NASA Contractor Report 3089

Investigation of the Multiple Model Adaptive Control (MMAC) Method for Flight Control Systems

M. Athans, Y. Baram, D. Castanon, K. P. Dunn,
C. S. Green, W. H. Lee, N. R. Sandell, Jr.,
and A. S. Willsky

NASA

NASA Contractor Report 3089

Investigation of the Multiple Model Adaptive Control (MMAC) Method for Flight Control Systems

M. Athans, Y. Baram, D. Castanon, K. P. Dunn,
C. S. Green, W. H. Lee, N. R. Sandell, Jr.,
and A. S. Willsky
Massachusetts Institute of Technology
Cambridge, Massachusetts

NASA

National Aeronautics
and Space Administration

Scientific and Technical
Information Office

1979

TABLE OF CONTENTS

vii

ix

xi

LIST OF TABLES

SYMBOLS

$\underline{A}$ Continuous time system matrix

$\underline{A}_{red}$ Short period dynamics continuous time system matrix

$\underline{A}_d$ Discrete-time system matrix

$\underline{A}_n$ System matrix of model in model-following design

$\underline{A}_p$ Implicit pilot-model system matrix

$\underline{A}(\gamma)$ System matrix for parameter value γ

$\underline{A}_i = \underline{A}(\gamma_i) = \underline{A}_d^i$ Discrete time system matrix for hypothesis model i, for parameter γ_i

$\underline{B}$ Continuous time input matrix

$\underline{B}_{red}$ Short period dynamics continuous time input matrix

$\underline{B}_d$ Discrete time input matrix

$\underline{B}_n$ Input matrix for model in model-following design

$\underline{B}_p$ Implicit input matrix for pilot model

$\underline{B}(\gamma)$ Input matrix for parameter values γ

$\underline{B}_i = \underline{B}(\gamma_i) = \underline{B}_d^i$ Discrete-time input matrix for hypothesis model i, for parameters γ_i

$\underline{C}$ Observation matrix

$\underline{C}(\gamma)$ Observation matrix for parameter values γ

$\underline{C}_i = \underline{C}(\gamma_i)$ Observation matrix for hypothesis model i, for parameters γ_i

$E\{(1)|(2)\}$ Conditional expectation of (1) given (2)

$\underline{G}_i$ Gain matrix for hypothesis model i

GR   Gearing ratio

G_q Steady-state gain between elevator deflection from trim and pitch rate.

G_q^i G_q for hypothesis model i.

G_α Steady-state given between elevator deflection from trim and angle of attack

G_α^i G_α for hypothesis model i

$\underline{H}^i (\underline{H}_i)$ Kalman Filter gains for hypothesis model i

H_i Hypothesis model i ($\underline{\gamma}=\underline{\gamma}_i$)

I Identity matrix

J_i Quadratic cost used for hypothesis model i

K Constant used in wind turbulence model

KF Kalman Filter

$\underline{K}$ Ricatti equation solution

L Scale length used in wind turbulence model

$\underline{L}$ Continuous time disturbance matrix

$\underline{L}(\gamma)$ Discrete time disturbance matrix for parameter values $\underline{\gamma}$

$\underline{L}(\underline{\gamma}_i)=\underline{L}_i$ Discrete time disturbance matrix for hypothesis model i, for $\underline{\gamma}=\underline{\gamma}_i$.

$\underline{L}_{red}$ Short-period continuous time disturbance matrix

M_i Steady state predicted covariance of $\underline{x}(t+1)$ given $Z(t)$

$MMAC$ Multiple Model Adaptive Control system

N Number of hypothesis models used

$N((1);(2))$ Gaussian distribution, mean (1), covariance (2)

$\underline{N}$ Noise covariance

$P(\underline{\gamma}_i)$ Probability of value of $\underline{\gamma}$ being $\underline{\gamma}_i$

P_i Identification probability corresponding to hypothesis model i

P_i^c Control Probability corresponding to hypothesis model i

$\underline{Q}_i$ State weighing matrix used in quadratic cost J_i

$\underline{R}_i$ Control weighing matrix used in quadratic cost J_i

$\underline{S}$ Covariance matrix for residual vector $\underline{\gamma}$

$\underline{S}_i$ Covariance matrix of residual vector $\underline{r}_i$ assuming hypothesis model i is time.

V_o True airspeed of aircraft.

WRS   Weighted sum of residuals squared

$Z(t)$ Set of post observations $\underline{z}(1),\ldots\underline{z}(t)$ and decision $\underline{u}(0),\ldots\underline{h}(t-1)$

a   Time constant used in actuator models

a_{ij} Element of matrix $\underline{A}$

a_y Lateral acceleration

a_z, a_{nz} Normal acceleration

b_i, b_{ij} Element of vector or matrix $\underline{B}$

g   Normal acceleration due to gravity

m   Dimension of the residual vector $\underline{r}$

$m(t)$ Weighted residual square signal

$m_i(t)$ Weighted residual square signal for hypothesis model i

$p(\gamma)$ Probability density of $\underline{\gamma}$

$p\{(1)|(2)\}$ Conditional probability density of (1) given (2)

p   Roll rate

q   Dynamic pressure

$q(t), q$ Pitch rate

r   Yaw rate

$\underline{r}$ Residual vector

$\underline{r}_i$ Residual vector for hypothesis model i

s   Symbol used in representation of transfer functions

s   Stick input

t	Time period
$\underline{u}$	Input vector
$\underline{u}_i$	Input vector suggested by hypothesis model i
$\underline{u}_m$	Input vector to model in model-following design
v	Velocity difference from trim
w	Normalized wind disturbance
$\underline{x}$	State vector
$\hat{\underline{x}}$	Optimal estimate of state vector
$\tilde{\underline{x}}_i(t)$	Predicted estimate of state vector by hypothesis model i at time t
$\hat{\underline{x}}_i(t)$	Updated estimate of state vector by hypothesis model i at time t
$\underline{z}$	Observation or measurement vector
$\hat{\underline{z}}$	Predicted measurement vector
$\underline{z}_m$	States of model in model-following design
$z_{(1)}$	Measurement reading of quantity (1)

Greek Symbols

α	Angle of attack deflection from trim value
β	Sideslip angle
$\beta_i, \beta_i{}^*$	Constants in conditional probability densities generated by hypothesis model i
$\underline{\gamma}$	Parameters describing possible models of the system
$\underline{\gamma}_i$	Parameters describing the ith hypothesis model used in MMAC
$\tilde{\delta}(\ )$	Dyrac delta function

δ_{ec}	Commanded elevator deflection from trim position
δ_a	Aileron deflection
δ_{ac}	Commanded aileron deflection
δ_r	Rudder deflection
δ_{rc}	Commanded rudder deflection
$\dot{\delta}_{ec}$	Commanded elevator deflection rate
$\dot{\delta}_{rc}$	Commanded rudder deflection rate
$\dot{\delta}_{ac}$	Commanded aileron deflection rate
$\delta(\ )$	Kronecker delta function
$\underline{\theta}$	Measurement noise vector
$\underline{\Theta}$	Measurement noise covariance
θ	Pitch angle deflection from trim value
$\eta_{(1)}$	Sensor noise in measurement of (1)
ϕ	Bank angle
ϕ_g	Spectral density of turbulence model
π	3.1415...
ξ	White noise disturbance
Ξ	Covariance of ξ
$\underline{\nu}$	White noise normalized disturbance
σ_ω	rms value of vertical gust velocity
$\epsilon_i(t|t)$	Conditional covariance of x(t) given Z(t)
$\epsilon_i(t+1|t)$	Conditional covariance of x(t+1) given Z(t)
ω	Frequency

General Abbreviations

$(1)_{LAT}$	Symbol 1, for the lateral system
$(1)_{LON}$	Symbol 1, for the longitudinal symbol

CHAPTER 1

INTRODUCTION, CONCLUSIONS, AND RECOMMENDATIONS FOR FUTURE RESEARCH

1.1. Introduction

This report presents the results of a research study which deals
with the feasibility of using an advanced adaptive control method, the
so called Multiple Model Adaptive Control (MMAC) method specifically
applied to the design of a stability augmentation control system for
the longitudinal and lateral dynamics of the NASA F-8C digital-flight-
by-wire aircraft. This study represents only one out of several
studies initiated by NASA Langley Research Center dealing with the de-
velopment and evaluation of different advanced control, identification,
and failure management strategies for the F-8C aircraft. Several of
these contributions appeared in an issue of the IEEE Transactions on
Automatic Control [1].

The paper by Elliott [2] presents an overview of the NASA F-8C
program. For the practically minded reader it is important to stress
that the results presented in this report represent a research effort
and a feasibility study, strongly influenced by certain design guidelines,
which will be described in detail later on, whose purpose was to make
the adaptive control problem for the F-8 aircraft intentionally difficult.
As explained in reference [2] the open loop characteristics of the F-8
aircraft are such that complex stability augmentation systems are not

necessary. In fact the F-8 aircraft does not require any sophisticated

control systems for adequate performance. Rather it serves as a test

bed for digital fly-by-wire studies, and as a vehicle by which several

methodologies for adaptive control, as well as failure detection and

redundancy management can be evaluated.

   For any conventional aircraft, the need for adaptive control

may occur if the aircraft is to be operated at a variety of operating

flight conditions as characterized by flight at different altitudes

and speeds,and under different conditions of wind turbulence. The dy-

namic characteristics of the aircraft change over its flight envelope

to a significant degree, since changes in dynamic pressure cause

changes in the aircraft aerodynamic forces and the effectiveness

of the control surfaces.   Thus a real-time adaptive control

system, based upon measurements obtained from the aircraft

sensors, has to determine in an approximate way the dynamic character-

istic of the aircraft at different points in its flight envelope.

One predominant parameter causing changes in the dynamic character

istics of any aircraft is, of course, dynamic pressure. If a

reliable estimate of the dynamic pressure is available, and reasonably

accurate aircraft models are available for each value of the dynamic

pressure, then one could design,in more or less straightforward manner, a

control system for the F-8 based upon the gain-scheduling approach; see

references [3],[4]. Gain scheduling has been long recognized as an

effective method for aircraft control given information about the dynamic

pressure.

The design guidelines under which this study was carried out were

such that an estimate of the dynamic pressure could not be obtained

using the sensors that were allowed. A parallel study, carried out by

a research team from Honeywell, Inc., see references [3],[4], directly

addressed the problem of estimating key aerodynamic parameters related

to dynamic pressure from longitudinal aircraft sensors, and then using

the estimate of dynamic pressure in order to do adaptive gain-scheduling.

The methodology employed in this study is philosophically different

than the one used by Honeywell, although the final implementation of

the adaptive control system presented in this study is quite similar,

from a structural and computational point of view.

1.2   Sensors

The performance of any aircraft command stability augmentation

system will be strongly influenced by the specific dynamics of the

aircraft, the available sensor measurements and their accuracy, and the

overall philosophy of designing the control system. The net outcome

should result in closed loop dynamics that have appealing handling

characteristics as far as the pilot is concerned.

In this study the dynamics of the aircraft were those of the F-8 aircraft. Since the objective of this study was to test the feasibility of the MMAC algorithm for aircraft control, the guidelines of the study were such that superior handling qualities were not one of the major required outputs of this study. Rather, the emphasis was on the adaptive identification and control aspects of the problem. This would then be strongly influenced by the sensors that one was allowed to use in the study, and the design methodology employed. Table 1.2.1 provides a list of the sensors that were used in the MMAC study. The general guidelines agreed upon by the NASA/LaRC and M.I.T./ESL was to utilize sensors that did not involve air data. Thus, sensors that utilize air data, such as sideslip vanes and angle of attack vanes were not used. Also, airspeed and accurate altitude information were excluded from the set of sensors that would be utilized. It should be noted that if accurate velocity and altitude sensors were used, then one could obtain an estimate of dynamic pressure, and one could construct the control system using simple gain-scheduling. In the absence of dynamic pressure estimates the adaptive control problem became particularly challenging. This dictates the complexity of the resultant MMAC design.

Once the question of available sensors was settled, the decision was made to fully take into account the stochastic aspects of these sensors. The design guidelines adopted were such that full use of Kalman filters was required. In the Honeywell study [4] no direct

TABLE 1.2.1.,

LIST OF AIRCRAFT SENSORS USED IN THE MMAC STUDY

Pitch Rate Gyro

Normal Accelerometer

Roll Rate Gyro

Yaw Rate Gyro

Lateral Accelerometer

Aileron Actuator *

Rudder Actuator *

Pitch Angle Gyro

Bank Angle Gyro

Altitude Sensor

---

* Sensors available for telemetering but not for control

Kalman filtering of the sensor measurements was made, except for iden-

tification purposes. In the MMAC design the use of Kalman filters for

processing the sensor measurements from both the longitudinal and lateral

dynamics had a two-fold purpose. First, the Kalman filters generated

state variable estimates which were then utilized by the control system,

and second, the Kalman filters also provided the necessary information

which acted as the input in the adaptive identification algorithm.

In order to minimize real-time computational requirements, the

decision was made to use only constant gain Kalman filters. The use of

time-varying Kalman filters may have improved the accuracy of the state

estimates and the performance of the identification algorithm. Time-

varying Kalman filters were not evaluated in this study, because it was

obvious that their real-time computational requirements were extensive.

1.3 Models

In any estimation and control system design, the performance of

both the estimation and the control algorithms is strongly influenced

by the accuracy of the dynamic models for the underlying system. In the

case of aircraft the most accurate dynamic models are those described

by nonlinear differential equations which include all the coupling terms

between the longitudinal and lateral dynamics.

The design guidelines agreed by NASA/LaRC and M.I.T./ESL were that only linear models associated with equilibrium flight could be used; these models did not include the coupling between the longitudinal and lateral dynamics; and they were described by linear time-invariant differential equations.

The operating envelope of the F-8 aircraft, defined in terms of altitude and speed, was approximated by using the linear equilibrium models of the aircraft at different flight conditions. These flight conditions, and their location in the flight envelope are summarized in Table 1.3.1. The numerical values used for the linearized open loop dynamics were provided by NASA/LaRC.

1.4 Control Philosophy

In this section the control philosophy is discussed, exclusive of the adaptive identification and control methods associated with the MMAC design. The key properties of the MMAC design will be discussed in detail in Chapter 2. This section outlines the methodology used for designing the control system given knowledge of the flight condition of the aircraft.

The design methodology consisted of two parts. First, it was agreed that one should understand the design of the regulator and gust alleviation system, i.e. the system that returns the aircraft to equilibrium flight, following any initial perturbations from it, and maintaining the aircraft on equilibrium flight in the presence of

TABLE 1.3.1.

FLIGHT CONDITIONS USED IN MMAC STUDY

Flight Condition No.	Altitude ft(met)	Mach No.	Dynamic Pressure lb/ft^2	(Newt/met^2)
#5	Sea level	.3	133.2	(6391)
#6	Sea level	.53	416.0	(19990)
#7	Sea level	.7	726.0	(34886)
#8	Sea level	.86	1098.0	(52762)
#10	20,000 (6096)	.4	109.0	(5237)
#11	20,000 (6096)	.6	245.0	(12205)
#12	20,000 (6096)	.8	434.0	(20854)
#13	20,000 (6096)	.9	550.0	(26429)
#14	20,000 (6096)	1.2	978.0	(46995)
#15	40,000 (12191)	.7	135.0	(6487)
#16	40,000 (12191)	.8	176.0	(8457)
#17	40,000 (12191)	.9	223.0	(10715)
#18	40,000 (12191)	1.2	397.0	(19077)
#19	40,000 (12191)	1.4	537.0	(25804)
#20	40,000 (12191)	1.6	703.0	(33781)

random turbulence inputs. Second, the regulator design was to be modified so as to be able to incorporate pilot commands.

For any given flight condition, the design guidelines required the construction of a complete Linear Quadratic Gaussian (LQG) design; see references [5], [6]. Both continuous-time and discrete-time designs were to be investigated.

Since the open loop dynamics change from flight condition to flight condition, several constant gain Kalman filters and control gains had to be obtained, using the standard LQG approach. The numerical values of the control gains were to be determined in order to provide the aircraft with certain desired closed loop characteristics, which changed from flight condition to flight condition. Therefore, one had to obtain a systematic way of defining the quadratic index of performance which changed in a natural way from flight condition to flight condition. The natural changes in the open loop dynamics as well as the changes in the performance index, resulted in different numerical values for the Kalman filter gains and the control gains for each flight condition.

It should be noted that significant simplifications can be made by modifying the LQG designs. This was not done, because the main thrust of the study was to understand the feasibility and performance of the MMAC method. At this point, it should be stressed that for any given known flight condition the transformation of the noisy sensor

measurements into commanded signals to the control surface actuators requires the use of a Kalman filter followed by the operation upon the estimated state variables by control gains. The next chapter shows how this design methodology is modified in order to obtain the overall adaptive identification and control system design, which is called the Multiple Model Adaptive Control (MMAC) method.

1.5 Brief Historical Perspectives

As explained in [9] there are several algorithms that employ a parallel structure of compensators to generate adaptive estimation and control algorithms. To the best of the authors' knowledge the first effort along these lines was that of Magill whose Ph.D. thesis culminated in [10]. Along similar veins Lainiotis and his students examined more general conditions for adaptive estimation (see [11] for a survey and discussion); Lainiotis calls these partitioned algorithms. Such ideas are also implicit in Aoki's book [12] and were also considered by Haddad and Cruz [13].

Multiple model type adaptive algorithms were considered by Stein [14] in his Ph.D. thesis, by Saridis and Dao [15], and by Lainiotis [16]-[17]. The properties of all these multiple model algorithms were examined by Willner [18] in his Ph.D. thesis. The structure of the specific MMAC algorithm used in this paper is akin to that by Deshpande et al. [19] and Athans and Willner [20] in which they examined a hypothetical STOL example. All these multiple model adaptive estimation and control algorithms represent blends of stochastic estimation and dynamic hypothesis testing

ideas. From an adaptive control point of view they are not dual control
approaches (see [9] and [21]). The F-8 specific design by Stein et al.
[4] can be also classified as a multiple model design.

1.6 Conclusions

This section contains a summary of the main study conclusions.
The conclusions will be divided into two separate categories, namely
conclusions with respect to the performance of the adaptive control
system based upon the MMAC method. Since all identification and control
simulations were based on a control system design that was based upon
linearized models of the aircraft, about equilibrium flight conditions,
the conclusions are only valid for maneuvering flight which does not
deviate extensively from equilibrium flight. Roughly speaking the main
conclusions pertain to flight or the F-8 aircraft throughout its flight
envelope, under the constraints that the pitch attitude of the aircraft
does not exceed 30°, and the bank angle of the aircraft does not exceed
45°. If these limits are exceeded the equilibrium models become grossly
invalid, and the MMAC design may yield poor performance and result in
instability.

1.6.1 Identification

As long as there is sufficient excitation of the aircraft, either
through pilot inputs or through turbulence inputs, the identification
performance of the MMAC algorithm is satisfactory. In general, the
accuracy and speed of the identification is better in the longitudinal
dynamics than the lateral dynamics. It should be noted that no ex-
ternal persistent excitation inputs were used in contradistinction to

the approach used by Honeywell [4]. In the absence of any persistent excitation, it is often difficult to obtain sufficient information from the noisy sensors to distinguish between flight conditions which are similar as far as the dynamic response of the aircraft is concerned. This does not necessarily imply a degradation in the performance of the adaptive control system.

1.6.2 Adaptive Control

The overall performance of the adaptive control system based upon the MMAC method was judged as satisfactory. As to be expected, the performance of the MMAC system was best when the flight conditions were close to the models used to implement the MMAC algorithm. In particular, the adaptive control system performed best when used as a regulator and as a wind gust alleviation system. The performance of the control system, viewed as a command augmentation system in the presence of pilot inputs, had certain inherent limitations due to the design methodology employed, which was not the best possible from the point of view of the aircraft handling qualities.

In general, the performance of the longitudinal control system in response to pilot inputs was better than the performance of the lateral control system. The lateral pilot command augmentation system, performed very well near its design point. The specific methodology employed in the design of the lateral control system was explicit model following of a lateral model which was velocity dependent: since the aircraft velocity was not to be measured (nor estimated in the MMAC approach) under the design ground rules, the lateral control system performed poorly when the actual velocity of the aircraft differed sig-

nificantly from the velocity employed for the model following base line case. In this respect, the aircraft could follow commanded changes in the bank angle quite well, at the expense of excessive sideslip angles.

As a general methodology, the MMAC method is more general than the method used by Honeywell [4], which is much more tailored to the characteristics of the F-8 aircraft. As such it deserves further study, as a general methodology, in view of the specific way that the method employs parallel computation. As the cost and reliability of digital microprocessors improve, the hardware implementation required by the MMAC algorithm becomes more and more viable.

1.7   Recommendations for Future Research

This section contains a list of specific recommendations for future research which are necessary for both improved understanding of the MMAC method as an adaptive design methodology, as well as for specific design changes that should be carried out before the present MMAC design is used in an actual flight test.

1.7.1   Identification Performance Using Real Data

Since there exists extensive data from the flight tests of the F-8 aircraft, the identification and estimation part of the MMAC algorithm can be tested, analyzed, and improved using this real data. The benefit of this study, will be to examine how the analytical models used in the development of the Kalman filters associated with the identification algorithm are compatible with the actual dynamics observed in flight. In this manner, one can test not only the identification accuracy and convergence speed of the

MMAC algorithm, but much more importantly one will obtain a much better idea of how to "tune" the Kalman filters for both the longitudinal and lateral dynamics. Through the use of real flight test data, one will be able to conclude how much information is provided by the longitudinal dynamics and how much information is provided from the lateral dynamics.

At the present time, based on the recently completed Ph.D. thesis of Baram [7], one has a much better, but by no means complete, theoretical understanding of the convergence properties of hypothesis-testing algorithms when the actual flight condition does not coincide with the flight conditions which have been used as models in the identification algorithm. The use of actual flight test data can increase the basic understanding of hypothesis testing based adaptive methods.

1.7.2 Improvements in Kalman Filter Design

The correct and accurate design of the discrete-time Kalman filters for both the longitudinal and lateral dynamics is very important. There are two reasons for having well-designed Kalman filters: first, the Kalman filters have to generate accurate estimates of the state variables to generate the commanded controls, and second, the residuals generated by the Kalman filters are the sole sources of information which drive the identification algorithm.

Since the longitudinal control system was designed only for the control of the short-period dynamics, the longitudinal Kalman filters received noisy information only from the normal accelerometer and the pitch rate gyro. The available measurement of elevator position was not used so that one would not have to face the problem of decomposing

the elevator measurement into a trim value and a pilot input. A great deal of improvement can be made in the Kalman filter design, if one augments the states so as to estimate the elevator trim. The design will be similar to the one used by Honeywell [4] although this would contribute to an increase in the complexity of each individual longitudinal Kalman filter and to the overall real time requirements of the MMAC algorithm. To increase the estimation accuracy and robustness of the individual Kalman filters one should change the design of the discrete Kalman filters using the recently developed techniques of the discrete time compensated Kalman filters, as described in the report by Lee and Athans [8], especially given the chosen relatively low sampling rate of 1/8 second. In addition, all the Kalman filters used in this study were designed for a fixed high level of turbulence. A more systematic study is needed, especially if the actual flight data is used, to investigate whether or not the longitudinal Kalman filters are sensitive to the level of turbulence used for their numerical design.

Similar comments could be made with respect to the design of the Kalman filters for the lateral dynamics. These Kalman filters will have to be very carefully tuned if indeed one wants to maximize the amount of information that could be extracted from lateral maneuvers of the aircraft. The Kalman filters employed for the lateral dynamics in this study were based upon equilibrium flight conditions. They do not perform adequately in the case of tight persistent turns, since these represent a different equilibrium flight for the aircraft. In the absence of such a study, one cannot conclude definitely what amount of information can be obtained

from the lateral dynamics as compared to the longitudinal dynamics.

1.7.3 Control System Design

The design of both the longitudinal and lateral control systems was based on the LQG methodology. There was little difficulty in designing adequate control systems for the regulator part of the design which can be used as a gust alleviation system. Improvements in the handling qualities are necessary for both the longitudinal and the lateral control system in the case of pilot inputs.

From the handling qualities point of view, the current longitudinal design is minimally adequate. One recommended change is to incorporate an additional integrator in the forward loop, using the results of Boussard and Safonov [28], which were not available at the time that the design was fixed. Effectively, such a change coupled with the low sampling rate employed in the design, will improve the performance of the longitudinal control system in the presence of sustained constant pilot inputs. In addition it will improve the performance of the longitudinal control system in the presence of constant but unknown wind forces which are not estimated by the Kalman filter.

The lateral control system employed for the gust alleviation case is good. However, the lateral control system used as a stability augmentation system in the presence of lateral commands by the pilot is not satisfactory. Its basic shortcoming, from a handling qualities point of view, is that it cannot produce coordinated turns throughout the flight envelope. This is not a shortcoming of the methodology employed, but rather is due to the design constraints of what informa-

tion is available from the sensors. In order to execute a coordinated turn, and minimize the resultant lateral acceleration, one must have a good estimate of the aircraft velocity. In the design employed, such an estimate of velocity was not available. The lateral control system was designed on the basis of a single nominal velocity of the aircraft, corresponding to a flight condition in the middle of the operating envelope of the aircraft, and this nominal value of the velocity was not changed as the aircraft executed maneuvers throughout its flight envelope. As a result the lateral control system performs very well as long as the actual velocity of the aircraft is near the design velocity. When the actual velocity of the aircraft differs significantly from the nominal velocity used in the design, the aircraft has to respond in such a way that excessive lateral accelerations and sideslip angles are generated in order to follow the commanded bank angles by the pilot. The discussion and simulation results given in Chapter 6 make this point clear. If a crude estimate of the velocity were available, then it would be a straightforward matter to change the numerical values of the control gains used in the lateral control system so that satisfactory performance can be obtained throughout the flight envelope.

The principal investigator in this effort was Michael Athans, and the principal co-investigator was Alan S. Willsky. The program manager was initially K. P. Dunn, followed by David Castañon. N. R. Sandell, Jr., Y. Baram, W. H. Lee, C. S. Greene, I. Segall and D. Orhlac also participated in this research. We gratefully acknowledge the aid and support of

CHAPTER 2

AN OVERVIEW OF THE MULTIPLE MODEL ADAPTIVE
CONTROL METHOD

2.1 Introduction

In this chapter an informal presentation of the key ideas associated with the Multiple Model identification and adaptive control algorithm are presented, so as to stress the intuitive aspects of this adaptive identification and control algorithm. A more rigorous treatment of the algorithm and its performance in the context of controlling the F-8C aircraft will be given in subsequent chapters of this report. Some well known facts about Kalman filters are included so as to establish notation. Finally, this chapter concludes with a brief description of the contents of the remaining chapters of this report.

2.2 Basic Idea of the Multiple Model Identification Algorithm

Consider the situation depicted in Figure 2.2.1 which shows a dynamic system subject to the influence of a multivariable control, $\underline{u}(t)$, and external disturbances. Assume that the system contains noisy sensors that generate a set of measurements which form the components of the measurements vector, denoted by $\underline{z}(t)$.   In the context of this study the true system represents the F-8C aircraft. The components of the control vector will be the commanded inputs to the surface actuators as generated by a combination of the pilot inputs and the signals generated by the stability augmentation system. The disturbances represent the forces on the aircraft generated by turbulence. The measurements are those generated by the aircraft sensors used in the design, as described in Chapter 1,
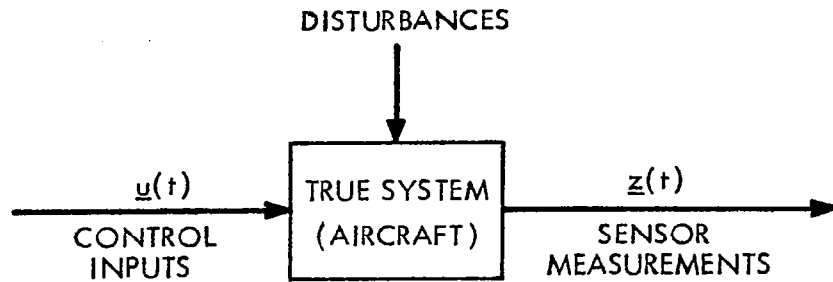
Figure 2.2.1   The structure of the system to be controlled.
In aircraft applications the control inputs
are the commanded inputs to the surface
actuators. Disturbances are due to wind
turbulence. The vector $\underline{z}$(t) denotes noisy
sensor measurements.

Table 1.2.1.

In general the noisy measurements generated by the sensors are not sufficient to obtain a good estimate of all the state variables of the true system. In these situations one must construct a Kalman filter whose objective is to process the noisy measurements and generate an estimate, $\hat{\underline{x}}(t)$, of the true state vector of the system that is generating the data. Figure 2.2.2 shows in block diagram form the true system which generates the data and the general structure of the Kalman filter. The Kalman filter contains a mathematical model of the true system. It generates a predicted measurement vector, $\hat{\underline{z}}(t)$, which is in some sense the best estimate of the actual measurement vector, $\underline{z}(t)$, generated by the true system. By subtracting the actual measurements from the pre-dicted measurements one obtains the so-called residual (innovations) vector $\underline{r}(t)$. The residual vector is multipled by the Kalman gain matrix which in turn drives the differential or difference state equations that represent the model of the true system. In this manner the Kalman filter generates a vector, $\hat{\underline{x}}(t)$, whose components represent the estimates of each and every state variable associated with the true system.

If the mathematical model employed in the Kalman filter is an adequate representation of the dynamics of the true system, it is well known that the residual vector, $\underline{r}(t)$ has certain special properties. In particular, the components of the residual vector will be white noise. One can calculate, off-line, the covariance matrix, $\underline{S}$, of the residual
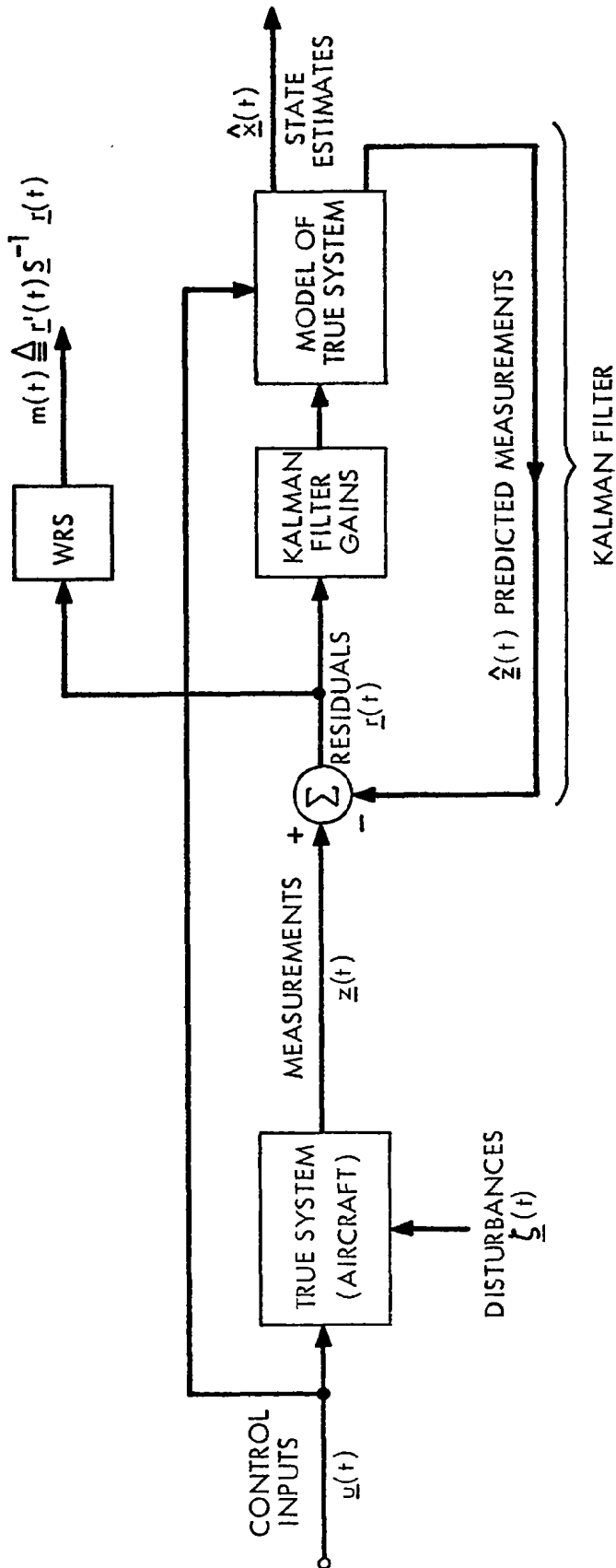
Figure 2.2.2   General structure of a Kalman filter. The weighted residual square (WRS) signal m(t) is generated from the residual vector, $\underline{r}(t)$, of the Kalman filter by the quadratic form $m(t) = \underline{r}'(t)\underline{S}^{-1}\underline{r}(t)$ where $\underline{S}$ is the covariance matrix of the residuals, m(t) in a scalar quantity.

vector $\underline{r}(t)$ given the mathematical model of the system and the statistical properties of the random processes which define the disturbances to the true system and the measurement noises associated with the physical sensors. For reasons that will become obvious in the sequel one can then process the residual vector, $\underline{r}(t)$, which is available in real time from the Kalman filter to generate a scalar quantity, denoted by $m(t)$, which is called the weighted residual square (WRS) signal. The mathematical definition of the signal $m(t)$ is as follows:

$$m(t) \overset{\Delta}{=} \underline{r}'(t)\underline{S}^{-1}\underline{r}(t) > 0 \qquad (2.2.1)$$

As the mathematical model of the true system used in the Kalman filter starts to deviate from the actual dynamic behavior of the true system which is generating the actual data, the residual vector, $\underline{r}(t)$, loses its "white" properties. Depending on the degree of modeling error the Kalman filter residuals become larger, correlated in time, and they may contain biases. Thus, by observing the time traces of the Kalman filter residuals, one can obtain a rough idea of whether or not the mathematical model used in a Kalman filter is a reasonable representation of the actual system dynamics. If the residuals are large, this is a clue that there is a mismatch between the actual system dynamics and the dynamics used to construct the Kalman filter.

The residual covariance matrix, $\underline{S}$, is always a positive definite matrix; hence the weighted residual square signal, m(t), as defined by Equation (2.2.1) will always be a positive quantity. If the mathematical model used in the Kalman filter is a very good approximation to the true system dynamics, the Kalman filter residuals will be small, and as a consequence the scalar m(t) will also be small. On the other hand, if the mathematical model used to construct the Kalman filter becomes a worse approximation to the true system dynamics, the residual vector will become larger, and as a consequence the WRS signal m(t) will become larger. Thus, the relative magnitude and stochastic behavior of the weighted residual square signal, m(t), as generated by any particular Kalman filter, provides a clue to the degree of "modeling error" between the true system dynamics and the mathematical model used to construct the Kalman filter.

Next, suppose that the designer does not have a good idea of the true dynamics of the physical system which is generating the actual data, $\underline{z}$(t). In this case, from prior considerations, he may hypothesize that the true system dynamics will be close enough to one out of N possible models. In aircraft applications, the fact that the aircraft, as it flies throughout its flight envelope, changes its dynamic characteristics causes the true system that is generating the data to be unknown to the designer. The designer may postulate the existence of several possible dynamic models of the aircraft, where each model represents the aircraft dynamics at different

flight conditions. Suppose that somehow the designer has selected N

different models for the possible description of the dynamics of the

aircraft. In this case, as illustrated in Figure 2.2.3, the designer

can construct a bank of Kalman filters where each Kalman filter is

driven simultaneously from the actual control vector, $\underline{u}(t)$, and the

actual measurement vector, $\underline{z}(t)$. Each Kalman filter, indexed by

$i = 1,2,...,N$, utilizes a different dynamic model for its implementation.

Thus each Kalman filter will generate a different estimate $\hat{\underline{x}}_i(t)$ of the

state of the system, and a different residual vector, $\underline{r}_i(t)$. Furthermore,

the covariance matrix $\underline{S}_i$ of the residual vector $\underline{r}_i(t)$ associated with each

Kalman filter will be different, because different dynamics are used to

implement each Kalman filter in Figure 2.2.3. The residual vector of

each Kalman filter can be further processed to generate a different scalar

WRS signal, $m_i(t)$, for each Kalman filter.

It should be intuitively obvious, that the differences between

the WRS signals, $m_i(t)$, will be strongly influenced not only by the dif-

ference between the actual system dynamics and the mathematical models

used in the bank of Kalman filters, but also by the control input, $\underline{u}(t)$,

which excites both the true system and every Kalman filter. If the control

input were sufficiently strong and excited all the significant dynamics

of the true system, then the WRS signals $m_i(t)$ would be larger and hence

the identification accuracy would improve. On the other hand, if the

control input did not sufficiently excite the dynamics of the true system
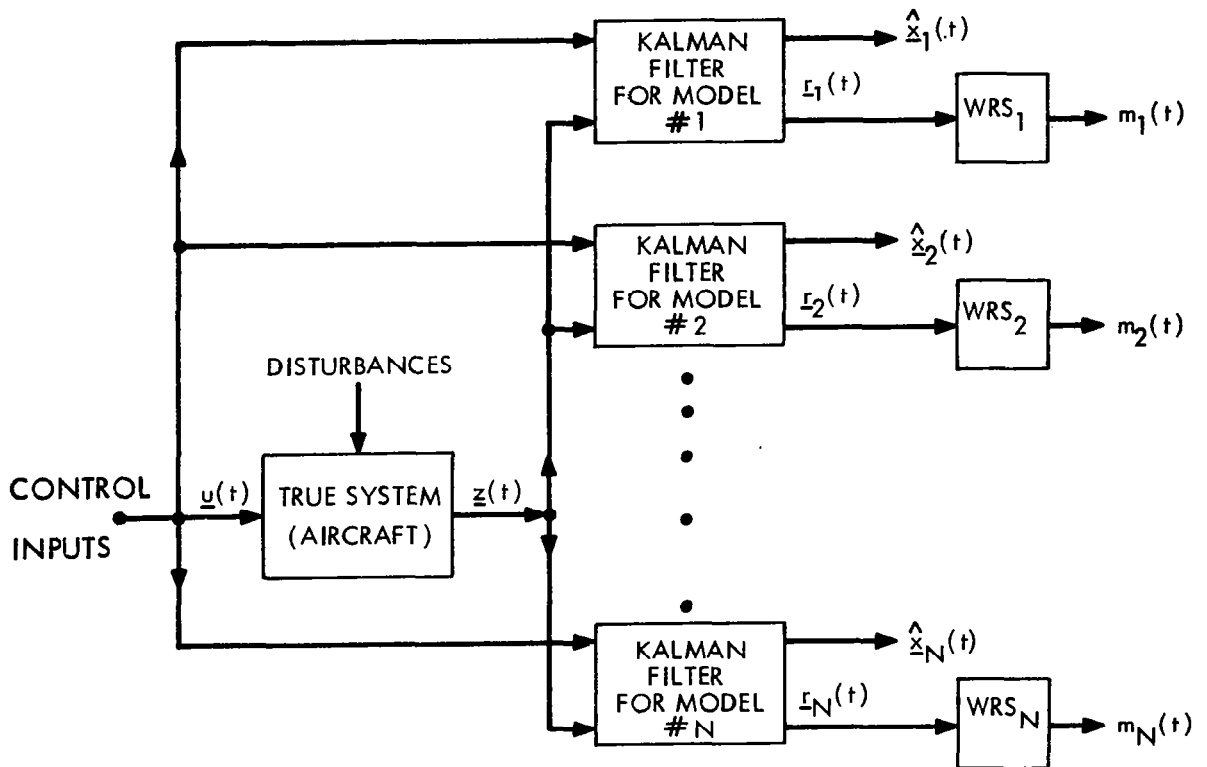
Figure 2.2.3   Structure of a bank of N Kalman filters (see Fig. 2.2.2)
that simultaneously generate state estimates, $\hat{\underline{x}}_i$(t), and

the WRS scalar signals m_i(t) that can be used for
identification.

then the existence of the wind disturbances and sensor noises, would make it relatively hard to tell which model best matched the dynamics of the true aircraft. Thus, in an ideal identification experiment one would like to apply relatively large signals to the true system so as to aid the identification accuracy. However, this may be completely against the requirements of the control system design, in which such large inputs are undesirable.

From the above discussion, it follows that the time evolution and relative size of the different WRS signals $m_i(t)$, contain information which can be used to determine the approximate dynamics of the true system. On the other hand, this information is not in the most appropriate form for either a precise definition of identification, or purposes of adaptive control. Under certain assumptions, discussed in Chapter 4, the information contained in the WRS signals $m_i(t)$ can be transformed into a conditional probability that the dynamics of the true system are close to the dynamics used in each Kalman filter.

2.3 Adaptive Control System Design by the MMAC Method

This section contains an informal description of the adaptive control system design associated with the MMAC concept. First, the design of the control system in the case of perfect identification is presented; then the design of the adaptive control system is illustrated. Suppose that the dynamics of the aircraft at a particular flight condition are known. Figure 2.3.1 illustrates the block diagram of the overall stability
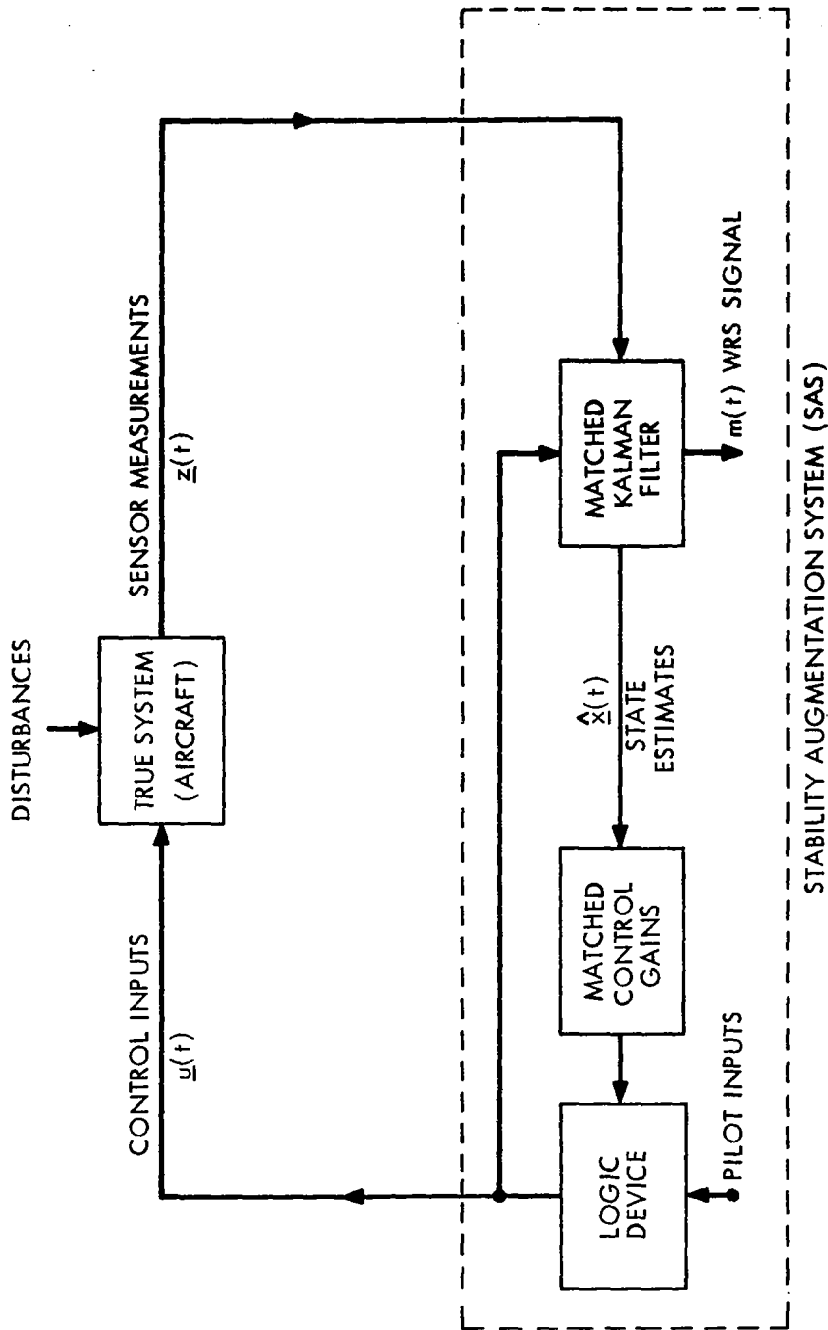
Figure 2.3.1 The general structure of the dynamic compensator or stability augmentation system (SAS) when the true aircraft dynamics are known so that matched Kalman filters and control gains can be computed.

augmentation system. The noisy sensor measurements, $\underline{z}(t)$, are used to drive a Kalman filter whose dynamics are matched to those of the aircraft. The Kalman filter generates an estimate, $\hat{\underline{x}}(t)$, which is multiplied by a set of control gains, selected to provide appropriate handling qualities for that particular flight condition. These control signals are then combined with the pilot input signals in order to generate the control vector, $\underline{u}(t)$, that is the command signal to the aircraft control actuators.

Figure 2.3.2 illustrates the structure of the overall multiple model adaptive control (MMAC) system. Using different models of the aircraft at different flight conditions, one designs the best stability augmentation system (SAS) for that particular flight condition. Each stability augmentation system would generate the optimal command control vector, $\underline{u}_i(t)$ to the aircraft under the assumption that the aircraft dynamics were identical to that of the i-th model. Since each stability augmentation system (see Figure 2.3.1) contains a Kalman filter, the WRS signals $m_i(t)$ are available and introduced to the probability evaluator, which in turn generates the probability, $P_i(t)$, that the aircraft is in the i-th flight condition. To generate the actual commanded control signals, $\underline{u}(t)$, to the aircraft actuators one multiplies the optimal control signal for each flight condition, $\underline{u}_i^*(t)$ by the probability, $P_i(t)$, that the aircraft is indeed in that flight condition and one adds the resultant signals to actually drive the aircraft actuators. Mathematically this defines the control vector $\underline{u}(t)$ as

$$\underline{u}(t) = \sum_{i=1}^{N} P_i(t)\underline{u}_i^*(t) \qquad (2.3.1)$$
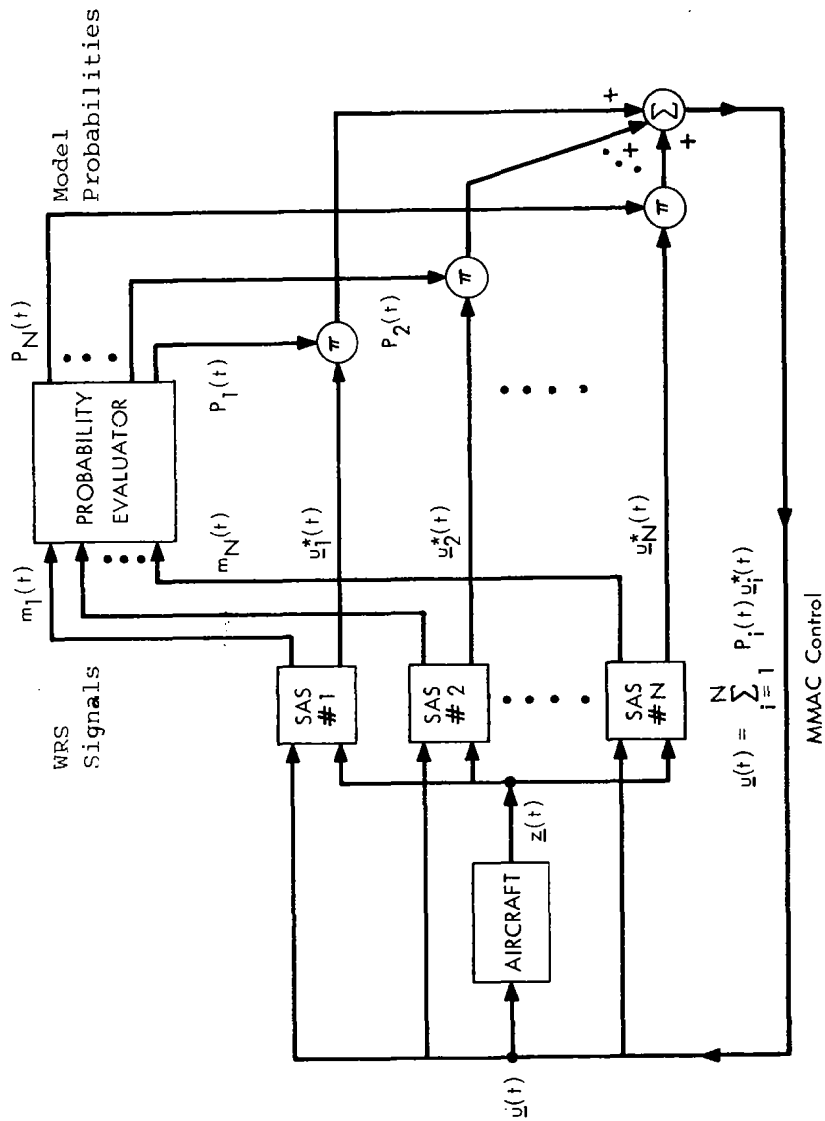
Figure 2.3.2   Complete structure of MMAC algorithm. Each SAS box is described by the functional diagram of Fig. 2.3.1 and generates the "optimal" control, $\underline{u}_i^*(t)$, for a given flight condition. The actual control, $\underline{u}(t)$, applied to the aircraft is the weighted probabilistic average.

When the aircraft coincides with one of the models used in the construction of a particular stability augmentation system, the probability associated with that model will eventually approach unity, so that the actual control applied to the aircraft will indeed be the optimal control as calculated by the specific stability augmentation system.

The overall performance of the MMAC scheme shown in Figure 2.3.2 will be influenced by a number of factors. Obviously the number, N, of the models available will influence the response of the overall system. The identification accuracy will be influenced by the amount of excitation available either through natural turbulence, or pilot inputs, or artificial persistent excitation (this was not used in this study). Ideally one would like to have as many models in the bank of the stability augmentation systems as possible. Since each model contains an internal Kalman filter, the real-time computational requirements of the MMAC algorithm will grow with the number of models. Thus tradeoffs between the effectiveness of the control system and the real-time computational requirements are necessary.

This completes the overview of the adaptive control system design. The remainder of this report discusses how each and every block in the entire control system was designed, and presents typical characteristics of this adaptive control algorithm using nonlinear simulations of the aircraft.

2.4 <u>Overview of Remaining Chapters</u>

The purpose of Chapter 3 is to define the variables and the struc-
ture of the differential equations associated with the longitudinal
and lateral dynamics of the F-8 aircraft. In the approach used, the
nonlinear differential equations describing the motion of the aircraft
were replaced by a set of linear differential equations, one set for
the longitudinal dynamics and another set for the lateral dynamics.
The different operating conditions were defined by the altitude of the
aircraft,its normal acceleration and its speed. This chapter also con-
tains the dynamics of the actuators, the modeling of the wind disturbances
as well as a description of the sensors used. The numerical values of
the coefficients that appear in the linear differential equations of
motion, for both the longitudinal and the lateral systems, are summarized
in Appendix A.

The purpose of Chapter 4 is to summarize the theory behind the MMAC
algorithm which was the basic adaptive design methodology used in this
study. Both the identification aspects as well as the control aspects of
this adaptive algorithm are presented in this chapter. Additional
theoretical backup is provided in Appendix C.

The purpose of Chapter 5 is to summarize the LQG based design used for
controlling the longitudinal system. In particular the philosophy and numerical
values associated with the quadratic index of performance used to design
the control system are indicated. The final quadratic performance index

penalizes a weighted combination of normal acceleration, pitch rate, and the time derivative of the commanded elevator signal. Further, the Kalman filter design for the longitudinal system, using only the noisy measurements of pitch rate and normal acceleration, is presented.

To incorporate pilot commands, the philosophy that the pilot only wishes to control the short-period dynamics was adopted. This chapter includes some simulations illustrating the operation of the pilot command system. The simulation results presented in this chapter represent the performance of the aircraft under perfect identification conditions; they serve as a bench mark for the subsequent adaptive control system simulations.

The purpose of Chapter 6 is to discuss the development of the control system for the lateral dynamics. The methodology employed was that of explicit model following. The chapter contains a discussion of the different types of quadratic performance criteria tried out. The final criterion included tradeoff terms involving the lateral acceleration, roll rate, sideslip angle, bank angle, as well as the time derivatives of the commanded aileron and rudder signals. The chapter concludes with the presentation of several simulations carried out at different flight conditions, different initial conditions, with and without turbulence, by comparing the open loop response of the aircraft versus the closed loop response of the aircraft in the lateral system. These simulations for the lateral system serve as a bench mark for further comparison with the adaptive lateral system.

The purpose of Chapter 7 is to present the performance of the MMAC algorithm for several simulations at different flight conditions. Simulations were carried out both in the absence and in the presence of turbulence. Several combinations of models were included in these simulation results. This chapter also contains an extensive set of experiments whose purpose is to demonstrate the amount of information available for identification, the performance of the identification algorithm, and the performance of the adaptive control system as a whole under stick commands.

The purpose of Chapter 8 is to describe a potential real time scheduling algorithm which is necessary in order to be able to carry out all the adaptive estimation, identification, and control algorithms in real time when the aircraft is flying throughout its entire envelope. This chapter describes a simple ad-hoc procedure that utilizes very gross altitude information, but no speed information whatsoever, in order to make a real-time decision about which subset of models are going to be used at each instant of time in the MMAC algorithm. This chapter includes selected simulation results of the MMAC algorithm as the aircraft undergoes piloted flight over large segments of its flight envelope.

The purpose of Chapter 9 is to summarize the main conclusions reached under this study.

CHAPTER 3

LINEARIZED AIRCRAFT EQUATIONS

3.1   Introduction

This chapter discusses the variables and equations which describe the aircraft behavior. As usual, lateral and longitudinal dynamics will be discussed separately. Based on these equations, decoupled longitudinal and lateral linear dynamic models of the aircraft are obtained at various flight conditions.

3.2   Reference Flight Conditions

Linearized models of the aircraft can be obtained about a number of equilibrium conditions. In this study, fifteen conditions were used, chosen throughout the aircraft flight envelope. Table 1.3.1 and Figure 3.2.1 describe the fifteen flight conditions for which NASA/LARC provided linearized data.

The flight conditions were characterized by altitude and Mach number, with dynamic pressure, trim, angle of attack and elevator position being specified as part of the flight condition. The true airspeed V_0 can be computed from

$$V_0 = \text{Mach no.} \times \text{speed of sound} \qquad (3.2.1)$$

3.3   Longitudinal Systems Equations

Table 3.3.1 contains a description of the variables which will be used in the linearized equations. The general form of these linearized
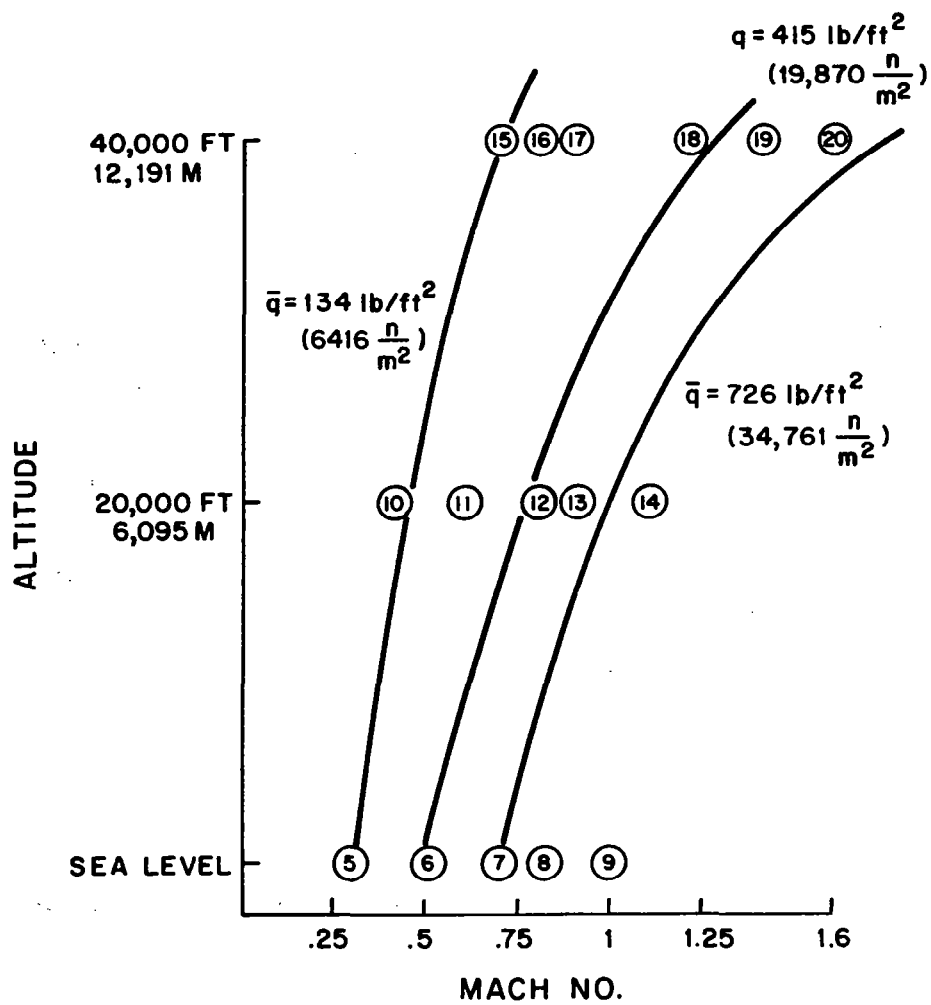
Figure 3.2.1 Location of selected Flight Conditions of F-8C.

TABLE 3.3.1

LONGITUDINAL VARIABLES

State Variable	Symbol	Units
Pitch rate	$q(t)$	radians/second
Velocity error from trim	$v(t)$	ft/sec (met/sec)
Angle of attack measured from trim condition	$\alpha(t)$	radians
Pitch attitude	$\theta(t)$	radians
Elevator deflection from trim condition	$\delta_e(t)$	radians
Commanded elevator deflection	$\delta_{ec}(t)$	radians
Wind disturbance (normalized)	$w(t)$	radians

commanded
elevator deflection → $\dfrac{a}{s+a}$ → actual
elevator position

δ_{ec} δ_e
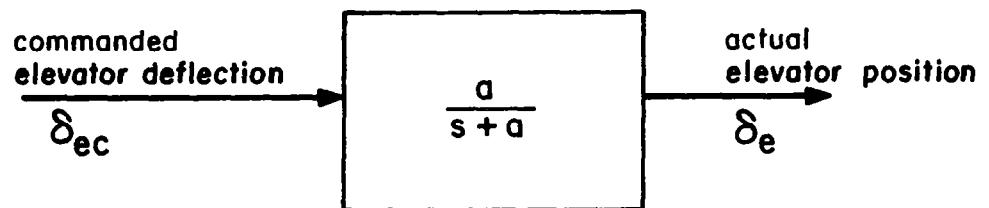
Figure 3.3.1   Actuator Model

equations is given by

$$
\frac{d}{dt}
\begin{bmatrix} q \\ v \\ \alpha \\ \theta \end{bmatrix}
=
\begin{bmatrix}
a_{11} & a_{12} & a_{13} & 0 \\
0 & a_{22} & a_{23} & -g \\
1 & a_{32} & a_{33} & 0 \\
1 & 0 & 0 & 0
\end{bmatrix}
\begin{bmatrix} q \\ v \\ \alpha \\ \theta \end{bmatrix}
+
\begin{bmatrix} b_1 \\ b_2 \\ b_3 \\ 0 \end{bmatrix}
\delta_e
\qquad (3.3.1)
$$

Equation (3.3.1) describes the general form of the linearized air-craft, ignoring actuator dynamics and disturbances. The elevator deflection δ_e is the output of an actuator driven by a commanded elevator angle δ_{ec}, as illustrated in Figure 3.3.1, so that

$$
\dot{\delta}_e(t) = -a\, \delta_{ec}(t) \qquad (3.3.2)
$$

where $a = 12$ is the time constant of the hydraulic actuator.

3.4 Wind Disturbances in the Longitudinal System

In modelling wind disturbances, the following power spectral density was used [2]

$$
\Phi_g = \frac{\sigma_w^2}{\pi} \frac{L}{V_0} \frac{4}{4 + \left(\dfrac{L}{V_0}\,\omega\right)^2} \qquad (3.4.1)
$$

where σ_w is the root mean square vertical gust velocity, L is the scale length in feet or meters, V_0 is the airstream velocity in ft/sec or m/second. Typical values of L and σ_w are shown in Tables 3.4.1 and 3.4.2.

The wind disturbance with power spectrum described by Eq. (3.4.1) can be considered as the output of a first-order linear system driven

TABLE 3.4.1

DEPENDENCE OF SCALE LENGTH L UPON ALTITUDE

Height	L
0 ft (0 met)	200 ft (61 met)
1000 ft (305 met)	1000 ft (305 met)
2500 ft (762 met)	2500 ft (762 met)
>2500 ft (762 met)	2500 ft (762 met)

TABLE 3.4.2

NUMERICAL VALUES OF σ_w FOR

DIFFERENT WEATHER CONDITIONS

Condition	σ_w
normal	6 ft/sec (1.83 met/sec)
cumulus	15 ft/sec (4.57 met/sec)
thunderstorm	30 ft/sec (9.15 met/sec)

by a zero mean white noise input, $\xi(t)$, as shown in Figure 3.4.1. The equation corresponding to this system is

$$w^\circ = -aw + \frac{K}{V_0} \xi(t) \qquad (3.4.2)$$

where

$$E\{\xi(t)\xi(s)\} = \delta(t-s) \qquad (3.4.3)$$

and $\delta(.)$ is the Dirac delta function.

Given the power spectrum of $w(t)$ given by Eq. (3.4.1), by choosing

$$a = 2 \frac{V_0}{L} \qquad (3.4.4)$$

$$K = \frac{2\sigma_w V_0}{\sqrt{\pi L V_0}} \qquad (3.4.5)$$

one obtains Eq. (3.4.2).

This normalized wind disturbance $w(t)$ in the longitudinal dynamics has the same influence on the remaining state variables as an angle of attack perturbation. Hence, $w(t)$ can be modeled as a state variable, and its effect on other state variables can be obtained from the previous linearized models. The linearized equations for the longitudinal system including wind effects and actuator dynamics are:
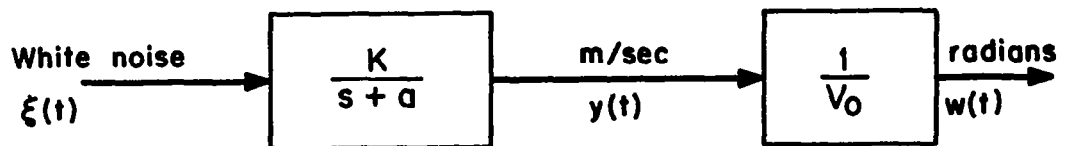
Figure 3.4.1   Normalized Wind Disturbance Generated by
              White Noise Input $\xi(t)$

$$\frac{d}{dt} \begin{Bmatrix} q(t) \\ v(t) \\ \alpha(t) \\ \theta(t) \\ \delta_e(t) \\ w(t) \end{Bmatrix} = \begin{bmatrix} a_{11} & a_{12} & a_{13} & 0 & b_1 & a_{13} \\ 0 & a_{22} & a_{23} & -g & b_2 & a_{23} \\ 1 & a_{32} & a_{33} & 0 & b_3 & a_{33} \\ 1 & 0 & 0 & 0 & 0 & 0 \\ 0 & 0 & 0 & 0 & -12 & 0 \\ 0 & 0 & 0 & 0 & 0 & -a \end{bmatrix} \begin{Bmatrix} q(t) \\ v(t) \\ \alpha(t) \\ \theta(t) \\ \delta_e(t) \\ w(t) \end{Bmatrix}$$

$$+ \begin{Bmatrix} 0 \\ 0 \\ 0 \\ 0 \\ 12 \\ 0 \end{Bmatrix} \delta_{ec}(t) + \begin{Bmatrix} 0 \\ 0 \\ 0 \\ 0 \\ 0 \\ \frac{K}{V_0} \end{Bmatrix} \xi(t) \qquad (3.4.6)$$

which is of the form

$$\overset{\circ}{\underline{x}}(t) = \underline{A}\,\underline{x}(t) + \underline{B}\,\delta_{ec}(t) + \underline{L}\xi(t)$$

Appendix A contains a complete list of the coefficients of the $\underline{A}$, $\underline{B}$, and $\underline{L}$ matrices for each flight condition.

3.5 Sensor Measurements in the Longitudinal Dynamics

The F-8C aircraft has noisy sensors which provide the measurements described in Table 3.5.1, which includes the variances of the measurement noise.

3-10

TABLE   3.5.1

NOTATION FOR NOISY LONGITUDINAL SENSORS

Sensor	Measurement equation	rms error
pitch rate	$z_q = q + \eta_q$	.489 deg/sec
velocity error	$z_v = v + \eta_v$	.6096 m/sec
pitch attitude	$z_\theta = \theta + \eta_\theta$	.2 deg
elevator angle	$z_{\delta_e} = \delta_e + \eta_{\delta_e}$	.1 deg
normal acceleration	$z_{a_z} = a_{n_z} + \eta_{a_z}$	.06 g's

The quantities η_q, η_v, η_θ, η_{δ_e} and η_{a_z} represent additive white measurement noises associated with the sensors. The dynamics of the sensors are modeled as unity gain transfer functions with no phase dynamics. The linearized measurement equations can be modeled as

$$\underline{z} = \underline{C} \begin{bmatrix} \underline{x} \\ w \end{bmatrix} + \underline{\xi}' \qquad (3.5.1)$$

where

$$\underline{z} = \begin{bmatrix} z_q \\ z_v \\ z_\theta \\ z_{\delta_e} \\ z_{a_z} \end{bmatrix}, \quad \begin{matrix} \underline{x} \\ w \end{matrix} = \begin{bmatrix} q \\ v \\ \alpha \\ \theta \\ \delta_e \\ w \end{bmatrix}, \quad \underline{\xi}' = \begin{bmatrix} \eta_q \\ \eta_v \\ \eta_\theta \\ \eta_{\delta_e} \\ \eta_{a_z} \end{bmatrix}$$

where $\underline{C}$ is a matrix, and $z(t)$ is the measurement vector.

Since q, v, θ and δ_e are already state variables, there is no problem obtaining the linearized matrix $\underline{C}$ for the first four measurement equations. The fifth measurement, normal acceleration, is defined as:

$$a_{n_z} = \frac{V_0}{g} \; (q - \dot\alpha - p\beta) - \cos\theta\cos\phi \qquad (3.5.2)$$

where V_0 is velocity, g is the gravitational constant, p, β, and ϕ are variables in the lateral system, respectively roll rate, sideslip angle

and bank angle, and the remaining variables are longitudinal variables. Equation (3.5.2) is a nonlinear equation which couples lateral and longitudinal variables. A way of linearizing and decoupling this observation equation is discussed in Appendix D. The resulting linearized equation for normal acceleration is

$$a_{n_z} = -\frac{V_0}{g} \; (-a_{32}v - a_{33}\alpha - b_3\delta_e) \qquad\qquad (3.5.3)$$

3.6 Reduced Dynamics for the Longitudinal System

The longitudinal models discussed in the previous sections contain state variables which have intrinsically different time constants. Variables such as velocity and flight path angle change slower (phugoid mode) than variables such as angle of attack, pitch rate, wind disturbance and elevator deflection. The latter variables represent the variables used in describing the short period dynamics of the aircraft. Models of the short-period longitudinal aircraft dynamics can be expressed as:

$$\frac{d}{dt} \begin{bmatrix} q \\ \alpha \\ \delta_e \\ w \end{bmatrix} = \begin{bmatrix} a_{11} & a_{13} & b_1 & a_{13} \\ 1 & a_{33} & b_3 & a_{33} \\ 0 & 0 & -12 & 0 \\ 0 & 0 & 0 & -a \end{bmatrix} \begin{bmatrix} q \\ \alpha \\ \delta_e \\ w \end{bmatrix}$$

$$+ \begin{bmatrix} 0 \\ 0 \\ 12 \\ 0 \end{bmatrix} \delta_{ec} + \begin{bmatrix} 0 \\ 0 \\ 0 \\ \frac{K}{V_0} \end{bmatrix} \xi(t)$$

$$\overset{\Delta}{=} \underline{A}_{red} \begin{bmatrix} q \\ \alpha \\ \delta_e \\ w \end{bmatrix} + \underline{B}_{red} \; \delta_{ec}(t) + \underline{L}_{red} \; \xi(t) \qquad (3.6.1)$$

where the elements of $\underline{A}_{red}$ have been indexed to identify them with elements of $\underline{A}$ in Eq. (3.4.6).

The measurement equations remain essentially the same as were discussed in Section 3.5. Available measurements in terms of the short-period variables are pitch rate, normal acceleration and elevator position. Since velocity is assumed to be constant in the short-period dynamics, the equation for normal acceleration (Eq. (3.5.3)), now becomes

$$a_{n_z} = -\frac{V_0}{g} \; (-a_{33}\alpha - b_3\delta_e) \qquad (3.6.2)$$

3-14

Appendix B contains a complete list of the reduced order longitudinal models for the fifteen flight conditions.

3.7 Linear Models of the Lateral Dynamics

Table 3.7.1 contains a description of the variables used in the lateral dynamics of the aircraft. Using these variables, the linearized equations are of the form

$$
\frac{d}{dt}
\begin{bmatrix} p \\ r \\ \beta \\ \phi \end{bmatrix}
= \underline{A}_{lat}
\begin{bmatrix} p \\ r \\ \beta \\ \phi \end{bmatrix}
+ \underline{B}_{lat}
\begin{bmatrix} \delta_a \\ \delta_r \end{bmatrix}
\tag{3.7.1}
$$

where the matrices $\underline{A}_{lat}$ and $\underline{B}_{lat}$ are coefficient matrices obtained for each flight condition. The numerical values of these matrices were supplied by NASA/LARC .

The actuator dynamics for the aileron and rudder actuators are modeled as first-order lags. In this study, the time constant for aileron actuators was equal to 30, and for rudder deflection, equal to 25, so that the differential equations which govern aileron and rudder deflections are:

$$
\frac{d}{dt} \delta_a = -30\delta_a + 30\delta_{a_c}
\tag{3.7.2}
$$

$$
\frac{d}{dt} \delta_r = -25\delta_r + 25\delta_{r_c}
\tag{3.7.3}
$$

Wind disturbances in the lateral system are modeled by the same gust spectrum discussed in Section 3.4. For the lateral system, one (normalized)

TABLE 3.7.1

LATERAL DYNAMICS VARIABLES

Variable Description	Symbol	Units
roll rate	$p(t)$	rad/sec
yaw rate	$r(t)$	rad/sec
sideslip angle	$\beta(t)$	rad
bank angle	$\phi(t)$	rad
aileron angle (asymmetric)	$\delta_a(t)$	rad
rudder angle	$\delta_r(t)$	rad
commanded aileron angle	$\delta_{a_c}(t)$	rad
commanded rudder angle	$\delta_{r_c}(t)$	rad
normalized wind turbulence	$w(t)$	rad

unit of turbulence w(t) has the same effect as a change in sideslip angle β. The equation for wind disturbances can then be written as

$$\dot{w}(t) = -aw(t) + \frac{K}{V_0} \xi(t) \tag{3.7.4}$$

where $\xi(t)$ is a white noise process of unity variance and a, K, have the values given in equations (3.4.4) and (3.4.5). Incorporating the effects of wind disturbances and actuator dynamics, the complete models of the lateral system of the aircraft are of the form:

$$\frac{d}{dt}
\begin{bmatrix} p \\ r \\ \beta \\ \phi \\ \delta_a \\ \delta_r \\ w \end{bmatrix}
=
\left[
\begin{array}{ccc:c}
 & & & a_{13} \\
 & \underline{A}_{lat} & \underline{B}_{lat} & a_{23} \\
 & & & a_{33} \\
\hdashline
 & & & a_{43} \\
 & & -30 \quad 0 & 0 \\
 & \underline{0} & 0 \quad -25 & 0 \\
 & & 0 \quad 0 & -a
\end{array}
\right]
\begin{bmatrix} p \\ r \\ \beta \\ \phi \\ \delta_a \\ \delta_r \\ w \end{bmatrix}$$

$$+
\begin{bmatrix} 0 & 0 \\ 0 & 0 \\ 0 & 0 \\ 0 & 0 \\ 30 & 0 \\ 0 & 25 \\ 0 & 0 \end{bmatrix}
\begin{bmatrix} \delta_{a_c} \\ \delta_{r_c} \end{bmatrix}
+
\begin{bmatrix} 0 \\ 0 \\ 0 \\ 0 \\ 0 \\ 0 \\ \frac{K}{V_0} \end{bmatrix}
\xi(t) \tag{3.7.5}$$

Appendix A contains a complete list of the coefficients for the matrices in Eq. (3.7.5) for each flight condition.

3.8 Sensor Measurements in the Lateral System

The set of lateral sensors used in the study is shown in Table 3.8.1. All but the first variable in Table 3.8.1 are state variables in the lateral system model, hence linear observation equations can be defined trivially for almost all measurements. For the first measurement, lateral accelera- tion is defined as

$$a_y(t) = \frac{V_0}{g} \ (\beta + r - p\alpha) - \sin\phi\cos\theta \qquad (3.8.1)$$

where V_0 is the airplane velocity, g is the gravity constant, and the other quantities are longitudinal and lateral state variables. Equation (3.8.1) is a nonlinear equation, using coupled dynamics for the longitu- dinal and lateral systems. How this equation is linearized is discussed in Appendix D. The resultant linear equation is

$$a_y = \frac{V_0}{g} \ (\beta + r - p\alpha_0) - \phi \qquad (3.8.2)$$

3.9 Concluding Remarks

In this chapter we presented the general structure of the linear differential equations that describe esquilibrium flight for the F8-C aircraft for both longitudinal and lateral motion. In addition, the sensors and their accuracies were described.

TABLE 3.8.1

NOTATION FOR LATERAL SENSORS

Sensor	Symbol	Equation	rms errors
Lateral acceleration	z_{a_y}	$z_{a_y} = a_y + \eta_{a_y}$	.15 deg/sec
Roll rate	z_p	$z_p = p + \eta_p$	.15 deg/sec
Yaw rate	z_r	$z_r = r + \eta_r$	.15 deg/sec
Aileron angle	z_{δ_a}	$z_{\delta_a} = \delta_a + \eta_{\delta_a}$	.1 deg
Rudder angle	z_{δ_r}	$z_{\delta_r} = \delta_r + \eta_{\delta_r}$	.1 deg
Bank angle	z_ϕ	$z_\phi = \phi + \eta_\phi$	.2 deg

CHAPTER 4

THE MULTIPLE MODEL ADAPTIVE CONTROL (MMAC) ALGORITHM: THEORY

4.1 Introduction

This chapter discusses the theory behind the MMAC algorithm, as a sampled-data control system for the F-8C aircraft. The two main parts of the algorithm are identification and control. The basic assumptions which lead to the development of a control system are reviewed, emphasizing potential areas of difficulty. Since the MMAC algorithm is a sampled data control system, all dynamic equations will be written as discrete-time difference equations.

4.2 Problem Formulation

Consider a linear discrete-time stochastic dynamic system whose dynamics depend on a constant parameter vector $\underline{\gamma}$ by the following difference equation

$$\underline{x}(t+1) = \underline{A}(\underline{\gamma})\underline{x}(t) + \underline{B}(\underline{\gamma})\underline{u}(t) + \underline{L}(\underline{\gamma})\underline{\xi}(t) \qquad (4.2.1)$$

where $\underline{x}(t)$ represents the state vector, $\underline{u}(t)$ the control or input vector, and $\underline{\xi}(t)$ is a zero-mean, stationary discrete white gaussian noise sequence with known covariance matrix $\underline{\Xi}$.. The vectors $\underline{x}(t)$, $\underline{u}(t)$ and $\underline{\xi}(t)$ are assumed to be elements of finite dimensional Euclidean spaces, with the matrices $\underline{A}$, $\underline{B}$, $\underline{L}$ appropriately dimensioned. The assumptions on the noise vector $\underline{\xi}(t)$ can be expressed as

$$E\{\underline{\xi}(t)\} = \underline{0} \qquad \text{for all } t \qquad (4.2.2)$$

$$E\{\underline{\xi}(t)\underline{\xi}'(s)\} = \underline{\underline{\Xi}}\tilde{\delta}(t-s) \qquad (4.2.3)$$

where $\tilde{\delta}(.)$ is the Kronecker delta function defined as :

$$\tilde{\delta}(t-s) = 1 \qquad \text{when } t = s$$

$$\qquad\qquad\qquad\qquad\qquad\qquad\qquad (4.2.4)$$

$$\tilde{\delta}(t-s) = 0 \qquad \text{if } t \neq s.$$

Additionally, there are stochastic measurement equations defined on the system, which may depend on the parameter γ as follows :

$$\underline{z}(t) = \underline{C}(\gamma)\underline{x}(t) + \underline{\theta}(t) \qquad (4.2.5)$$

In Eq. (4.2.5), $\underline{z}(t)$ is the actual measurement vector at time t, an element of a finite-dimensional Euclidean space, and $\underline{C}$ is an appropriately dimensioned matrix; the vector $\underline{\theta}(t)$ represents measurement noise, and it is assumed to be a stationary, zero mean, discrete Gaussian white noise sequence, independent of $\underline{\xi}(t)$. That is,

$$E\{\underline{\theta}(t)\} = \underline{0} \qquad (4.2.6)$$

$$E\{\underline{\theta}(t)\underline{\theta}'(s)\} = \underline{\Theta}\tilde{\delta}(t-s) \qquad (4.2.7)$$

$$E\{\underline{\theta}(t)\underline{\xi}'(s)\} = \underline{0} \qquad (4.2.8)$$

$$\underline{\Theta} > \underline{0} \qquad \text{for all } t \qquad (4.2.9)$$

The last assumption (4.2.9) implies a positive definite noise covariance for all time.

Consider now the parameter vector $\underline{\gamma}$. It is assumed to be an element of a finite-dimensional space. The degree of accuracy by which the elements

of γ are known depend upon the accuracy of the modeling process. The MMAC algorithm considers γ as a random vector, about which certain a priori information exists. All prior information about γ can be captured in its prior probability density function, denoted by $p(\gamma)$.

It is clear that the numerical values of the parameter vector γ would alter the system dynamics, and influence both the control gains and Kalman filter gains. Thus, the problem of obtaining estimates of γ from the actual noisy sensor measurements is important.

In aircraft applications in general the parameter vector γ would capture all underlying variables, such as dynamic pressure and configuration changes, which would crucially affect the linearized aircraft dynamics under equilibrium flight. The MMAC method then assumes that these crucial parameter values cannot be measured directly, but rather they have to be inferred from noisy sensors.

4.3 Identification and Estimation

Under the assumption that both γ and $\underline{x}(t)$ are random variables belonging to finite dimensional Euclidean spaces, successful control of the system described by Eq. (4.2.1) depends on accurate identification of the value of γ and accurate estimation of the state $\underline{x}(t)$, on the basis of the noisy measurements. Several algorithms, notably the extended Kalman filter [22], [23] exist which can be used to approach the joint problem of estimation and identification. However, in the presence of large para- meter uncertainties, even these sophisticated algorithms break down. A different approach, based on additional assumptions is needed; the MMAC

approach was used exclusively in this study. In order to handle the uncertainty in the parameter vector $\underline{\gamma}$ assume that its parameter space can be quantized (divided) into a finite number of regions, each region represented by a specific parameter value $\underline{\gamma}_i$. That is, suppose that there are N vectors $\underline{\gamma}_1$, $\underline{\gamma}_2$, ..., $\underline{\gamma}_N$ chosen throughout the parameter space. Additionally, assume that the true value of $\underline{\gamma}$ is one of these N values for all time. Effectively, by the above assumptions, the parameter space is being reduced to a finite set. Needless to say, the above assumption is not true in real situations. This point will be discussed later on.

Under the assumptions stated above, equations (4.2.1) and (4.2.5) can be rewritten

$$\underline{x}(t+1) = \underline{A}_i\underline{x}(t) + \underline{B}_i\underline{u}(t) + \underline{L}_i\underline{\xi}(t) \tag{4.3.1}$$

$$\underline{z}(t) = \underline{C}_i\underline{x}(t) + \theta(t) \tag{4.3.2}$$

where i = 1, 2, ..., N, using the obvious notational abbreviation

$$\underline{A}_i \triangleq \underline{A}(\underline{\gamma}_i), \ \underline{B}_i \triangleq \underline{B}(\underline{\gamma}_i), \ \underline{C}_i \triangleq \underline{C}(\underline{\gamma}_i), \ \underline{L}_i = \underline{L}(\underline{\gamma}_i)$$

The a priori probability density of $\underline{\gamma}$ can now be stated as $p(\underline{\gamma}) = \{P(\underline{\gamma}_1), \underline{P}(\underline{\gamma}_2), ..., P(\underline{\gamma}_N)\}$. The problem of parameter identification can be viewed as a hypothesis testing problem, in which there are N hypotheses H_i, where the random variable H is such that

$$H = H_i \quad \text{if} \quad \underline{\gamma} = \underline{\gamma}_i \tag{4.3.3}$$

Initially, all the information which is known about the system is

given in $p(\underline{\gamma})$. Define the initial probabilities $P_i(0)$ by

$$P_i(0) \triangleq P(\gamma_i) \triangleq P(H = H_i). \tag{4.3.4}$$

Suppose one applies a sequence of deterministic inputs $\underline{u}(0)$, $\underline{u}(1)$,...,
$\underline{u}(t-1)$ to the system, and obtains measurements $\underline{z}(1)$, $\underline{z}(2)$, ..., $\underline{z}(t)$.
The problem at hand consists of using these measurements to provide both
a good estimate of the state $\underline{x}(t)$ and the parameter $\underline{\gamma}$. Define the infor-
mation (data) set of time t, Z(t), as follows:

$$Z(t) = \{\underline{z}(1), \underline{z}(2), ..., \underline{z}(t), \underline{u}(0), \underline{u}(1), ..., \underline{u}(t-1)\} \tag{4.3.5}$$

Additionally, define the conditional probabilities

$$P_i(t) = \text{Prob. } \{H = H_i | Z(t)\}. \tag{4.3.6}$$

Thus, the posterior probability density of the hypothesis variable H given
the measurements Z(t) is given

$$p(H|Z(t)) = \sum_{i=1}^{N} P_i(t)\delta(H - H_i) \tag{4.3.7}$$

where $\delta(.)$ is the Dirac delta function. The joint estimation and identifi-
cation problem consists of determining the probability densities and condi-
tional expectation $p(H|Z(t))$ and $E(\underline{x}(t)|Z(t))$.

Figure 4.3.1 contains a summary of the system and identification
problem. Appendix C contains a derivation of the expressions for the
conditional probability densities of H and $\underline{x}(t)$. As shown in Appendix C
these conditional probabilities can be calculated in real time in a recur-

DYNAMIC SYSTEM

$$\underline{x}(t+1) = \underline{A}_i\underline{x}(t) + \underline{B}_i\underline{u}(t) + \underline{L}_i\underline{\xi}(t)$$

$$\underline{z}(t) = \underline{C}_i\underline{x}(t) + \underline{\theta}(t)$$

$\underline{u}(t)$

CONTROL
INPUT
VECTOR

$\underline{z}(t)$

NOISY SENSOR
MEASUREMENT
VECTOR
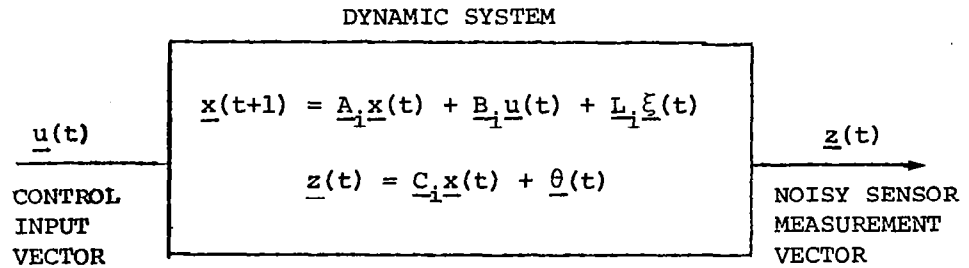
$$Z(t) = \{\underline{z}(1), \ldots, \underline{z}(t), \underline{u}(0), \ldots, \underline{u}(t-1)\}$$

$$H = H_i \Longleftrightarrow \underline{\gamma} = \underline{\gamma}_i$$

Estimation problem: find $\bar{E}(\underline{x}(t)|Z(t))$

Identification problem: find $P(H|Z(t))$

Figure 4.3.1   The Nature of the Joint Estimation and
Identification Problem

sive manner, using Bayes' rule [6], [23]

$$P_i(t) = \frac{p(\underline{x}(t)|H_i, Z(t-1), \underline{u}(t-1))}{\sum\limits_{j=1}^{N} p(\underline{x}(t)|H_j, Z(t-1), \underline{u}(t-1))P_j(t-1)} P_i(t-1) \qquad (4.3.8)$$

$$\hat{\underline{x}}(t) \triangleq E\{\underline{x}(t)|Z(t)\} = \sum\limits_{i=1}^{N} P_i(t)E\{\underline{x}(t)|Z(t), H_i\} \qquad (4.3.9)$$

As explained in Appendix C, the probability densities involved in the right-hand sides of equations (4.3.8) and $.3.9) are Gaussian, because when hypothesis H_i is assumed true, the system in Figure 4.3.1 becomes a linear, time invariant, Gaussian-driven system. Furthermore, the conditional expected value $\hat{\underline{x}}_i(t) = E\{\underline{x}(t)|Z(t), H_i\}$ can be constructed by a linear time-varying Kalman-Bucy filter [5], [6].

The basic formulae of Kalman filters are well known. From each Kalman filter, indexed by $i = 1, 2, \ldots, N$, one obtains the value of the corresponding residual vector $\underline{r}_i(t)$, defined as

$$\underline{r}_i(t) \triangleq \underline{z}(t) - \underline{C}_i E\{\underline{x}(t)|Z(t-1), \underline{u}(t), H_i\}. \qquad (4.3.10)$$

Additionally, the covariance matrix of the residual vector $\underline{r}_i(t)$, defined as $\underline{S}_i(t)$, can be computed off-line. With this nomenclature, Equation (4.3.8) is shown in Appendix C to give

$$P_i(t+1) = \frac{p(\underline{z}(t+1)|H_i, \underline{u}(t), Z(t)) \; P_i(t)}{\sum\limits_{j=1}^{N} p(\underline{z}(t+1)|H_j, \underline{u}(t), Z(t)) \; P_j(t)} \qquad (4.3.11)$$

$$= \frac{\beta_i(t+1) \ e^{-\frac{1}{2} (\underline{r}_i'(t+1)\underline{S}_i^{-1}(t+1)\underline{r}_i(t+1))}}{\sum\limits_{j=1}^{N} \beta_j(t+1) \ e^{-\frac{1}{2} (\underline{r}_j'(t+1)\underline{S}_j^{-1}(t+1)\underline{r}_j(t+1))} P_j(t)} \ P_i(t) \quad (4.3.12)$$

where the scalars $\beta_i(t)$ are defined by

$$\beta_i(t) = (2\pi)^{-\frac{m}{2}} [\det \underline{S}_i(t)]^{-\frac{1}{2}}, \ i = 1, 2, \ldots, N \quad (4.3.13)$$

and m is the dimension of the vector $\underline{r}_i(t)$, (m is equal to the number of measurements). The matrices $\underline{S}_i(t)$ and the scalars $\beta_i(t)$ can be computed a priori in an off-line fashion as described in Appendix C. Using equations (4.3.12) and (4.3.13) in conjunction with N Kalman filters, as described in Figure 4.3.2, one is able to compute the evolution of the hypothesis probabilities and the conditional expected value of the system state.

Because of the stationary properties of the time system, one can consider the operation of the system in steady state. In this case, the residual covariance matrix is stationary, so that the matrices S_i and the scalars β_i^* are constants, as described in Appendix C. The system probabilities in steady state operation are given by

$$P_i(t) = \frac{\beta_i^* \exp(-\frac{1}{2}\underline{r}_i'(t)\underline{S}_i^{-1}\underline{r}_i(t))}{\sum\limits_{j=1}^{N} \left[\beta_j^* \exp(-\frac{1}{2}\underline{r}_j'(t)\underline{S}_j^{-1}\underline{r}_j(t))\right] P_j(t-1)} \ P_i(t-1) \quad (4.3.14)$$
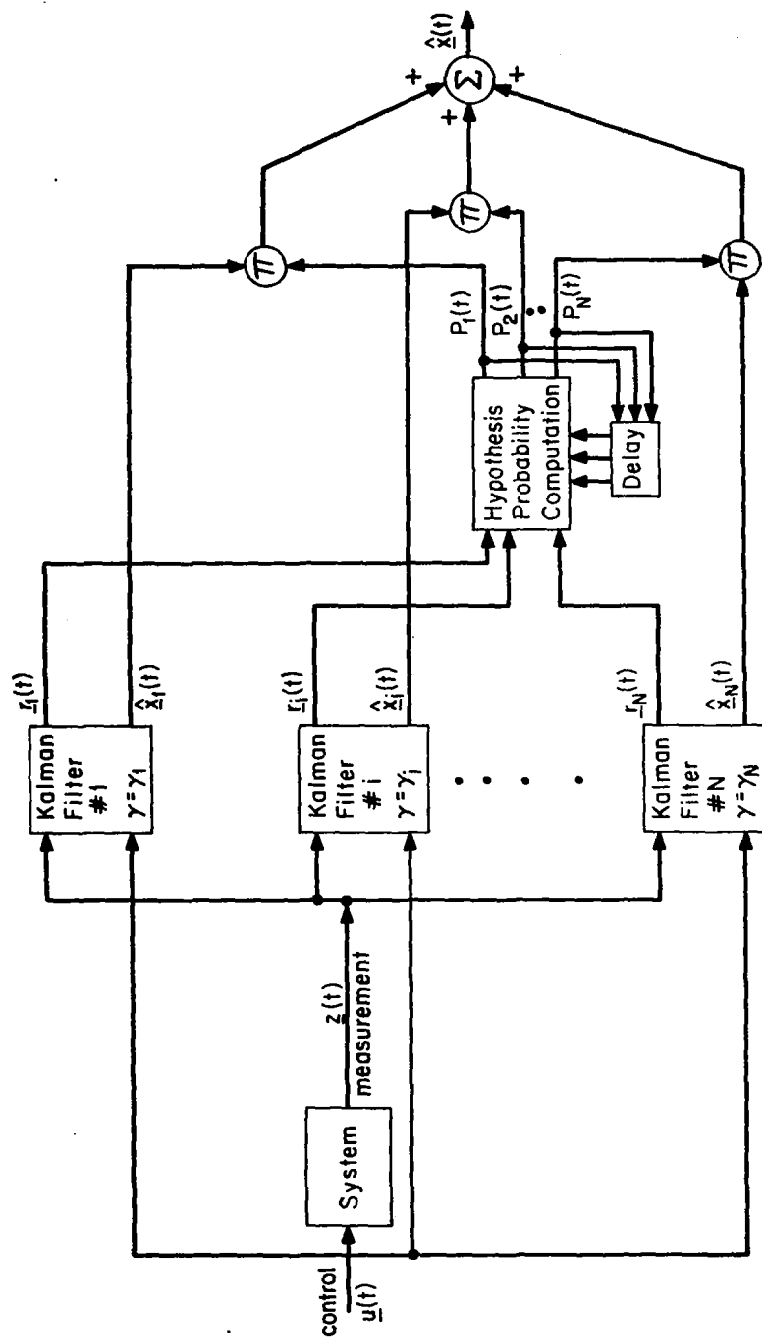
Figure 4.3.2 Multiple Model Identification and Estimation.
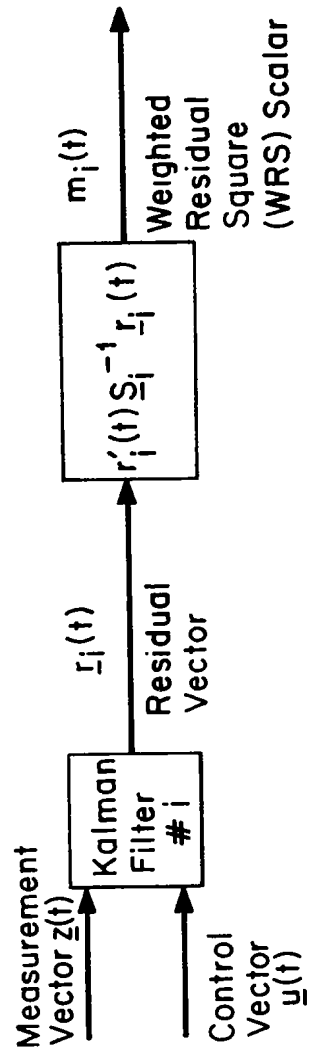
Figure 4.3.3   Block Diagram of the Generation of
WRS $m_i(t)$ from each Kalman Filter

Equation (4.3.14) can be written in a somewhat simpler form by defining the <u>weighted residual signals</u> (WRS) $m_i(t)$ as follows (see Fig. 4.3.3)

$$m_i(t) \triangleq \underline{r}_i'(t) \underline{S}_i^{-1} \underline{r}_i(t), \quad i = 1,2,\ldots,N \tag{4.3.15}$$

It should be stressed that each WRS $m_i(t)$ is a scalar quantity, and each is generated by a Kalman filter (later chapters show several time histories of the WRS $m_i(t)$).

Using this notation, the formula for the probability update (4.3.14) can be written as

$$P_i(t) = \frac{\beta_i^* \exp\{-\tfrac{1}{2}m_i(t)\}}{\sum\limits_{j=1}^{N} \beta_j^* \exp\{-\tfrac{1}{2}m_j(t)\} P_j(t-1)} P_i(t-1) \tag{4.3.16}$$

4.4 Discussion of Identification

The MMAC identification algorithm has some interesting asymptotic properties. Hawkes and Moore [24] have established that, under general conditions and the assumptions of the previous section, the model probabilities are such that

$$P_i(t) \to 0 \quad \text{if } H \neq H_i$$

$$\tag{4.4.1}$$

$$P_i(t) \to 1 \quad \text{if } H = H_i \quad \text{(true model)}$$

as $t \to \infty$. This is true only if the true model is in the set of hypotheses.

Consider the equation describing the evolution of the probabilities $P_i(t)$, equations (4.3.1). With some algebraic manipulation, one obtains

$$P_i(t) - P_i(t-1) = \left[\sum_{j=1}^{N} P_j(t-1)\beta^*_{\cdot j} \, e^{-\frac{1}{2} \underline{r}'_j(t)\underline{S}_j^{-1}\underline{r}_j(t)} \right]^{-1} \cdot$$

$$P_i(t-1) \left[(1-P_i(t-1))\beta^*_i \, e^{\frac{1}{2} \underline{r}'_i(t)\underline{S}_i^{-1}\underline{r}_i(t)} - \sum_{j \neq 1} P_j(t-1)\beta^*_j \exp(-\frac{1}{2} \underline{r}'_j(t)\underline{S}_j^{-1}\underline{r}_j(t)) \right]$$

(4.4.2)

Heuristically, one expects that, as the system is subject to persistent excitation, the residuals of the true model Kalman filter, nominally the ℓth one, will be small, while the residuals of the mismatched Kalman filters ($i \neq \ell$, $i = 1, 2, \ldots, N$) will be large. Thus, if ℓ indexes the correct model, one has

$$\underline{r}'_\ell(t)\underline{S}_\ell^{-1}\underline{r}_\ell(t) \ll \underline{r}'_i(t)\underline{S}_i^{-1}\underline{r}_i(t) \quad \text{all } i \neq \ell \ (\ell : \text{true model}) \quad (4.4.3)$$

If this condition persists, it implies that

$$\frac{e^{-\frac{1}{2} \underline{r}'_i(t)\underline{S}_i^{-1}\underline{r}_i(t)}}{e^{-\frac{1}{2} \underline{r}'_\ell(t)\underline{S}_\ell^{-1}\underline{r}_\ell(t)}} \quad \tilde{} \quad 0 \quad (4.4.4)$$

Hence, the correct probability will grow as

$$P_\ell(t) - P_\ell(t-1) = \frac{P_\ell(t-1)(1-P_\ell(t-1))\beta^*_j \exp(-\frac{1}{2} \underline{r}'_\ell(t)\underline{S}_\ell^{-1}\underline{r}_\ell(t))}{\sum_{j=1}^{N} P_j(t-1)\beta^*_j \exp(-\frac{1}{2} \underline{r}'_j(t)\underline{S}_j^{-1}\underline{r}'_j(t))} > 0 \quad (4.4.5)$$

For the incorrect models, the same assumptions yield

$$P_i(t) - P_i(t-1) = \frac{-P_i(t-1)P_\ell(t-1)\beta_\ell^* \exp(-\frac{1}{2}\underline{r}_\ell'(t)\underline{S}_\ell^{-1}\underline{r}_\ell(t))}{\sum\limits_{j=1}^{N} P_j(t-1)\beta_j^* \exp(-\frac{1}{2}\underline{r}_j'(t)\underline{S}_j^{-1}\underline{r}_j(t))} < 0 \quad (4.4.6)$$

Hence, assuming that the Kalman filter residuals will behave as expected, the identification scheme will converge to the true model. However, when the Kalman filters do not possess these regularity assumptions, the identification scheme does not work well. For instance, consider the case that, in a prolonged sequence of measurements, the residuals $\underline{r}_j(t)$ turn out such that

$$\underline{r}_1'(t)\underline{S}_1^{-1}\underline{r}_1(t) \approx r_2'(t)\underline{S}_2^{-1}\underline{r}_2(t) \quad \cdots \quad \approx \underline{r}_N'(t)\underline{S}_N^{-1}\underline{r}_n(t) \quad (4.4.7)$$

Under these conditions, equation (4.4.2) becomes

$$P_i(t) - P_i(t-1) \approx \frac{P_i(t-1)\sum\limits_{j\neq 1}(\beta_i^* - \beta_j^*)P_j(t-1)}{\sum\limits_{j=1}^{N}\beta_j^* P_j(t-1)} \quad (4.4.8)$$

Consider the largest β_j^*, indexed as k. Then equation (4.4.9) indicates that $P_k(t) - P_k(t-1)$ is always positive unless $P_k(t) = 1$. Thus, the identification converges to the system whose β_j^* value is the largest, not necessarily the true system. Since the β_j^* values are determined a priori from design parameters (as indicated in Appendix C), this behavior must be considered in the design of the Kalman filter.

A typical situation when equation (4.4.7) holds true is when the true

system is at rest (i.e., $\underline{x}(t) = \underline{0}$) and the excitation of the system, $\underline{\xi}(t)$, is actually much smaller in covariance than the modeled covariances. In this case, all of the residuals $\underline{r}_i(t)$ will be essentially zero, satisfying equation (4.4.7) and give rise to the β* dominance identification effect. The implications are that this effect can occur in the absence of significant excitation of the system, or when the Kalman filters are designed for a much larger process noise $\underline{\xi}(t)$ than is actually encountered in the true system.

When the value of the true parameter $\underline{\gamma}$ is not included in the finite parameter set $\{\underline{\gamma}_1, \ldots, \underline{\gamma}_N\}$, Hawkes and Moore [24] showed that the probabilities converge to the "nearest" element of the set. That is,

$$P_i(t) \to 1 \qquad \text{if and only if } d(\underline{\gamma}, \underline{\gamma}_i) \leq d(\underline{\gamma}, \underline{\gamma}_j) \qquad (4.4.9)$$

$$\text{for all } j = 1, \ldots, N.$$

The distance between two parameters is defined in terms of the Kullback [25] information measure, as discussed in [24].

However, the theoretical proofs of convergence for the MMAC algorithm have neglected two fundamental aspects of the physical problems connected with adaptive control: the convergence proofs have all dealt with undriven, open loop systems. In reality, the identification algorithm must operate within a closed-loop system, where inputs based on measurements are applied to the system. The question of convergence under closed-loop conditions has not been addressed in the literature.

The second aspect which has been neglected in the literature is the assumption that $\underline{\gamma}$ is constant. In many adaptive systems, $\underline{\gamma}$ is a time-varying

hypothesis. Some preliminary studies by Athans and Chang [26] indicate that performance of the identification algorithm is closely related to the time-scale of the parameter variations.

4.5 The MMAC Algorithm: Control Approach

In Section 4.3, the MMAC identification algorithm was used to obtain the probabilities $P_i(t)$ for any string of inputs applied to the system. However, the objective of the control system is finding the control inputs to the system. The basic approach follows the outline of hypothesis testing described in Section 4.3.

Under the assumption that hypothesis H_i was true, the system equations become

$$\underline{x}_i(t+1) = \underline{A}_i\underline{x}_i(t) + \underline{B}_i\underline{u}(t) + \underline{L}_i\underline{\xi}(t) \qquad (4.5.1)$$

$$\underline{z}(t) = \underline{C}_i\underline{x}(t) + \underline{\theta}(t) \qquad (4.5.2)$$

Assuming perfect knowledge of the state dynamics and measurement equations, the optimal control $\underline{u}_i(t)$ can be computed for each model indexed by i. This is accomplished through the solution of a Linear-Quadratic-Gaussian optimization problem [5], as described in Appendix F. The optimal control $\underline{u}_i(t)$ is obtained by linear feedback of the conditional expected value of $\underline{x}(t)$ for each model

$$\underline{u}_i(t) = -\underline{G}_i\hat{\underline{x}}_i(t) \qquad (4.5.3)$$

where $\underline{G}_i$ is a constant control gain matrix and $\hat{\underline{x}}_i(t)$ is obtained from the Kalman filter matched to the ith model.

The optimal control $\underline{u}_i(t)$ can be computed in parallel for each hypothesis (model) indexed by $i = 1,\ldots,N$. The MMAC control approach is then very simple: the individual control inputs are combined in a weighted average using the identification probabilities. That is, the actual control applied to the system is given

$$\underline{u}(t) = \sum_{i=1}^{N} P_i(t)\underline{u}_i(t) = -\sum_{i=1}^{N} P_i(t)\underline{G}_i\hat{\underline{x}}_i(t) \qquad (4.5.4)$$

The complete control and identification scheme is shown in block diagram form in Figure 4.5.1.

Willner [18] established using dynamic programming that the control law obtained using equation (4.5.4) was optimal in minimizing a quadratic cost criterion only over a single time step. That is, when the system dynamics and the horizon of the cost criterion is larger than one time period, the MMAC controller is a suboptimal control, even when all other assumptions discussed in Section 4.3 still hold. Hence the MMAC control algorithm represents a computationally simple suboptimal adaptive approach towards control of the F-8C aircraft. It must be emphasized that there is no theory guaranteeing the success or performance of this approach; this is a major motivation for extensive research into the feasibility of this approach.

4.6 Modification of the MMAC Algorithm

The theory behind the MMAC design deals with identifying and controlling a system represented by a linear time-invariant finite dimensional

4-17
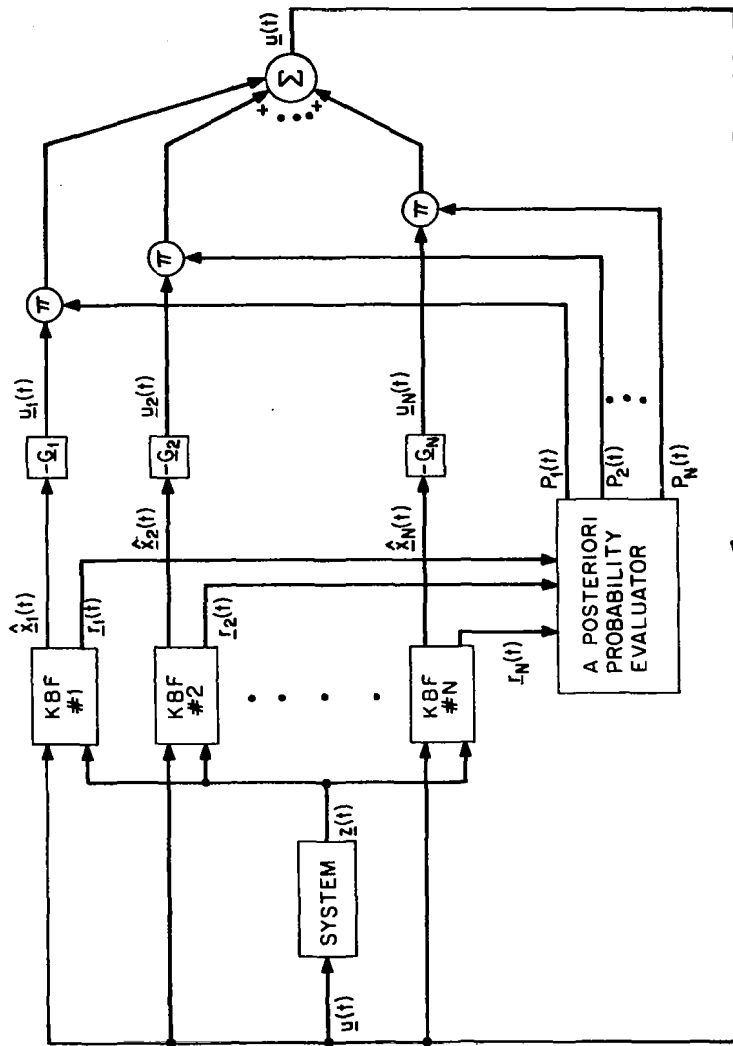
Figure 4.5.1 MMAC Identification and Control Scheme

mathematical model. The F-8C aircraft is a non-linear, time-varying

plant which is subjected to a variety of pilot commands. Several modifi-

cations of the MMAC design were introduced to compensate for the differences

between the theoretical assumptions behind the MMAC and the true properties

of the F-8C aircraft. One of the crucial questions dealing with the

convergence of the identification algorithm is the availability of infor-

mation [24], [7] to separate the various hypotheses. Sources of information

include pilot commands, turbulence, gusts or other types of excitation.

Some studies in adaptive control of aircraft [27] include a low intensity

test signal designed to provide information to the identification system.

The basic MMAC algorithm includes no such signal; thus, when the MMAC

lacks information, the identification system will have difficulties identify-

ing the right hypothesis. This occurs when the aircraft is trimmed,

flying at equilibrium level flight under no turbulence. Under such circum-

stances, the β^* dominant identification effect mentioned in Section 4.4 occurs.

It should be noted that the β^* dominant effect was not known when this

study commenced. It was observed in simulations and in the absence of any

theory, led to ad - hoc modification of the MMAC System.

In order to compensate for the β^* dominant effect, one can modify the

evolution of the identification probabilities $P_i(t)$ described in equation (4.3.16)

According to equation (4.4.7), the β^* dominant effect occurs when all the WRS

signals $m_i(t)$ are near zero. The modification consists of stopping the

identification algorithm when there is not enough information. The MMAC

algorithm monitors all of the $m_i(t)$, and updates its identification probabil-

ities as

$$P_i(t+1) = P_i(t) \text{ if } m_i(t) < T_H, \quad i = 1,\ldots,N \qquad (4.6.1)$$

$$P_i(t+1) = \frac{\beta*_i \, P_i(t)e^{-m_i(t)}}{\sum\limits_{j=1}^{N} \beta*_j \, P_j(t)e^{-m_j(t)}} \qquad \text{otherwise.} \tag{4.6.2}$$

The values of the thresholds T_H were determined by trial and error. The values used in the designs were:

$$\begin{aligned}
&\text{Longitudinal System Threshold} = 1\\
&\text{Lateral System Threshold} = 5
\end{aligned} \tag{4.6.3}$$

Notice that there are two separate thresholds for the longitudinal and lateral systems. The MMAC algorithm contains separate identification and control systems for the longitudinal and lateral systems. In principle the information provided by the two systems could be combined to improve identification. Under the assumption that the longitudinal and lateral systems are completely decoupled and uncorrelated, the identification probabilities can be combined, according to the following equations.

Let $\underline{S}_{i \ LON}, \underline{S}_{i \ LAT}$ denote the residual covariance matrices of the Kalman filters, for the i-th flight condition, associated with the longitudinal and lateral dynamics respectively. Define

$$\beta_i*_{LON} = (2\pi)^{-\frac{m_{LON}}{2}} (\det \underline{S}_{i \ LON})^{-1/2} \tag{4.6.4}$$

$$\beta_i*_{LAT} = (2\pi)^{-\frac{m_{LAT}}{2}} (\det \underline{S}_{i \ LAT})^{-1/2} \tag{4.6.5}$$

where m_{LON} and m_{LAT} are the number of longitudinal and lateral sensors. Let $\underline{r}_{i \ LON}(t)$ and $\underline{r}_{i \ LAT}(t)$ denote the Kalman filter residual vectors

at time t, for flight condition i, associated with the longitudinal and
lateral dynamics respectively. Define the WRS signals:

$$m_{i\ LON}(t) \triangleq \underline{r}'_{i\ LON}(t)\underline{S}^{-1}_{i\ LON}\underline{r}_{i\ LON}(t) \qquad (4.6.6)$$

$$m_{i\ LA} \triangleq \underline{r}'_{i\ LAT}(t)\underline{S}^{-1}_{i\ LAT}\underline{r}_{i\ LAT}(t) \qquad (4.6.7)$$

Then the overall probability that the aircraft is in flight condition i
at time t, is generated by the recursive formula

$$P_i(t) = P_i(t-1)\beta^*_{iLON}\beta^*_{iLAT}\ \exp\{-m_{iLON}(t)/2\}\exp\{-m_{i\ LAT}(t)/2\}\ /$$

$$\sum_{j=1}^{N} P_j(t-1)\beta^*_{jLON}\beta^*_{jLAT}\ \exp\{-m_{jLAT}(t)/2\}\ \exp\{-m_{j\ LON}(t)/2\} \qquad (4.6.8)$$

The β* dominance effect discussed above now refers to the relative magnitude
of

$$\beta^*_i \triangleq \beta^*_{iLON}\beta^*_{iLAT} \qquad (4.6.9)$$

obviously the method should be expected to work well when both longitudinal
and lateral Kalman filters are correctly designed so that the residuals
of the "matched" Kalman filters are smaller than those of the "mismatched"
ones.

The reason the MMAC algorithm does not combine the lateral and
longitudinal identification probabilities lies in the differences between
the mathematical assumptions and the actual problem posed by the F-8C
aircraft. Throughout most of the flight envelope the linearized equations
of the F-8C aircraft will differ from all of the hypotheses in the MMAC
algorithm. In this situation, it is not clear that combining the information

will improve the overall identification. In many cases, one can observe the information obtained in one system dominating the overall identification. Section 7.3 contains the mismatched stability tables showing the effects of erroneous identification on the stability of the aircraft. A close examination of these tables will show several combinations which are stable in one system, say longitudinal, and unstable in the other system. Should the information from the longitudinal system dominate the identification schemes are used, each system can quickly recognize when the airplane is unstable and alter its identification. Figure 4.6.1, shows typical aircraft responses with identification. Note the instabilities in the lateral system variables.

One final modification was made in the MMAC identification algorithm: the identification probabilities $P_i(t)$ were bounded away from zero. In principle the identification algorithm is trying to identify a fixed, time-invariant hypothesis; in actual practice, this hypothesis changes with time as the F-8C aircraft travels through its envelope. Thus, the MMAC algorithm must be able to react to a time-varying true hypothesis. Bounding the probabilities away from zero corresponds to limiting the importance of past information, enabling the identification system to react quickly to new information. Trial and error established these lower bound to be 10^{-4}. Hence, the updated identification probabilities were modified as follows:

$$\underline{P}_i(t) = P_i(t) \text{ if } P_i(t) \geq 10^{-4}$$ (4.6.10)

$$= 10^{-4} \text{ otherwise}$$

The modified identification probabilities, denoted by $P_i^M(t)$, were obtained by

$$P_i^M(t) = \frac{\underline{P}_i(t)}{\displaystyle\sum_{j=1}^{N} \underline{P}_j(t)}$$ (4.6.11)

One of the undesirable properties of the MMAC identification algorithm
is its sensitivity and quick response to information.* When the airplane
is subjected to high levels of turbulence, the randomness of this turbulence
is reflected in the identification probabilities. Figures 4.6.2 and 4.6.3
represent typical airplane responses under various levels of turbulence.
Notice the fast transitions in the identification probabilities $P_i(t)$. Each
transition, however, changes the feedback gains in the control system, thereby
changing the aircraft response to pilot inputs. These transitions occur
under turbulence, or when two or more hypothesis are equally "close" in a
probabilistic sense to the true aircraft. The net result is a control system
which feels very uneven to the pilot. In order to smooth out the changes
in the control system and to eliminate some of the random effects in the
identification, the identification probabilities were low-pass filtered to
produce control probabilities; trial-and-error experiments set the filter
time constant at 2 seconds. Figure 4.6.5 describes the low-pass filter
introduced. The control probabilities are given by

$$P_i^C(t) = .94041 \ P_i^C(t-1) + .05959 \ P_i^M(t) \tag{4.6.12}$$

Figure 4.6.5 shows the control probability evolutions using the low-pass
filtering scheme to smooth out the control action.

---

*
    These important sensitivity properties were not known when this study
was initiated. In point of fact, the overall nonlinear nature of the MMAC
System (Figure 4.3.2) precludes any analytical insight. Thus, extensive
stochastic simulations are necessary to evaluate any MMAC design.
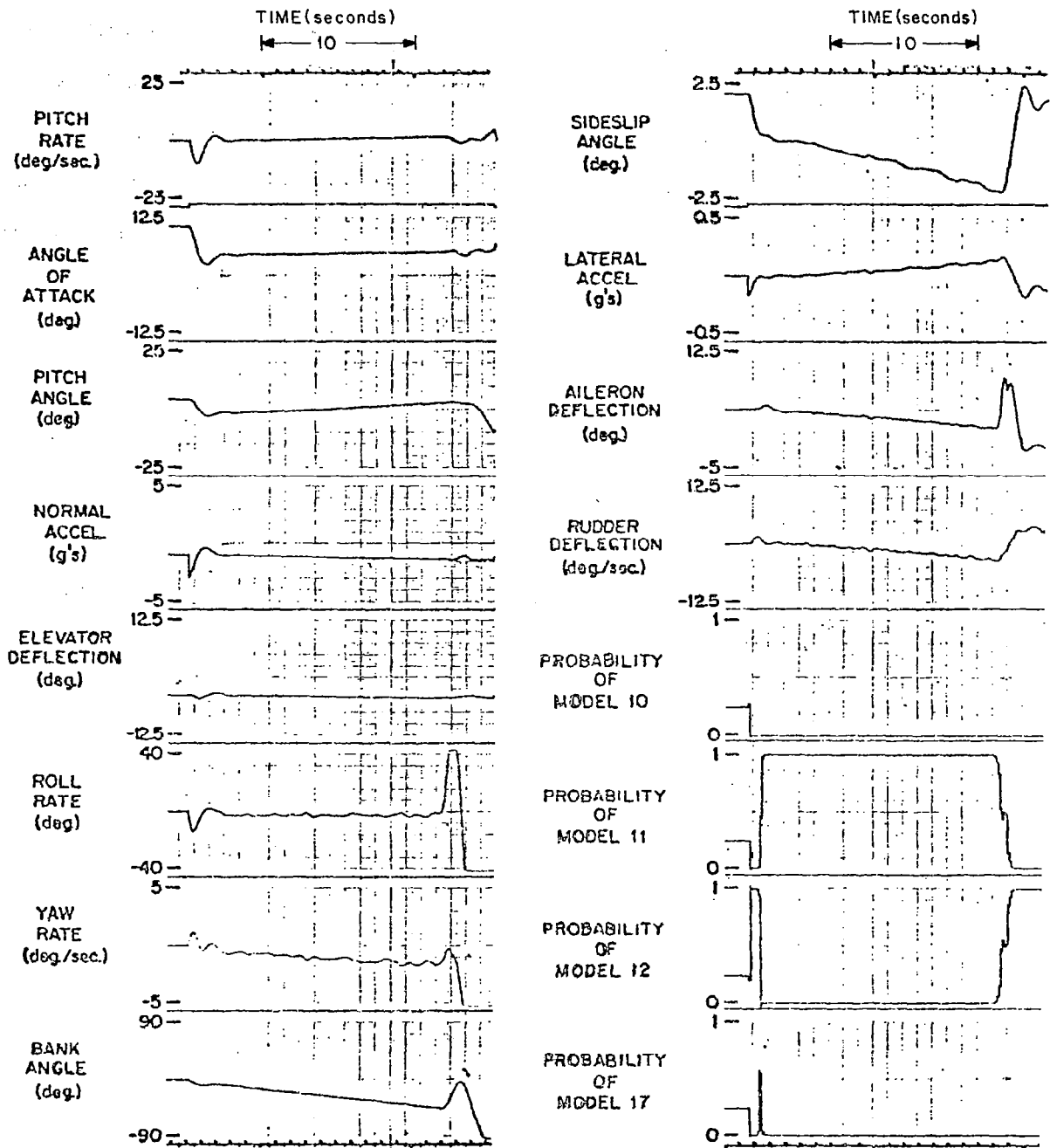
Figure 4.6.1   Aircraft responses to 6°α, 2°β initial gusts,
no turbulence, altitude 6096 meters, speed .6 Mach,
using combined identification
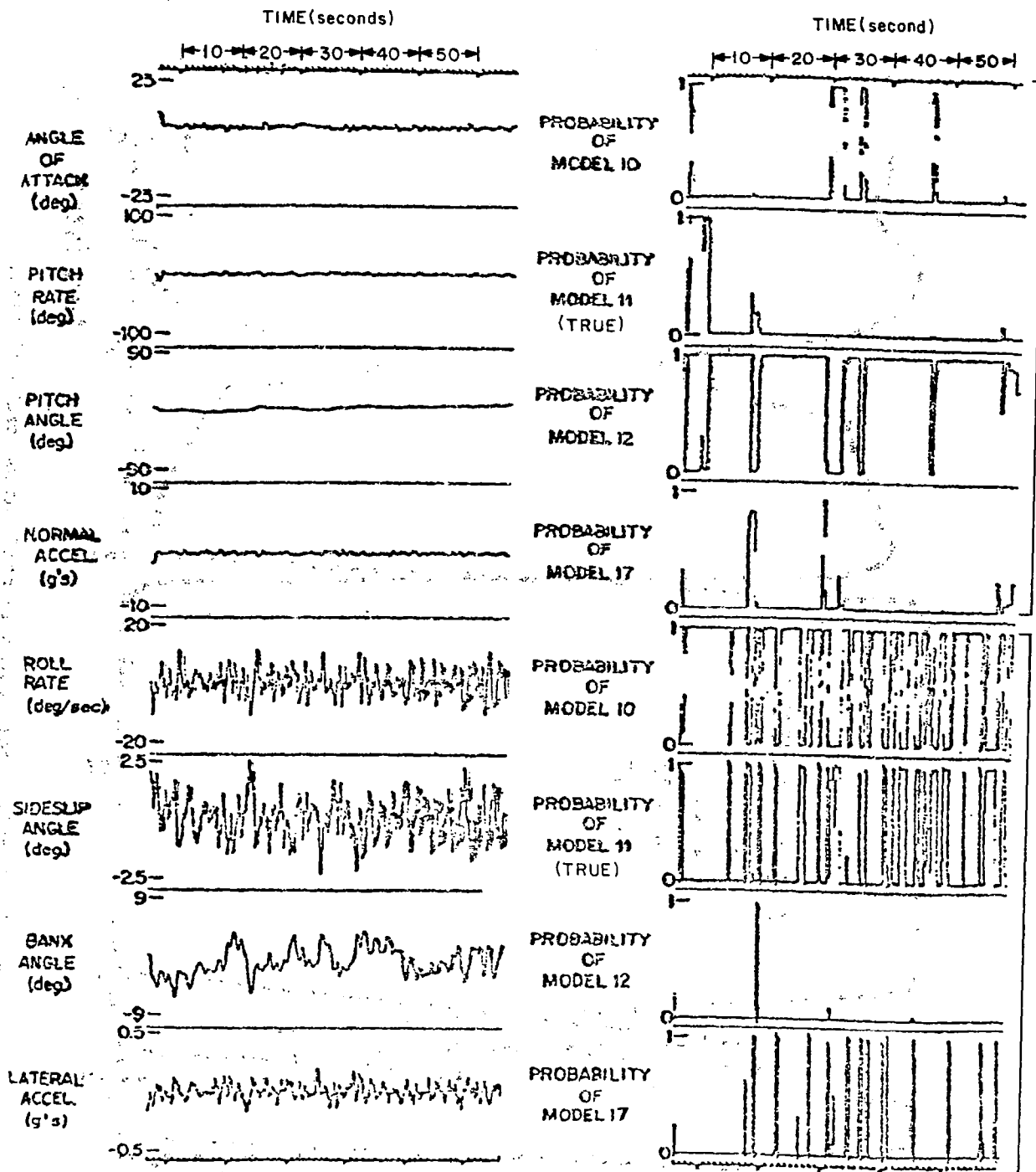
Figure 4.6.2   Aircraft responses to 6°α , 2°β initial gusts,
4.57 m/sec rms turbulence, altitude 6096 meters,
speed .6 Mach, displaying identification probabilities
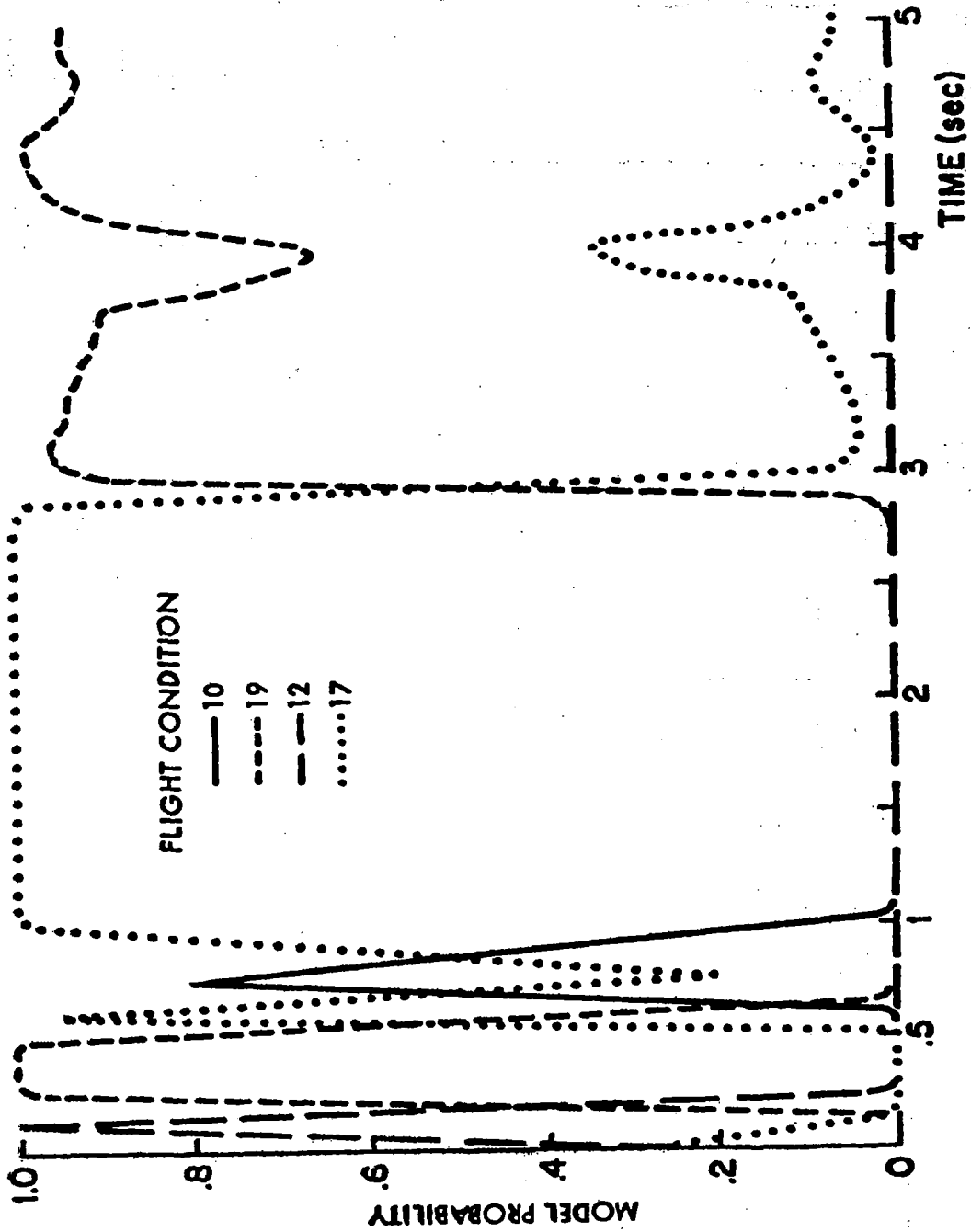
Figure 4.6.3   Longitudinal system identification probabilities,
altitude 6096 meters, speed .6 Mach (F.C. 11),
4.57 m/sec rms turbulence
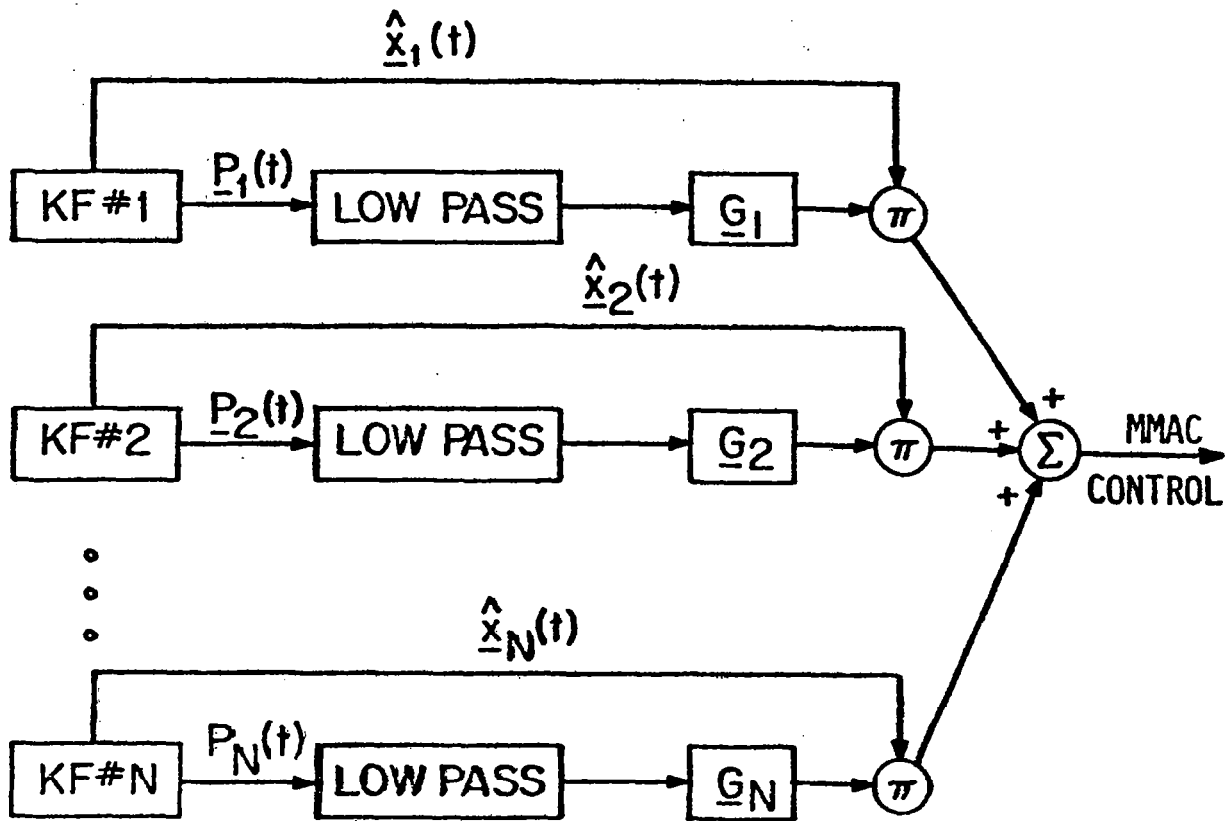
Figure 4.6. 4   Description of Low-Pass Filtering Approach
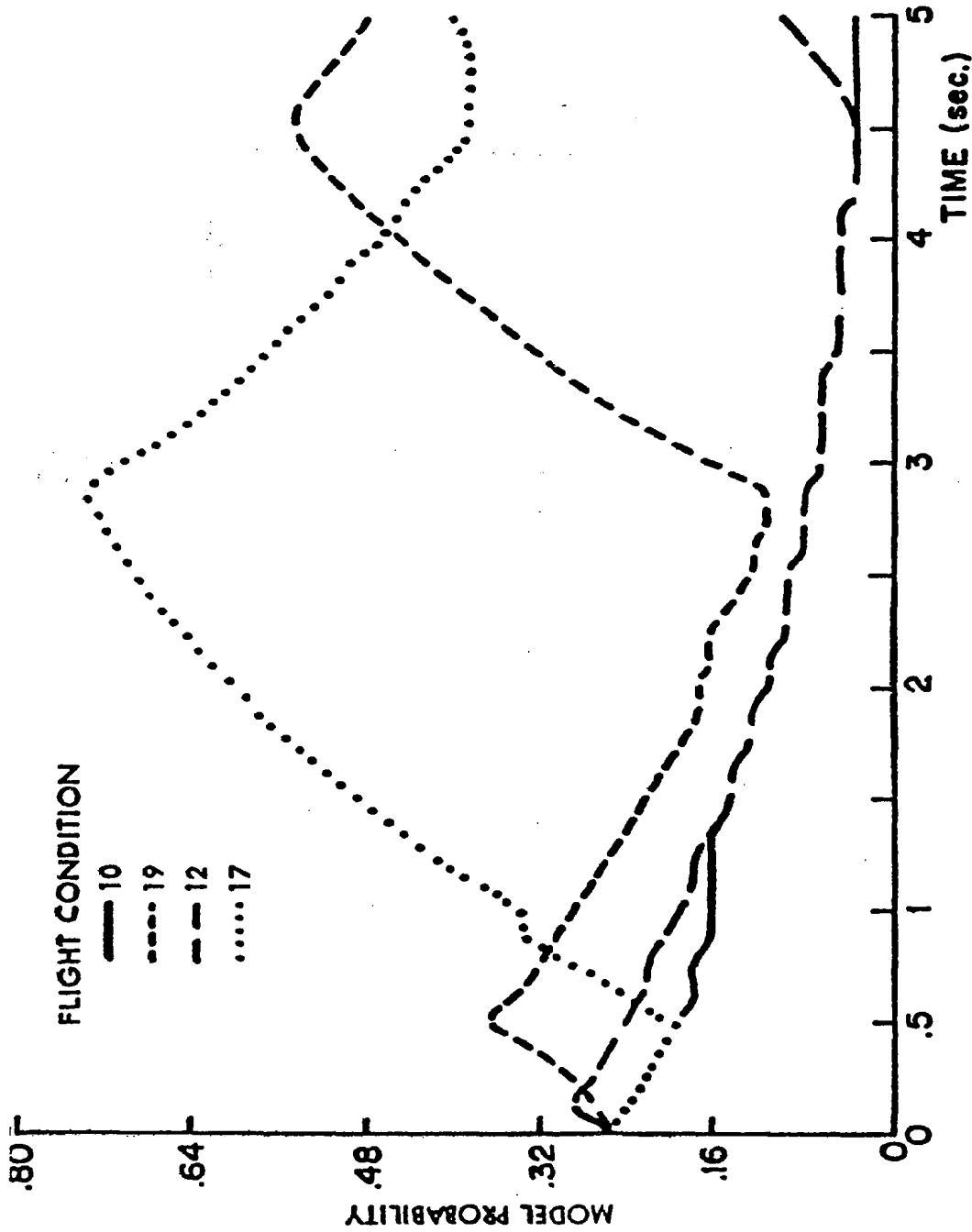
Figure 4.6.5   Longitudinal system control probabilities,
altitude 6096 meters, speed .6 Mach (F.C. 11),
4.57 m/sec rms turbulence

CHAPTER 5

LONGITUDINAL AXIS CONTROL AUGMENTATION SYSTEM

5.1 Introduction

This chapter describes the specific development of the control

designs for the longitudinal dynamics for the fifteen flight conditions.

In addition to discussing the development stages, sample simulations of

the final design are included at various operating conditions, to illus-

trate the operation of the control system.

5.2 Longitudinal Axis Linearized Model

The states used in the longitudinal system were discussed previously

in Section 3.4. As a design choice, the control variable was chosen to

be the commanded elevator rate, $\dot{\delta}_{e_c}$, the opposed to the commanded elevator

position δ_{e_c} . This choice of control variable has some advantages:

one can then incorporate a saturation constraint of 25 degrees per second

on the commanded elevator rate. The control penalty

on $\dot{\delta}_{e_c}$ can be adjusted to keep the system operating without saturation.

Combining this choice of control with equations (3.4.6), the longitudinal

system model has the form:

$$\frac{d}{dt} \begin{Bmatrix} q \\ v \\ \alpha \\ \theta \\ \delta_e \\ w \\ \delta_{e_c} \end{Bmatrix} = \begin{pmatrix} \begin{array}{ccc} \underline{A} & \vdots & \underline{B} \\ (6 \times 6) & \vdots & (6 \times 6) \\ \cdots & \cdots & \cdots \\ \underline{0} & \vdots & \underline{0} \\ (6 \times 1) & \vdots & (1 \times 1) \end{array} \end{pmatrix} \begin{Bmatrix} q \\ v \\ \alpha \\ \theta \\ \delta_e \\ w \\ \delta_{e_c} \end{Bmatrix} + \begin{Bmatrix} \underline{0} \\ (1 \times 6) \\ \cdots \\ 1 \end{Bmatrix} \dot{\delta}_{e_c}$$

$$+ \begin{Bmatrix} \underline{L} \\ (1 \times 6) \\ \cdots \\ 0 \end{Bmatrix} \xi(t) \tag{5.2.1}$$

The control system was designed using linear quadratic control theory [6], described in Appendix F. A quadratic performance index was selected with general structure

$$J_i \triangleq \int_0^\infty (\underline{x}'(t)\underline{Q}_i\underline{x}(t) + \underline{u}'(t)\underline{R}_i\underline{u}(t))\,dt \tag{5.2.2}$$

where the weighting matrices $\underline{Q}_i$, $\underline{R}_i$ are indexed as to possibly vary for each flight condition.

In the initial design it was decided that one should relate the maximum deviations of several variables in a cost functional of the form

given in equation (5.2.2). These variables were pitch attitude θ,
pitch rate q, normal acceleration a_{nz} and commanded elevator rate $\dot{\delta}_{e_c}$.
This yields a performance index of the form

$$J_{lon} = \int_0^\infty \left(\frac{a_{nz}(t)}{a_{nz\ max}^i}\right)^2 + \left(\frac{q(t)}{q_{max}^i}\right)^2 + \left(\frac{\theta(t)}{\theta_{max}^i}\right)^2 + \left(\frac{\dot{\delta}_{e_c}(t)}{\dot{\delta}_{e_c\ max}^i}\right)^2 \ dt$$

$$(5.2.3)$$

All of the variables included in the cost function J_{lon} are either
state or control variables, except a_{nz}. The linearized relationship for
a_{nz} derived in Appendix D is

$$a_{nz}(t) = \frac{V_0}{g} (k_1 v(t) + k_2 \alpha(t) + k_3 \delta_e(t)) \qquad . \qquad (5.2.4)$$

Effectively the structure of the criterion implies that, if the maximum
values of normal acceleration, pitch rate or pitch attitude occurred,
one would be willing to saturate the elevator rate to remove them. For
the preliminary design the following numerical values were used, as
suggested by the NASA Langley Research Center technical staff.

$$\left.\begin{aligned} a_{nz\ max}^i &= 6 \text{ g's} \\[1.5em] q_{max}^i &= \frac{10g}{V_i} \\[1.5em] \theta_{max}^i &= \frac{6g}{V_i a_{33}^i} \end{aligned}\right\} \qquad (5.2.5)$$

$$\dot{\delta}^i_{e_c max} = .435 \frac{rad}{sec} = 25 \frac{deg.}{sec.} \qquad (5.2.6)$$

where V_i is the aircraft speed (Mac no. × speed of sound) and a_{33} is

an element of the linearized $\underline{A}$ matrices discussed in Chapter 3. The

resulting $\underline{Q}_i$ and $\underline{R}_i$ matrices can then be computed for each flight condition

using the values of the linearized models given in Appendices A and D.

5.3 Reduced Model Longitudinal Design

Using the Linear Quadratic design methodology, control gains were

designed for the seven state model of equation (5.2.1) at each flight condi-

tion. The closed-loop responses of the linearized models were studied to

evaluate performance; it was decided that the design should be modified

to exclude feedback gain on the pitch angle θ and the velocity deviation v.

The primary reasons for this modification were: first, the gains on the

velocity deviation were very small for all flight conditions. Second,

as part of the ground rules it was desirable to avoid using the pitch and

velocity sensors. The pitch angle θ(t) is weakly observable from the system

dynamics, so that in the absence of pitch measurements, large estimation

errors would be obtained which could adversely affect the performance of

the control system since the optimal gains include a significant gain on

the estimated pitch attitude. Finally, it was decided that variations in

θ and v occurred in a slow mode so that the pilot would be able to control

variations in pitch and velocity.

In order to eliminate feedback from undesirable states such as θ and

v, reduced-order "short-period" approximation models were used. These

models were discussed in Chapter 3 and Appendix B. Since pitch angle is no longer a variable in the reduced model, the performance index (5.2.3) was modified to

$$J_{i \ LON} = \int_0^\infty \left\{ \left[\frac{a_{nz}(t)}{a_{nz \ max}^i} \right]^2 + \left[\frac{q(t)}{q_{max}^i} \right]^2 + \left[\frac{\dot{\delta}_{e_c}(t)}{\dot{\delta}_{e_c max}} \right]^2 \right\} dt \quad (5.3.1)$$

where

$$a_{nz} = - \frac{V_i}{g} \ (k_2 \alpha(t) + k_3 \dot{\delta}_e(t)) \qquad (5.3.2)$$

Using the same values of $a_{nz \ max}^i$, q_{max}^i and $\dot{\delta}_{e_c max}$ given by eqs. (5.2.5) and (5.2.6), the reduced order linear quadratic optimization problem was solved, obtaining gains which depended only on q, α, δ_e, δ_{e_c} and w.

The reduced-order gain designs were simulated using the full state linearized models, to evaluate the change in performance using the reduced-order model design. From the viewpoint of transient responses to the variables of interest (normal acceleration, pitch rate, angle of attack), the transient responses to initial conditions were almost identical for both the full-state design and the reduced-order design. Thus, the short-period motion of the aircraft was dominated by the relative tradeoff between maximum normal acceleration $a_{nz \ max}$ and maximum pitch rate q_{max}. The reduced-order gains tended to be smaller than their full-state counterparts. The major difference in the performances of the two designs were that, in the simulations of the reduced-order design, velocity error v and pitch attitude deviation θ were not reduced to zero.

This performance was deemed acceptable, since the drift was slow enough for a human pilot to correct.

Using the reduced-order design procedure, feedback gains were obtained for different values of the cost matrices $\underline{Q}_i$. In particular, the parameter changed was q^i_{max}, with values defined as

$$q^i_{max} = \frac{10g}{V_i} , \frac{8g}{V_i} , \frac{6g}{V_i} , \frac{4g}{V_i} \qquad (5.3.3)$$

Figure 5.3.1 contains a plot of the closed-loop complex eigenvalues of the reduced system. These correspond to the "optimal" short-period dynamics. Notice that, for each choice of q^i_{max}, the poles for supersonic and subsonic flight conditions lie along lines of constant damping ratios. This result is of particular interest, since it reflects that the implicit cost adjustment in the matrix $\underline{Q}_i$ produced a constant damping ratio. Table 5.3.1 summarizes the damping ratios for different weightings.

5.4 C*-Design Using Reduced Order Dynamics

The problem of obtaining desirable handling qualities in the control system was approached from a C*-criterion point of view. The C* criterion is one of several measures which may be used to evaluate handling qualities of aircraft. Appendix J explains in detail the C* criterion.

Essentially, the C* quantity represents a tradeoff between normal acceleration and pitch rate. This balance between normal acceleration and pitch rate can be used in defining a new performance index of the form:
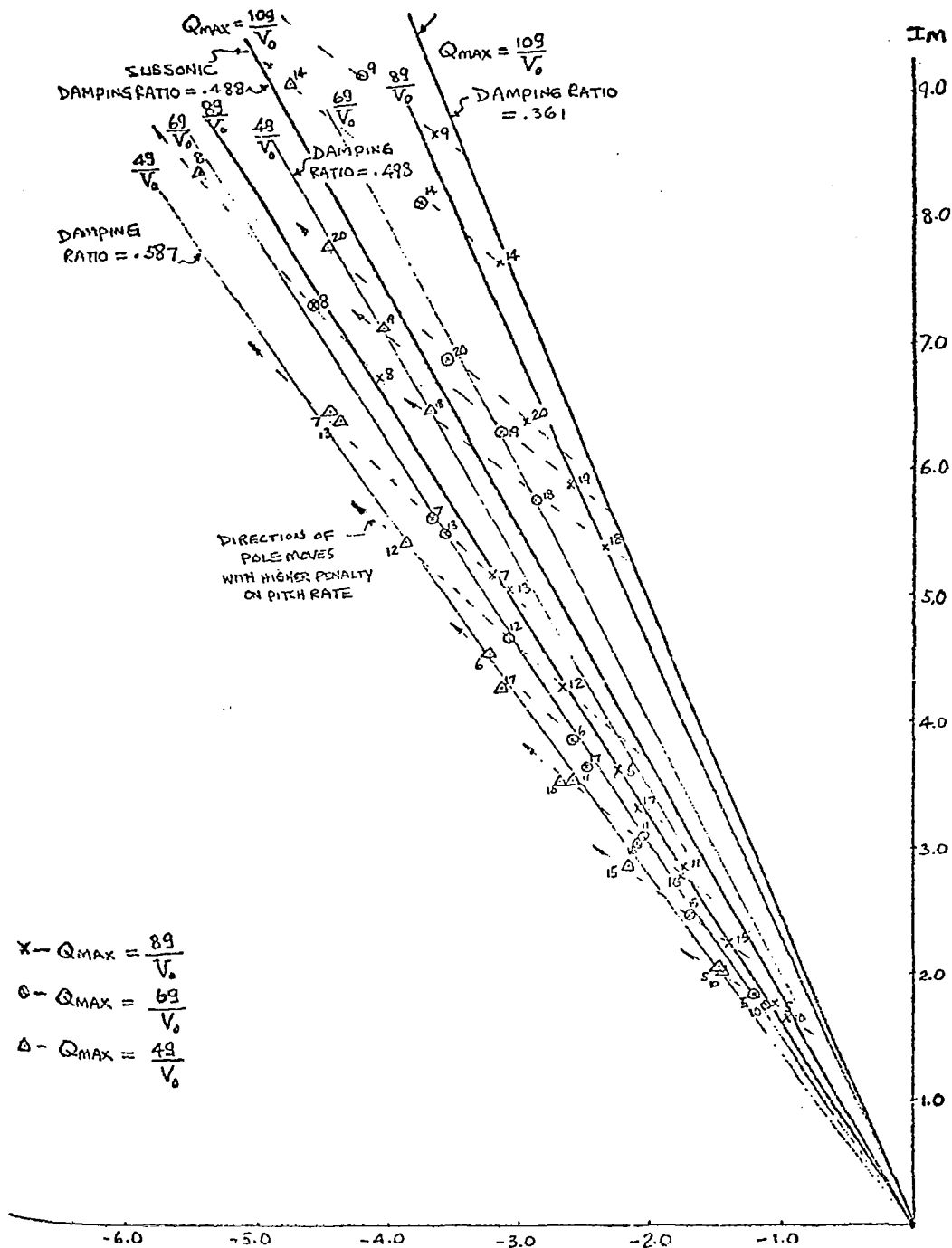
Figure 5.3.1   Closed-loop complex poles for different pitch rate penalties

TABLE 5.3.1

DAMPING RATIO FOR CLOSED-LOOP SHORT PERIOD
POLES AS A FUNCTION OF MAXIMUM PITCH RATE
PENALTY, q_{max}^i, IN (5.3.1).

q_{max}	Damping ratio for all subsonic conditions	Damping ratio for all supersonic conditions
$10g/V_o$	0.488	0.361 .
$8g/V_o$	0.530	0.402
$6g/V_o$	0.552	0.449
$4g/V_o$	0.587	0.498

$$J_{C*}^i = \int_0^\infty (C*(t)^2 + k_1^i (\dot{\delta}_{e_c})^2) dt \qquad\qquad (5.4.1)$$

where

$$C*(t) = k_2^i a_{nz}(t) + k_3^i q(t) \qquad\qquad (5.4.2)$$

Note the ith superscript on the performance index and the weighings, indicating the dependence of the performance index on flight condition.

The performance index J_{C*}^i has an implicit balance between normal acceleration and pitch rate, determined by the constants k_2^i and k_3^i. These constants were chosen to be

$$k_3^i = 10; \; k_2^i = 1. \qquad\qquad (5.4.3)$$

independent of flight condition. Various choices for k_1^i were tried, obtaining optimal gains for the reduced models for each choice; upon evaluation of the various responses under closed-loop conditions, the optimal weight k_1^i was chosen to be

$$k_1^i = \left(\frac{1}{.435}\right)^2 = 5.252467 \qquad\qquad (5.4.4)$$

This criteria was chosen for the final design of the fixed point controller. Appendix I contains a table of the optimal continuous-time gains for each flight condition. The optimal closed-loop poles are shown in figure 5.4.1.
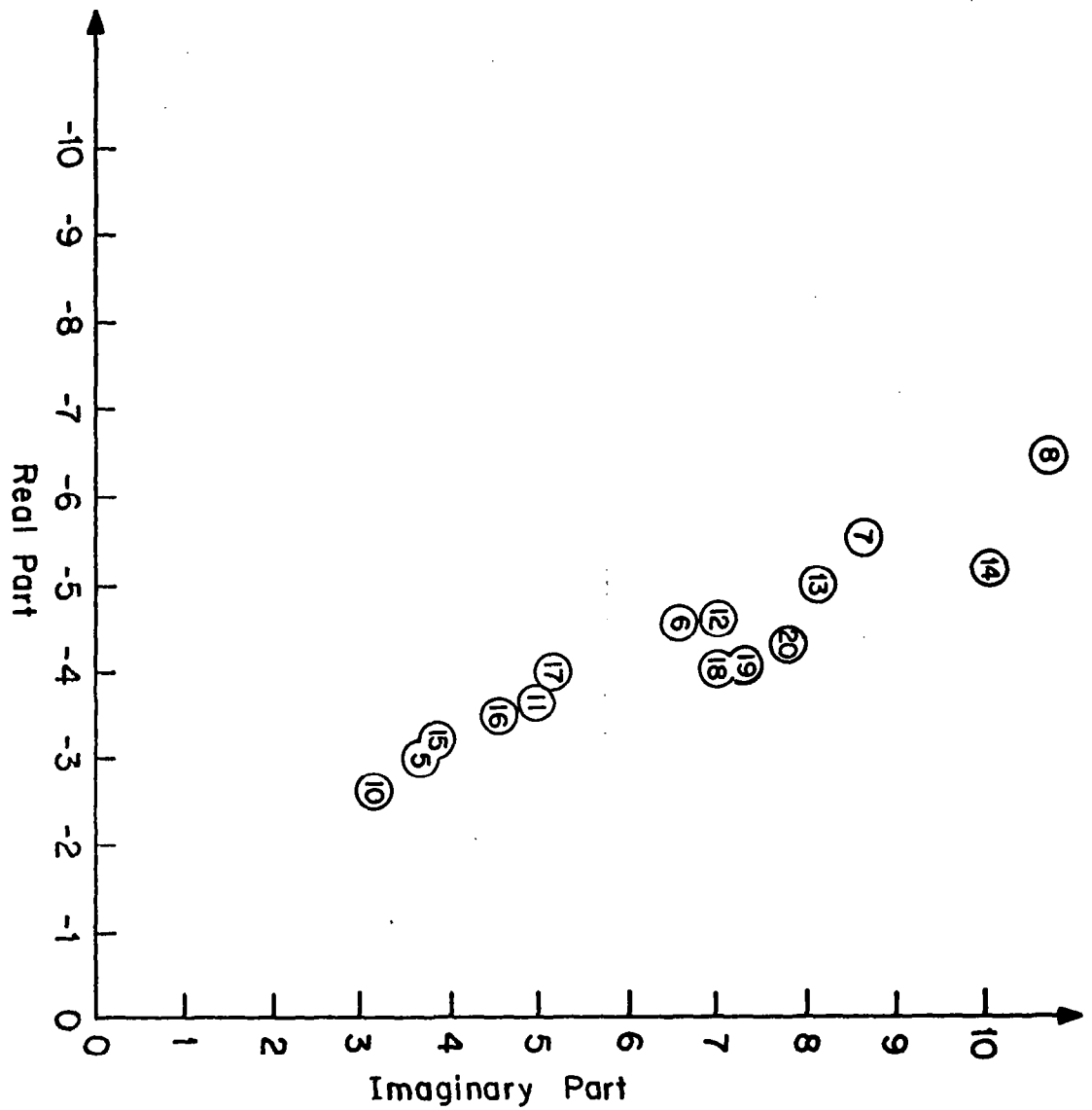
Figure 5.4.1   Complex Eigenvalues of Closed-loop Longitudinal System

5.5 Discrete-time LQG Design

Using the Linear Quadratic Gaussian approach discussed in Appendix F, the continuous-time gains obtained in the previous section were converted to discrete-time gains. The final discrete-time gains are tabulated in Appendix H. Following the methodology of Appendix C, Kalman filters were designed using measurements of pitch rate and normal acceleration, based on the equivalent linear discrete-time models described in Appendix E. Although an elevator position measurement was available, it was not used because of its trim dependence.

The steady-state Kalman filter gains were determined using the sensor covariances quoted in Table 3.5.1, using a 15 ft/sec rms value in the wind disturbance model of Section 3.4. They are listed in Appendix K. Closed-loop eigenvalues for the complete discrete time system are listed in Appendix L.

5.6 Longitudinal Pilot Command System

The basic regulator scheme used in the MMAC control system was described in Sections 5.1 - 5.5. In this section the regulator design is modified to incorporate pilot commands. The basic operation of the pilot command system is structured as follows: the stick position is translated into an elevator deflection input by multiplying it by a gear ratio. This commanded elevator deflection is translated into reference values of pitch rate and angle of attack using gains computed in the next section. These three reference values are subtracted from the estimate of the corresponding state variables to produce error signals, which in

turn get multiplied by the optimal regulator gains to generate a control signal. Figure 5.6.1 illustrates this deterministic scheme.

Pitch rate and angle of attack were chosen to be the controlled variables, as they are the dynamic variables mostly controlled and responded to by the pilot. This choice also simplifies the on-line computation of commanded variables, as only short-period dynamics need be considered. The regulator drives the aircraft to obtain the commanded state values; handling qualities are not explicitly considered, as the responses are based on the regulator design, which partly addressed this question.

The complete controller structure for a given flight condition is shown in Figure 5.6.2. Notice that, in the absence of pilot inputs, the individual controller design is essentially the LQG controller discussed in previous sections. Thus, this design preserves the regulator properties, extending the structure to incorporate pilot commands.

The gains between pitch rate and elevator deflection input, and between angle of attack and the input are obtained from a steady-state analysis of the short-period dynamics. The short-period dynamics of the aircraft, ignoring the actuator dynamics, can be modeled as in Chapter 3 by:

$$\frac{d}{dt} \begin{bmatrix} q \\ \alpha \end{bmatrix} = \begin{bmatrix} a_{11} & a_{13} \\ a_{31} & a_{33} \end{bmatrix} \begin{bmatrix} q \\ \alpha \end{bmatrix} + \begin{bmatrix} b_1 \\ b_3 \end{bmatrix} \delta_e \qquad (5.6.1)$$

For the steady state, one sets $\dot{q} = \dot{\alpha} = 0$, to obtain the algebraic equation

$$\begin{bmatrix} a_{11} & a_{13} \\ a_{31} & a_{33} \end{bmatrix} \begin{bmatrix} q \\ \alpha \end{bmatrix} = \begin{bmatrix} -b_1 \\ -b_3 \end{bmatrix} \delta_e \qquad (5.6.2)$$
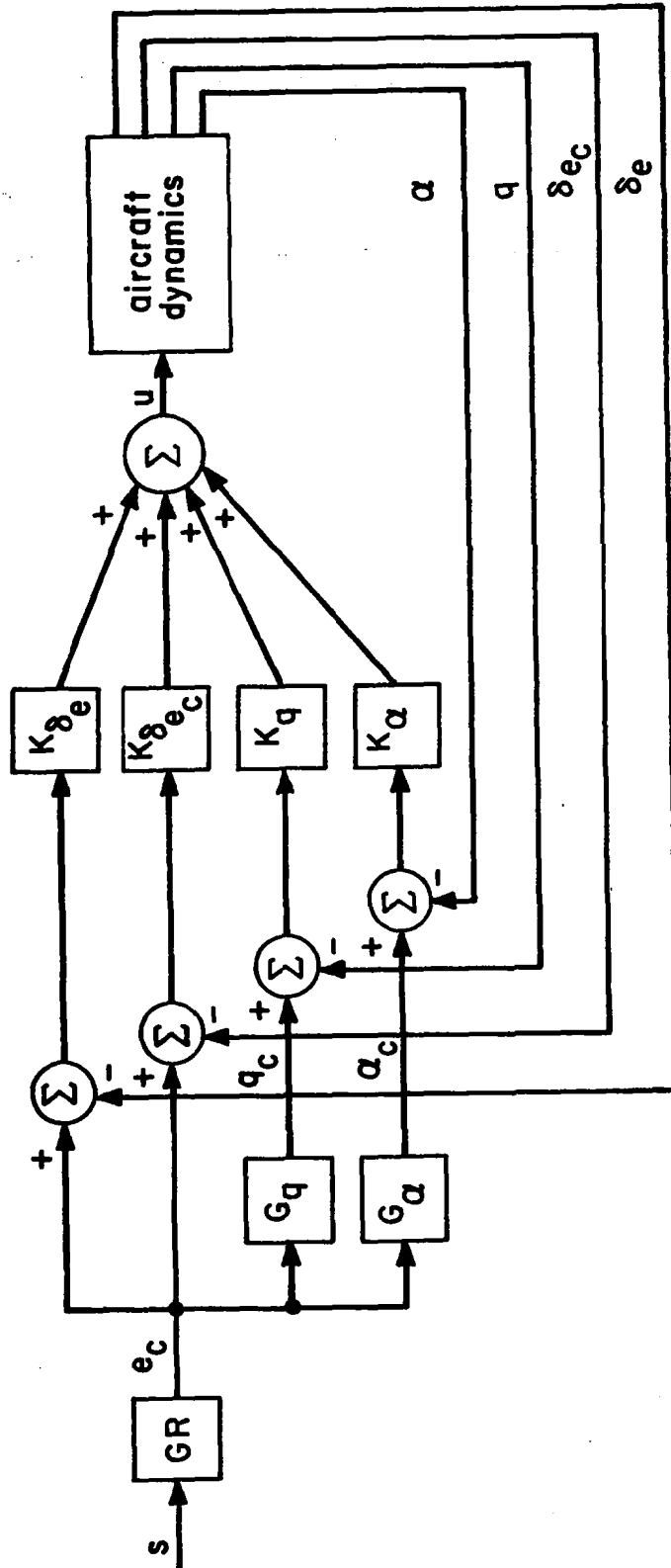
Figure 5.6.1   Deterministic Longitudinal Pilot Command System
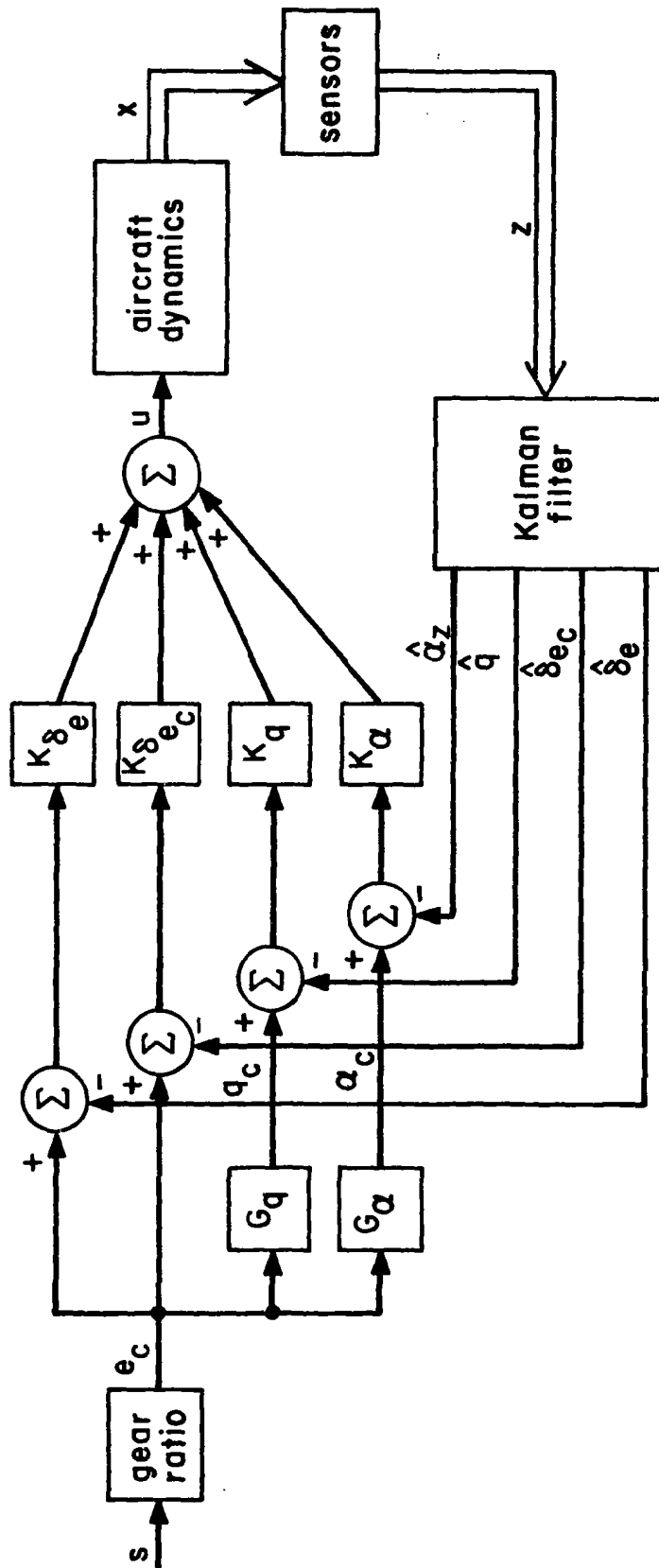
Figure 5.6.2 Stochastic Longitudinal Pilot Command System

The steady-state gains are now readily obtained by

$$G_q = \frac{q}{\delta_e} = \frac{-b_1 a_{33} + b_3 a_{13}}{a_{11} a_{33} - a_{13} a_{31}} \tag{5.6.3}$$

$$G_\alpha = \frac{\alpha}{\delta_e} = \frac{-b_3 a_{11} + b_1 a_{31}}{a_{11} a_{33} - a_{13} a_{31}} \tag{5.6.4}$$

Table 5.6.1 contains the values of the steady-state gains G_q and G_α for all flight conditions.

The steady-state gains depend on the relationships between elevator deflection and the resulting short-period steady state, which depends only on the aerodynamic properties of the aircraft. These gains are independent of the regulator design or the control scheme, and remain unchanged if a discrete-time controller is used.

The selection of the gains does not involve handling qualities, nor does it guarantee satisfactory aircraft performance. The control gain design used in the regulator controller in Section 5.1 - 5.5 was achieved using handling qualities considerations. Simulation results indicate that the proposed steady state gain scheme coupled with the regulator design yield satisfactory responses to pilot commands. Notice that the gearing ratio between the pilot stick and elevator deflection is left as a design parameter to be adjusted, which will change the sensitivity of the system to pilot actions. Nominally, this value has been set to

$$\text{Gearing Ratio} = 4.75 \text{ deg/in} \quad (1.87 \text{ deg/cm}) \tag{5.6.5}$$

which was suggested by Langley staff.

TABLE 5.6.1

TABLE FOR GAINS THAT APPEAR IN LONGITUDINAL COMMAND SYSTEMS

(see Figure 5.6.2)

Flight Condition	GAIN G_q	GAIN G_α
5	-.987	-1.2817
6	-1.9024	-1.3882
7	-2.4096	-1.2265
8	-3.0430	-1.1218
10	-.6239	-1.2079
11	-1.1072	-1.3454
12	-1.7531	-1.4520
13	-1.9191	-1.3159
14	-.5826	-.3525
15	-.8412	-1.9356
16	-.9429	-1.8695
17	-.5958	-1.0260
18	-.3253	-.4627
19	-.2973	-.4272
20	-.2399	-.4121

5.7 Modifications of Controller Design

The longitudinal system models were all linearized about different trim conditions, namely the nominal values of angle of attack, pitch angle and elevator deflection. Table 5.7.1 contains the trim conditions for the fifteen flight conditions in the MMAC. The linearized equations in Appendix A .describe the evolution of deviations of the variables from their equilibrium values. Thus, in order to output a command to the aircraft, it is necessary to. know the reference trim values of elevator position.

There are various ways of handling the trim problem in the longitudinal system. One way is to treat the trim values of elevator as a state variable to be estimated, together with the other variables. This method represented additional complexity, and did not seem accurate enough, thus it was rejected.

Another possible way of handling trim is to use a self-trimming controller design such as P-I controller [28], [29]. Preliminary studies by Lee, Athans et al.[29] provided the foundation for a sampled-data P-I-D controller which would result in neutral speed stability. Figure 5.7.1 contains a typical controller design. However. this controller design was not fully available and implemented in a stochastic framework during the course of this study.

Since it attempts to control only the short-period response of the aircraft, the MMAC system was coupled with filtering schemes which attenuated low frequencies (hence reducing trim effects). Additionally, the control variable was chosen to be $\dot{\delta}_{ec}$, to introduce some integral control and reduce steady-state errors. These are the modifications to the MMAC control

TABLE   5.7.1

TRIM VALUES FOR FLIGHT CONDITIONS

(see Table 1.3.1)

Flight Condition	Trim Angle of Attack and Pitch Angle (Degrees)	Trim Elevator (Degrees)	Trim Forward Velocity (m./sec)
5	7.991	-3.960	101.36
6	2.989	-2.495	180.18
7	1.921	-2.455	238.16
8	1.536	-2.537	292.66
10	9.270	-5.549	124.81
11	4.429	-3.663	189.13
12	2.626	-2.615	252.66
13	2.250	-2.650	281.58
14	1.490	-2.131	379.26
15	7.035	-4.791	205.08
16	5.371	-3.891	235.17
17	4.257	-3.521	264.94
18	2.822	-4.463	353.80
19	2.736	-4.416	412.79
20	2.063	-3.465	472.00
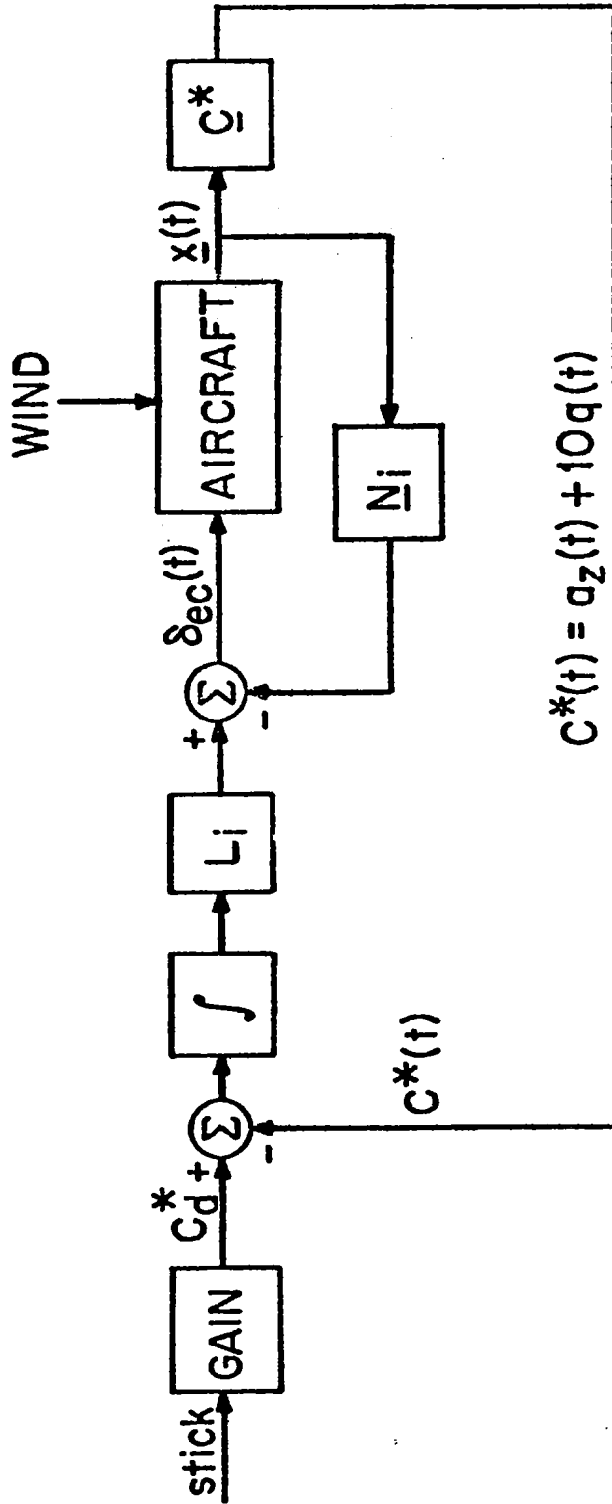
GAINS L_i AND $\underline{N}_i$ CHANGE WITH FLIGHT CONDITION.

Figure 5.7.1   Structure of P-I Controller

$$C^*(t) = a_z(t) + 10q(t)$$

algorithm which enable it to account for the trim effects in the filtering scheme.

Figure 5.7.2 contains a diagram of the longitudinal control scheme of the MMAC with the filtering included. The combined commands of the pilot stick and trim integrator are separated into a high-frequency and a low-frequency component by a second-order high pass filter. Experimentation established the break frequency to be 0.4 radians/second. The discretized equations for the filter are given in Appendix M.

Additionally, the pitch rate and normal acceleration measurements are high-pass filtered as described in Appendix M. The high-frequency measurements and commands are then processed by the MMAC control system described in Sections 5.1 - 5.6. This produces a desired elevator command $\overset{\bullet}{\delta}_{ec}$. This command is then added to the low-passed components of the stick and trim integrator to produce the complete command to the aircraft.

This control scheme does not provide neutral speed stability. However, it reduces the effects of trim differences throughout the flight envelope on identification, and it allows the pilot to trim the aircraft using the trim integrator. Isolating the high-frequency components of commands and measurements is consistent with the philosophy of controlling only the short-period response of the aircraft.

5.8 Performance of the Longitudinal Control System

Figures 5.8.1 to 5.8.12 illustrate the performance of the longitudinal regulator system over the flight envelope of the F-8 aircraft. The aircraft is subjected to a six degree alpha gust initially; the transient
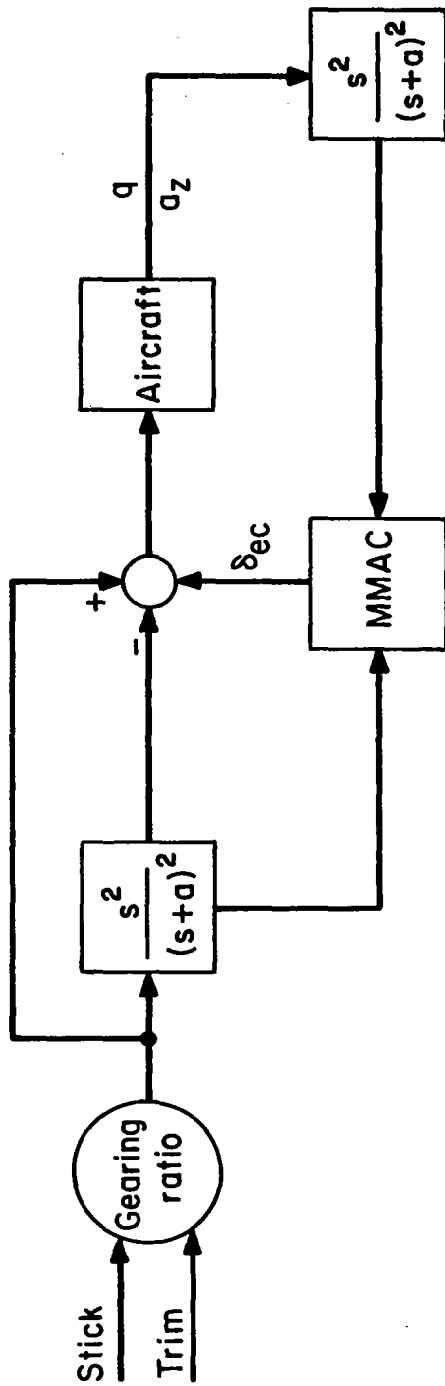
Figure 5.7.2   High-pass Filtering of Trim Effects in MMAC

response of the aircraft is shown under no turbulence and 4.57 m/sec rms turbulence. The figures contrast the uncontrolled (open-loop) response of the aircraft with the controlled regulator response. The simulations were obtained at NASA Langley Research Center using a full state non-linear model of the F-8C aircraft.

The simulations conducted with no turbulence highlight the gust-alleviation damping of the MMAC system at various flight conditions. When the turbulence level is 4.57 m/sec rms, the simulations highlight the MMAC system's ability to reduce the rms level of continuous turbulence. All closed loop simulations were done using the full sampled data stochastic design using a sampling period of 1/8 second.

Figures 5.8.13 to 5.8.15 contain the airplane responses to a doublet command in the longitudinal system at six selected flight conditions. The steady-state gain design for the MMAC system was used in conjunction with the high-pass filtering scheme which separated stick commands into long-term and short-term commands. The short-term commands are used in driving the MMAC command system; the MMAC commands are subsequently added to the long-term commands to form the total command to the aircraft. The longitudinal stick response shown is the short-term command mentioned. The simulations describe the designed responses of the MMAC control system under perfect identification.

It should be noted that all closed loop simulations used the complete sampled data stochastic design, with Kalman filters and instrument noise, at a sampling period of 1/8 seconds.
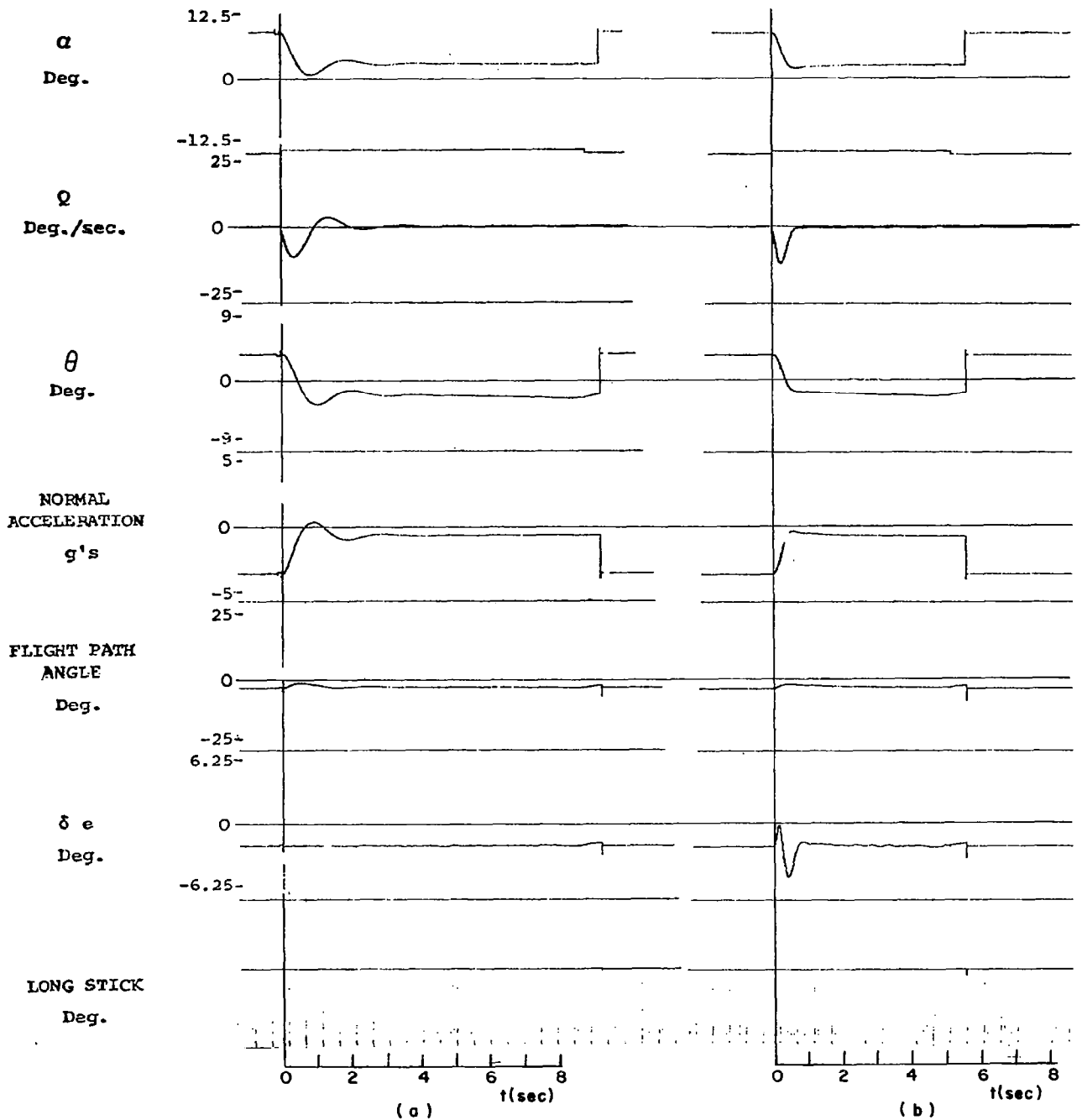
Figure 5.8.1 Longitudinal system responses to initial 6°α perturbation,
no turbulence, altitude 304.8 meters, speed .53 Mach

(a) open loop responses
(b) closed loop responses
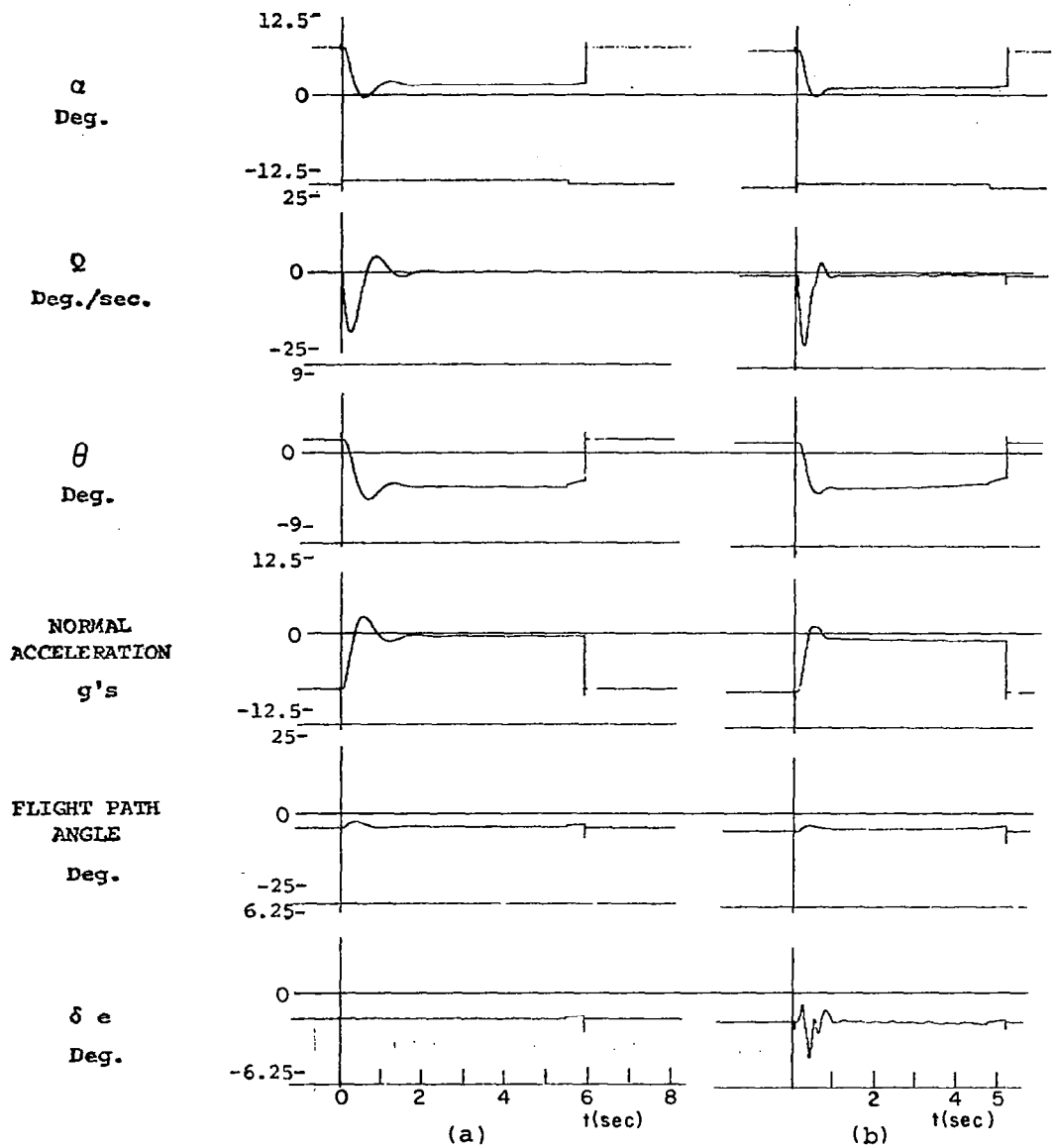
Figure 5.8.2   Longitudinal system responses to initial 6°α perturbation,
no turbulence, altitude 304.8 meters, speed .86 Mach

(a)   open loop responses
(b)   closed loop responses
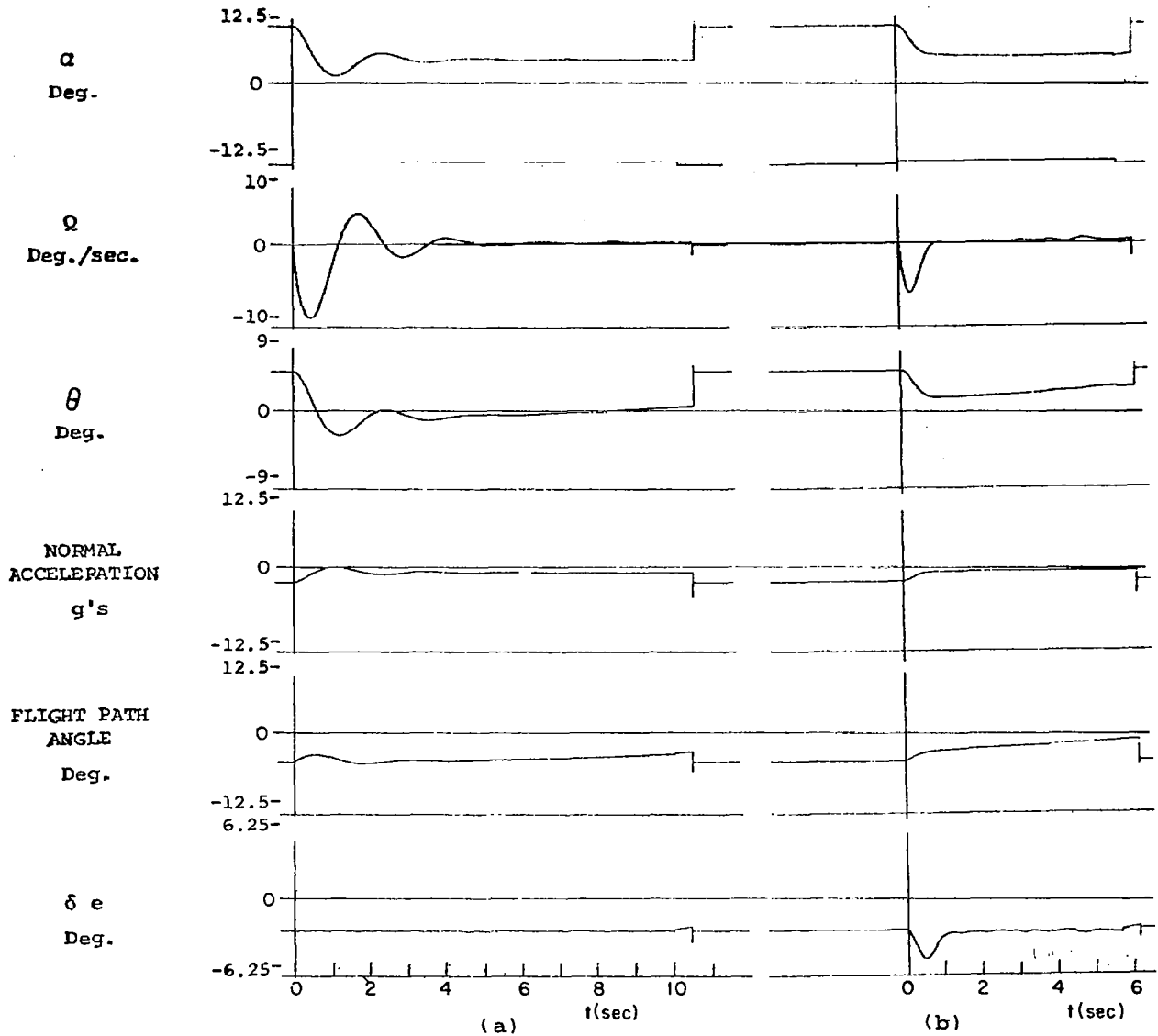
Figure 5.8.3 Longitudinal system responses to initial 6°α perturbation, no turbulence, altitude 6096 meters, speed .6 Mach

(a) open loop responses
(b) closed loop responses
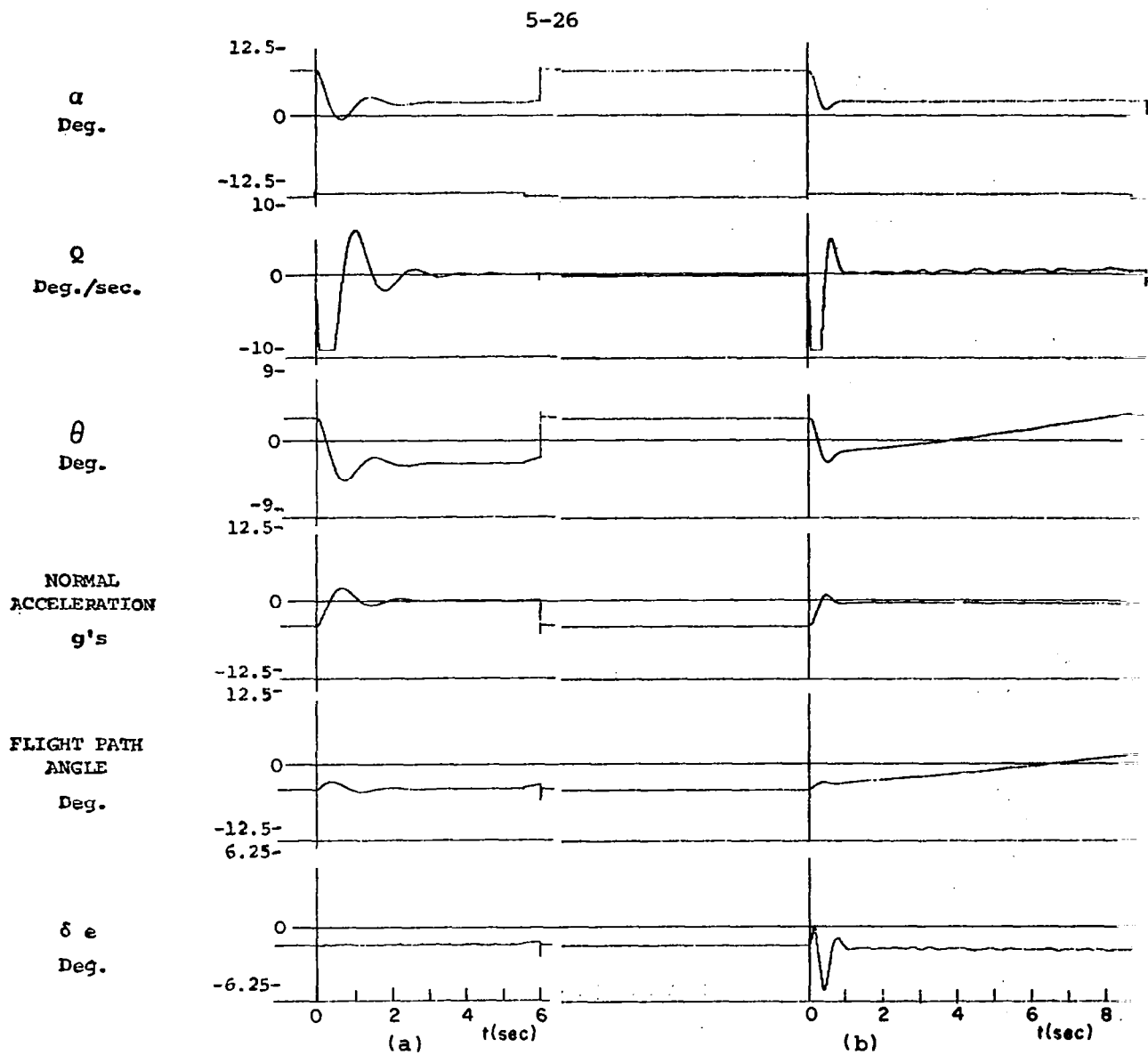
Figure 5.8.4 Longitudinal system responses to initial 6°α perturbation,
no turbulence, altitude 6096 meters, speed .9 Mach

(a) open loop responses
(b) closed loop responses
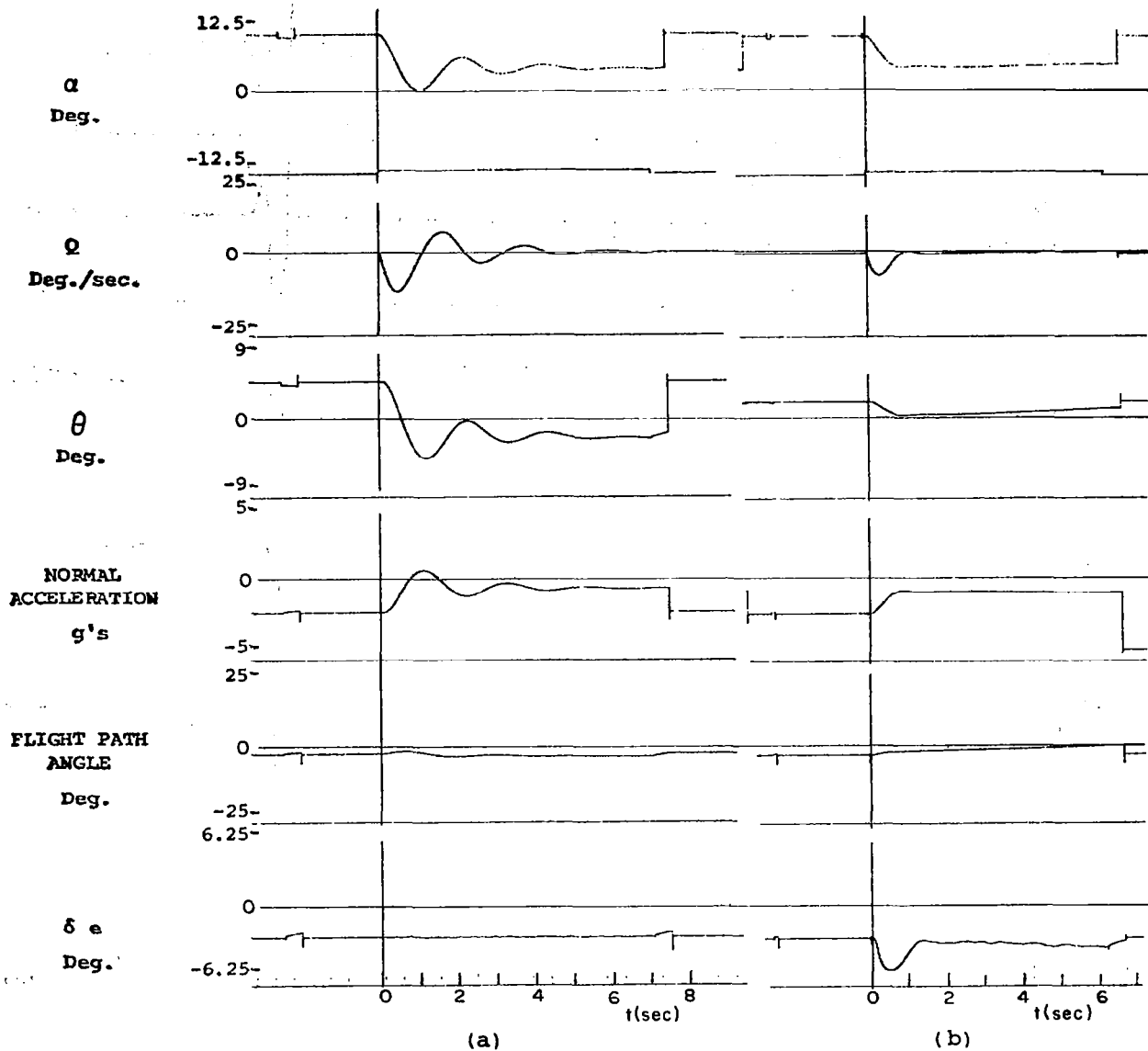
Figure 5.8.5 Longitudinal system responses to initial 6°α perturbation,
no turbulence, altitude 12192 meters, speed .9 Mach

(a)   open loop responses
(b)   closed loop responses
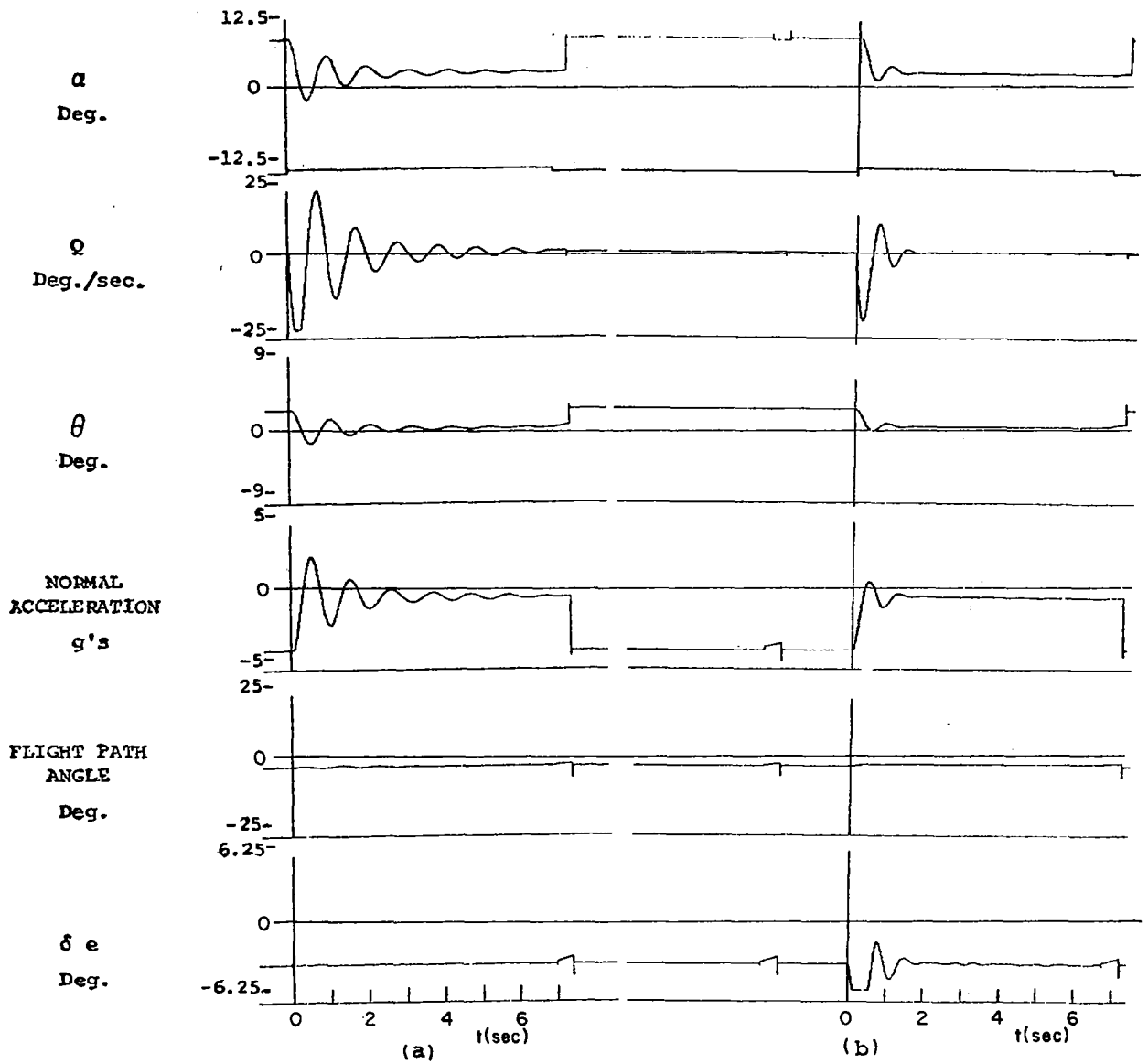
Figure 5.8.6 Longitudinal system responses to initial 6°α perturbation, no turbulence, altitude 12192 meters, speed 1.4 Mach

(a) open loop responses
(b) closed loop responses
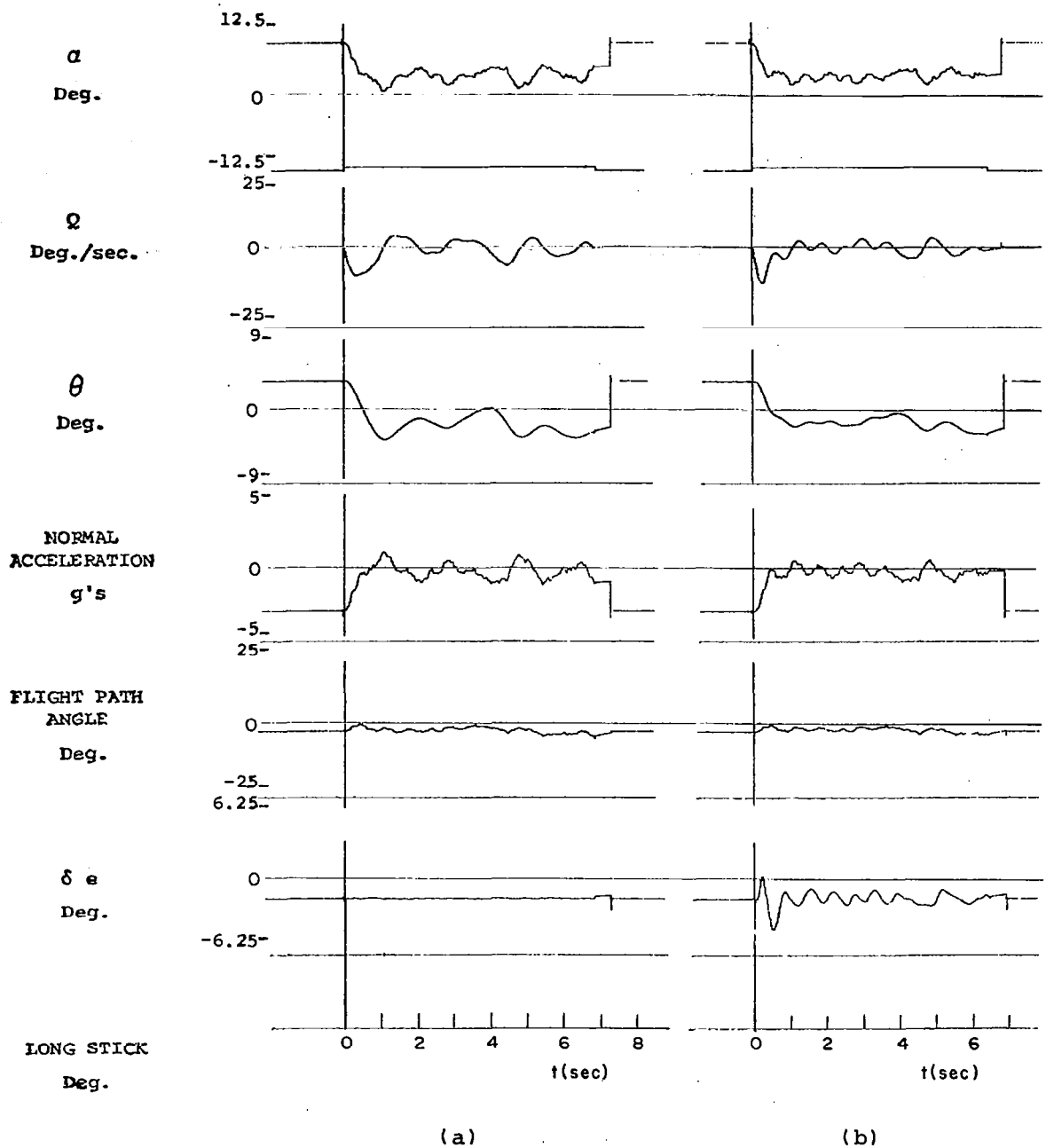
Figure 5.8.7 Longitudinal system responses to initial 6°α perturbation,
turbulence level 4.57 m/sec rms, altitude 304.8 meters,
speed .53 Mach

(a) open loop responses
(b) closed loop responses
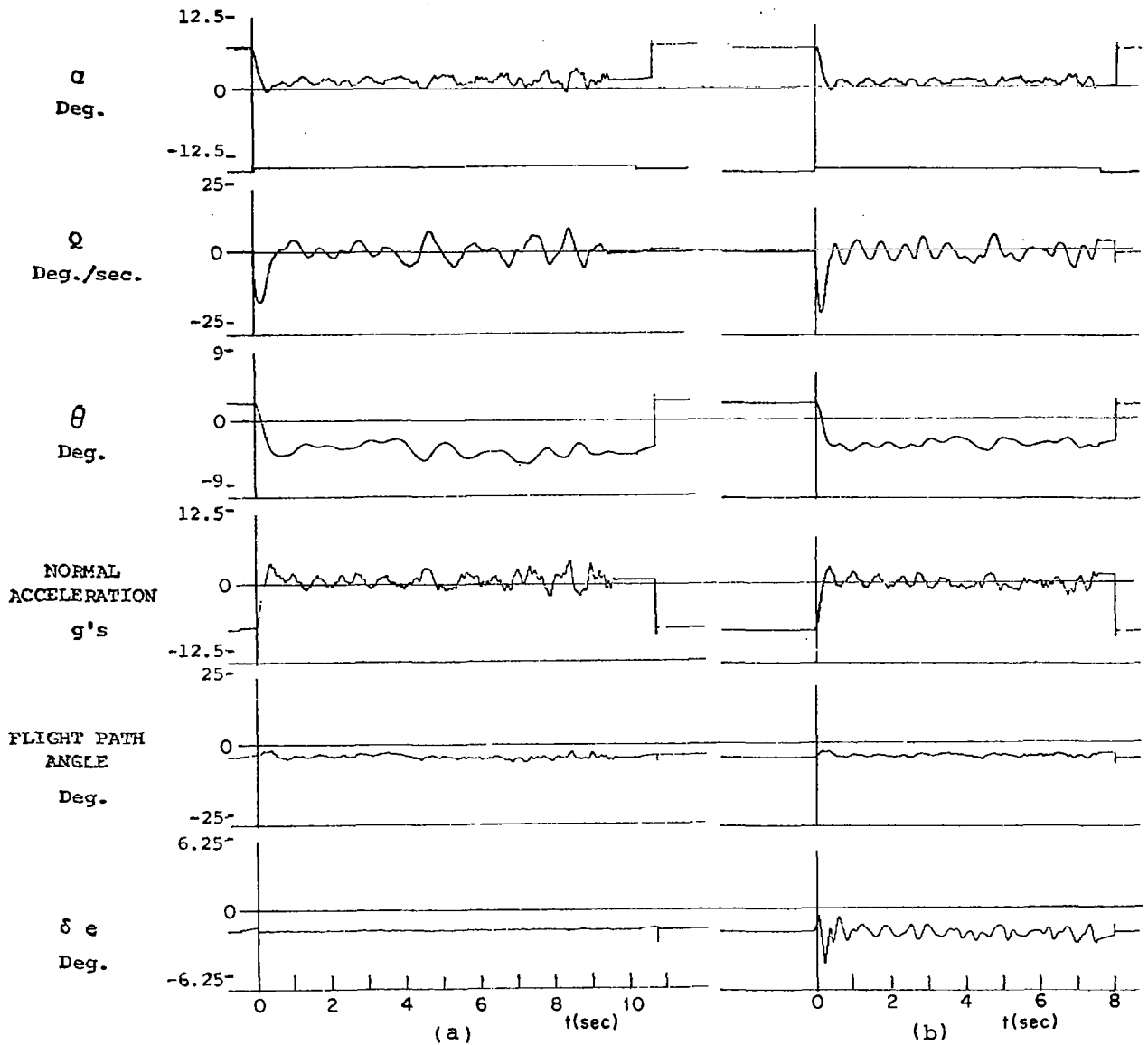
Figure 5.8.8   Longitudinal system responses to initial 6°α perturbation,
turbulence level 4.57 m/sec rms, altitude 304.8 meters,
speed .86 Mach

(a)   open loop responses
(b)   closed loop responses
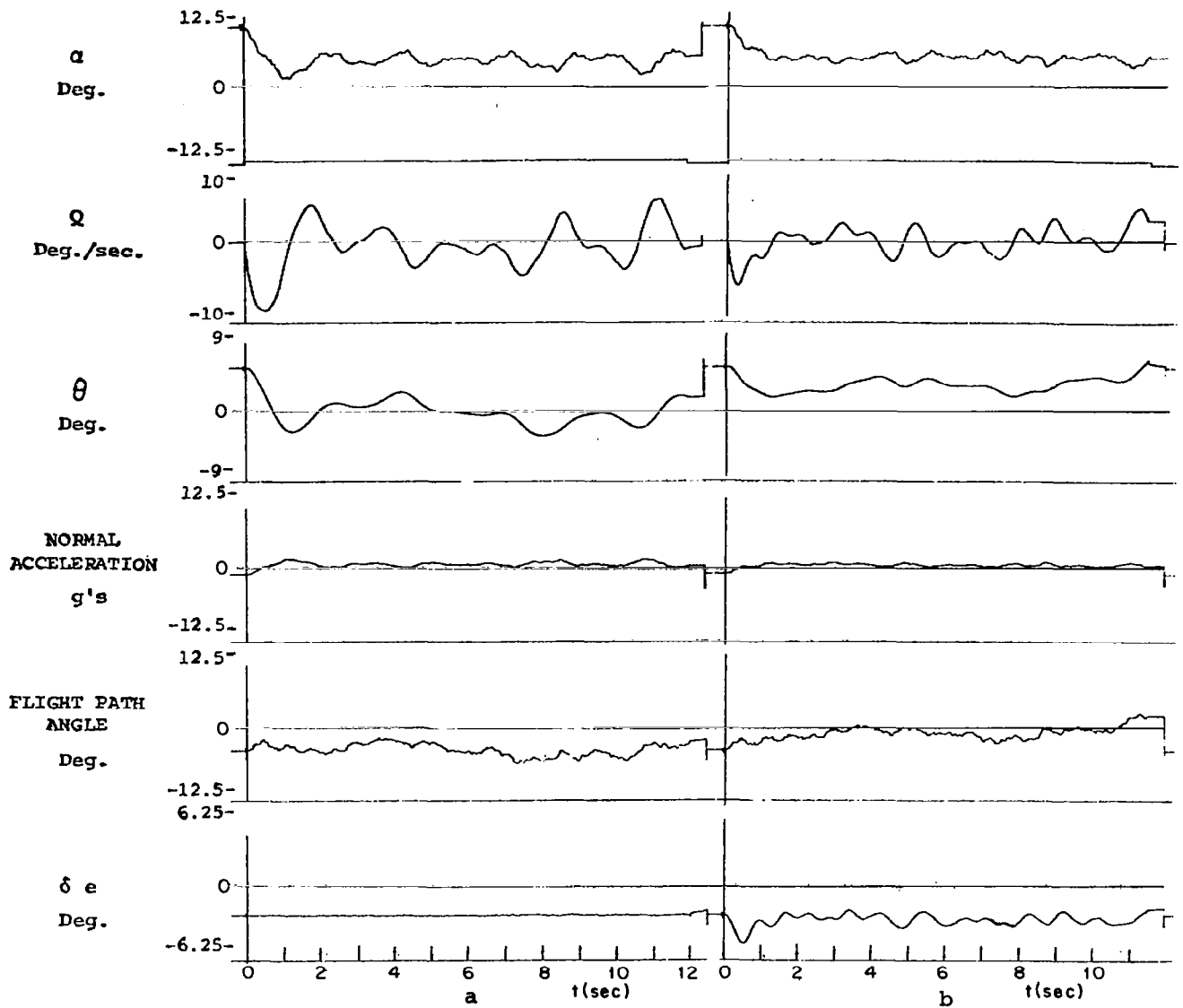
Figure 5.8.9 Longitudinal system responses to initial 6°α perturbation,
turbulence level 4.57 m/sec rms, altitude 6096 meters,
speed .6 Mach

(a) open loop responses
(b) closed loop responses
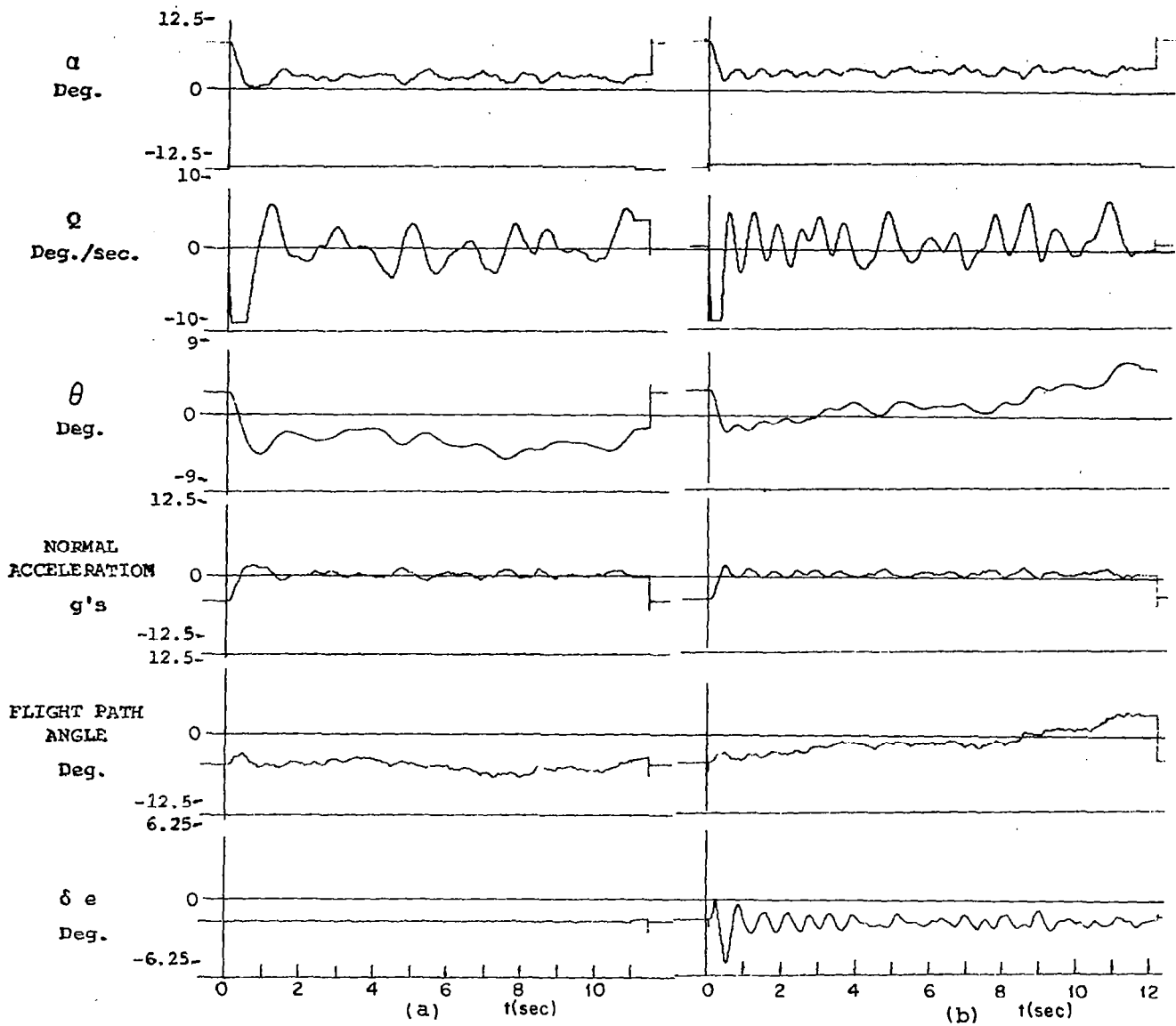
Figure 5.8.10   Longitudinal system responses to initial 6°α perturbation,
turbulence level 4.57 m/sec rms, altitude 6096 meters,
speed .9 Mach

   (a)   open loop responses
   (b)   closed loop responses
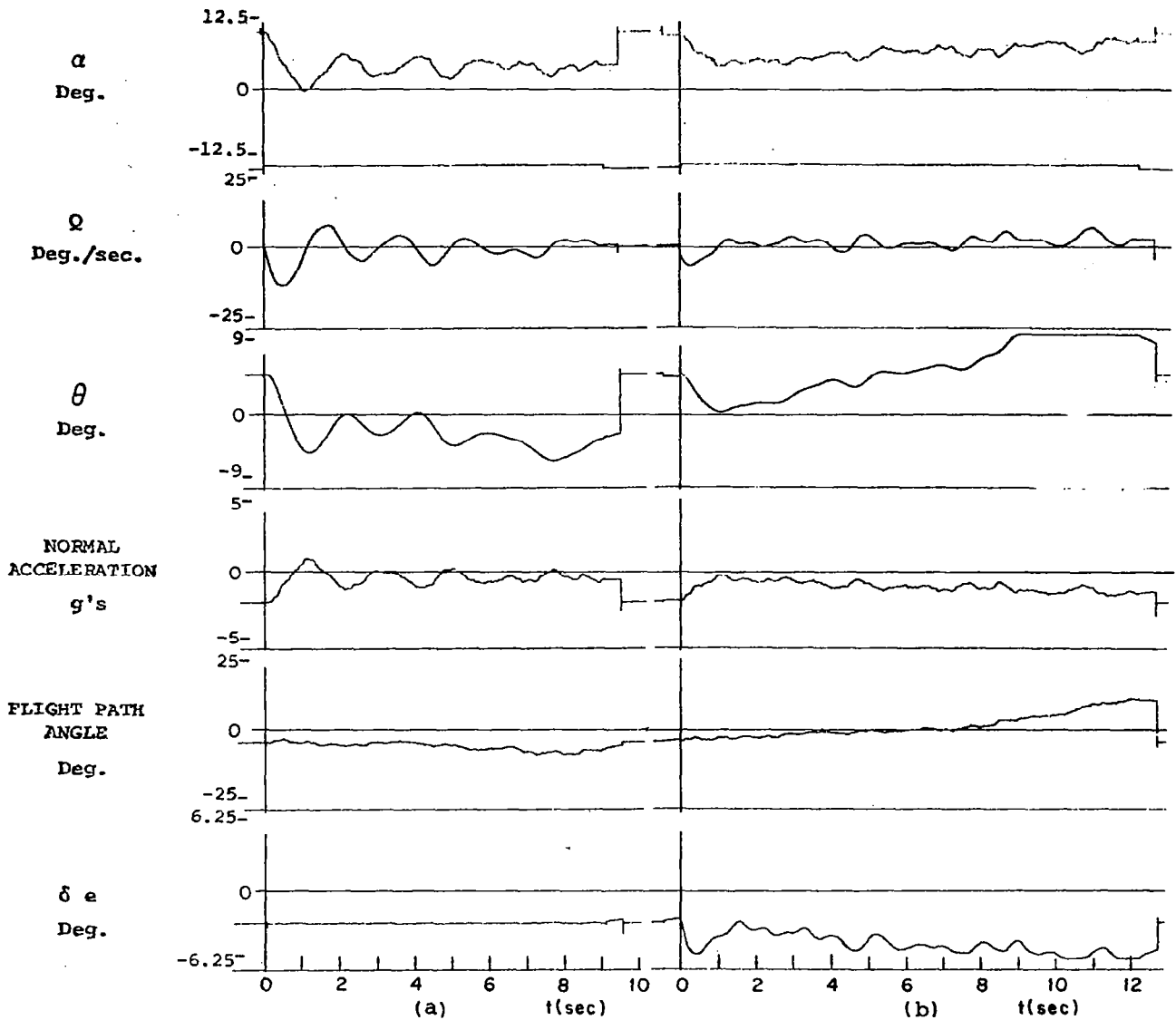
Figure 5.8.11 Longitudinal system responses to initial 6°α perturbation,
turbulence level 4.57 m/sec rms, altitude 12192 meters,
speed .9 Mach

(a) open loop responses
(b) closed loop responses
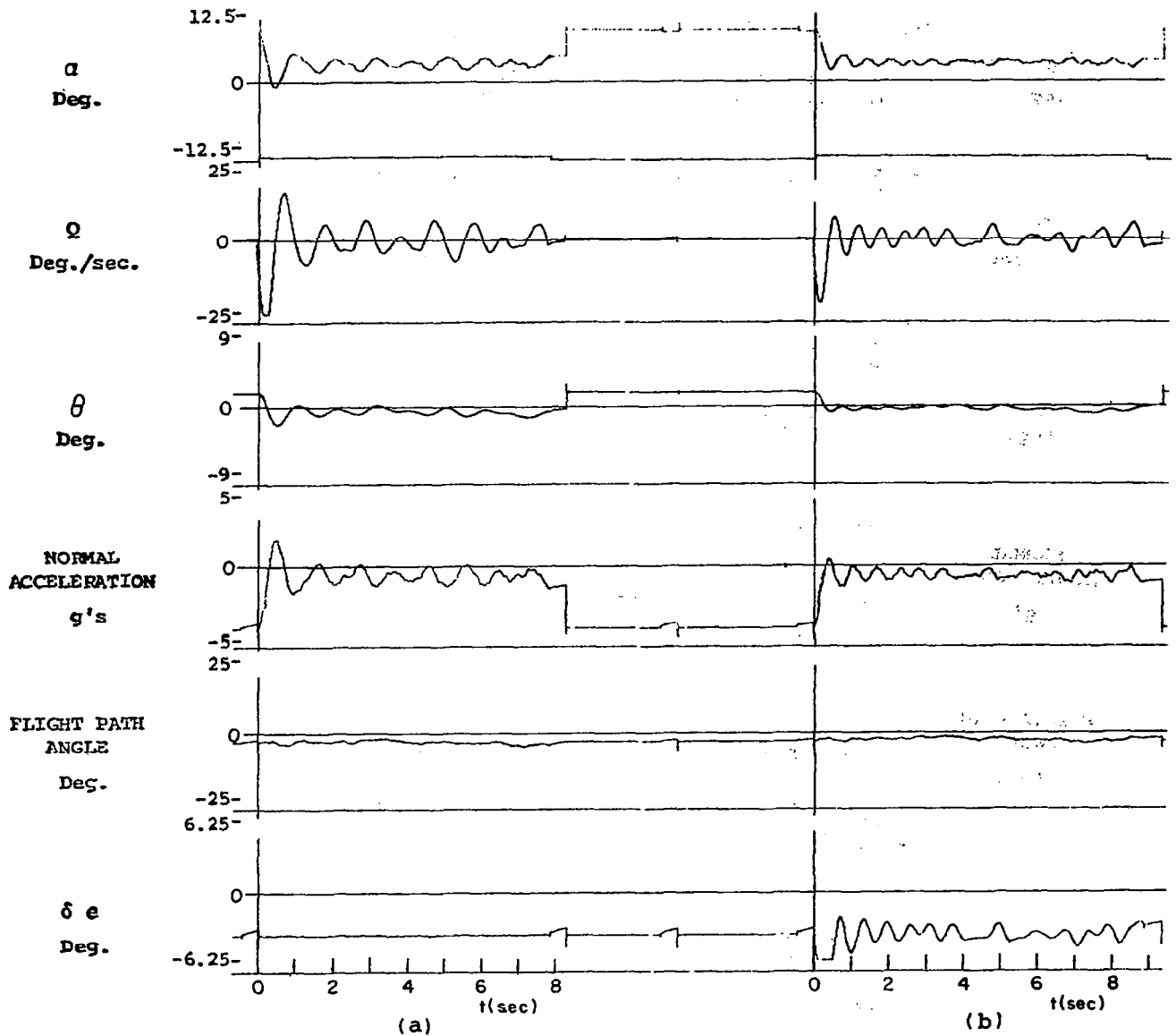
Figure 5.8.12   Longitudinal system responses to initial 6°α perturbation,
turbulence level 4.57 m/sec rms, altitude 12192 meters,
speed 1.4 Mach

   (a)   open loop responses
   (b)   closed loop responses
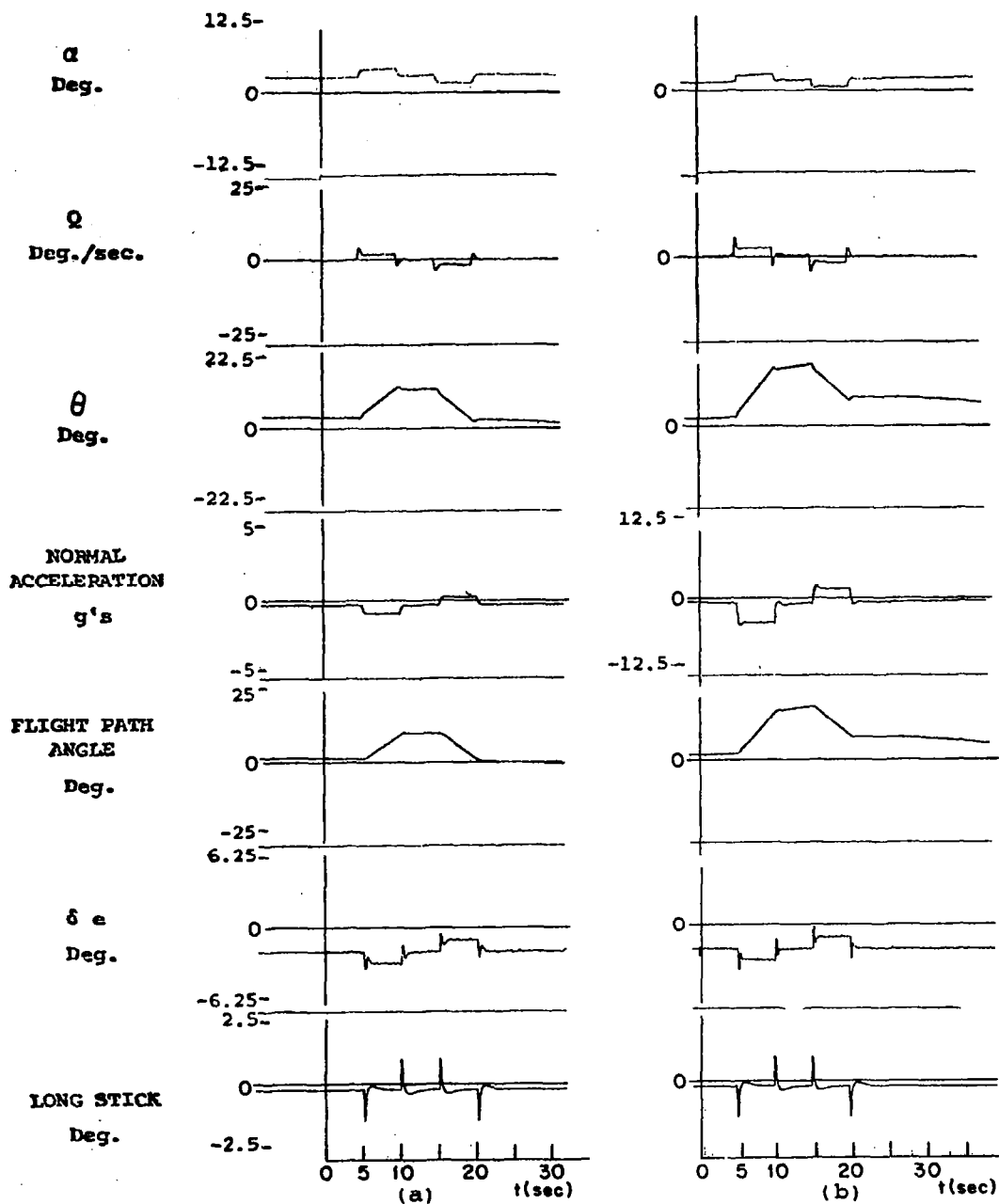
Figure 5.8.13 Longitudinal system responses to elevator doublet command, no turbulence, altitude 304.8 meters

(a)   closed loop responses, speed .53 Mach
(b)   closed loop responses, speed .86 Mach
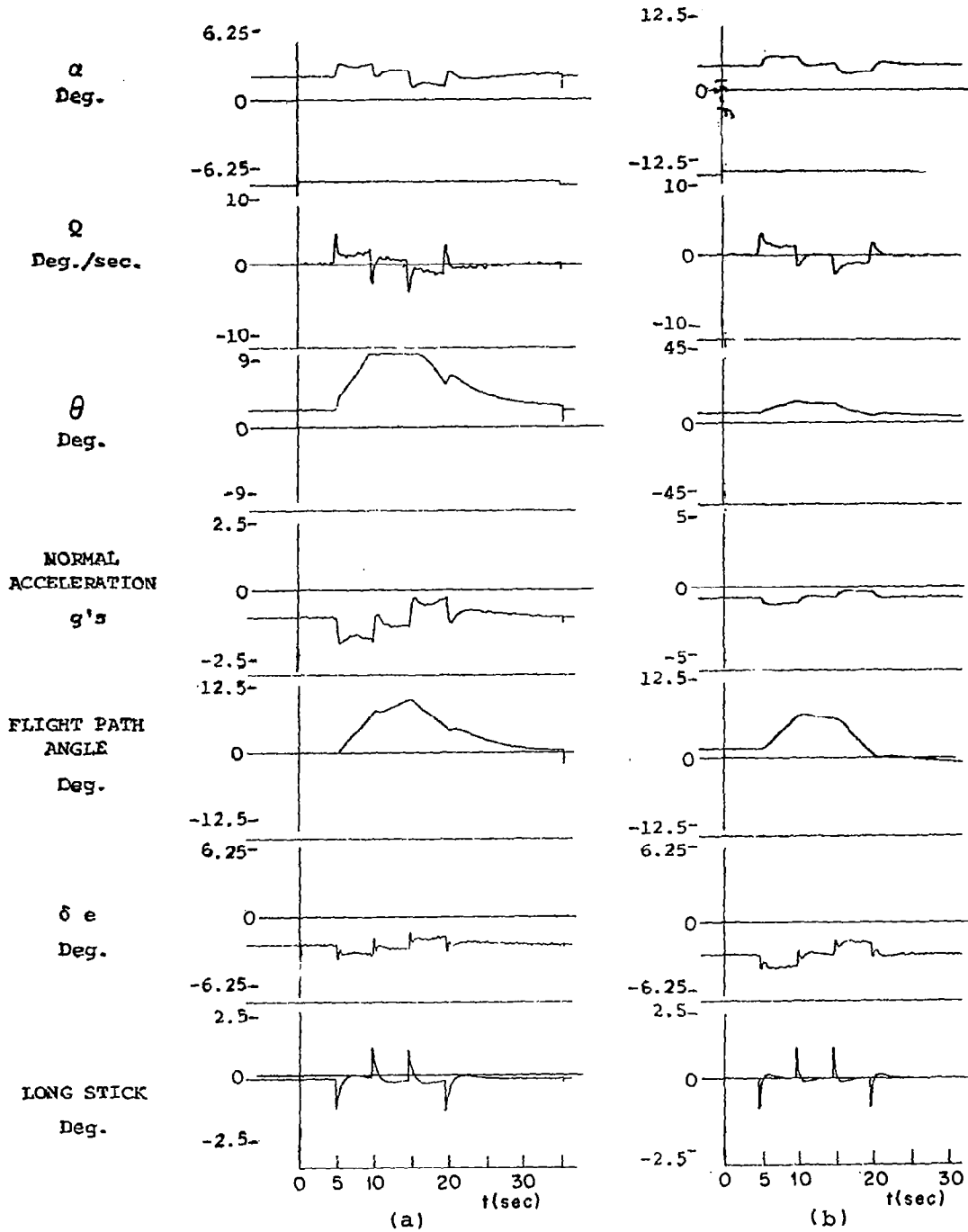
Figure 5.8.14   Longitudinal system responses to elevator doublet command, no turbulence, altitude 6096 meters

(a)   closed loop responses, speed .6 Mach
(b)   closed loop responses, speed .9 Mach
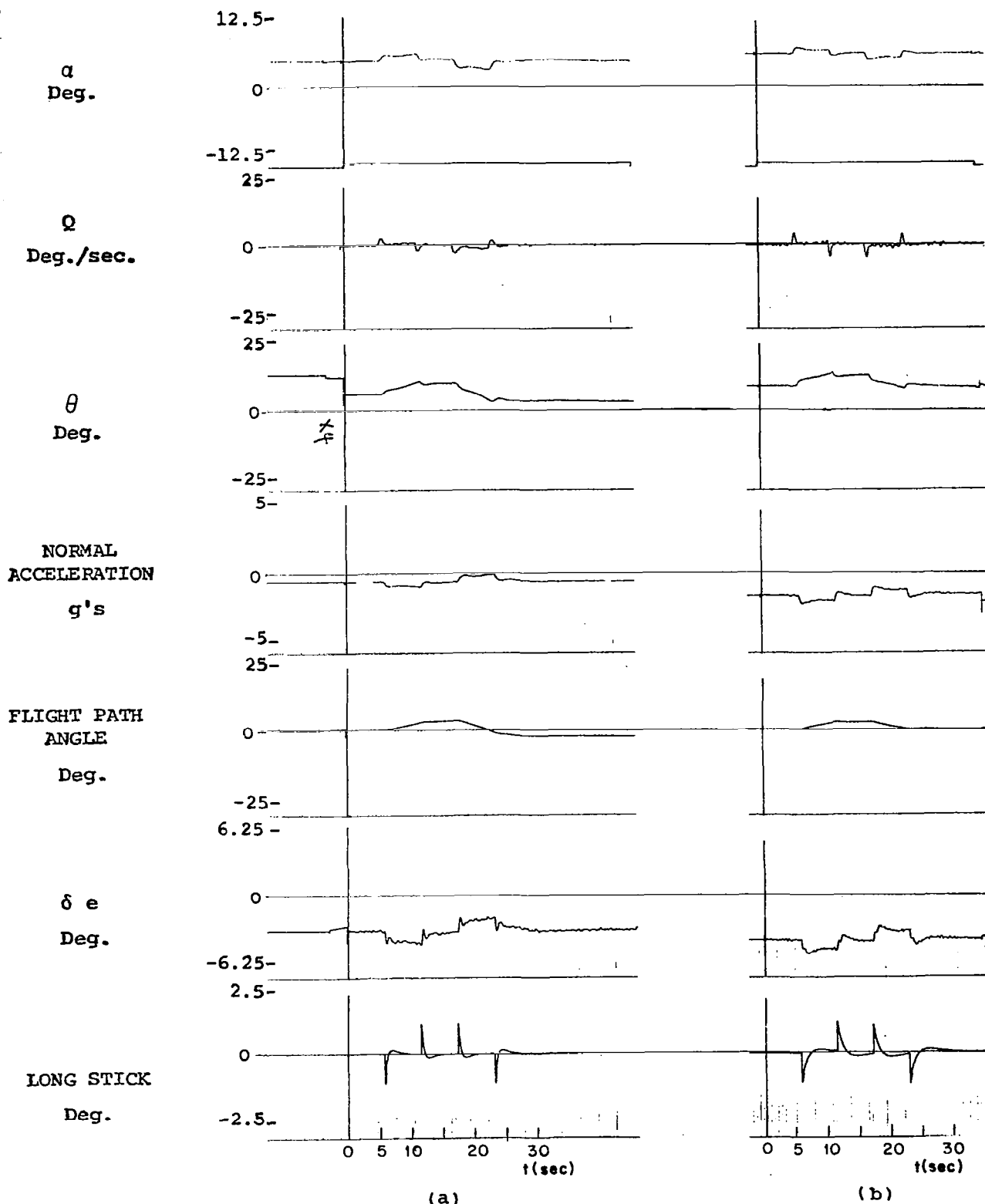
Figure 5.8.15   Longitudinal system responses to elevator doublet command,
no turbulence, altitude 12192 meters

(a)   closed loop responses, speed .6 Mach
(b)   closed loop responses, speed 1.4 Mach

CHAPTER 6

LATERAL AXIS CONTROL AUGMENTATION SYSTEM

6.1 Introduction

This chapter discusses the fixed-point controller designs for the lateral system. The regulators for the individual lateral models were designed using the procedures outlined in Appendix F. The overall design philosophy closely paralleled that used for the longitudinal system but the two controllers were designed independently. After choosing control variables, the development of the cost function is discussed. To incorporate pilot commands, an explicit model-following method was used.

6.2 Choice of Control Variables

As presented in Chapter 3, the model for the lateral states of the aircraft has its input variables the commanded aileron and rudder positions. One decision which was made early in the design process was to actually control rates of these variables. The reasons for making this decision have been discussed in [20], [21]; namely, the presence of integrators in the control loops could be used to compensate for steady-state errors. Thus, the first step in the regulator design was to augment the model given in Chapter 3 to provide for the two integrators necessary to generate position from rate.

The model following problem has been discussed in many papers [32], so only the briefest development is presented here. Model following is essentially a straight-forward extension of regulator theory in which the error between the actual state and the model (i.e., desired) state is penalized.

Assume (6.2.1) represents a given model which describes the behavior to be emulated.

$$\dot{\underline{z}}_M = \underline{A}_M \underline{z}_M + \underline{B}_M \underline{u}_M \tag{6.2.1}$$

The control problem can be posed using the model of (6.2.1) directly, but as is well known, this leads to a control scheme which anticipates the values of $\underline{u}_M$ (i.e., the pilot inputs). This is clearly unreasonable so some assumption must be made as to the character of these inputs. We therefore assume that the signals $\underline{u}_M$ are themselves outputs of a model driven by white Gaussian noise as in

$$\dot{\underline{u}}_M = \underline{A}_p \underline{u}_M + B_p \underline{\nu} \tag{6.2.2}$$

where $\underline{\nu}$ is zero mean white gaussian noise.

One can now combine the aircraft model of Chapter 3 with equations (6.2.1) and (6.2.2) to get

$$\frac{d}{dt}\begin{bmatrix} \underline{x} \\ \underline{z}_M \\ \underline{u}_M \end{bmatrix} = \begin{bmatrix} \underline{A}_{lat} & \vdots & \underline{0} & \vdots & \underline{0} \\ \underline{0} & \vdots & \underline{A}_M & \vdots & \underline{B}_M \\ \underline{0} & \vdots & \underline{0} & \vdots & \underline{A}_p \end{bmatrix}\begin{bmatrix} \underline{x} \\ \underline{z}_M \\ \underline{u}_M \end{bmatrix} + \begin{bmatrix} \underline{0} \\ \underline{0} \\ B_p \end{bmatrix}\nu + \begin{bmatrix} \underline{B}_{lat} \\ 0 \\ 0 \end{bmatrix}\begin{bmatrix} \dot{\delta}_{ac} \\ \dot{\delta}_{rc} \end{bmatrix} \tag{6.2.3}$$

A cost function of the form

$$J = \int_0^{\infty} [(\underline{x} - \underline{H}_M \underline{z}_M)^T \underline{Q}(\underline{x} - \underline{H}_M \underline{z}_M) + \underline{u}^T \underline{R}\underline{u}]dt \tag{6.2.4}$$

with $\underline{u}^T = [\dot{\delta}_{ac} \; \vdots \; \dot{\delta}_{rc}]$ can now be posed so that a control law

$$\underline{u} = [\underline{G}_x \; \vdots \; \underline{G}_z \; \vdots \; \underline{G}_u][\underline{x}^T \; \vdots \; \underline{z}_M^T \; \vdots \; \underline{u}_M^T]^T \quad \text{can be found.}$$

A few comments on the solution of this problem are in order. First of all, as posed above, this is a straightforward variant of the regulator problem discussed in Appendix F and so is easily solved in theory. Secondly, the Separation Theorem implies that the optimal gains $\underline{G}_x$, $\underline{G}_z$ and $\underline{G}_u$ do not depend in any way on the statistics of the white driving noise nor on the value of $\underline{B}_p$. Thus, these are of no further concern. Last, upon writing the Riccati equation for the model following problem some one-way separations become evident. Thus, the control gain $\underline{G}_x$ depends only upon the values of $\underline{A}_{lat}$, $\underline{B}_{lat}$, $\underline{Q}$ and $\underline{R}$ and is therefore independent of the model to be followed. In fact, the matrix $\underline{G}_x$ is exactly the one resulting from solving the conventional regulator problem (i.e., with $\underline{z}_M \equiv \underline{0}$). Furthermore, $\underline{G}_z$ is independent of all assumptions on the pilot input model (i.e., $\underline{A}_p$, $\underline{B}_p$, etc.). Therefore, the choice of models for the input (i.e., $\underline{A}_p$, $\underline{B}_p$) has a minimal effect on the overall solution. Figures 6.2.1 shows the resultant lateral systems designs.

The model used in the model-following scheme has been provided by the Langley staff as a linear model of an aircraft which would be well rated by a pilot. The dynamic equations are
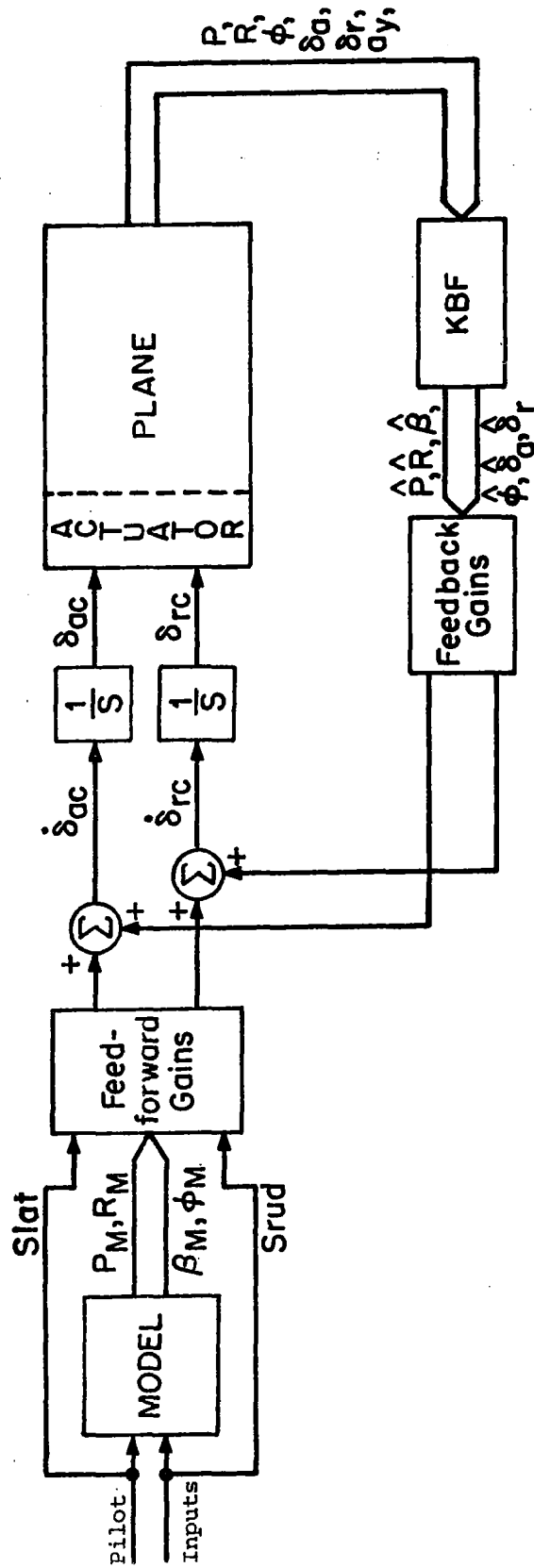
Figure 6.2.1   Structure of Lateral Controller for each Model

$$\dot{\underline{x}}_M(t) = \begin{bmatrix} -4 & .865 & -10. & 0 \\ .04 & -.507 & 5.87 & 0 \\ 0 & -1.0 & -7.43 & g/V_0 \\ 1 & 0 & 0 & 0 \end{bmatrix} \underline{x}_M + \begin{bmatrix} 20 & 3.3 \\ 0 & -3.1 \\ 0 & 0 \\ 0 & 0 \end{bmatrix} \underline{u}_M \qquad (6.2.5)$$

where

$$\underline{x}_M' = [p_M, \ r_M, \ \beta_M, \ \varphi_M]$$

and

$$\underline{u}_M' = [\delta_{ail}, \ \delta_{\gamma ud}].$$

It should be noted that the lateral model of Eq. (6.2.5) is flight condition dependent through the term g/V_0. Hence, the desired lateral response of the aircraft, as dictated by the lateral model (6.2.5), will change from flight condition to flight condition. Essentially, the term g/V_0 allows the aircraft to execute coordinated turns without excessive sideslip and lateral accelerations at different speeds.

On the other hand, under the design ground rules the measurement of the aircraft velocity V_0 could not be included in the implementation of the control system. Since the model (6.2.5) is an integral part of control system, see Fig. 6.2.1, a constant value for V_0 had to be selected. The one selected was that corresponding to flight condition #11 (V_0 = 189.13 m/sec or 620.5 ft/sec) for all subsequent simulations.

The choice of a constant V_0 for the model represents a serious shortcoming as far as the handling lateral quantities of the aircraft

for large bank angles are concerned. If the actual velocity of the
aircraft is near the selected value V_0, then the aircraft lateral
response should be satisfactory. On the other hand, when the
aircraft velocity is drastically different from V_0 one may need
to have excessive sideslip and lateral acceleration in order to hold
bank angle at its commanded value. This will be illustrated in
Section 6.4.

It should be remarked that the shortcoming, of the possible poor
lateral responses are not due to the MMAC philsophy, but rather due to
the fact that the aircraft velocity was not measured nor estimated
in the design.

As discussed earlier, a stochastic model of the form of equation
(6.2.2) is needed to model the actual pilot inputs. It should be pointed
out that all of the control gains ($\underline{G}_x$, $\underline{G}_z$, and $\underline{G}_u$) are independent of
$\underline{B}_p$ and the statistics of $\underline{v}$. Thus, they are ignored in the following.

Many models of the form of (6.2.2) are possible. In the design
presented here, $\underline{A}_p = 0$ was used to obtained the $\underline{G}_u$ feedback gain. This
was chosen principally to help the controller anticipate the model re-
sponse and thereby keep the model-following errors small.

6.3 Cost Function Development

Designing a quadratic cost function which would provide good aircraft
response at all flight conditions proved to be a difficult task. This is
in contrast to the longitudinal system where a minimum number of iterations
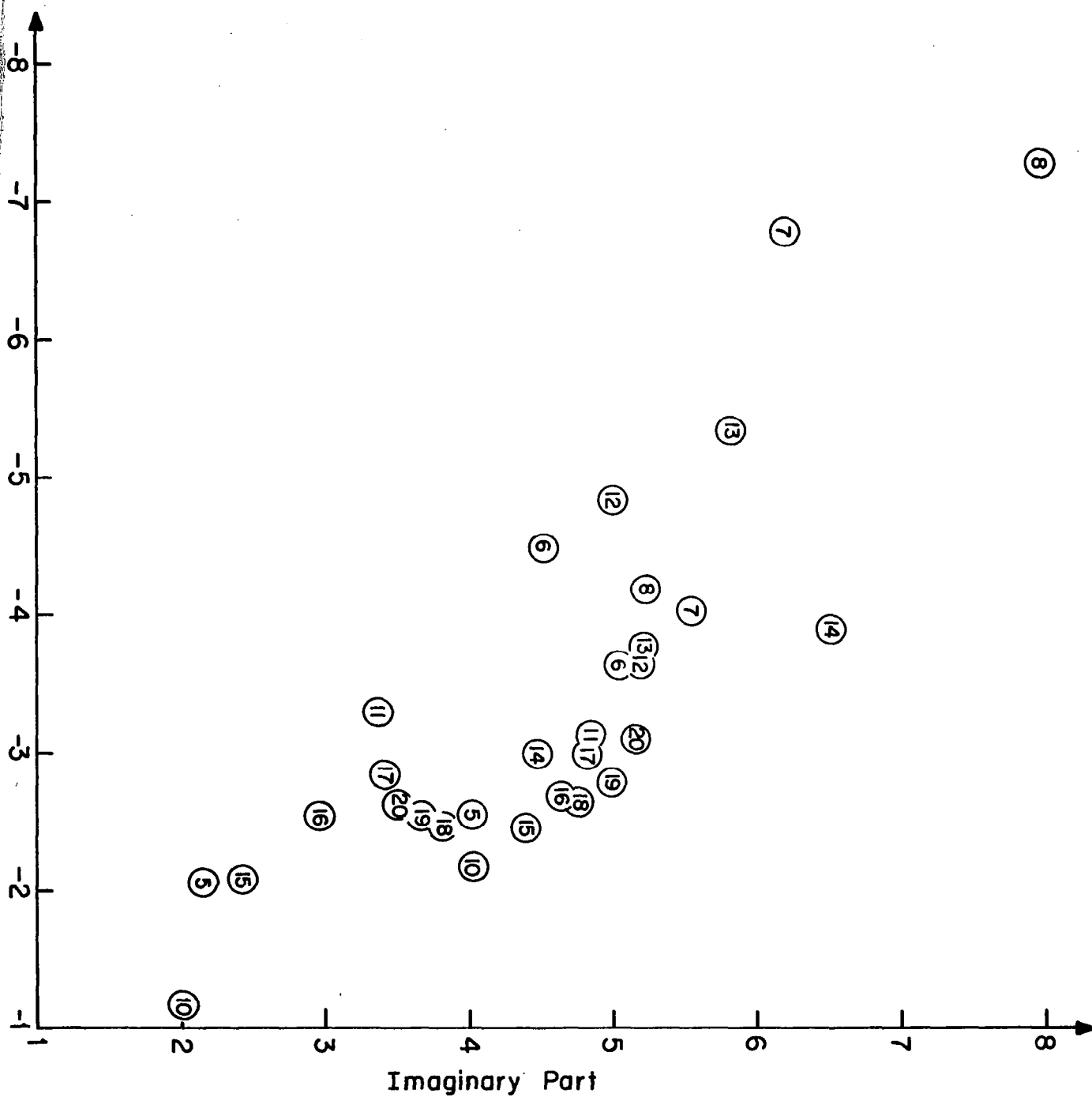
Figure 6.3.1   Complex Eigenvalues of Closed-loop Lateral Control System

were needed. This complication is partly due to a tight coupling between the various modes in the lateral dynamics, and the use of a specific model following concept.

The basic philosophy for determining the control and state penalties for the first iteration in the design was to determine those qualities considered important in aircraft performance, and then to weigh these quantities in the cost function by the inverse of the maximum allowable deviations in the quantities of interest. After discussions with NASA staff, it seemed that the most important quantity to penalize was the lateral acceleration. For the control penalty the rate saturation value was used. The aileron rate saturation value δ_{amax} was modified by a factor of two-thirds to reflect a greater willingness on the part of the pilot to saturate the rudder rate $\dot{\delta}_{rmax}$ compared to the aileron rate.

For the regulator, this leads to a cost function of the form,

$$ J_1(u) = \int_0^\infty \left(\frac{a_y(t)}{a_{ymax}}\right)^2 + \left(\frac{\dot{\delta}_{ac}(t)}{\frac{2}{3}\dot{\delta}_{amax}}\right)^2 + \left(\frac{\dot{\delta}_{rc}(t)}{\dot{\delta}_{rmax}}\right)^2 \; dt \qquad (6.3.1) $$

$\dot{\delta}_{amax}$ and $\dot{\delta}_{rmax}$ were given by hardware limitations while for a_{ymax} a value of .25 g's was decided upon. A summary of the progression of cost functions is shown in Table 6.3.1. These cost functions have been discussed in [30].

In order to overcome the poor convergence of the sideslip angle and the fast convergence of the bank angle, penalties on sideslip angle and

roll rate were added. The weights of the penalties on these variables were determined largely by limited trial-and-error. It was desirable to make this added penalty not affect the good qualities of response already achieved with respect to lateral acceleration and also to make any variations due to differences between flight conditions "automatic". Therefore, it was decided to add a fraction of the roll rate and sideslip angle penalties to the penalty function. After some experimentation, values of 10% of the penalty due to lateral acceleration alone were chosen. Thus, the cost function became:

$$J_2(u) = J_1(u) + \int_0^\infty [K_1 p^2(t) + K_2 \beta^2(t)] dt \qquad (6.3.2)$$

with

$$K_1 = .1\left(\frac{V_0}{g} (a_{31} - \alpha_0)\right)^2 \qquad (6.3.3)$$

and

$$K_2 = .1\left(\frac{V_0}{g} a_{33}\right)^2 \qquad (6.3.4)$$

A relatively mild penalty on bank angle was added to the cost function to prevent the aircraft from banking excessively; thus the cost function became:

TABLE 6.3.1

SUMMARY OF COST FUNCTION PROGRESSION FOR THE LATERAL DYNAMICS

Variable penalized	1	2*	3	4
$\dot{\delta}_{amax}$	$\frac{2}{3}(140°/sec)$	$\frac{2}{3}(140°/sec)$	$\frac{2}{3}(140°/sec)$	$\frac{2}{3}(140°/sec)$
$\dot{\delta}_{rmax}$	70°/sec	70°/sec	70°/sec	70°/sec
a_{ymax}	.25 g's	.25 g's	.25 g's	.25 g's
p_{max}^{**}	0	K_1^*	K_1	K_1
β_{max}^{**}	0	K_2^*	K_2	K_2
ϕ_{max}	0	0	45°	15°

*K_1 and K_2 were derived largely by trial and error resulting in many variations between iteration 1 and 2.

**K_1 and K_2 are given in the text, Eqs. (6.2.3) and (6.2.4)

$$J_3(u) = J_2(u) + \int_0^\infty \left[\frac{\phi(t)}{\phi_{max}}\right]^2 dt \qquad (6.3.5)$$

It was found that in order to design the model-following scheme used to implement pilot commands, the bank angle penalty had to be included; the value of ϕ_{max} was chosen to be 15°. The resulting cost function for the model-following problem can then be interpreted as:

$$J(u) = \int_0^\infty \left[\frac{a_y - a_{y_{model}}}{a_{y_{max}}}\right]^2 + \left[\frac{p - p_{model}}{p_{max}}\right]^2 + \left[\frac{\beta - \beta_{model}}{\beta_{max}}\right]^2$$

$$+ \left[\frac{\phi - \phi_{model}}{\phi_{max}}\right]^2 + \left[\frac{\dot{\delta}_{ac}}{\frac{2}{3}\dot{\delta}_{amax}}\right]^2 + \left[\frac{\dot{\delta}_{rc}}{\dot{\delta}_{rmax}}\right]^2 \quad dt \quad (6.3.6)$$

In converting equation (6.3.6) into the form of (6.2.4) it is necessary to use a linear approximation to the a_y and $a_{y_{model}}$ terms. This approximation is discussed further in Appendix E. Controller gains were then calculated for all flight conditions using this cost function.

Using the equivalent discrete-time models of Appendix E, Kalman filters were designed to operate at a sampling interval of 1/8 sec., using measurements of roll rate, yaw rate, bank angle, lateral acceleration, aileron

and rudder angles, assuming the sensor noise rms values quoted in
Table 3.8.1, and a 4.75 m/sec rms value in the wind disturbance
model of Section 3.4.

The feedback gain from the wind state was set to zero, because
of the slow convergence of the Kalman filter estimate for the wind
state. The feedforward and feedback gains were converted to equi-
valent discrete-time gains with a sampling interval of 1/8 sec. as
described in Appendix F. The discrete time control gains are shown
in Appendix H. Kalman filter gains and discrete-time control and
filter eigenvalues are listed in Appendices K and L, respectively.
Figure 6.3.1 contains a plot of the continuous-time complex
eigenvalues.

6.4 Simulation Results

In this section some simulation results are shown for six selected flight
conditions. The first simulations give the response to beta gust (sideslip)
disturbances for both the unaugmented airplane and the regulated one. The
simulations were conducted at both no turbulence and 4.57 m/sec
rms wind turbulence. They highlight the improvements introduced by
the MMAC system in gust-alleviation, and in reducing the rms level of
continuous turbulence effects. Figures 6.4.1 to 6.4.6 contain the
lateral system responses to a 2° beta gust under no turbulence
at various flight conditions. These simulations highlight the damping

of the effects of initial gusts. Figures 6.4.7 to 6.4.12 contain the lateral system responses to a two-degree beta gust under a 4.57 m/sec. rms turbulence level. These simulations highlight the reduction of the rms level of continuous disturbance. The simulations were conducted using NASA Langley's nonlinear simulation of the F-8C aircraft.

Figures 6.4.13 to 6.4.18 illustrate the response of the aircraft to a 2° doublet command in the lateral stick at various flight condi-tions. Both the model states and the aircraft states are shown; no turbulence is used in these runs. These results indicate that both the roll rate and bank angle follow the model well. Further, when the aircraft is near flight condition 11 (the flight condition around which the model is based in terms of the numerical value of V_0) the lateral acceleration remains small. However, for other flight conditions (i.e., see Figure 6.4.17) lateral acceleration becomes large. Also, sideslip angle does not follow the model.

As mentioned in Section 6.2 these problems are primarily due to:

(a) Using a fixed model based on FC 11.

(b) The use of an approximation in computing $a_{y_{model}}$ in equation (6.3.6) resulting in $a_{y_{model}}$ being nonzero.

A change in the model to be followed is clearly indicated, possibly resulting in a simpler model which would not involve sideslip

angle or lateral acceleration. The essential idea would be to remove

the $a_{y_{model}}$ term from equation (6.3.6) and thereby always require a_y

to near zero.

It should be noted that no rudder pedal response characteristics

have been presented. The philosophy followed was to design a feet-on-

the-floor controller in which the rudder surface would be automatically

controlled. Thus, the rudder pedal response was not of concern.

Additionally, the simulations were conducted using a complete sampled-

data LQG controller, with Kalman filters and instrument noises included.
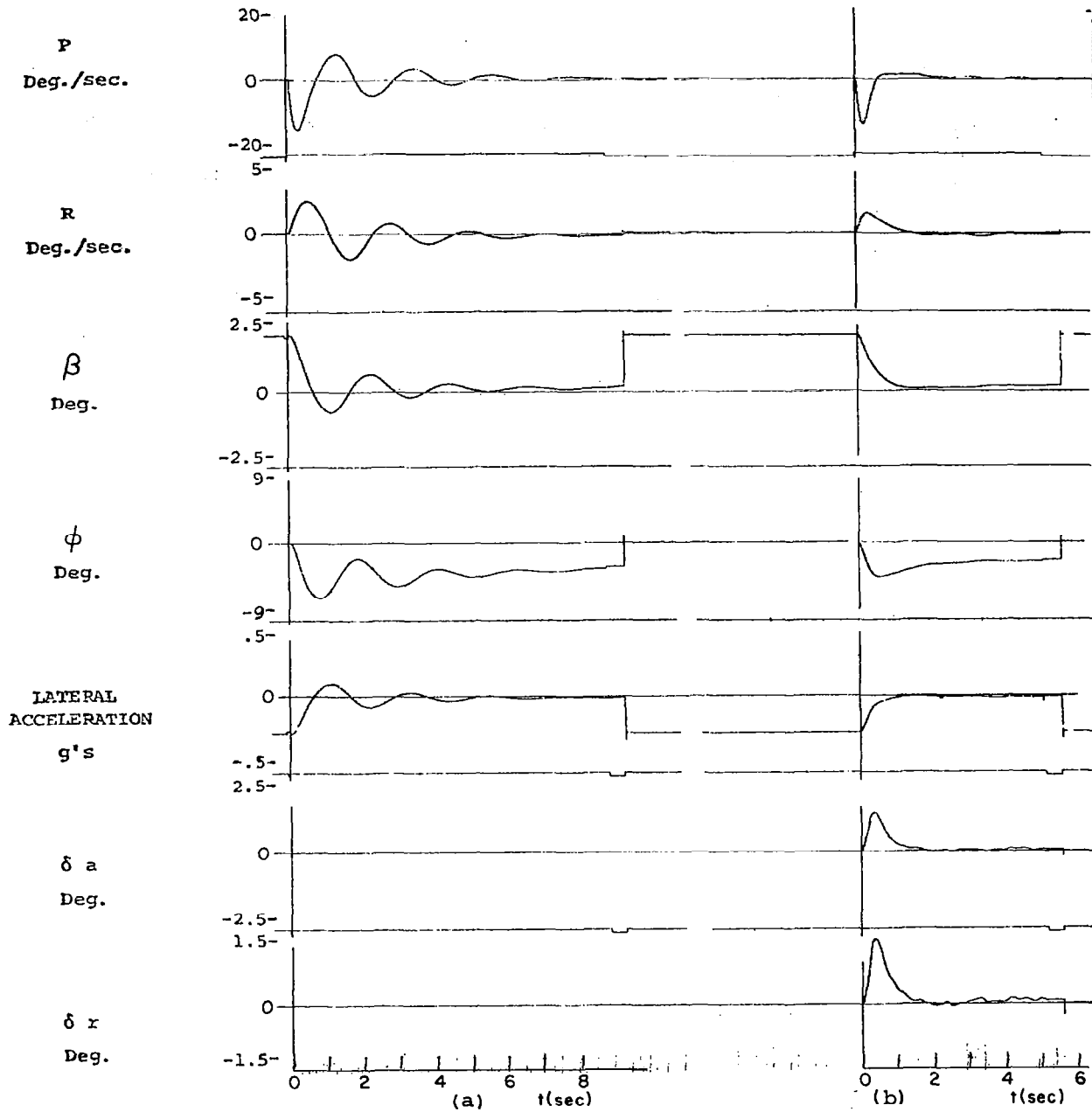
Figure 6.4.1   Lateral system responses to initial 2° β perturbation, no turbulence, altitude 304.8 meters, speed .53 Mach

(a)   open loop responses
(b)   closed loop responses
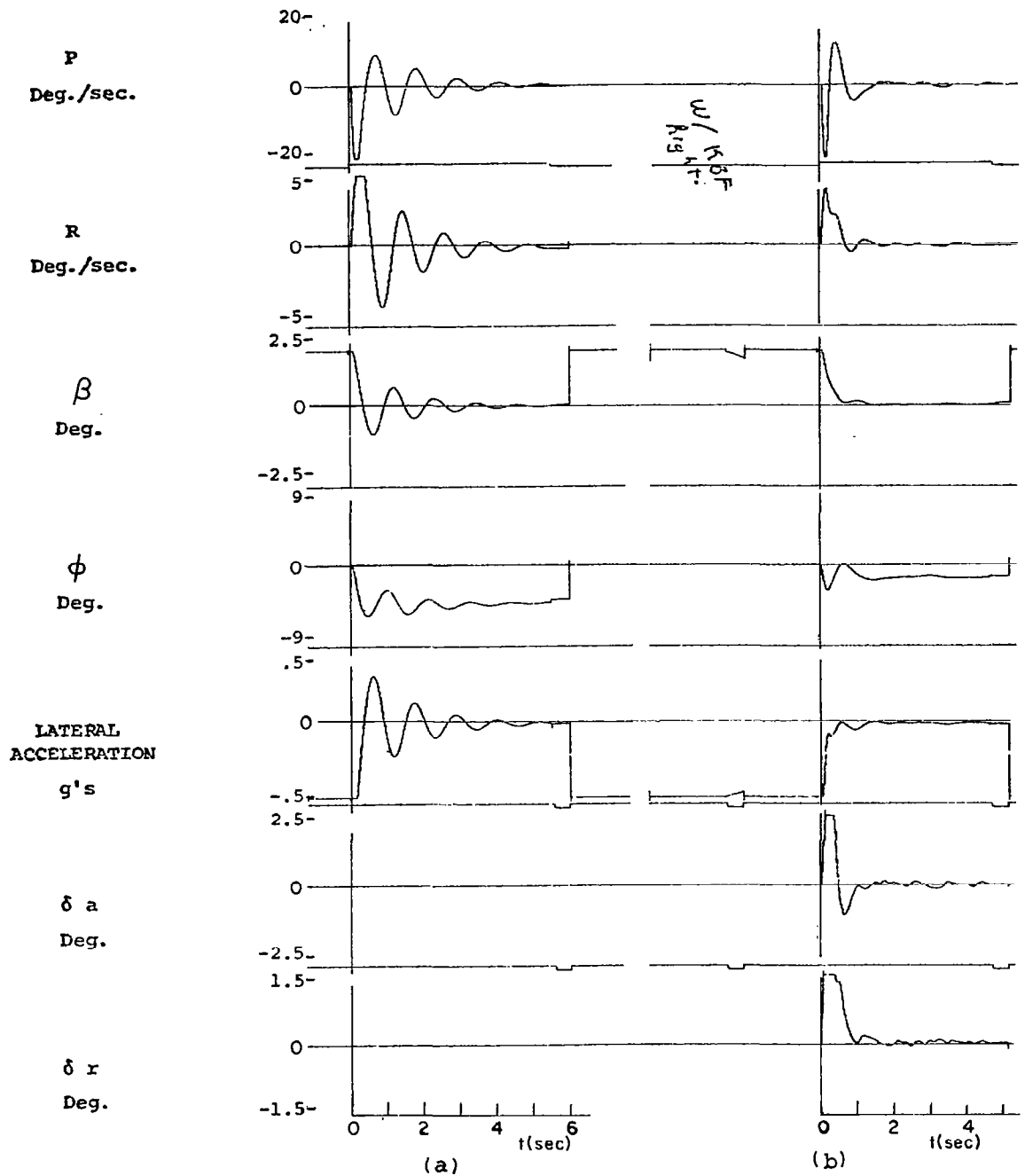
Figure 6.4.2   Lateral system responses to initial 2°β perturbation, no
turbulence, altitude 304.8 meters, speed .86 Mach

(a)   open loop responses
(b)   closed loop responses
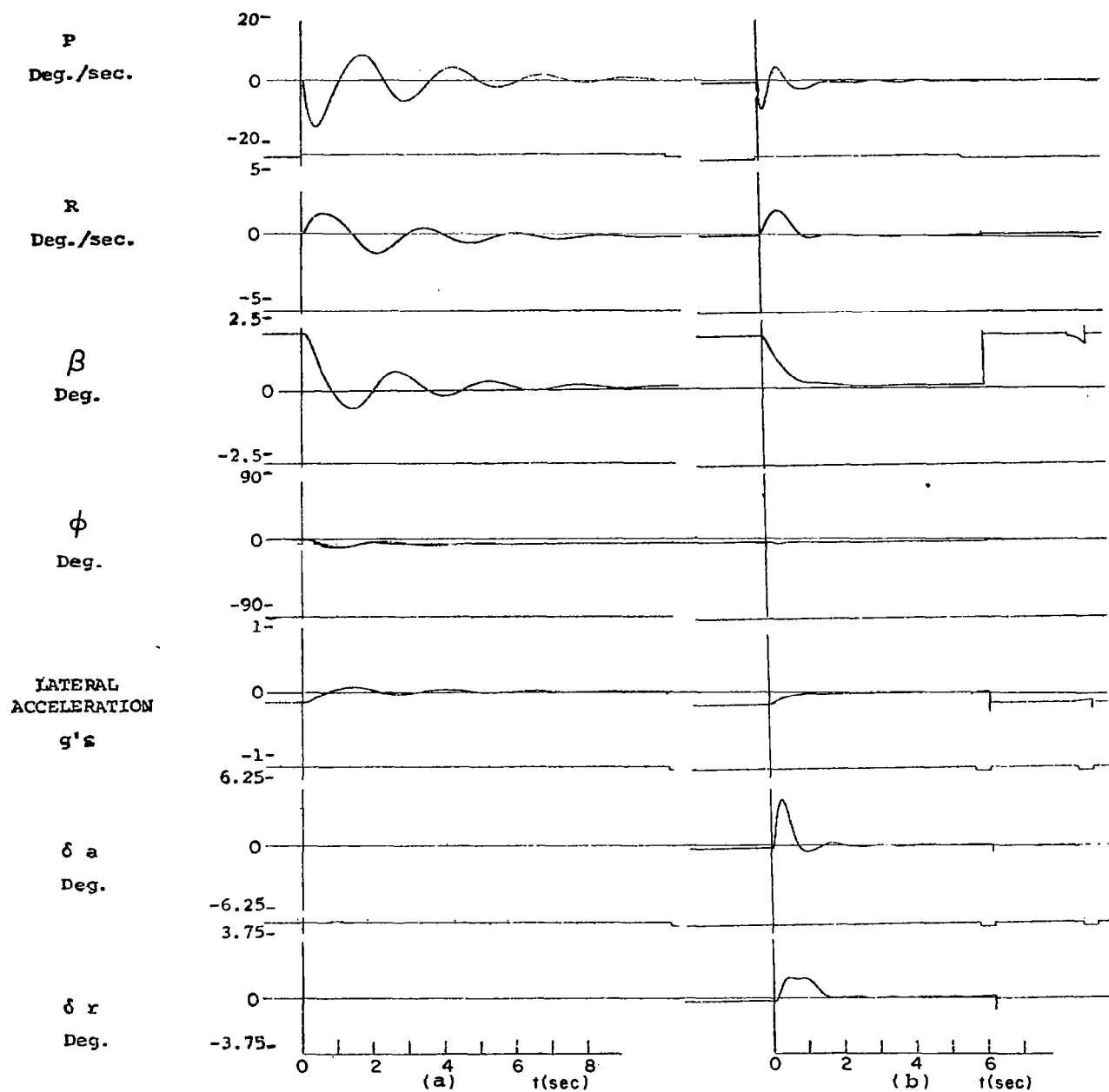
Figure 6.4.3 Lateral system responses to initial 2° β perturbation, no
turbulence, altitude 6096 meters, speed .6 Mach

(a) open loop responses
(b) closed loop responses
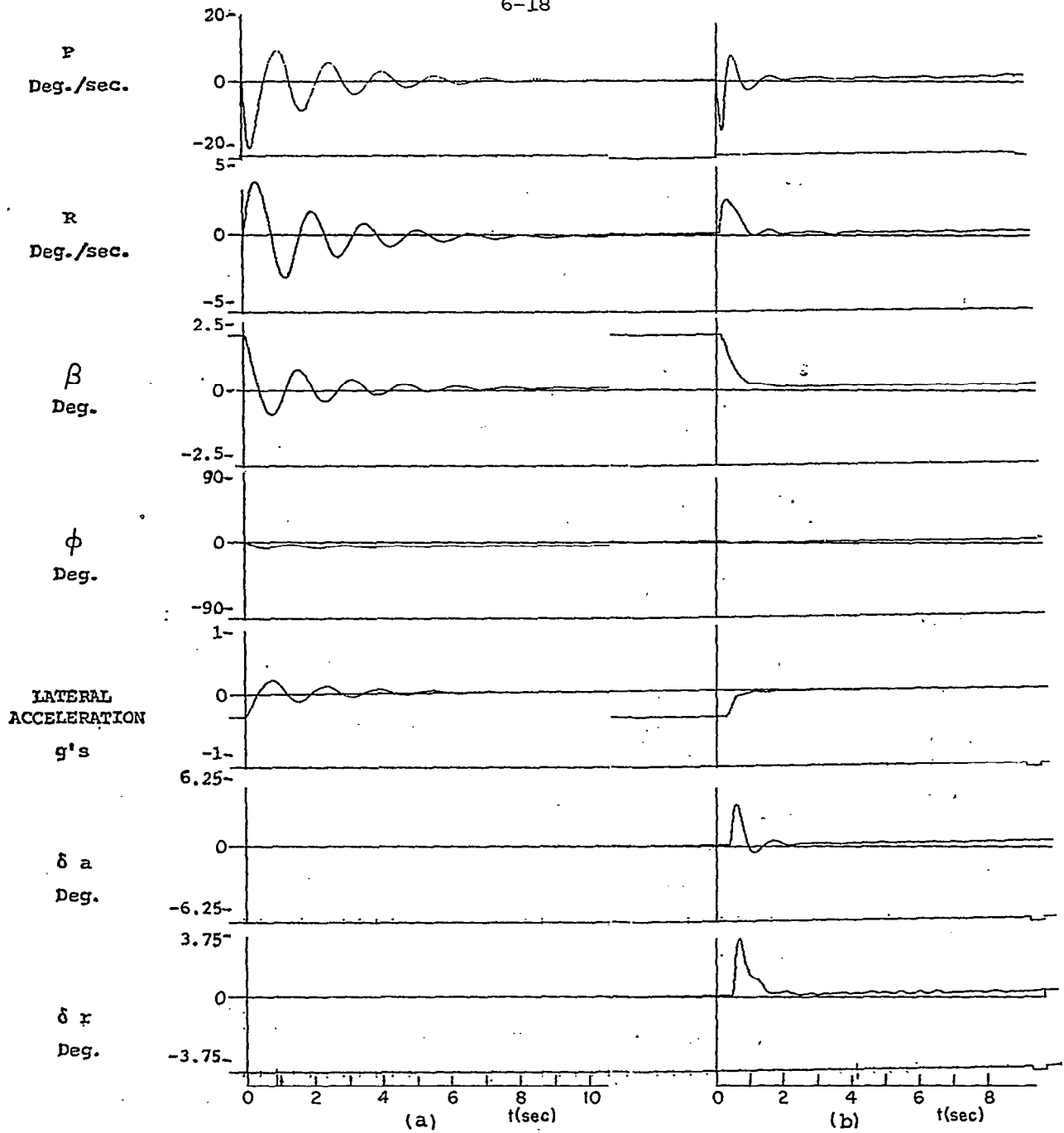
Figure 6.4.4   Lateral system responses to initial 2° β perturbation, no
turbulence, altitude 6096 meters, speed .9 Mach

(a)   open loop responses
(b)   closed loop responses
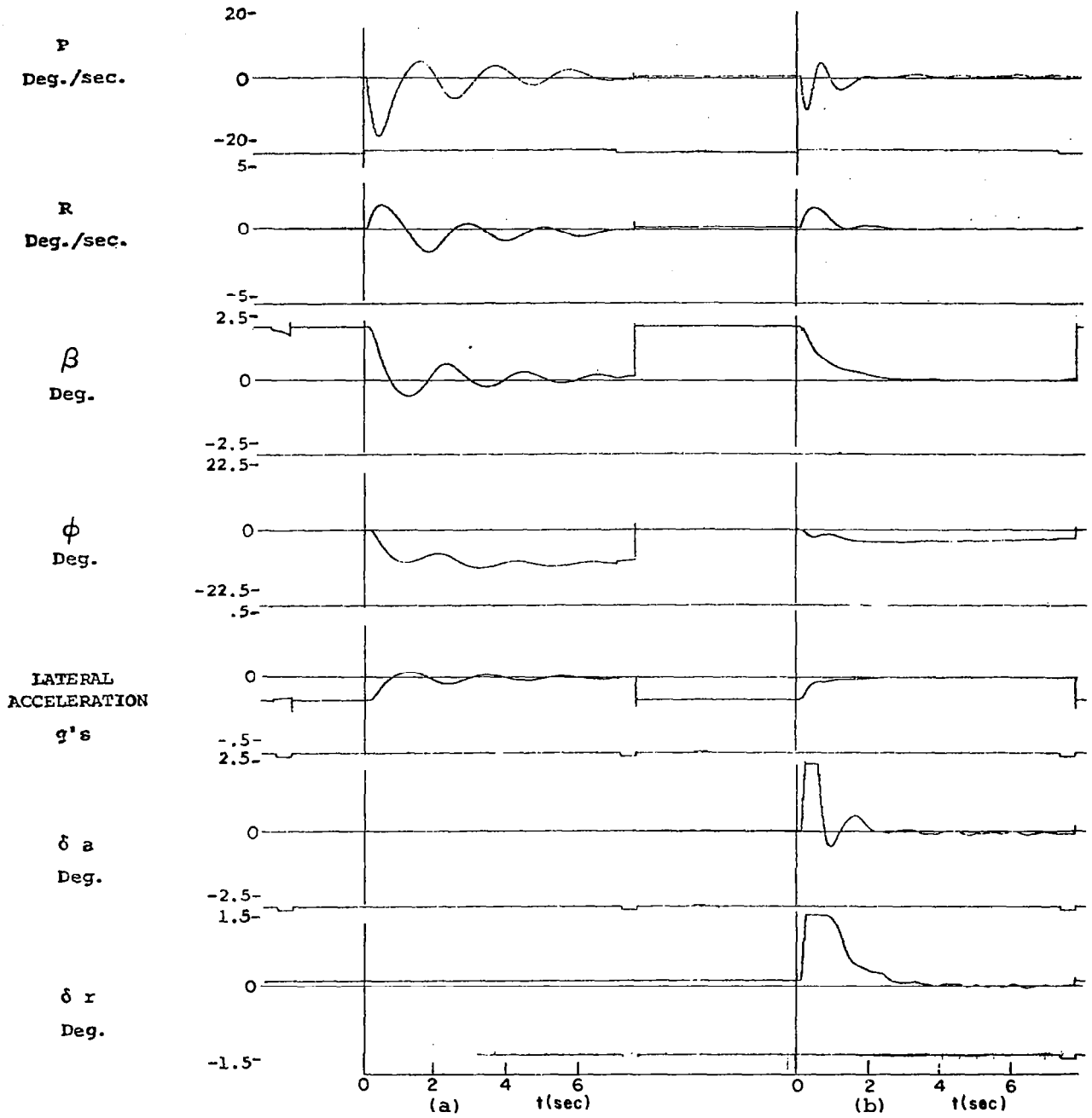
Figure 6.4.5 Lateral system responses to initial 2° β perturbation, no
turbulence, altitude 12192 meters, speed .9 Mach

(a)   open loop responses
(b)   closed loop responses
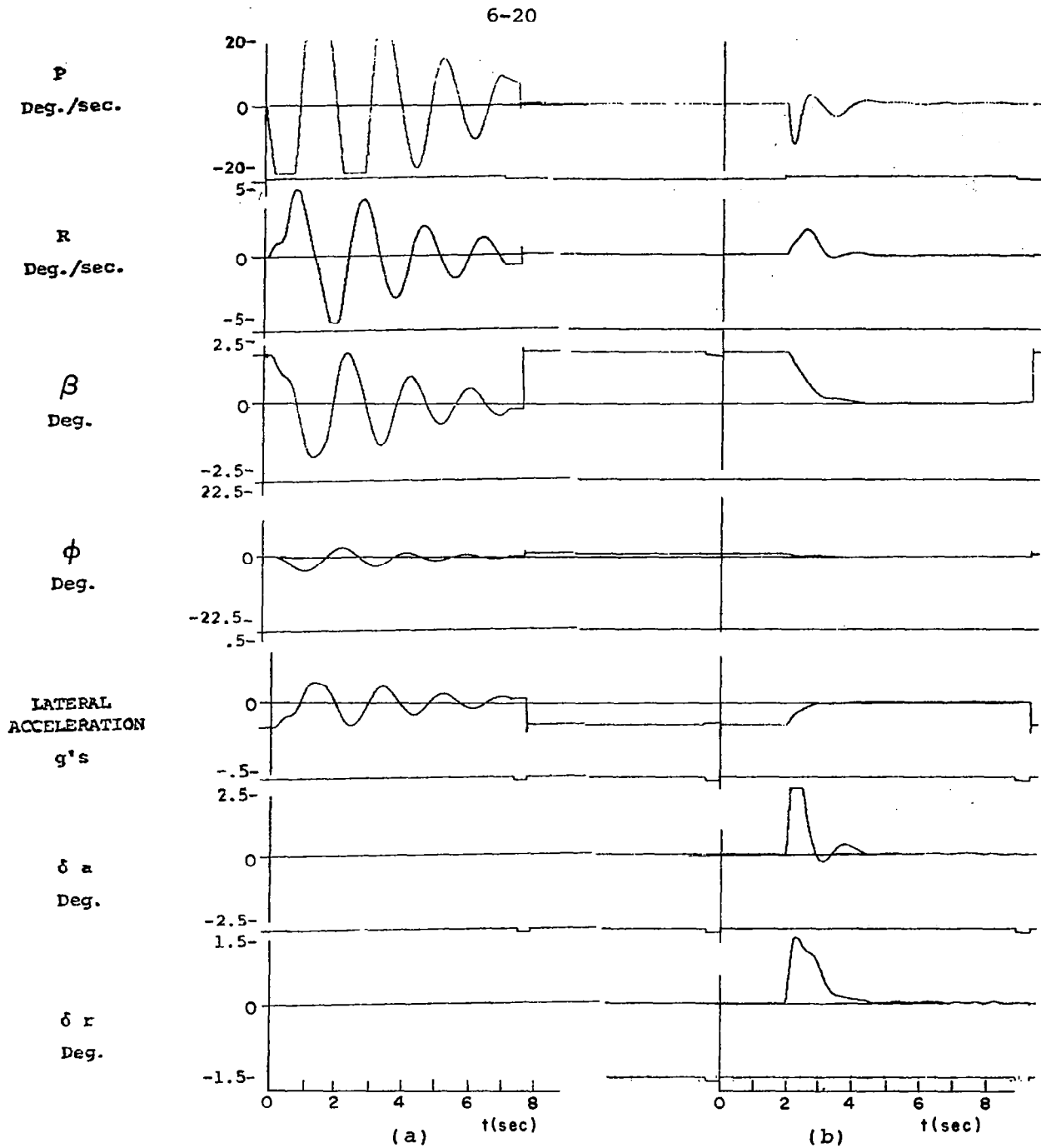
Figure 6.4.6   Lateral system responses to initial 2° β perturbation, no
turbulence, altitude 12192 meters, speed 1.4 Mach

(a)   open loop responses
(b)   closed loop responses
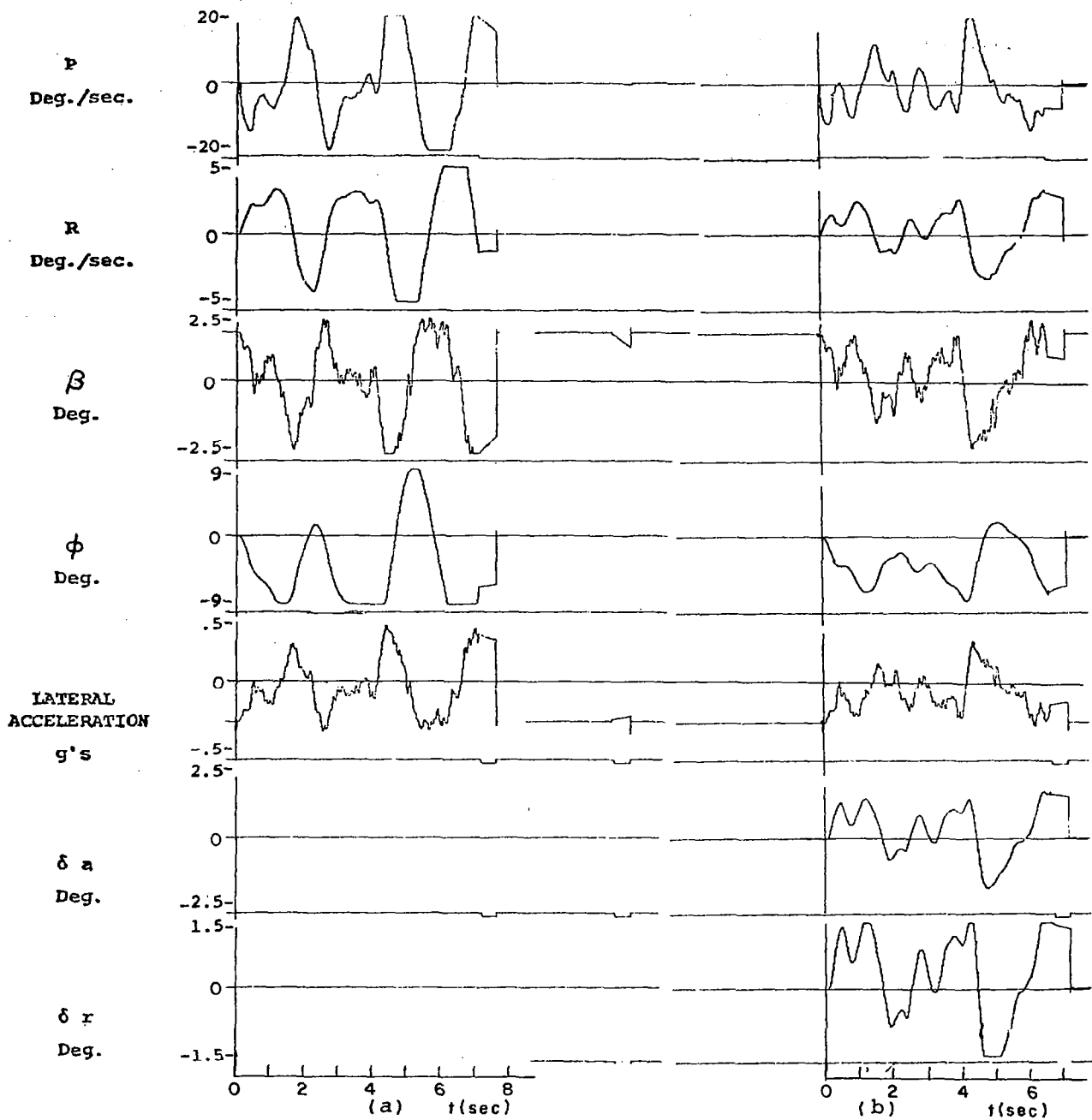
Figure 6.4.7   Lateral system responses to initial 2°β perturbation,
turbulence level 4.57 m/sec rms, altitude 304.8 meters,
speed .53 Mach

(a)   open loop responses
(b)   closed loop responses
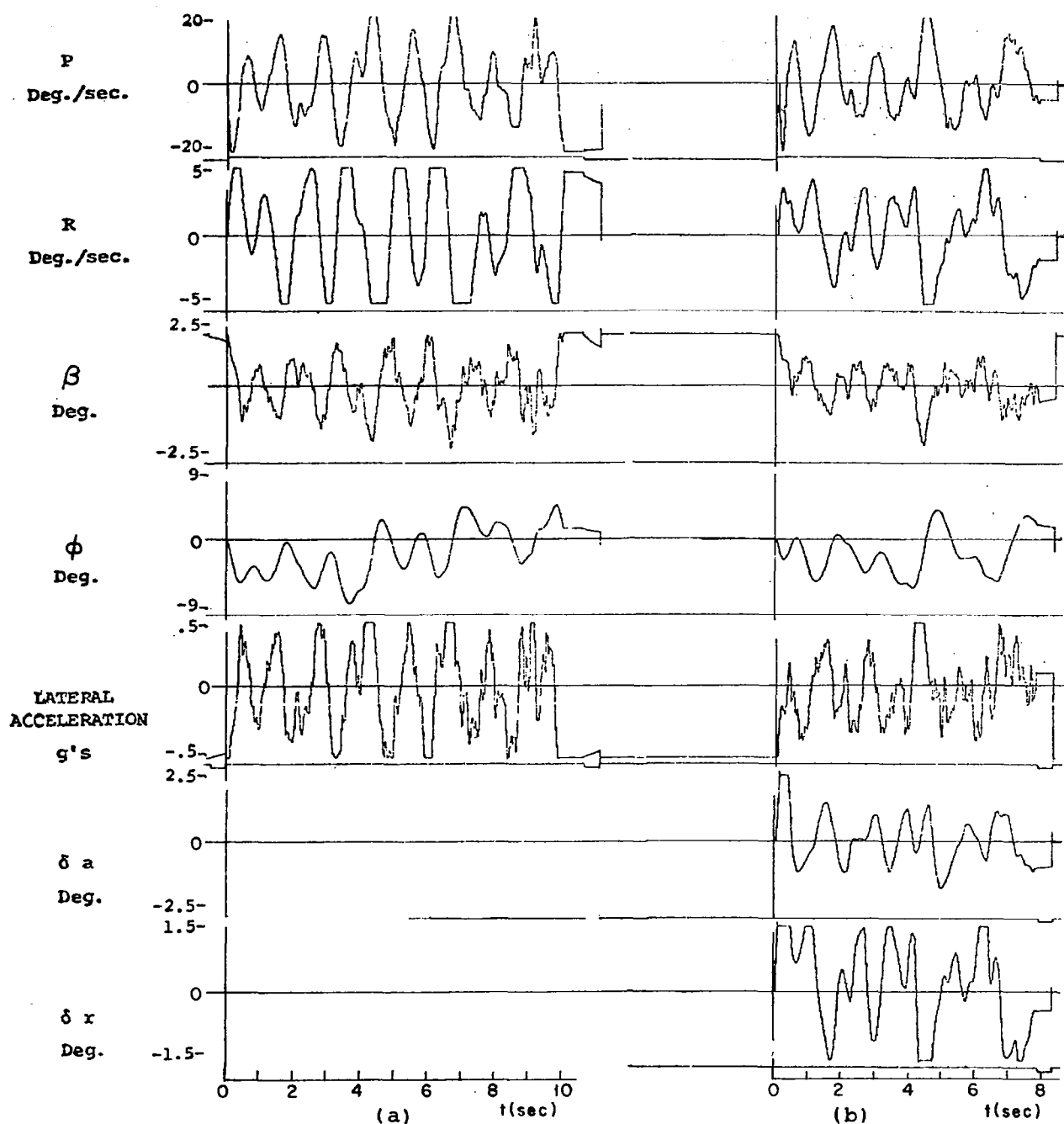
Figure 6.4.8   Lateral system responses to initial 2°β perturbation,
               turbulence level 4.57 m/sec rms, altitude 304.8 meters,
               speed .86 Mach

               (a)   open loop responses
               (b)   closed loop responses
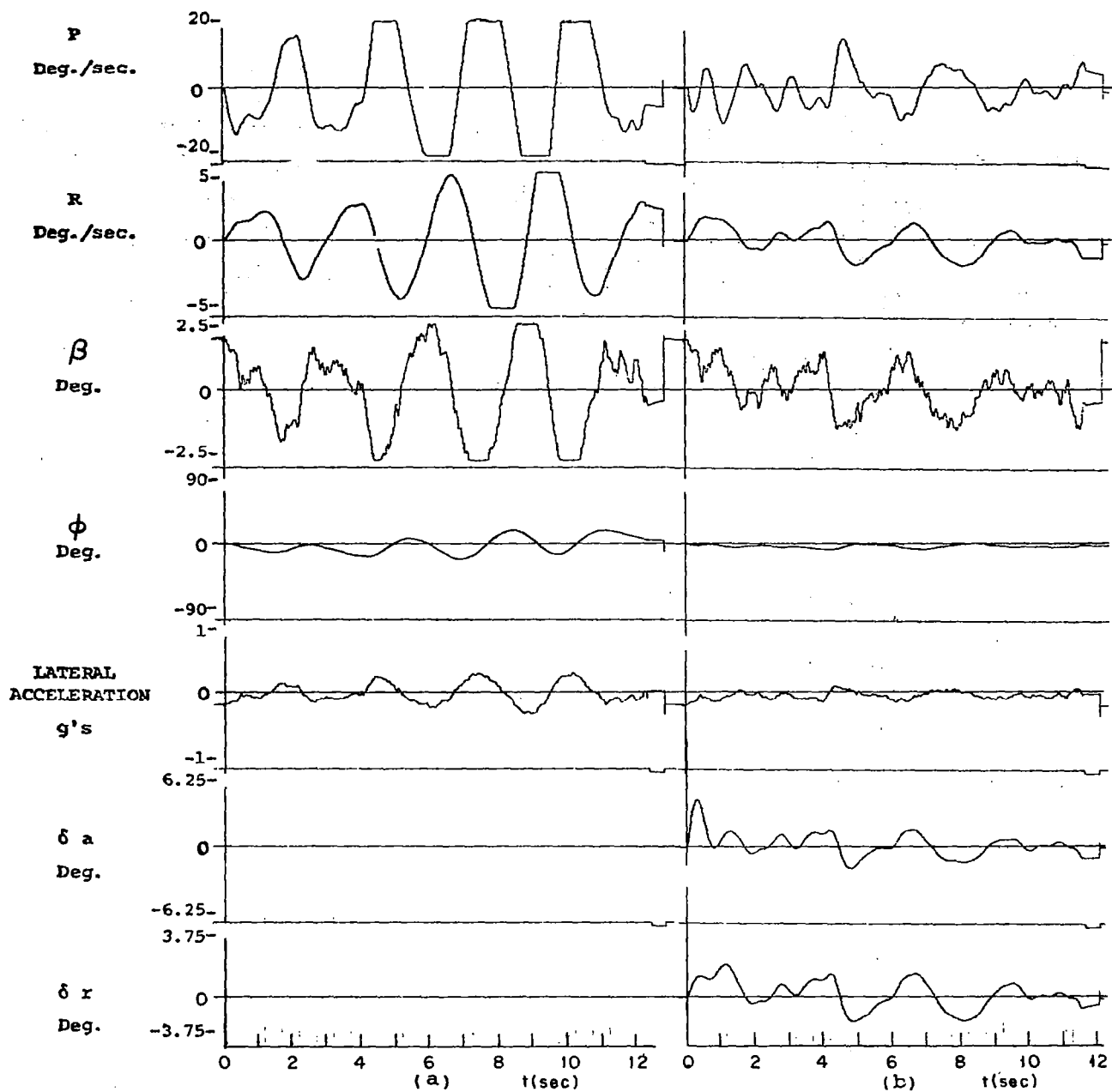
Figure 6.4.9   Lateral system responses to initial 2°β perturbation,
turbulence level 4.57 m/sec rms, altitude 6096 meters,
speed .6 Mach

(a)   open loop responses
(b)   closed loop responses
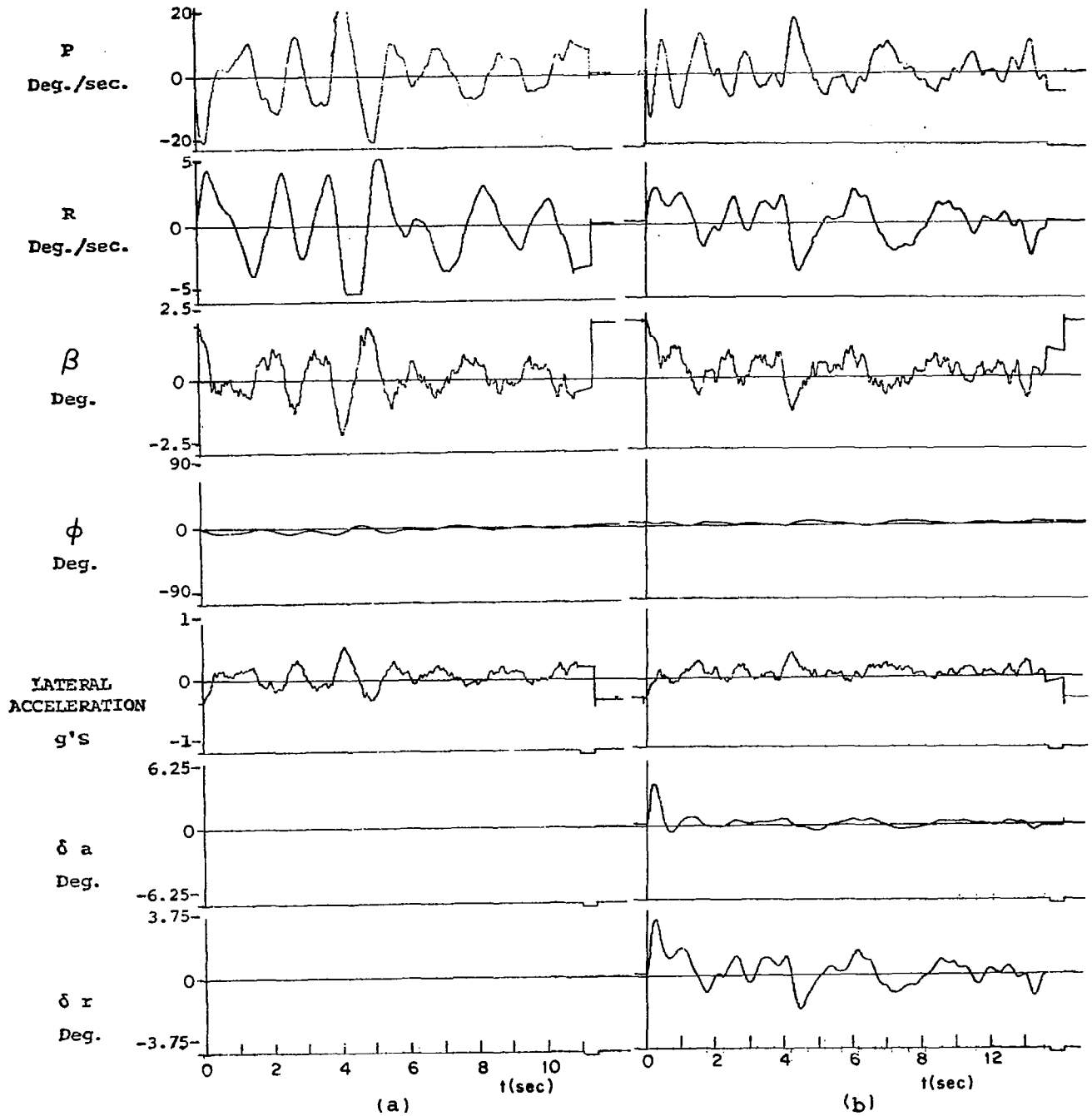
Figure 6.4.10 Lateral system responses to initial 2°β perturbation, turbulence level 4.57 m/sec rms, altitude 6096 meters, speed .9 Mach

(a) open loop responses
(b) closed loop responses
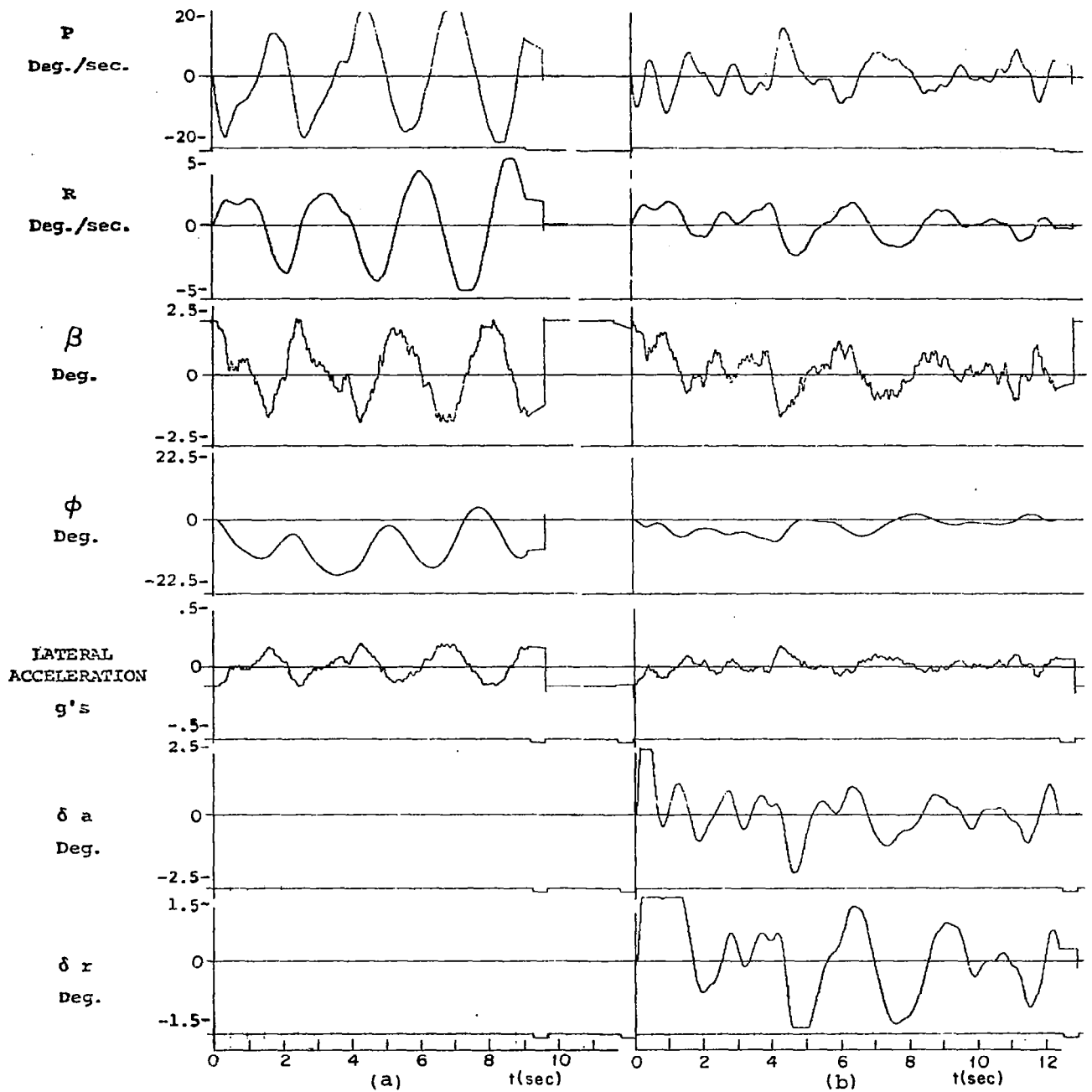
Figure 6.4.11   Lateral system responses to initial 2°β perturbation,
turbulence level 4.57 m/sec rms, altitude 12192 meters,
speed .9 Mach

(a)   open loop responses
(b)   closed loop responses
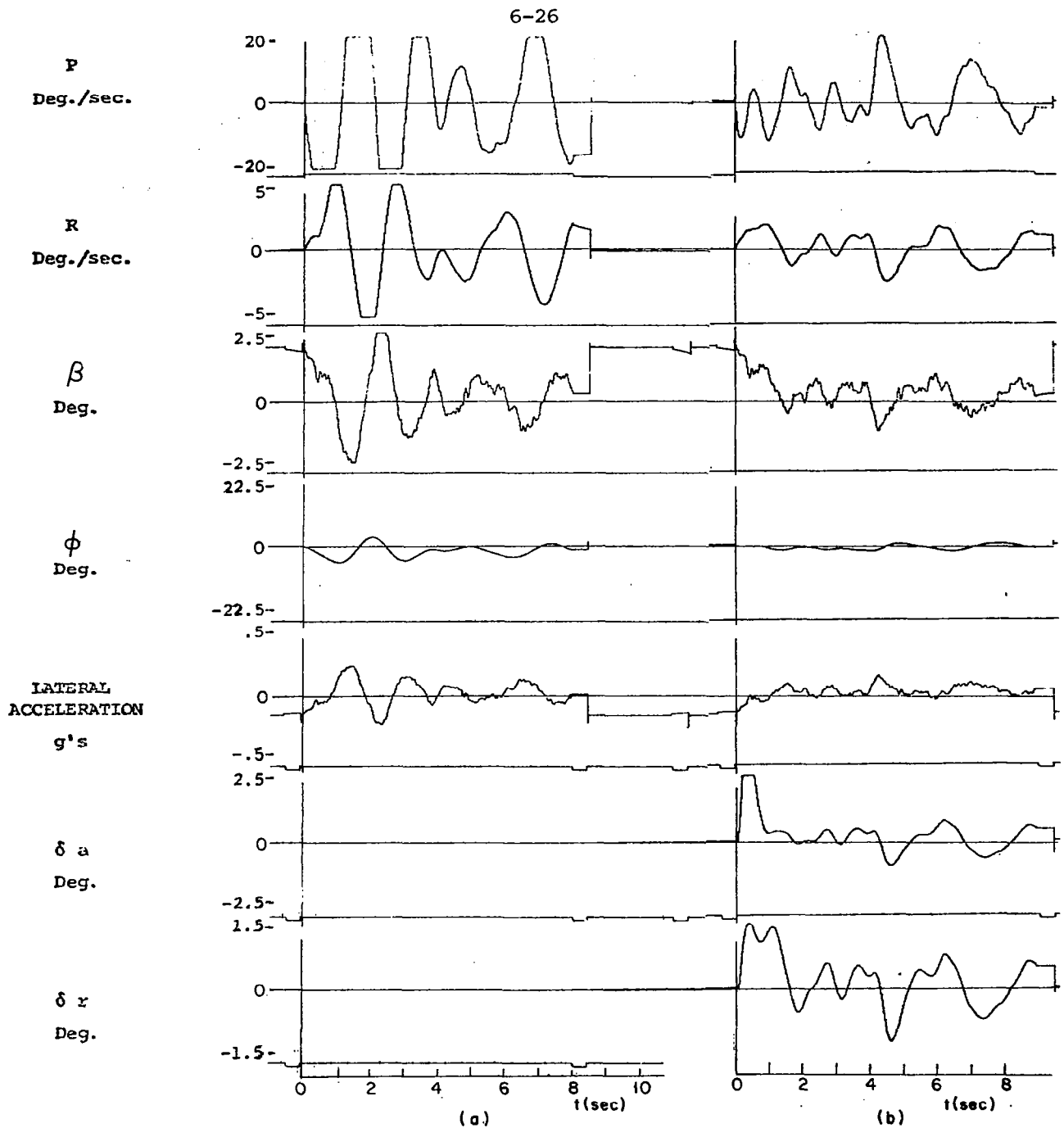
Figure 6.4.12 Lateral system responses to initial 2°β perturbation,
turbulence level 4.57 m/sec rms, altitude 12192 meters,
speed 1.4 Mach

(a)   open loop responses
(b)   closed loop responses
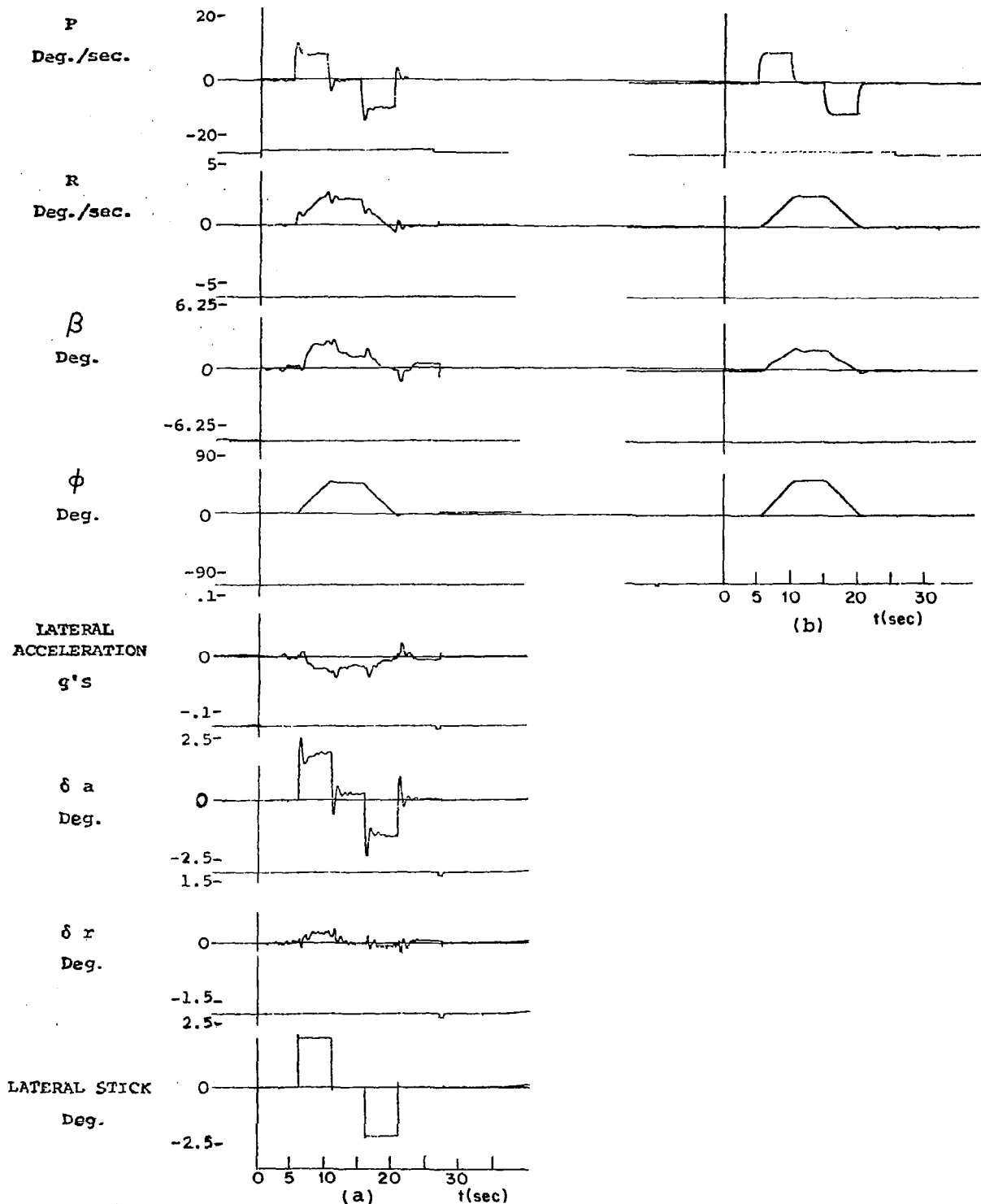
Figure 6.4.13 Lateral system responses to aileron doublet command, no turbulence, altitude 304.8 meters, speed .53 Mach

(a) closed loop responses
(b) model responses used in model-following scheme
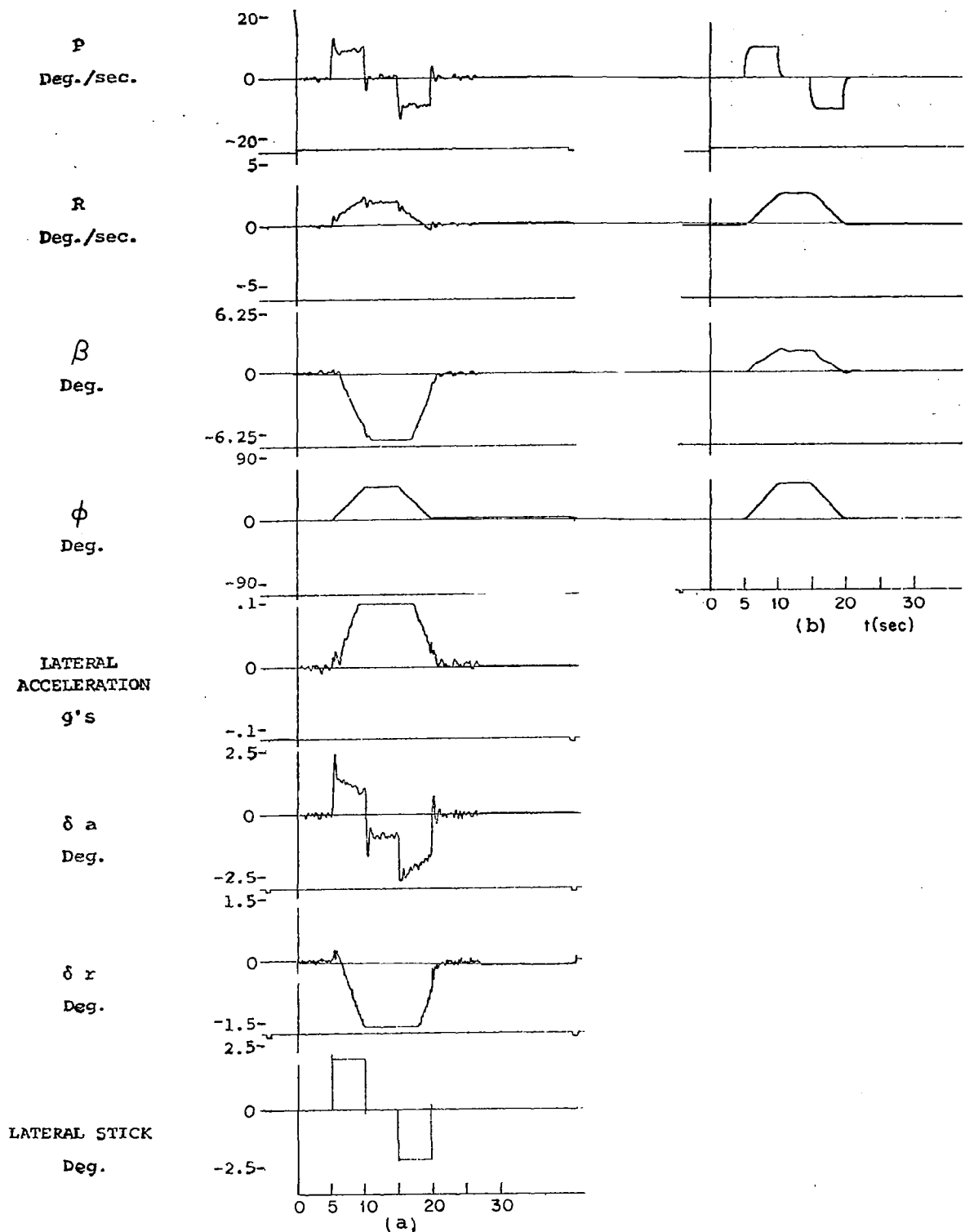
Figure 6.4.14   Lateral system responses to aileron doublet command, no
turbulence, altitude 304.8 meters, speed .86 Mach

(a)   closed loop responses
(b)   model responses used in model-following scheme
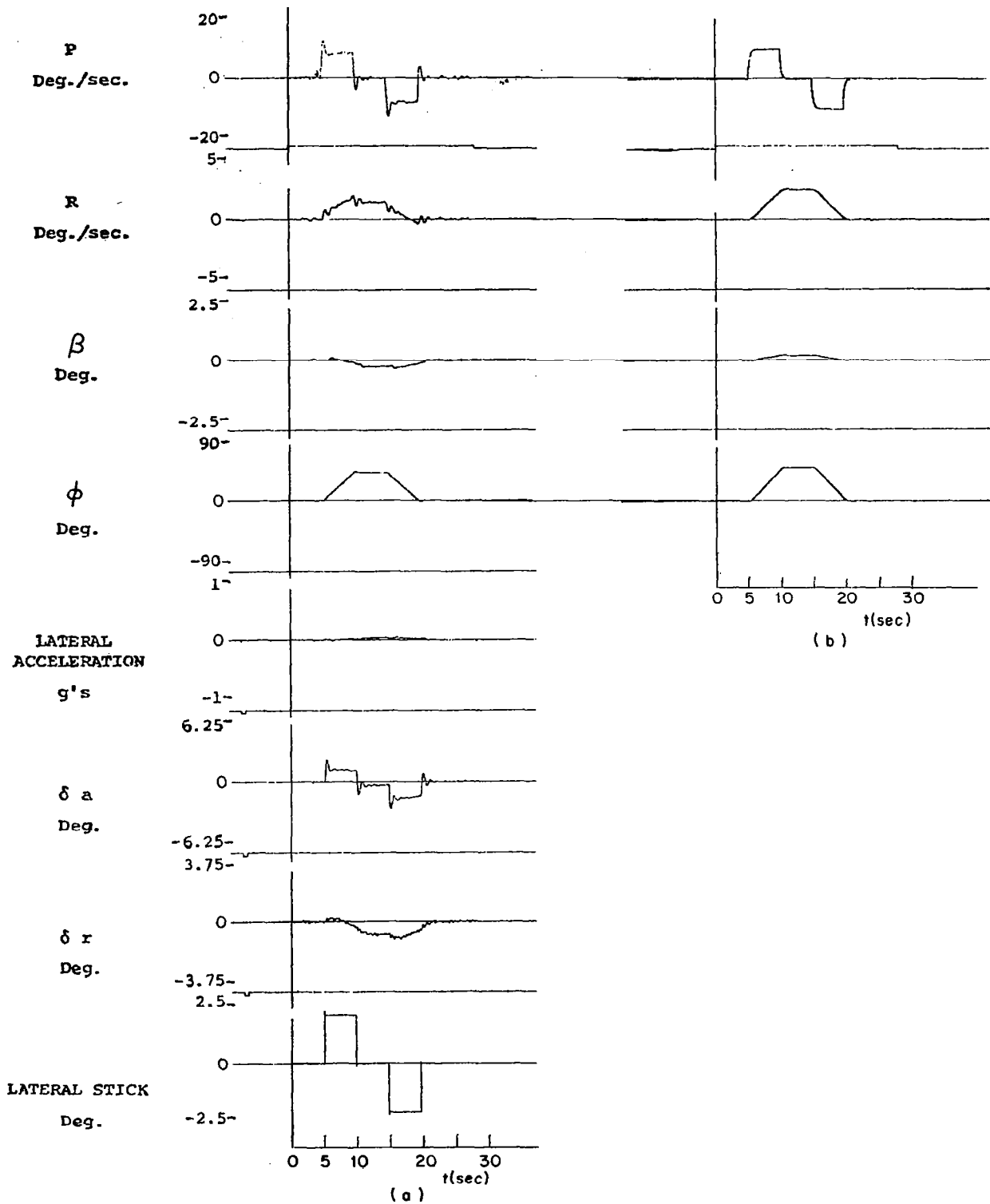
Figure 6.4.15   Lateral system responses to aileron doublet command, no
turbulence, altitude 6096 meters, speed .6 Mach

(a)   closed loop responses
(b)   model responses used in model-following scheme
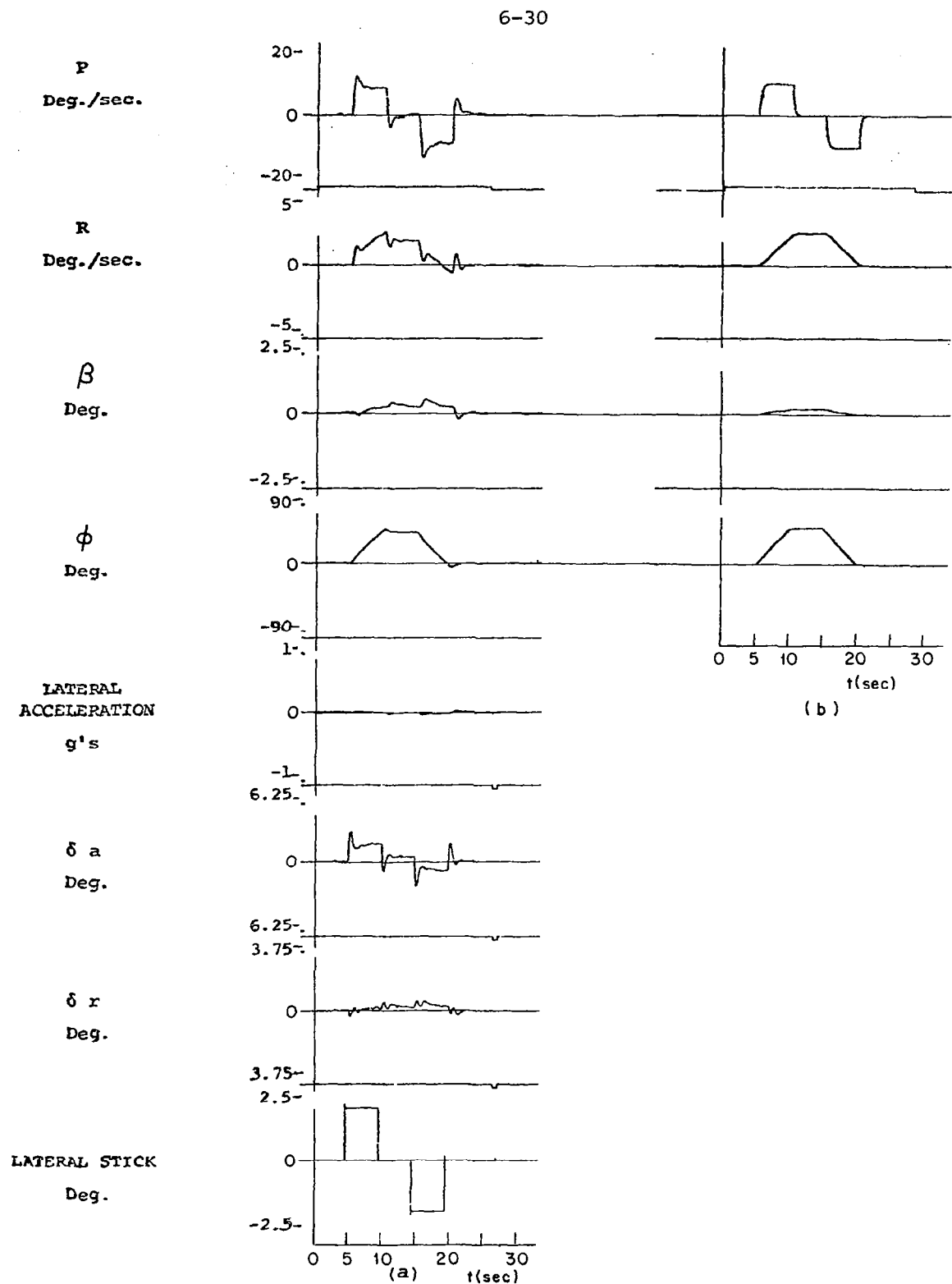
Figure 6.4.16   Lateral system responses to aileron doublet command, no
turbulence, altitude 6096 meters, speed .9 Mach

(a)   closed loop responses
(b)   model responses used in model-following scheme
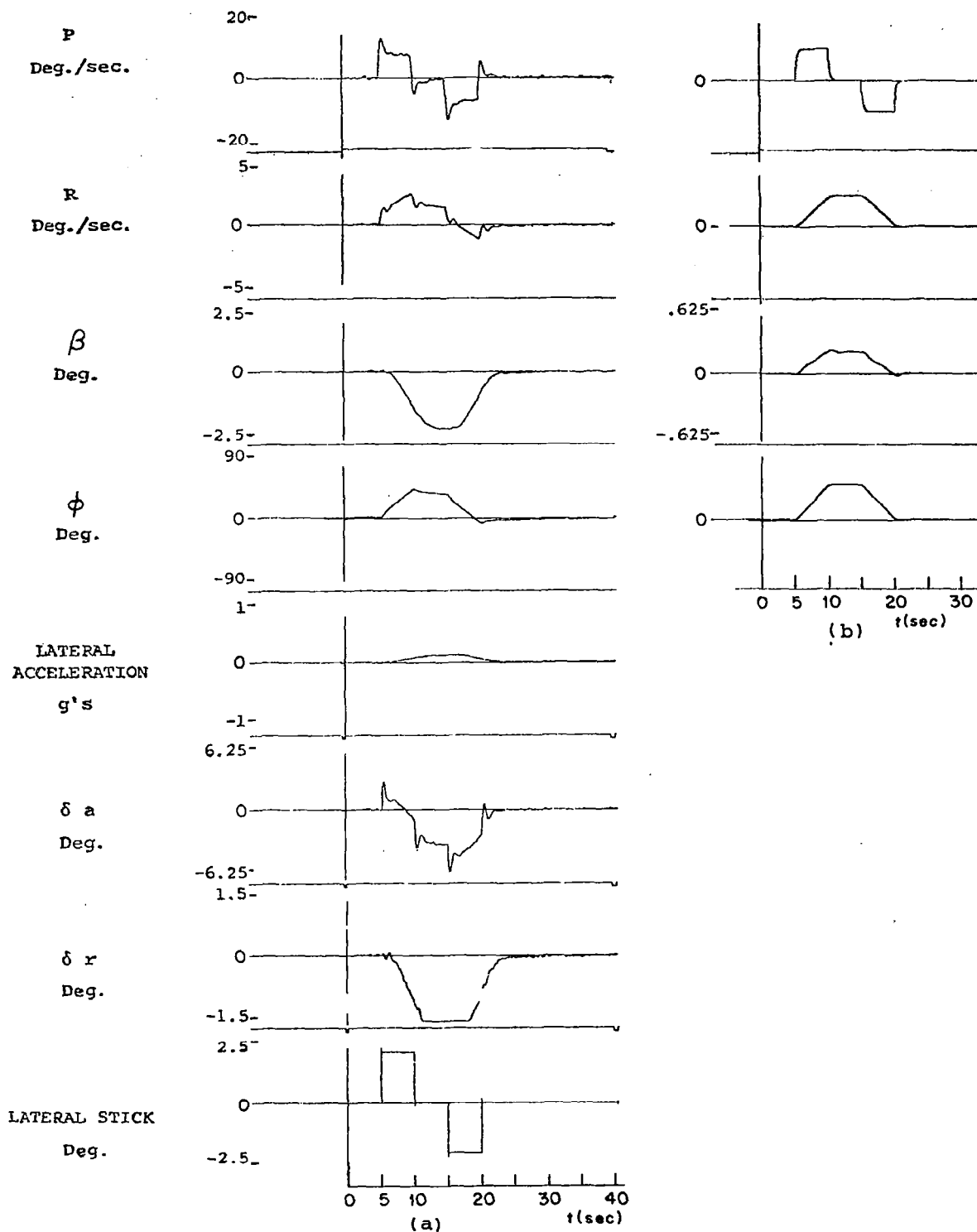
Figure 6.4.17   Lateral system responses to aileron doublet command, no
                 turbulence, altitude 12192 meters, speed .9 Mach

                 (a)   closed loop responses
                 (b)   model responses used in model-following scheme

                 Note excessive sideslip to follow bank angle
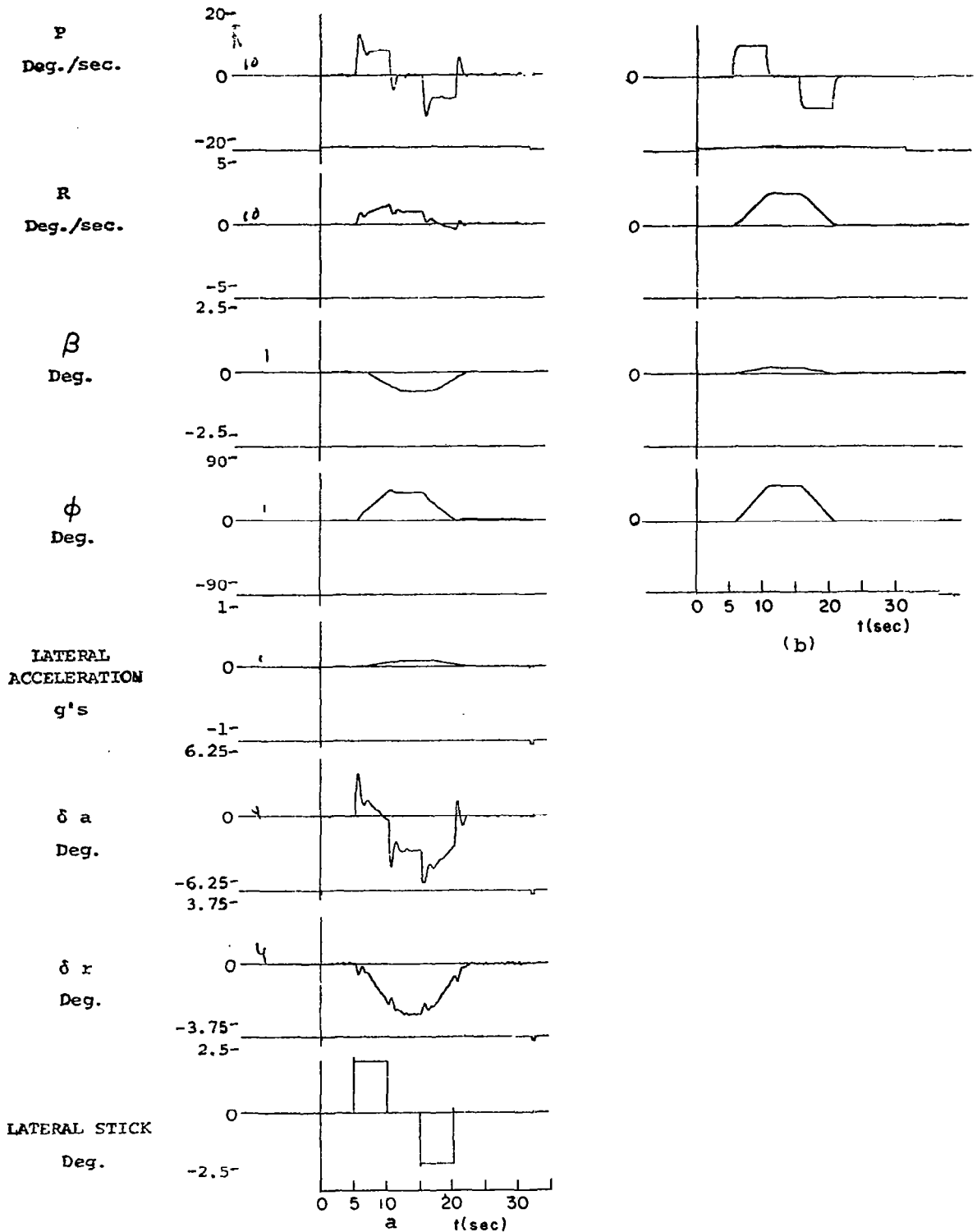
Figure 6.4.18   Lateral system responses to aileron doublet command, no
turbulence, altitude 12192 meters, speed 1.4 Mach

(a)   closed loop responses
(b)   model responses used in model-following scheme

CHAPTER 7

MMAC EXPERIMENTS

7.1 Introduction

This chapter discusses simulation results obtained using Langley Research Center's nonlinear simulation of the F-8C aircraft. To test the gust alleviation properties of the MMAC, the aircraft was initially trimmed at various altitudes and speeds, then subjected to a 6° angle of attack (α) gust and a 2° sideslip angle (β) gust.

To test the response of the MMAC system under pilot commands, the aircraft was subjected to doublet commands in the longitudinal and lateral axes. The models in the MMAC were all initialized with equal probability. The simulations show both the aircraft responses and the identification responses of the MMAC system. Various levels of turbulence were used in these experiments. Three test flight conditions, at various altitudes and speeds, have been chosen to illustrate the performance of the MMAC across the F-8C flight envelope.

7.2 MMAC Control Systems

The fixed-point controllerdesigns of Chapters 5 and 6 were combined with the MMAC identification algorithm, to yield MMAC control systems for the longitudinal and lateral axes. Figures 7.2.1 and 7.2.2 illustrate the operation of these MMAC control systems.
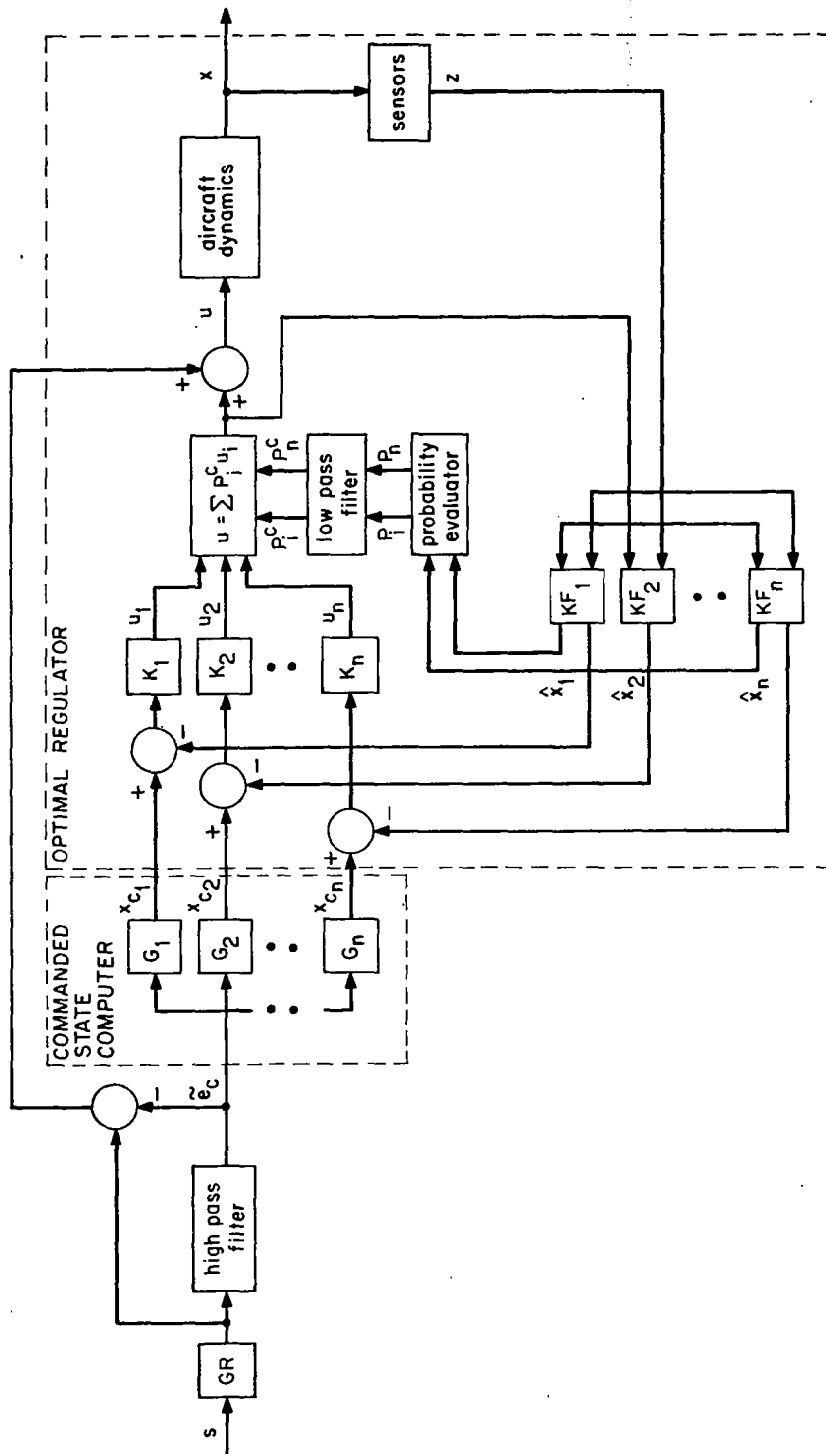
Figure 7.2.1   MMAC control system for longitudinal axis

LATERAL MMAC-MODEL FOLLOWING SYSTEM

Note:
Pi is the a posteriori probability that Model i is true.
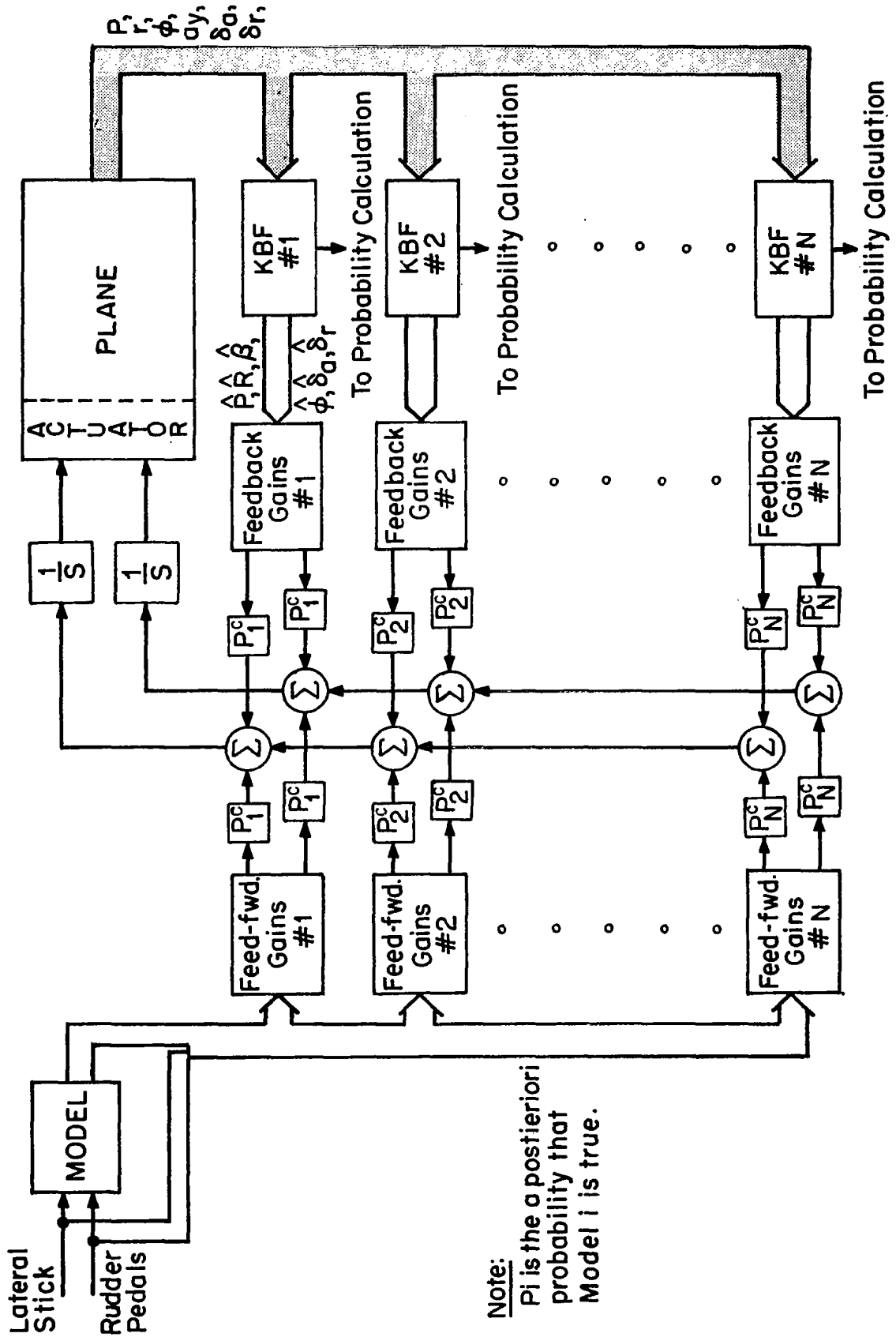
Figure 7.2.2   MMAC Control System for Lateral Axis

For testing the response of the MMAC controlled aircraft to stick inputs, a doublet command of twenty seconds duration, as depicted in Figure 7.2.3, was applied to either the lateral or longitudinal systems. For the longitudinal system, the pilot stick command is separated into slow and fast commands using a high-pass filter. The fast command is processed by the MMAC control system; this control system computes an optimal command for each possible flight condition, using the design of Sections 5.1 to 5.8. These individual commands are combined into a weighted average using the control probabilities discussed in Section 4.6. This processed "fast" control is combined with the "slow" control to produce the complete command applied to the aircraft.

The lateral system controller works on a different principle. The lateral stick command drives the lateral system model described in Chapter 6. The states of the lateral model are used in computing optimal commands for each possible flight condition using the model-following scheme described in Chapter 6. The individual commands are combined into a weighted average using the control probabilities of Section 4.6 to produce the command applied to the aircraft.

In both the longitudinal and lateral systems, sensors measure the aircraft responses. These responses are used to drive Kalman filters for each possible flight condition. The residual signals of these filters are used in evaluating the identification and control probabilities, as described in Chapter 4.
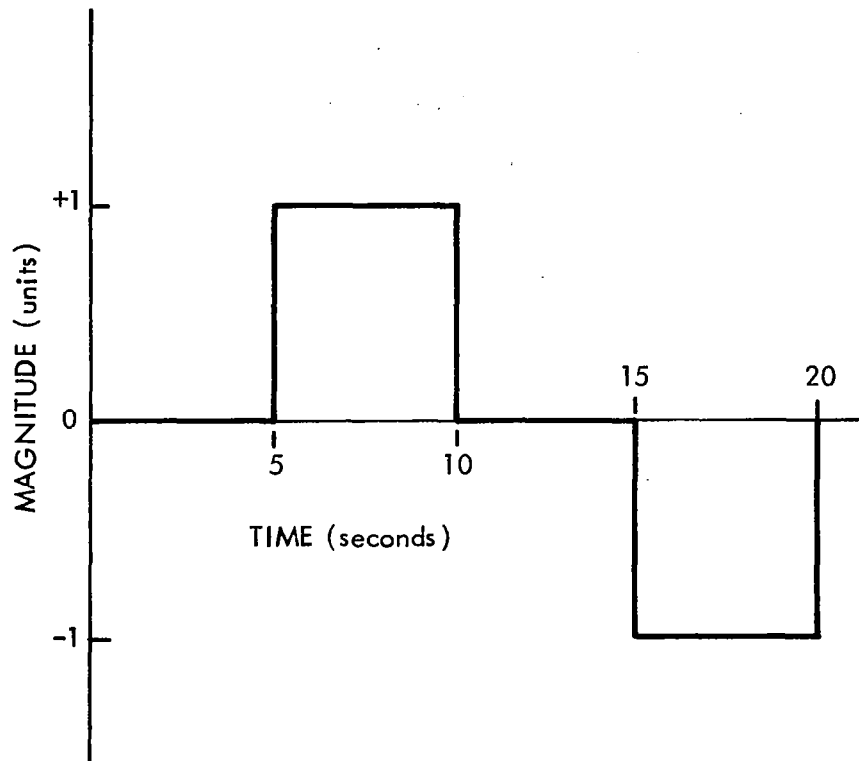
Figure 7.2.3   Doublet command used in aircraft simulations

The main feature of the MMAC controller is that all N hypothesis flight conditions have an individual controller designed on LQG principles. The outputs of these controllers are combined probabilistically to obtain the complete command applied to the aircraft.

7.3 Stability Tables for Mismatched Controllers

The MMAC algorithm frequently identifies a flight condition which is different from the true condition of the aircraft. Using only the linearized discrete time representations of the aircraft as discussed in Chapter 3, one can examine the effect of this mismatching in terms of the stability of the system. Denote the true aircraft linearized matrices by superscript t. Assume the MMAC algorithm is using flight condition i. In the absence of pilot commands, the deterministic system equations are

$$\underline{x}(t+1) = \underline{A}_d^t \, \underline{x}(t) + \underline{B}_d^t \, \underline{u}(t) \tag{7.3.1}$$

$$\underline{u}(t) = -\underline{G}^i \, \hat{\underline{x}}(t) \tag{7.3.2}$$

$$\hat{\underline{x}}(t) = \tilde{\underline{x}}(t) + \underline{H}^i (z(t) - \underline{C}^i \, \tilde{\underline{x}}(t)) \tag{7.3.3}$$

$$\tilde{\underline{x}}(t) = \underline{A}_d^i \, \hat{\underline{x}}(t-1) + \underline{B}_d^i \, \underline{u}(t-1) \tag{7.3.4}$$

$$\underline{z}(t) = \underline{C}^t \, \underline{x}(t) \tag{7.3.5}$$

Combining these equations yields the following system equations

$$\underline{x}(t+1) = \underline{A}_{d}^{t}\,\underline{x}(t) + - \underline{B}_{d}^{t}\,\underline{G}^{i}\hat{\underline{x}}(t) \tag{7.3.6}$$

$$\hat{\underline{x}}(t+1) = \underline{A}_{d}^{i}\,\hat{\underline{x}}(t) + -\underline{B}_{d}^{i}\underline{G}^{i}\,\hat{\underline{x}}(t) + \underline{H}^{i}\underline{C}^{i}\underline{A}_{d}^{t}\underline{x}(t)$$
$$- \underline{H}^{i}\underline{C}^{i}(\underline{A}_{d}^{i} - \underline{B}_{d}^{i}\underline{G}^{i})\hat{\underline{x}}(t) - \underline{H}^{i}\underline{C}^{i}\underline{B}^{t}\underline{G}^{i}\hat{\underline{x}}(t) \tag{7.3.7}$$

This can be represented as

$$\begin{pmatrix} \underline{x} \\[2mm] \tilde{\underline{x}} \end{pmatrix}(t+1) = \begin{pmatrix} \underline{A}^{t}d & -\underline{B}_{d}^{t}\underline{G}^{i} \\[3mm] \underline{H}^{i}\underline{C}^{i}\underline{A}_{d}^{t} & (I-\underline{H}^{i}\underline{C}^{i})(A_{d}^{i}-B_{d}^{i}G_{d}^{i}) - \underline{H}^{i}\underline{C}^{i}\underline{B}^{t}\underline{G}^{i} \end{pmatrix} \begin{pmatrix} \underline{x} \\[2mm] \tilde{\underline{x}} \end{pmatrix}(t) \tag{7.3.8}$$

The eigenvalues of the matrix in equation (7.3.8) indicate whether the mismatched combination of identified and true system is an unstable combination. Two tables are presented for each system. The first table declares a combination unstable if any eigenvalues are greater than one. The second table, to allow for numerical errors, declares a combination unstable if any eigenvalues are greater than 1.005. As seen in Appendix L, many of the filter and control eigenvalues are 1.0, so the second table yields a truer measure of the instabilities present. These tables will be useful in interpreting the simulation results that follow in this Chapter.

TABLE 7.3.1

LONGITUDINAL SYSTEM

STABILITY SUMMARY TABLE

U=Unstable (1.0), * =stable

CONTROLLER

TRUE FC	5	6	7	8	10	11	12	13	14	15	16	17	18	19	20
5	*	*	*	*	*	*	U	U	*	*	*	U	*	U	*
6	U	*	*	*	U	*	U	U	*	U	U	U	*	U	*
7	U	*	*	*	U	U	U	U	*	U	U	U	*	U	*
8	U	U	*	*	U	U	U	U	*	U	U	U	U	U	*
10	*	*	*	*	*	*	U	U	*	U	U	U	*	U	*
11	*	*	*	*	U	*	U	U	*	*	U	U	*	U	*
12	U	*	*	*	U	*	*	U	*	U	U	U	*	U	*
13	U	U	U	U	U	U	*	*	*	U	U	U	*	*	*
14	U	U	*	*	U	U	U	U	*	U	U	U	U	U	*
15	*	*	*	*	U	U	U	U	*	*	U	U	*	U	*
16	*	*	*	*	*	*	U	U	*	*	*	U	*	U	*
17	U	U	U	U	U	*	*	U	*	*	*	*	U	*	*
18	U	*	*	*	U	U	U	U	*	U	U	U	*	U	*
19	U	*	*	*	U	U	U	U	*	U	U	U	*	U	*
20	U	*	*	*	U	U	*	U	*	U	U	U	*	U	*

U=Unstable (1.005), * =stable

TRUE FC	5	6	7	8	10	11	12	13	14	15	16	17	18	19	20
5	*	*	*	*	*	*	*	*	*	*	*	*	*	*	*
6	U	*	*	*	U	*	*	*	*	U	*	*	*	*	*
7	U	*	*	*	U	U	*	*	*	U	U	U	*	*	*
8	U	U	*	*	U	U	U	U	*	U	U	U	U	U	*
10	*	*	*	*	*	*	*	*	*	*	*	*	*	*	*
11	*	*	*	*	U	*	*	*	*	*	*	*	*	*	*
12	U	*	*	*	U	*	*	*	*	U	U	*	*	*	*
13	U	*	*	*	U	U	*	*	*	U	U	U	*	*	*
14	U	U	*	*	U	U	U	U	*	U	U	U	U	*	*
15	*	*	*	*	*	*	*	*	*	*	*	*	*	*	*
16	*	*	*	*	*	*	*	*	*	*	*	*	*	*	*
17	*	*	*	*	U	*	*	*	*	*	*	*	*	*	*
18	U	*	*	*	U	U	*	*	*	U	U	U	*	*	*
19	U	*	*	*	U	U	*	*	*	U	U	U	*	*	*
20	U	*	*	*	U	U	*	*	*	U	U	U	*	*	*

TABLE 7.3.2

LATERAL SYSTEM

STABILITY SUMMARY TABLE

U=Unstable (1.0) * =stable

CONTROLLER

TRUE FC	5	6	7	8	10	11	12	13	14	15	16	17	18	19	20
5	*	*	*	*	*	U	U	U	U	U	*	*	*	*	*
6	*	*	*	*	*	*	U	U	U	*	*	*	U	*	*
7	*	*	*	*	U	*	U	U	U	U	*	*	U	*	*
8	*	*	U	*	U	*	*	*	*	U	*	U	U	*	*
10	*	*	*	*	*	U	U	U	U	U	*	*	U	U	*
11	*	*	*	*	*	*	U	U	U	*	*	U	U	*	*
12	*	*	*	*	U	*	*	*	U	*	*	*	*	*	*
13	*	*	*	*	U	*	*	*	U	*	*	*	*	*	*
14	*	*	*	*	*	*	*	*	*	*	*	*	U	*	*
15	U	*	*	*	*	*	U	U	U	*	*	*	U	*	*
16	U	*	*	*	*	*	U	U	U	*	*	*	*	*	*
17	U	*	*	*	*	*	U	U	U	*	*	*	*	*	*
18	*	*	*	*	*	*	*	*	U	*	*	*	*	*	*
19	*	*	*	*	*	*	U	U	U	*	*	*	*	*	*
20	U	U	*	*	U	U	U	U	U	U	U	U	U	U	*

U=Unstable (1.005) * =stable

TRUE FC	5	6	7	8	10	11	12	13	14	15	16	17	18	19	20
5	*	*	*	*	*	U	U	U	U	U	*	*	*	*	*
6	*	*	*	*	*	*	U	U	U	*	*	*	U	*	*
7	*	*	*	*	U	*	*	*	U	U	*	*	U	*	*
8	*	*	*	*	U	*	*	*	*	U	*	*	U	*	*
10	*	*	*	*	*	U	U	U	U	U	*	*	*	U	*
11	*	*	*	*	*	*	U	U	U	*	*	*	U	*	*
12	*	*	*	*	U	*	*	*	U	*	*	*	*	*	*
13	*	*	*	*	U	*	*	*	U	*	*	*	*	*	*
14	*	*	*	*	*	*	*	*	*	*	*	*	*	*	*
15	*	*	*	*	*	*	U	U	U	*	*	*	U	*	*
16	*	*	*	*	*	*	U	U	U	*	*	*	*	*	*
17	*	*	*	*	*	*	U	U	U	*	*	*	*	*	*
18	*	*	*	*	*	*	*	*	U	*	*	*	*	*	*
19	*	*	*	*	*	*	U	U	U	*	*	*	*	*	*
20	*	*	*	*	U	U	U	U	U	U	U	U	U	U	*

7.4 Simulations at Sea Level

The test flight condition used in these simulations was flight condition 7; the aircraft was initially trimmed at level flight near flight conditions 7 and 8 at an altitude of 1000 ft. (304.8 m.) and a speed of .7 Mach. The aircraft was then subjected to a combined $6°\alpha$, $2°\beta$ gusts.

Figure 7.4.1 contains the longitudinal system transient responses corresponding to a MMAC system with perfect identification (that is, one which always identifies flight condition 7 with probability 1), a MMAC system with models 6, 7, 8 and 10 as hypothesis; and a MMAC system with models 6, 8, 18 and 19 as hypothesis. Figure 7.4.2 contains the lateral system responses of those experiments. Figure 7.4.3 contains both the lateral and longitudinal system responses for an MMAC system with models 7, 8, 18 and 19. The major differences in the initial transient response of the four simulations are due to the different models involved in the various MMAC systems. Since the initial model probabilities are set equal, the initial control gains consist of an average of the four sets of control gains in the MMAC system. This difference is clearly seen in the lateral system responses.

The low-pass filter which smooths out the identification probabilities for control purposes prevents an initial rapid change of the control gains, so the initial transient response is controlled

by the initial combination of models. After one second, the MMAC

identification has a sizable effect in changing the control gains.

Figure 7.4.4 contains the time history of the control probabilities

for two MMAC systems. The difference in the lateral responses in

Figures 7.4.2 and 7.4.3 is due to the different control gains:

Flight condition 6 for MMAC with models 7-8-6-10, and Flight conditions

18 and 19 for MMAC with models 7-8-18-19.

Figures 7.4.5 and 7.4.6 contrast the perfect identification

response with the MMAC responses when the aircraft is operating

under heavy turbulence (4.57 m/sec rms). Figures 7.4.7 and 7.4.8

display MMAC responses of the aircraft over a 35-second simulation

while the aircraft is subject to moderate turbulence (1.22 m/sec rms).

Figures 7.4.9, 7.4.10 and 7.4.11 show the time histories of the control

probabilities and the weighted sum of residuals (WRS) denoted by $m(t)$

for these simulations. The histories of $m(t)$, i.e., the weighted sum

of residuals, give an indication of the information used by the MMAC

algorithm for identification purposes. They also offer an indication

of the separation between the various hypotheses used in the MMAC system.

In these simulations, the low turbulence level provides a consistent

excitation. However, after the initial transient dies out, it is dif-

ficult to distinguish between the various hypotheses; this is reflected

in the changing control probabilities.

The important element to notice in Figure 7.4.7 is the slow

rise in pitch angle. This corresponds to the phugoid mode of the

aircraft, which is excited in the control of the initial transient.

Since the MMAC attempts to control only the short-period response of the aircraft, it does not affect the slow phugoid oscillations.

Overall, the aircraft responses obtained using MMAC controllers closely matched the responses obtained using the gains with perfect identification. The major exception occurred when gains from super-sonic flight conditions were used to control the aircraft at subsonic flight conditions.

The performance of the MMAC identification algorithms is illustrated in Figures 7.4.4, 7.4.9, 7.4.10 and 7.4.11. The lon-gitudinal identification system has difficulty distinguishing between flight conditions 6 and 7 in the absence of turbulence. The open-loop models for these conditions are different; however, when a controller is added, the closed-loop systems are very difficult to distinguish. This is reflected in the similar aircraft responses in Figure 7.4.1 (a) and (b). This difficulty is also present when moderate turbulence is introduced, although in a lesser degree, as illustrated by Figure 7.4.9. The identification system for the lateral axis performed poorly throughout these experiments, identifying supersonic, 40,000 feet altitude flight conditions when the aircraft was flying at sea level.

Figure 7.4.12 shows the longitudinal system responses of four MMAC systems to elevator doublet commands. The decay observed in the longi-tudinal stick position is the effect of the high-pass filtering scheme

discussed in Chapter 5, used to eliminate trim effects and to
separate short-period responses from long-period responses. The
simulations in Figure 7.4.12 were conducted under no turbulence.
Simulation (a) used an MMAC system with hypotheses models 7, 8, 6,
10. Simulation (b) used an MMAC system with hypotheses 7, 8, 6, 20,
all close in dynamic pressure. Simulation (c) used an MMAC system
with hypotheses 7, 8, 18, and 19, and simulation (d) used an MMAC
system with hypotheses 6, 8, 18, 19. Note the close performance of
these four MMAC systems; the aircraft responses in simulations (c)
and (d) indicate a slight drift in pitch angle, due to the presence
of two supersonic hypothesis models in the MMAC system. This close-
ness indicates a degree of robustness in the MMAC algorithm with
respect to the model hypotheses used.

Figures 7.4.13 and 7.4.14 show the control probability responses
for these four experiments, together with the weighted sum of square
residuals (m(t) time histories) for each hypothesis model. Figure 7.4.13
and Figure 7.4.14a illustrate that the identification scheme chooses the
correct hypothesis while the aircraft is maneuvering. In all three cases
flight condition 7 was identified correctly. Once the maneuver stops, the
residuals become close to zero, and as such the identification scheme
lacks information. In the absence of information the identification
scheme falls into the $\beta*$ behavior mentioned in Chapter 4, but with no
ill effects on the aircraft responses, as flight condition 6 is a close
neighbor of the true flight condition. Table 7.4.1 contains a list of
the $\beta*$ values for each flight condition. Note in Figure 7.4.13a that

the β^*-dominant model is flight condition 10; however, the mismatch stability tables in Section 7.3 indicate that model 10 is an unstable choice. This is quickly indicated by an increase in m(t) corresponding to model 10, thereby changing identification to model 6. This β^* behavior can be eliminated through proper tuning of the threshold mentioned in Chapter 4, recognizing when there is a lack of information.

The key point to notice is that flight condition 7 was identified correctly while the aircraft was maneuvering, even in the absence of elevator measurements. The m(t) traces for models 6,7, and 8 are remarkably similar, yet the identification scheme is able to choose correctly. When the correct hypothesis is not included in the system, Figure 7.4.14 b indicates that identification is uncertain during the maneuver, affecting performance.

Figure 7.4.15 shows the responses of a repeat of three of the experiments in Figure 7.4.13, conducted under 1.22 m/sec. rms turbulence. The presence of turbulence should provide enough information to avoid the β^* behavior. Figure 7.4.16 contains the longitudinal control probability and m(t) responses. The β^* behavior encountered in the previous experiments is not present in these simulations. This figure suggests that the presence of mild turbulence actually hinders the identification of the true system during maneuvers. During the five second quiet period before the doublet command starts, the turbulence level drives the identification towards the correct model. At

the start of the command, there is some confusion between models 7 and 8, which is eventually resolved correctly. The responses in Figure 7.4.15 are quite good; the supersonic hypotheses have a reduced effect because of the identification changes in the preliminary quiet periods.

Figure 7.4.17 describes the lateral system responses to a doublet command in the lateral system, under no turbulence. The bank angle response is very good, holding lateral acceleration to a minimum. The MMAC system did not include the true hypothesis, model 7, in this experiment. The important aspect of this experiment is the difference in the m(t) responses when there is a command, and when there is no command. When there is a doublet command, only the close neighbors of the true hypothesis, models 6 and 8, are identified. When the doublet command stops, Model 18 is suddenly identified. The resulting combination produces a stable system in spite of inaccurate identification. These results substantiate the theory that the MMAC algorithm tends to identify only "stable" combinations of time system and hypothesis controller. This experiment also indicates a basic inaccuracy in the lateral identification system in the absence of commands, corroborating the results of the gust-alleviation experiments.

7.5 Simulations at 20,000 Feet (6096 meters)

The test flight condition chosen at this altitude was flight condition 11, with a speed of .6 Mach. The first set of experiments correspond to a combined 6° angle of attack (α-gust) and 2°

TABLE 7.4.1

β* VALUES OF FLIGHT CONDITIONS

Flight Condition	Longitudinal β*	Lateral β*
8	54	29,044
7	86	38,100
14	86	54,601
6	127	47,069
13	132	62,612
20	135	69,951
19	139	66,707
12	146	65,498
18	153	68,941
11	194	73,415
5	195	57,670
17	203	75,185
16	210	77,470
15	224	80,508
10	236	82,577
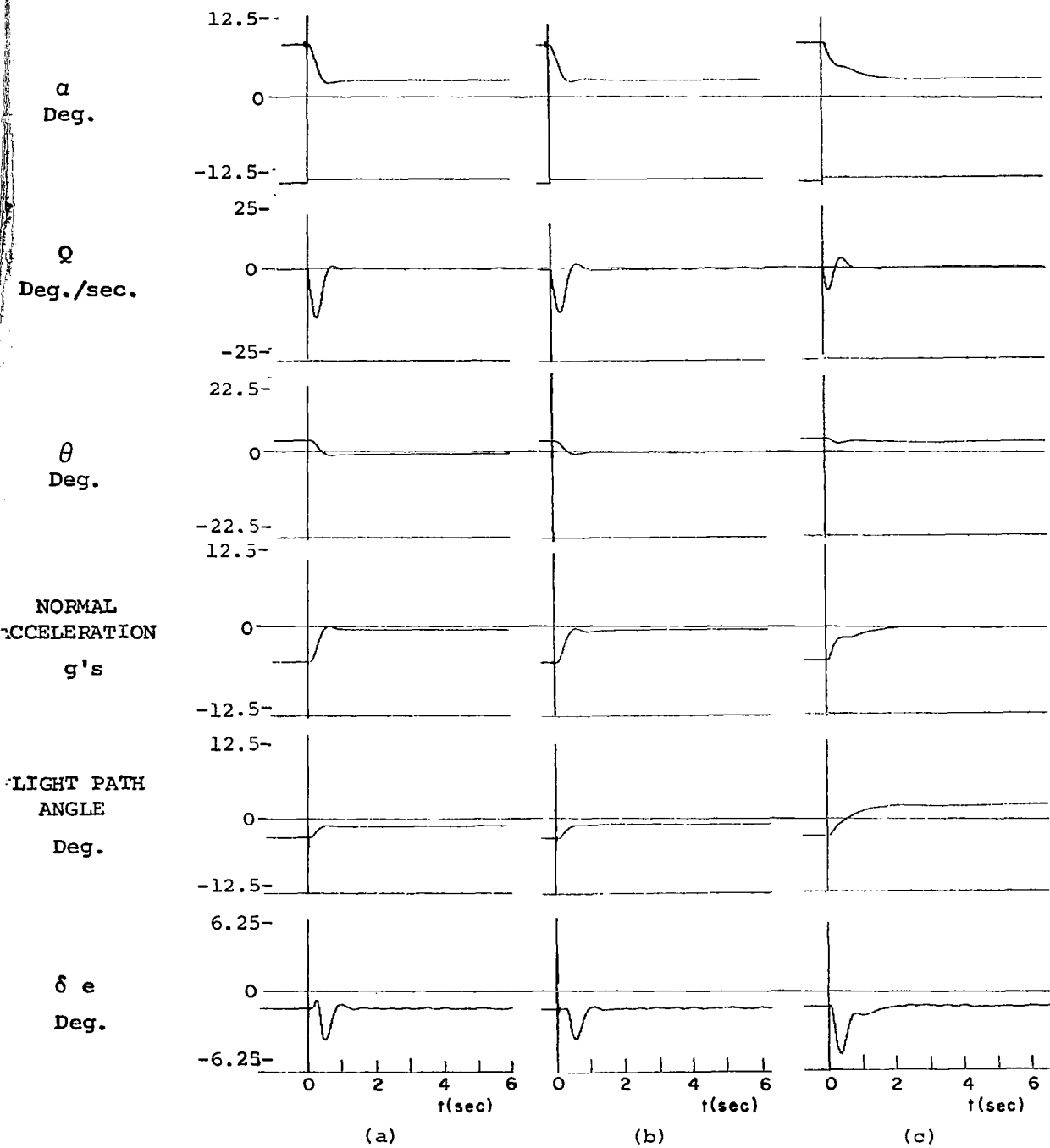
Fig. 7.4.1   Longitudinal responses to 6°α, 2°β initial conditions,
no turbulence, altitude 304.8 meters, speed .7 Mach

(a)   Perfect identification responses
(b)   MMAC responses, Models 6,7,8,10
(c)   MMAC responses, Models 6,8,18,19
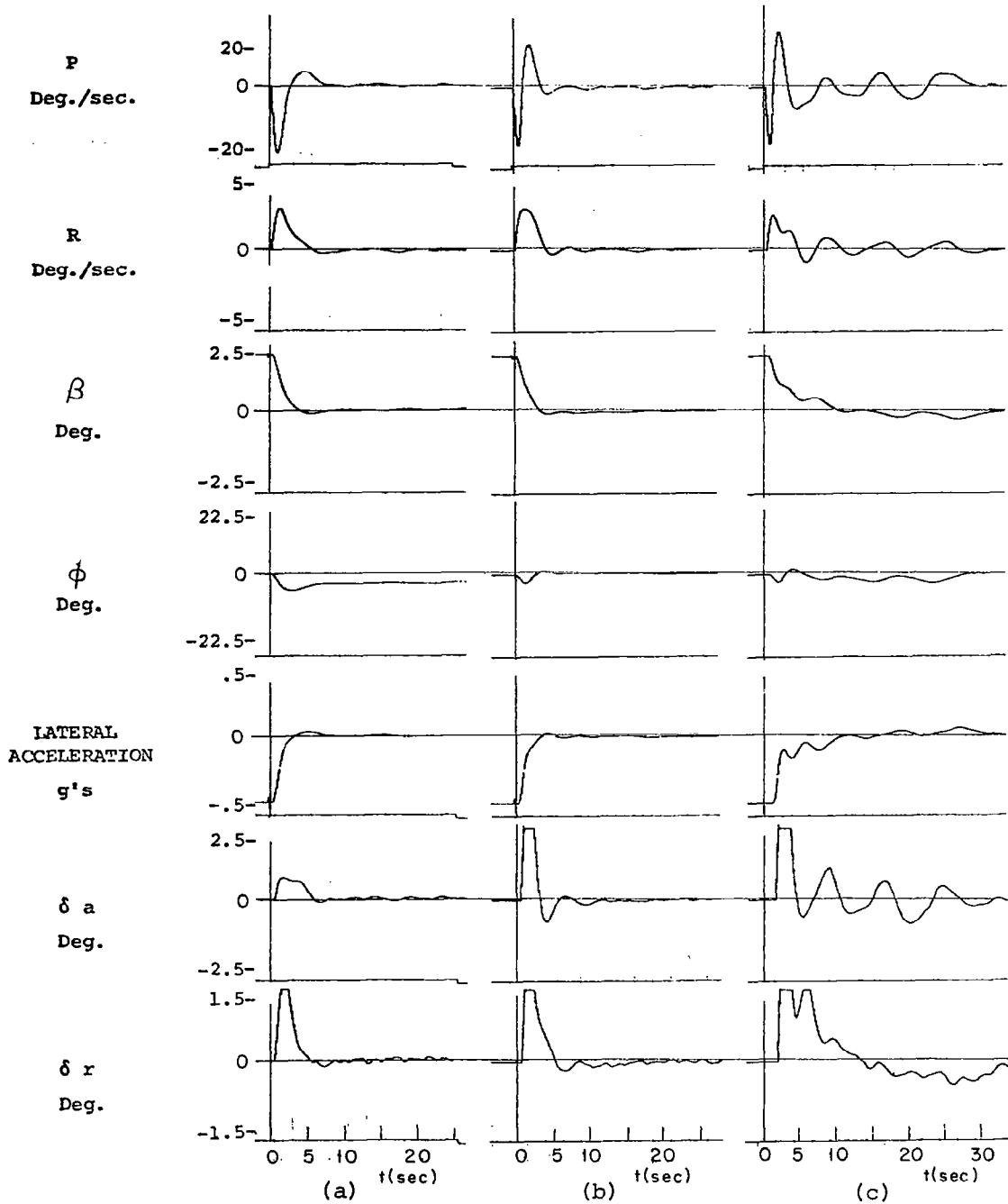
Figure 7.4.2 Lateral responses to 6°α, 2°β initial conditions,
no turbulence, altitude 304.8 meters, speed .7 Mach

(a)   Perfect identification responses
(b)   MMAC responses, Models 6,7,8,10
(c)   MMAC responses, Models 6,8,18,19
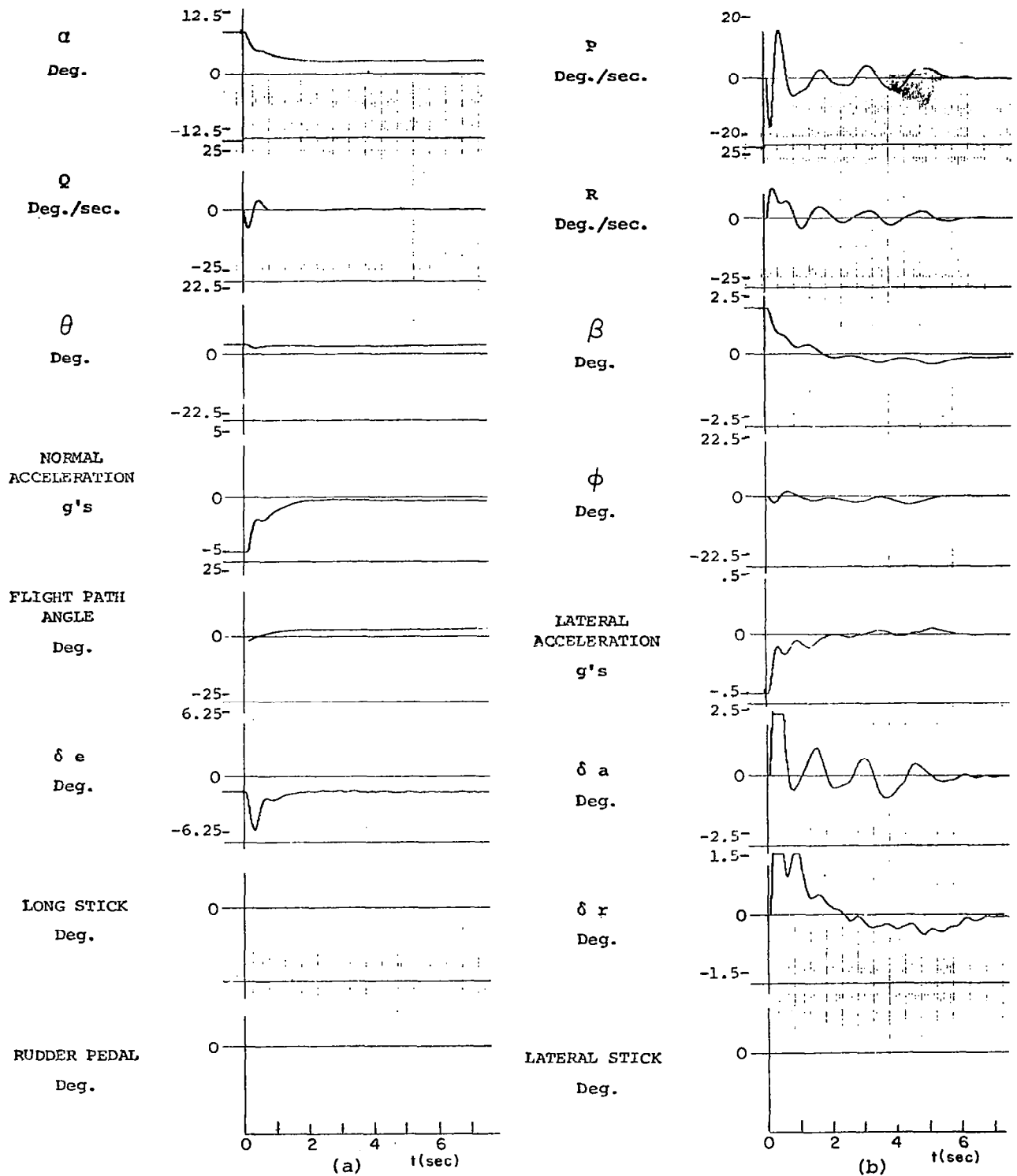
Figure 7.4.3   Longitudinal and Lateral responses to 6°α, 2°β
                initial conditions, no turbulence, altitude
                6096 meters, speed .7 Mach
                MMAC models 7,8,18,19
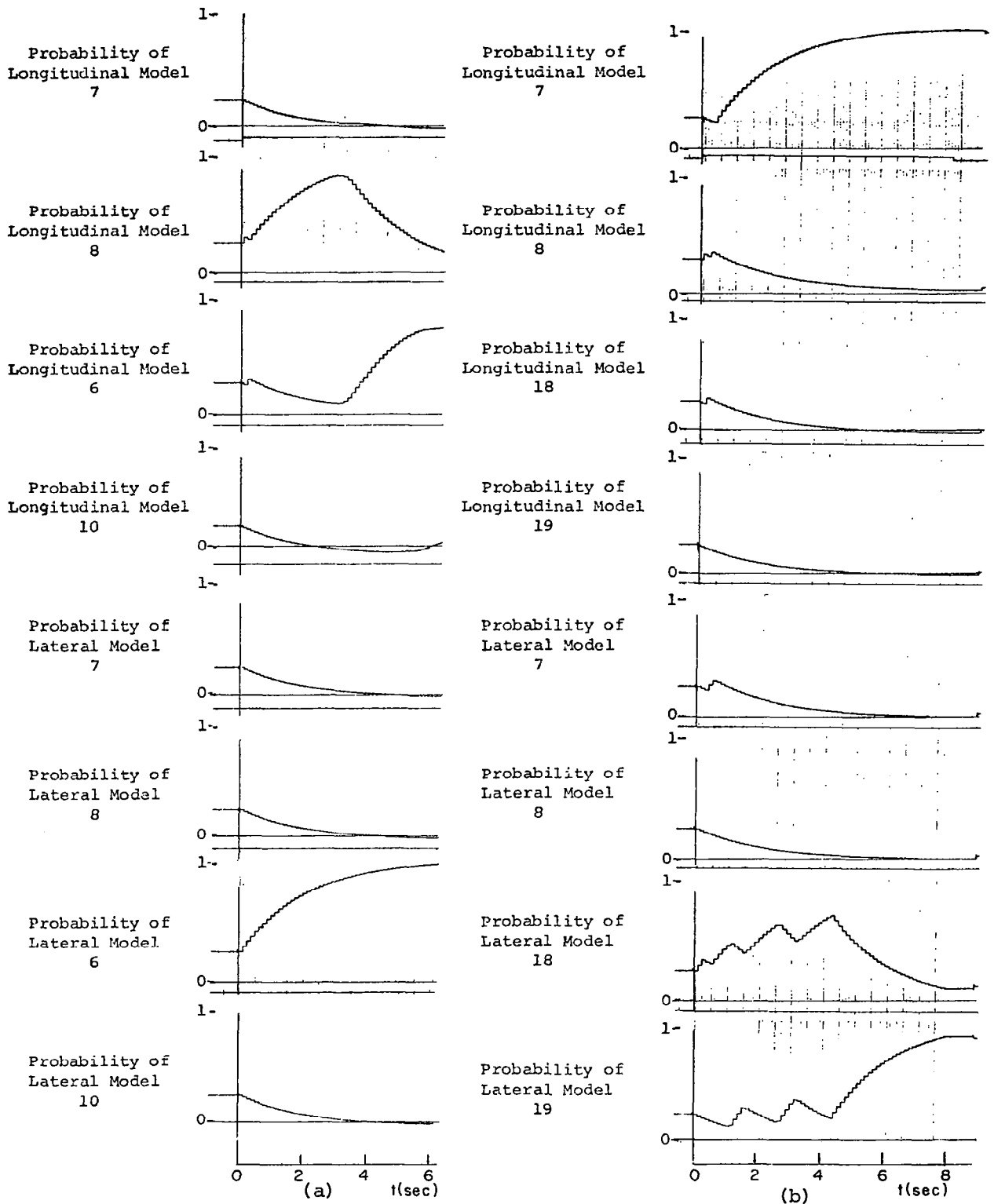
Figure 7.4.4   Control probability responses to 6°α, 2°β initial conditions,
                no turbulence, altitude 304.8 meters, speed .7 Mach

                (a)   MMAC responses, Models 6,7,8,10
                (b)   MMAC responses, Models 7,8,18,19
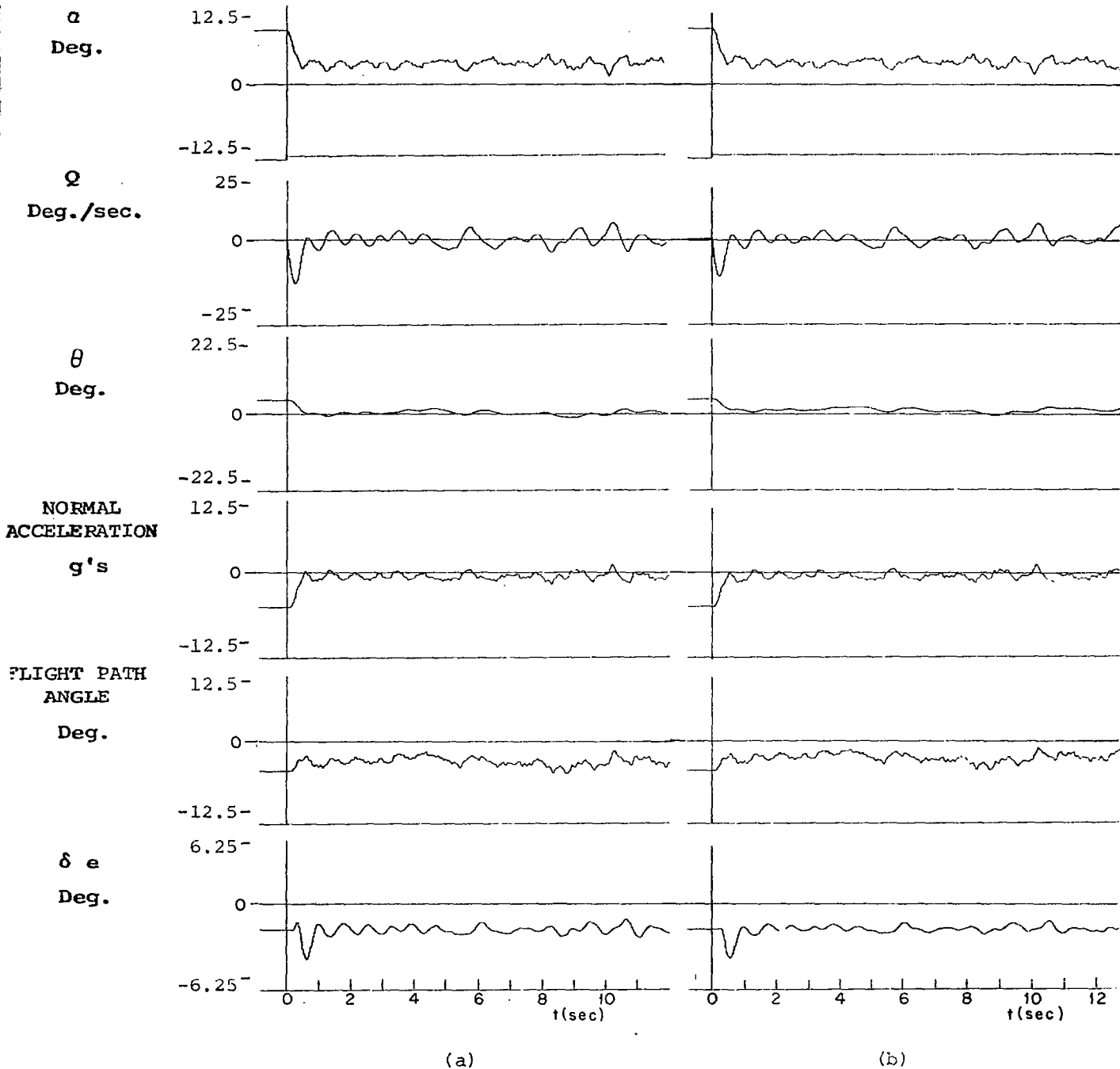
Figure 7.4.5   Longitudinal responses to 6°α, 2°3 initial
                conditions in 4.57 m/sec rms turbulence at
                304.8 meters altitude, speed .7 Mach

                (a)   Perfect identification responses
                (b)   MMAC responses, Models 6,7,8,10
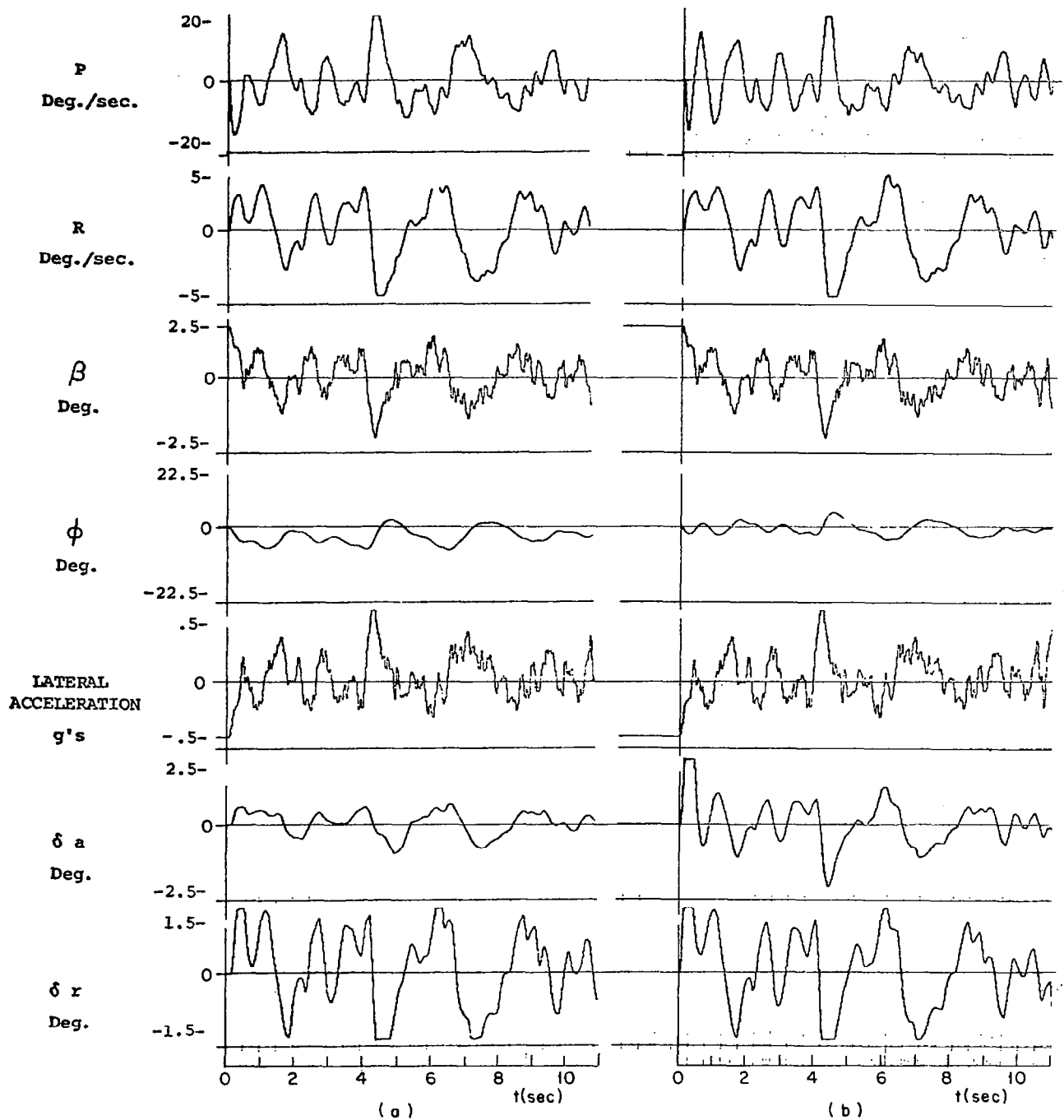
Figure 7.4.6   Lateral responses to 6°α, 2°β initial conditions
in 4.57 m/sec rms turbulence, altitude 304.8 meters,
speed .7 Mach

(a)   Perfect identification responses
(b)   MMAC responses, Models 6,7,8,10
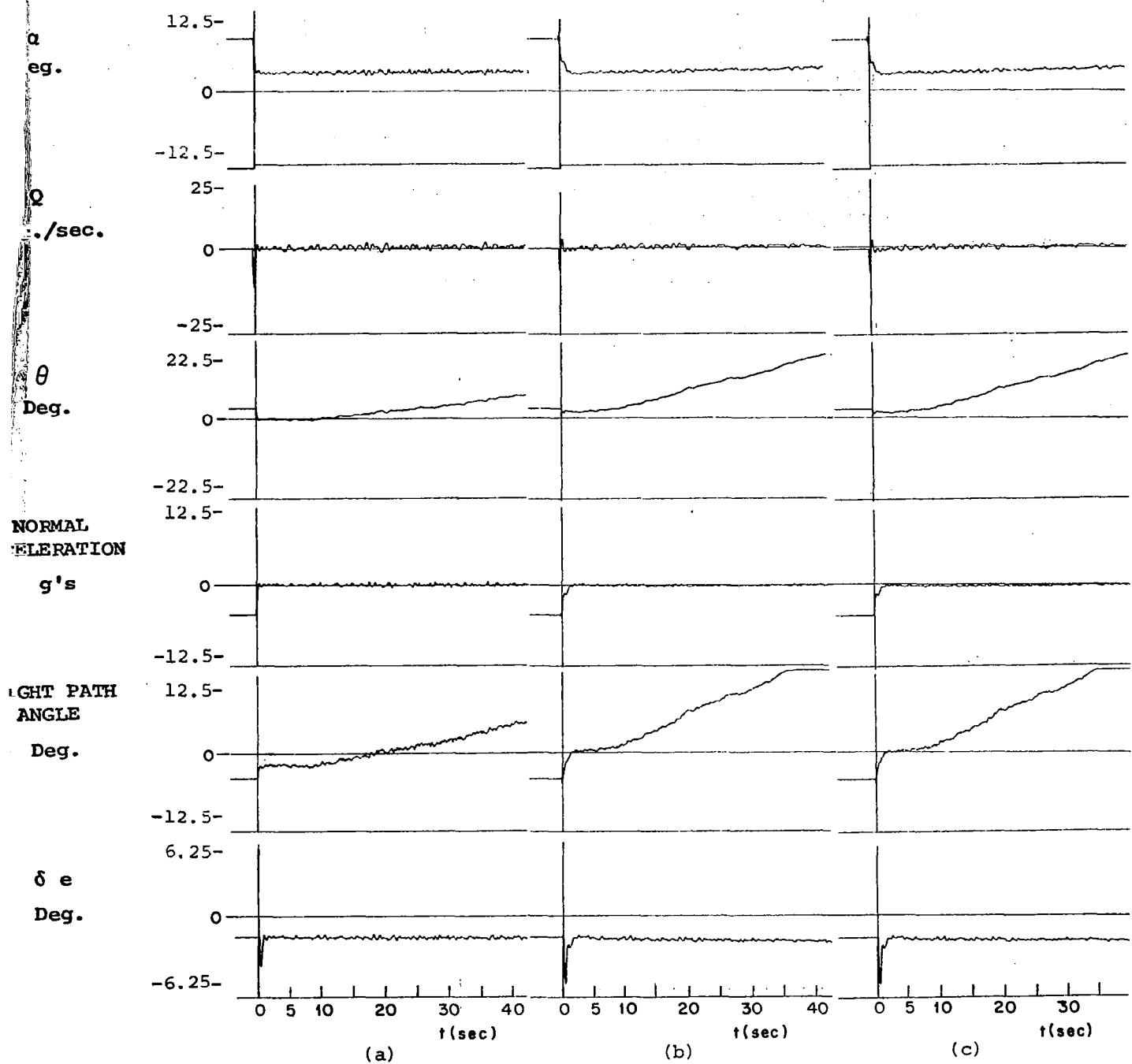
Figure 7.4.7 Longitudinal Responses to 6°α,2°β initial conditions, 1.22 m/sec rms turbulence, altitude 304.8 meters, speed .7 Mach

(a) MMAC responses, Models 6,7,8,10
(b) MMAC responses, Models 7,8,18,19
(c) MMAC responses, Models 6,8,18,19
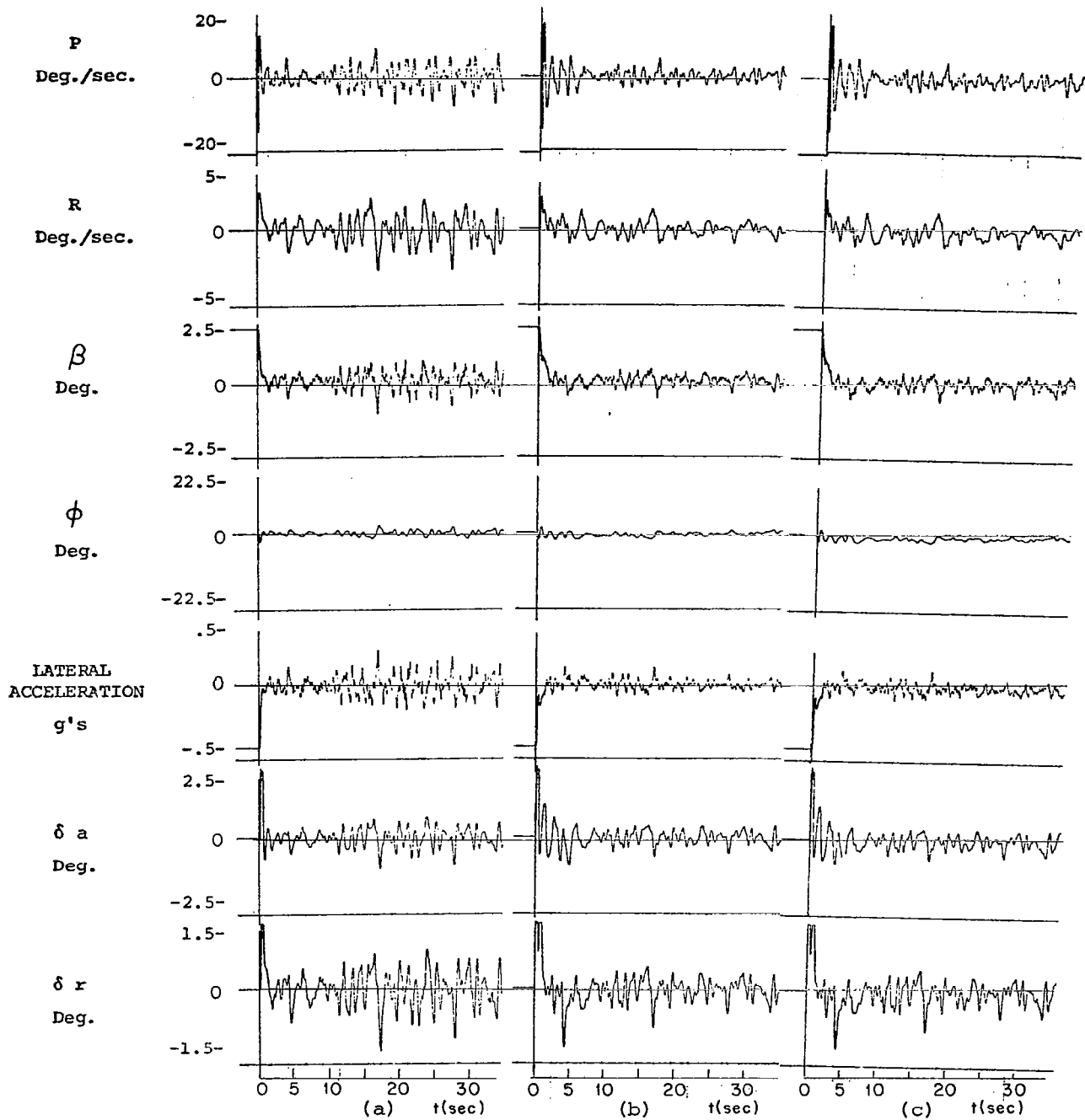
Figure 7.4.8   Lateral responses to 6°α, 2°β initial conditions,
1.22 m/sec rms turbulence, altitude 304.8 meters, speed
.7 Mach

(a)   MMAC responses, Models 6,7,8,10
(b)   MMAC responses, Models 7,8,18,19
(c)   MMAC responses, Models 6,8,18,19
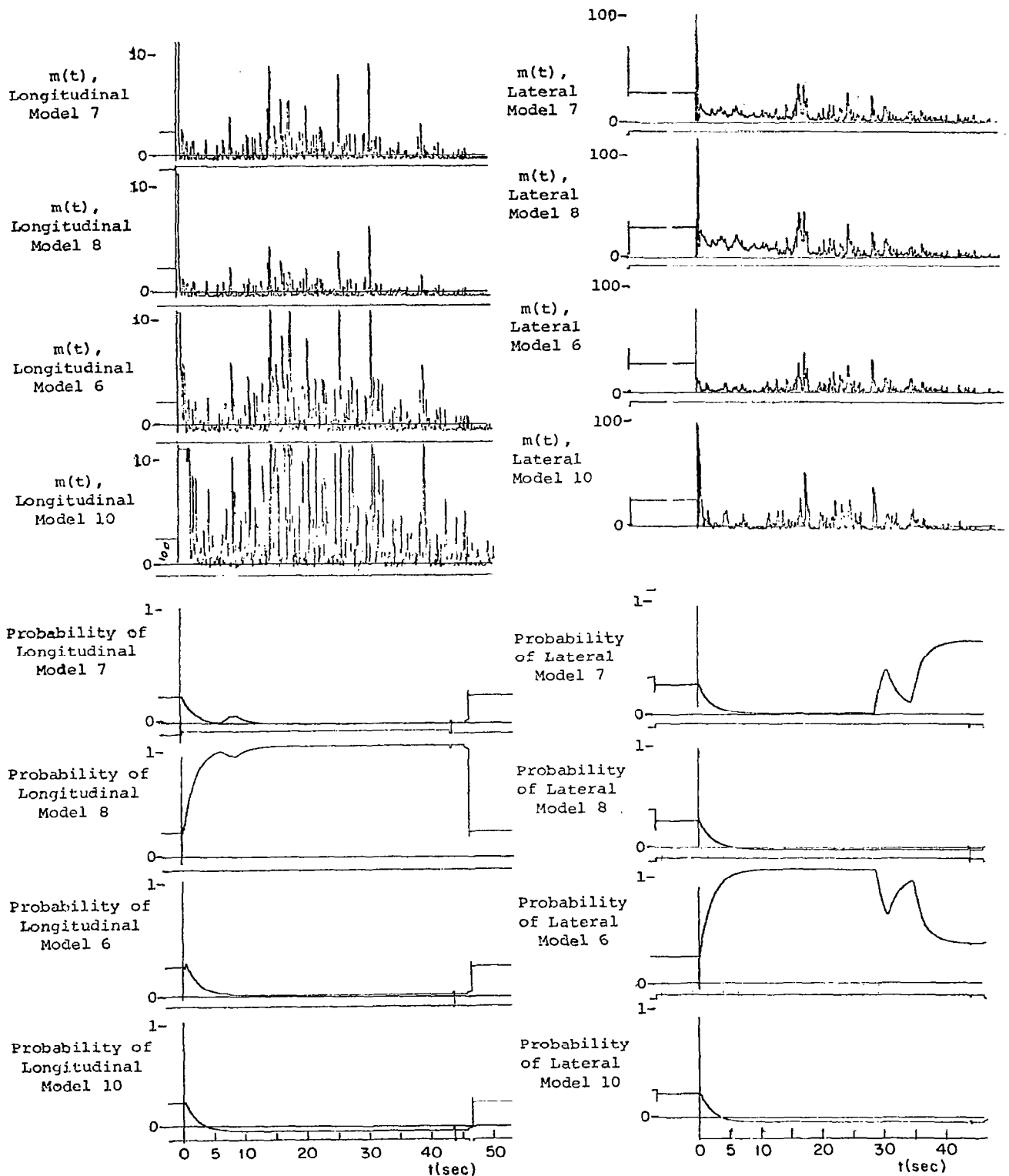
Figure 7.4.9   Control Probability and m(t) responses to 6°α, 2°β
initial conditions, 1.22 m/sec rms turbulence,
altitude 304.8 meters, speed .7 Mach
MMAC Models 6,7,8,10
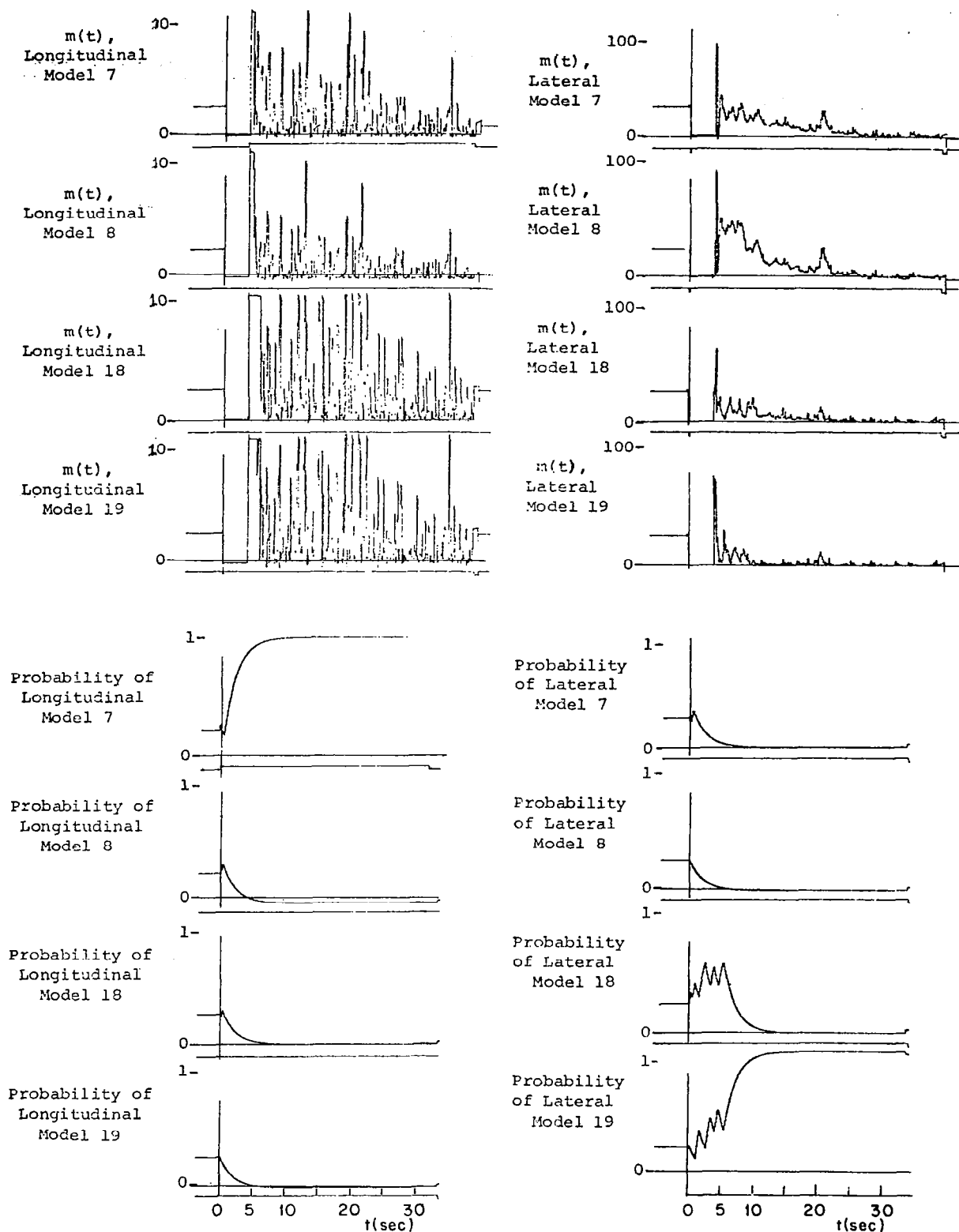
Figure 7.4.10   Control Probability and m(t) responses to 6°α, 2°β
                  initial conditions, 1.22 m/sec rms turbulence,
                  altitude 304.8 meters, speed .7 Mach
                  MMAC Models 7,8,18,19
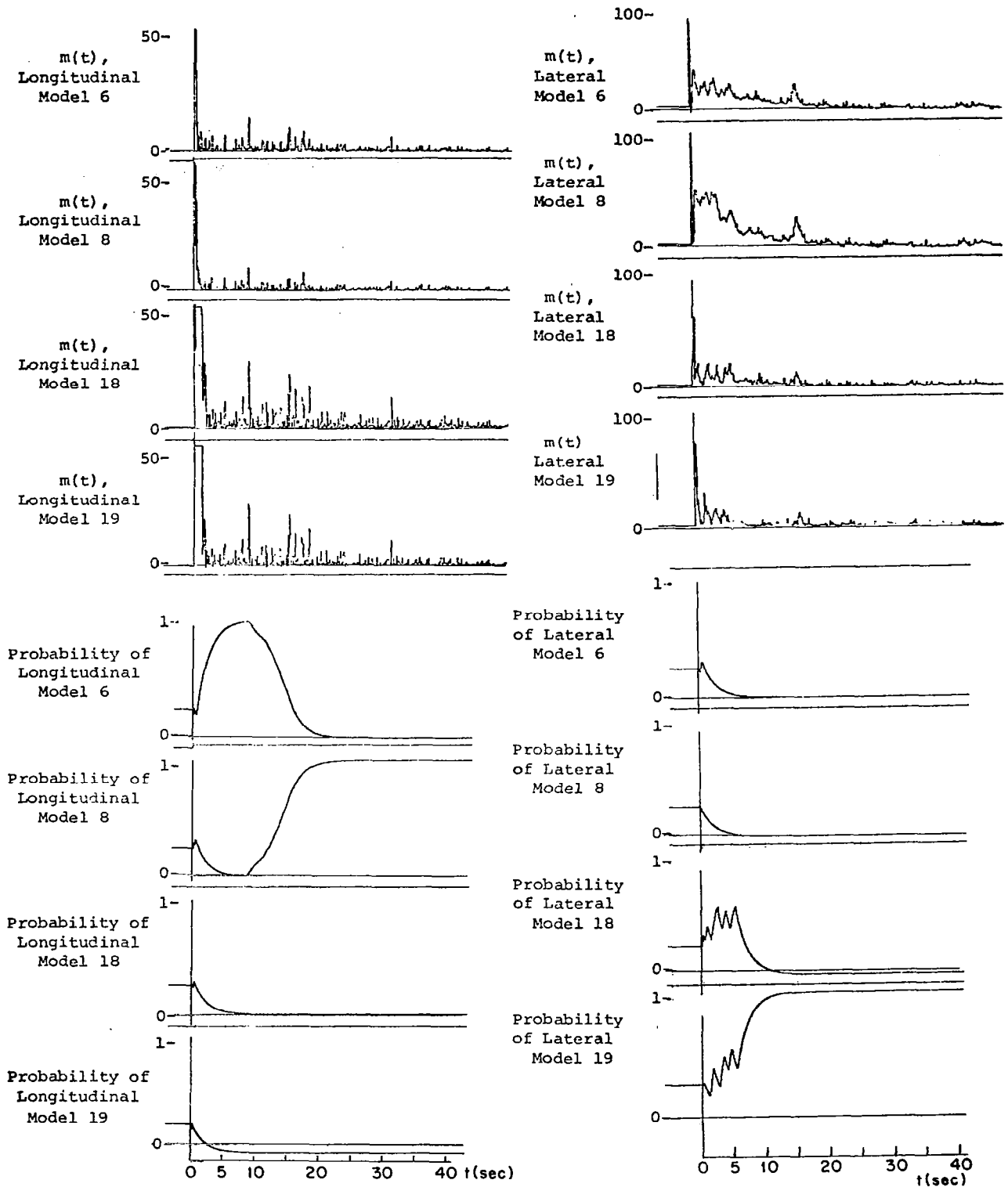
Figure 7.4.11   Control Probability and m(t) responses to 6°α, 2°β
initial conditions, 1.22 m/sec rms turbulence,
altitude 304.8 meters, speed .7 Mach
MMAC Models 6,8,18,19
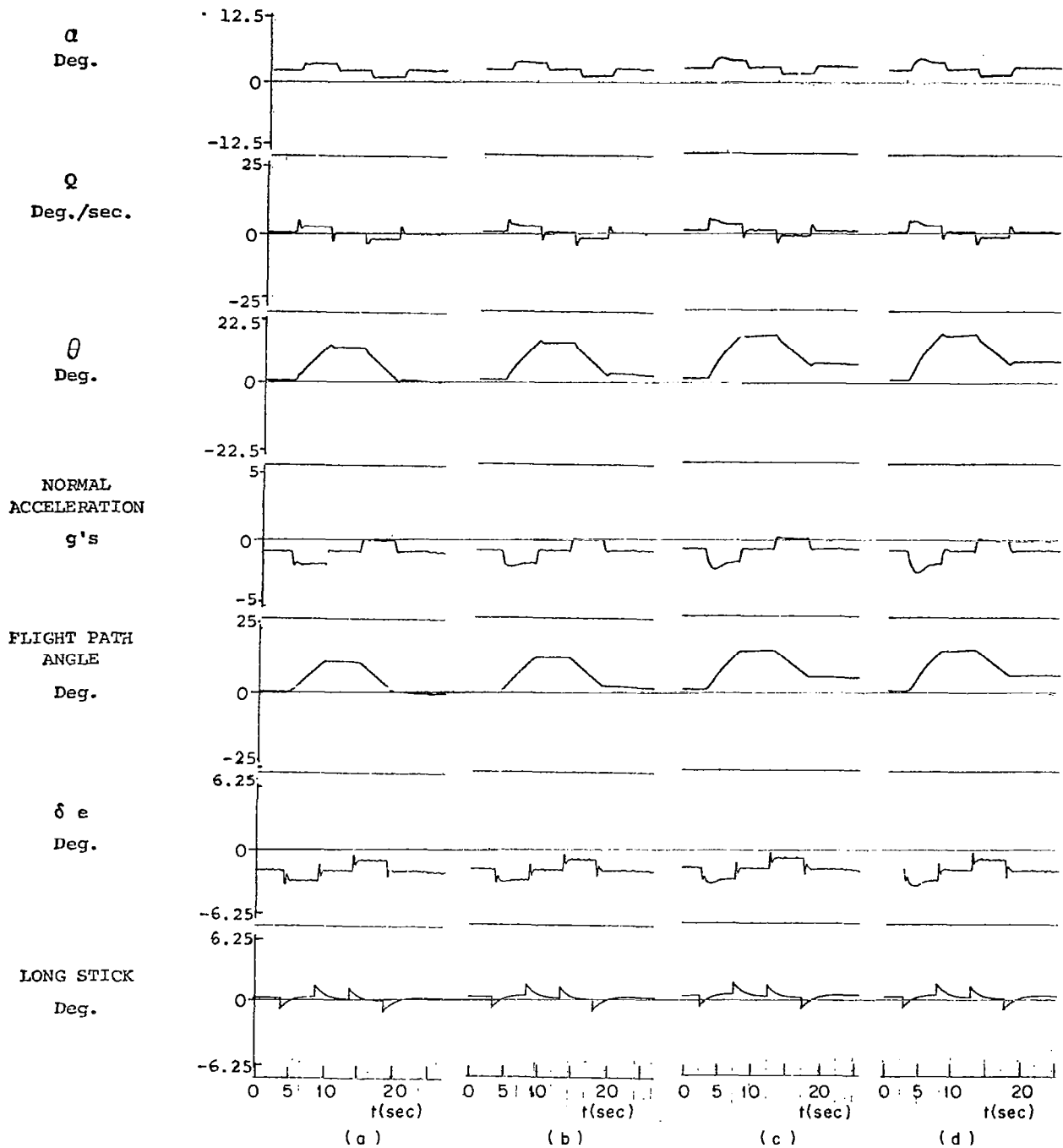
Figure 7.4.12   Longitudinal responses to elevator doublet command,
no turbulence, altitude 304.8 meters, speed .7 Mach

(a)   MMAC responses, models 6,7,8,10
(b)   MMAC responses, models 6,7,8,20
(c)   MMAC responses, models 7,8,18,19
(d)   MMAC responses, models 6,8,18,19
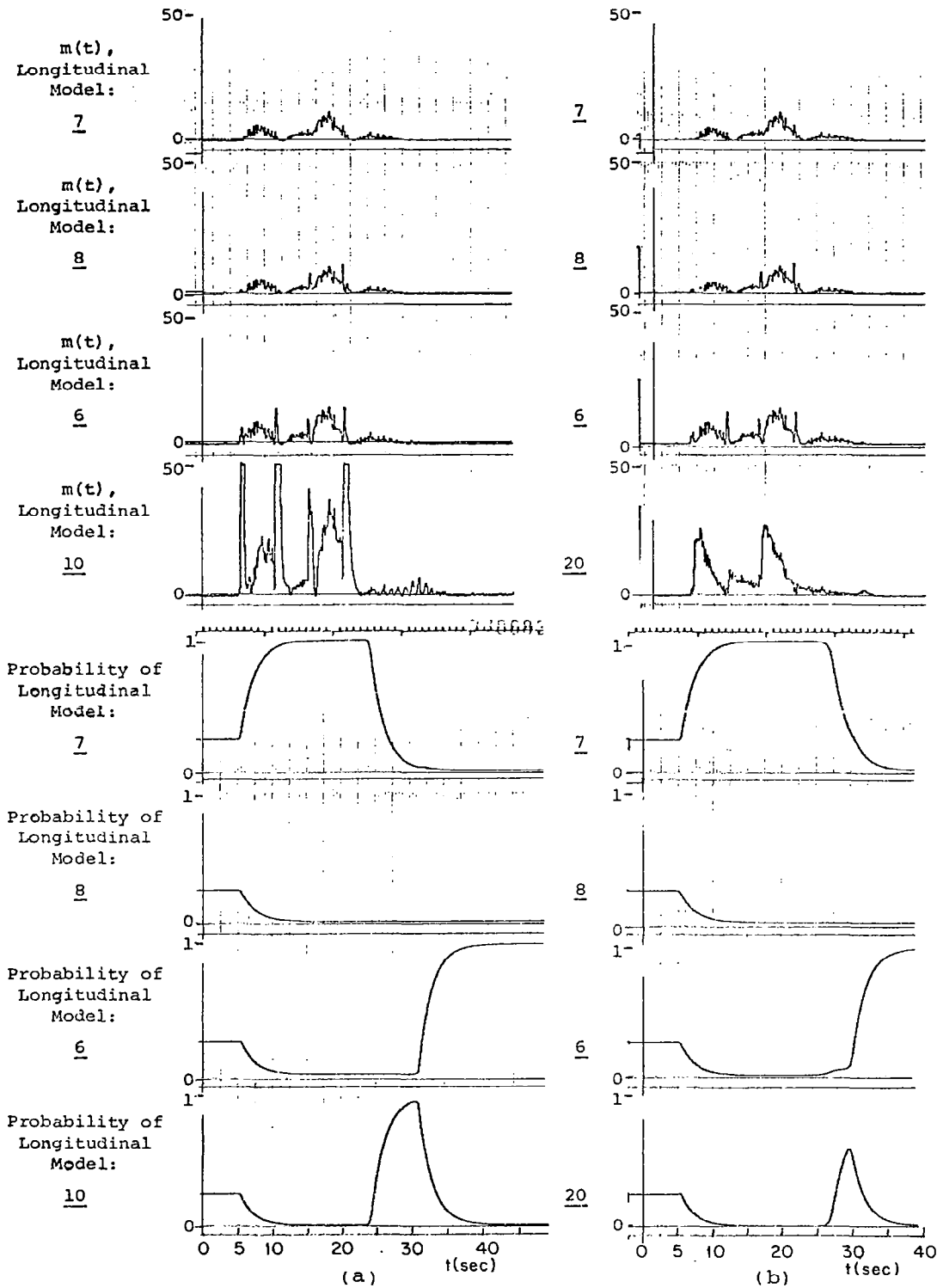
Figure 7.4.13   Longitudinal control probability and m(t) responses
                 to elevator doublet command, no turbulence, altitude
                 304.8 meters, speed .7 Mach

                 (a)   MMAC responses, models 6,7,8,10
                 (b)   MMAC responses, models 6,7,8,20
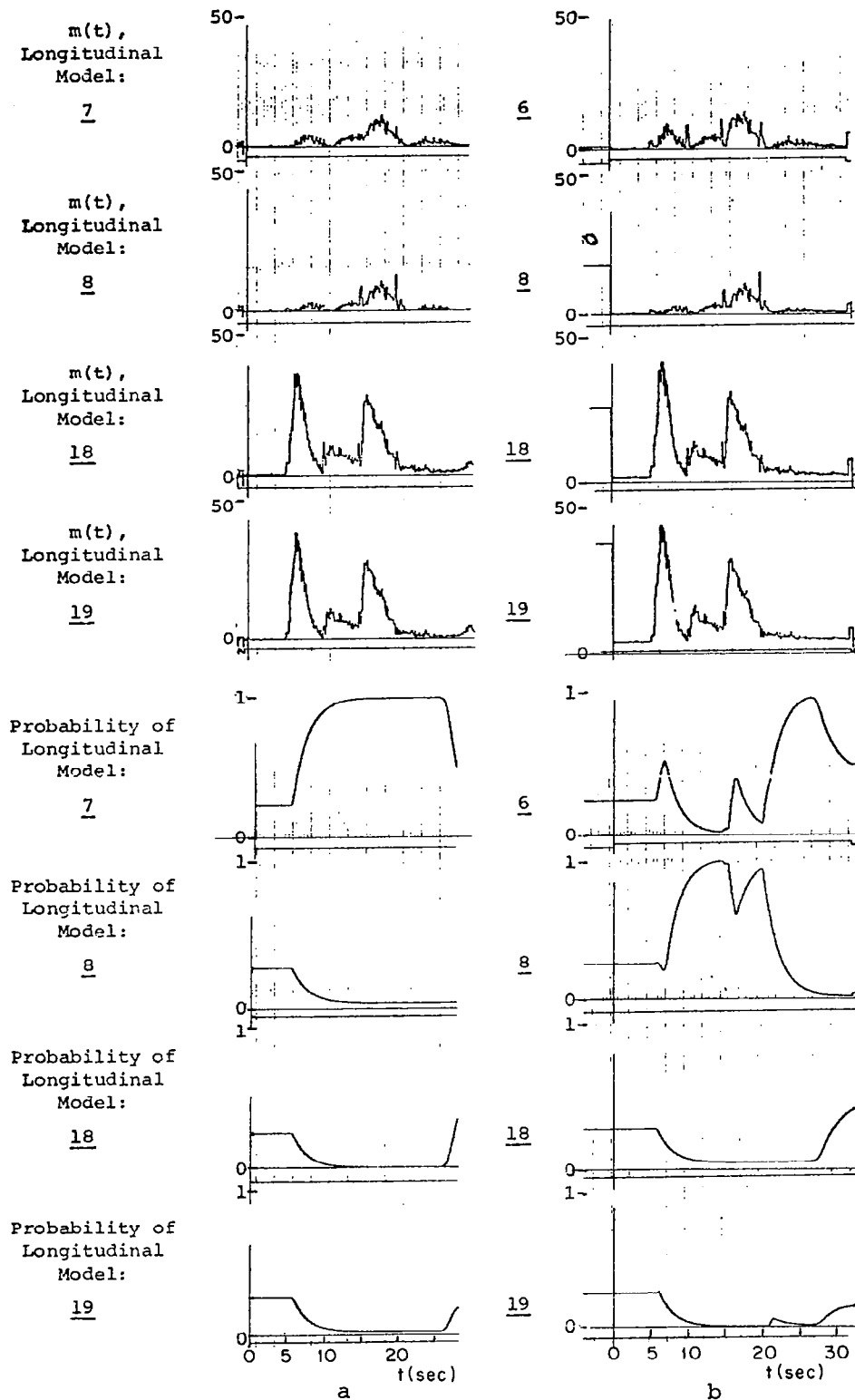
Figure 7.4.14   Longitudinal control probability and m(t) responses
to elevator doublet command, no turbulence, altitude
304.8 meters, speed .7 Mach

(a)   MMAC responses, models 7,8,18,19
(b)   MMAC responses, models 6,8,18,19
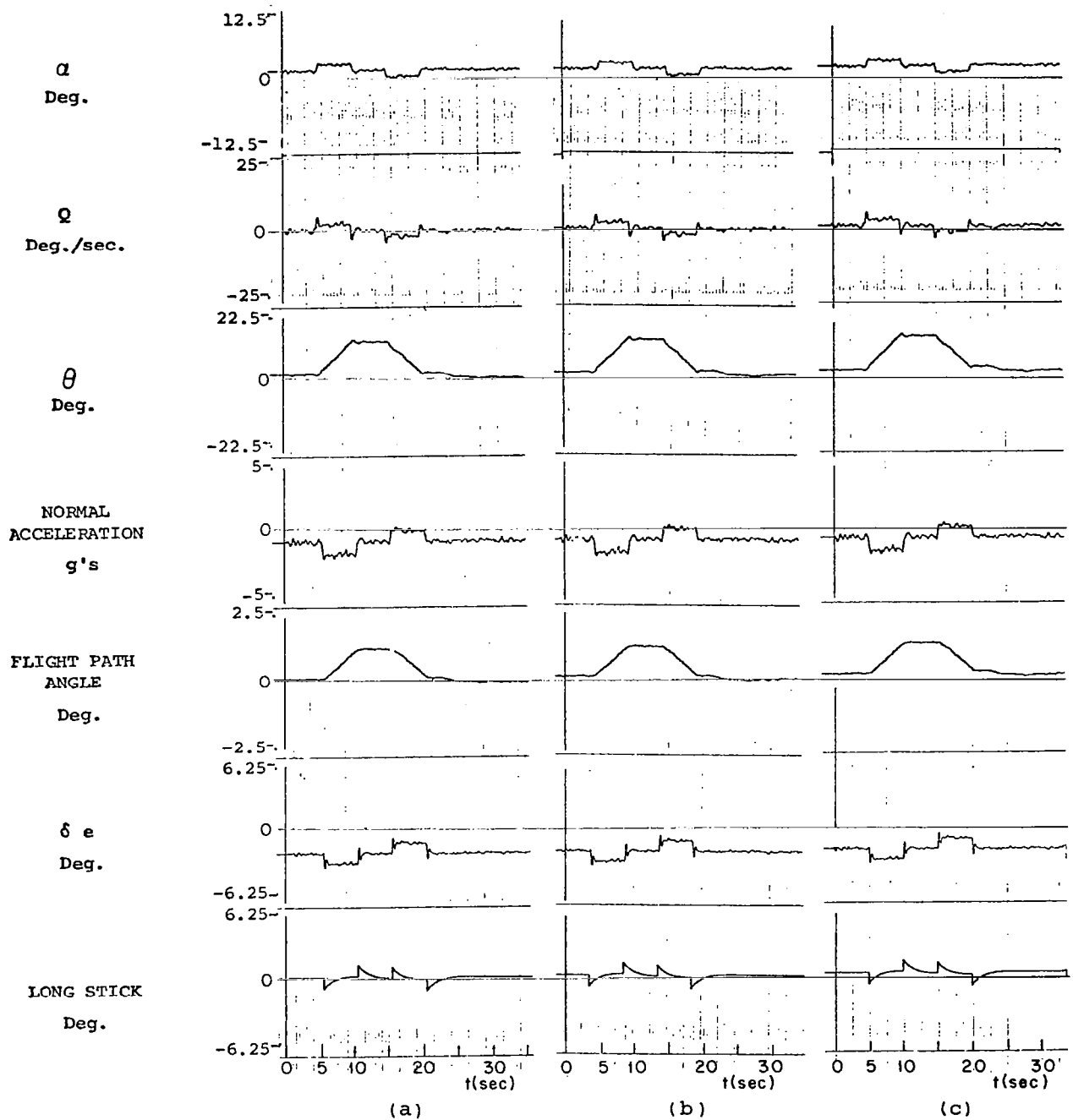
Figure 7.4.15   Longitudinal responses to elevator doublet command,
1.22 m/sec rms turbulence, altitude 304.8 meters, speed
.7 Mach

(a)   MMAC responses, models 6,7,8,10
(b)   MMAC responses, models 6,7,8,20
(c)   MMAC responses, models 7,8,18,19
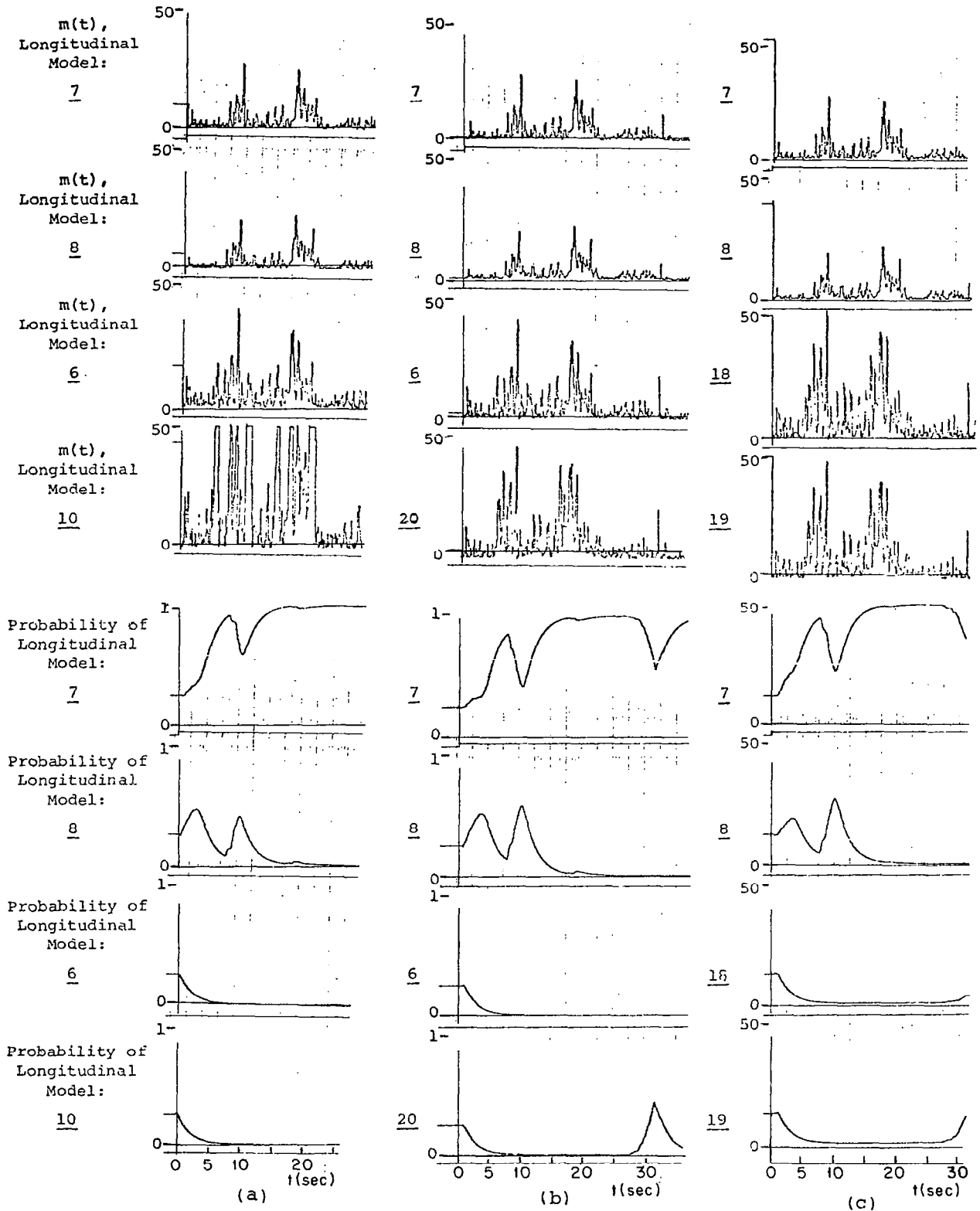
Figure 7.4.16 Longitudinal control probability and m(t) responses
to elevator doublet command, 1.22 m/sec rms turbulence,
altitude 304.8 meters, speed .7 Mach

(a) MMAC responses, models 6,7,8,10
(b) MMAC responses, models 6,7,8,20
(c) MMAC responses, models 7,8,18,19
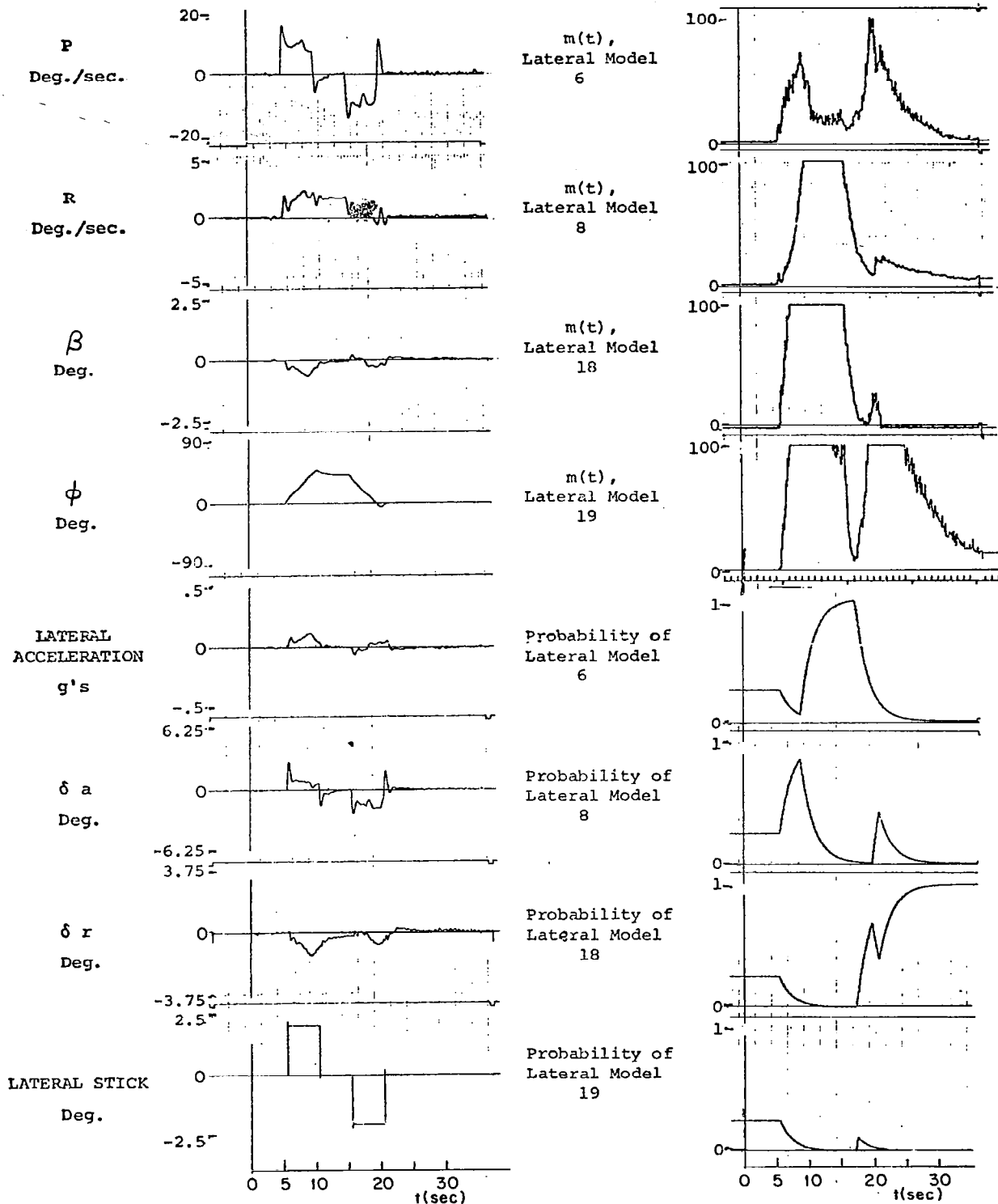
Figure 7.4.17   Lateral responses to aileron doublet command, no turbulence, altitude .304.8 meters, speed .7 Mach, MMAC models 6,8,18,19.

sideslip angle (β-gust) perturbation. The Kalman filter states are ini-tially set to zero so that the initial perturbations are not readily estimated. The aircraft is not subject to turbulence.

Figures 7.5.1, 7.5.2 and 7.5.3 show three sets of responses, corres-ponding to pitch rate, normal acceleration and lateral acceleration responses respectively. The experiments show the open-loop behavior of the aircraft, the perfect identification response, and two MMAC responses. Note the close correspondence of the MMAC responses to the perfect iden-tification response. The initial perturbations are eliminated quickly, so that, in the absence of turbulence, the aircraft reaches equilibrium flight.

Figure 7.5.4 contains the trajectories of the longitudinal identi-fication probabilities of an MMAC simulation. Note the quick identifi-cation of the true model in less than one second, even though the Kalman filters are not correctly initialized and all measurements are noise-corrupted. The lag in proper identification corresponds to the lag in the Kalman filters correctly updating its state estimates.

The second set of experiments corresponds to a repetition of the first experiments, now at cumulus level turbulence (4.57 m/sec rms). Figures 7.5.5, 7.5.6 and 7.5.7 contain the pitch rate, normal accelera-tion, and lateral acceleration responses of the aircraft. Again, note the similarity between MMAC controllers and the perfect identification controller. Figures 7.5.8 and 7.5.9 show the control probabilities for

the longitudinal and lateral system respectively, using a MMAC controller with hypotheses 10, 11, 12, 17. The lateral system erroneously identifies flight condition 10, a close neighbor of flight condition 11. The performance is hardly affected by this misidentification.

Figures 7.5.10 and 7.5.11 show the control probabilities used in the MMAC controller with hypotheses 10, 19, 12, 17. The continuous transitions in the probabilities reflect the amount of excitation caused by the cumulus disturbances. No clear identification is obtained in the transient period. However, the aircraft responses are still satisfactory.

The third set of simulations were conducted at zero turbulence. The Kalman filters were correctly initialized in these experiments. Figure 7.5.12 shows the longitudinal responses of three MMAC systems. Figure 7.5.13 shows the lateral responses of these systems; and Figure 7.5.14 shows the control probabilities associated with these systems. Note the similarity in the responses, even though the third MMAC system hypotheses are 6, 13, 16, 17, and the true aircraft is at flight condition 11. Checking the mismatched stability tables of Section 7.3, one sees that there are several unstable combinations possible with flight condition 11. Flight conditions 12 and 13 are unstable in the lateral system, as is flight condition 10 in the longitudinal system. The differences in lateral system responses in the last simulation are due to a partial initial identification of model 13. The MMAC system corrects

this identification error in short order, never completely using model 13 for control purposes. In the longitudinal system, no troubles were encountered when the unstable model 10 was included, since the identification did not choose that hypothesis.

Figure 7.5.15 contains three simulation responses to doublet stick commands: column (a) represents the longitudinal aircraft responses with perfect identification, column (b) represents the longitudinal aircraft responses with an MMAC controller using hypothesis models 10, 11, 12 and 17, and column (c) represents the longitudinal aircraft responses with an MMAC controller using hypothesis models 10, 12, 17 and 18. No turbulence was included in these experiments. The simulations illustrate the close responses of the MMAC-controlled aircraft to the responses of the aircraft with perfect identification. The responses were similar even when the "true" hypothesis was not included in the MMAC system. Figure 7.5.16 also compares the performance of an MMAC-controlled system with a system using perfect identification. These two experiments were conducted with no turbulence, and the break frequency for the high-pass filters described in Chapter 5 was set at one radian per second. The performance of the perfect identification system and the MMAC system with hypotheses 6, 13, 17 and 19 are seen to be quite close, even though none of the MMAC hypotheses are similar to the true flight condition. This suggests that, in the absence of accurate hypotheses, the identification system chooses controllers which approximate the desired closed-loop responses.

Figure 7.5.17 shows the evolution of the control probabilities in the MMAC experiments in Figures 7.5.15 and 7.5.16. Initially, there is a

quiet period with no information available so the MMAC identification does

not choose any models. After five seconds, the pilot commands starts. Fig-

ure 7.5.17(a) shows that the true model is correctly identified once the

command starts. Figure 7.5.17 indicates that, in the absence of the true

hypothesis, a close neighbor (flight condition 10) is identified with

little effect on the aircraft responses, as evidenced by Figure 7.5.15(c).

The identification is slower in this case, reflecting the fact that

flight condition 10 is not the true flight condition.

Figure 7.5.17(c) describes the evolution of the identification pro-

abilities for an MMAC system with hypotheses 6, 13, 16, 17. The identifi-

cation converges to flight condition 13. Interestingly, the aircraft

responses were very similar to those obtained under perfect identifica-

tion, even though the hypothesis models were different from the true

hypothesis.

Figure 7.5.18 is a repetition of the experiments in Figure 7.5.15,

using a break frequency in the high-pass filter of .1 radians per sec-

ond. The three sets of responses can be virtually superimposed, even

when the true hypothesis is not included. Figure 7.5.19 describes the

longitudinal control probability and m(t) responses for the experiments

in Figures 7.5.18 (b) and (c). When the true hypothesis (model 11) is

included in the MMAC system, the identification scheme selects it

during the doublet command. Once the command dies, β^* behavior is ob-

served, where model 10, corresponding to the largest β^*, is identified.

Figure 7.5.19 (b) shows uncertain identification between two close neigh-

bors of the true hypothesis (models 10 and 12) during the command period,

followed by β^*-identification behavior.

Figure 7.5.20 describes the longitudinal MMAC response of the aircraft with hypotheses 10, 11, 12 and 17, and with hypotheses 10, 12, 17, 18, when the aircraft is subjected to 1.22 m/sec rms turbulence. Again the responses of the aircraft when the true flight condition was a hypothesis are almost identical to the responses when the true flight condition was not included as a hypothesis. Figure 7.5.21 shows the evolution of the control probabilities and the weighted sums of residuals (m(t)) for the longitudinal system. The presence of moderate turbulence provides information to the identification system, as evidenced by the plots of the weighted sum of residuals. However, one should notice how close the traces of $m_i(t)$ are for each hypothesis, indicating the limited amount of information available. When the MMAC hypothesis are models 10, 11, 12 and 17, the MMAC correctly identifies model 11, but only when the pilot command starts. When model 11 is excluded, the MMAC identification converges on model 12, a close neighbor of model 11, again when the command starts. These experiments indicate that the presence of turbulence does not provide sufficient information to correctly identify the true hypothesis. Examining the traces of the $m_i(t)$, this means that in the absence of pilot commands, turbulence alone does not create sufficient difference in the weighted sum or residuals to use for identification.

Figures 7.5.23 and 7.5.22 show aircraft responses to doublet commands in the lateral system. The lateral pilot command system is based

on a model-following scheme. This scheme, described in Chapter 6, proved

to be somewhat incompatible with the MMAC algorithm. When identification

changes in the MMAC algorithm, the control gains from the model to the

aileron and rudder commanded rates change also, as indicated in Chapter 6

and Appendices G and H. Hence, although the reference values provided by

the model remain unchanged with identification, the commanded aileron and

rudder rates are affected.

Figure 7.5.24 contains the control probability responses for these

experiments. When the true model is included in the MMAC system, it is

identified promptly during maneuvers, resulting in a good response, as

seen in Figure 7.5.22 b. In the absence of the true model, the identi-

fication scheme chooses a close neighbor, model 12, which is mismatched

unstable according to Section 7.3. The ensuing identification switches

can do little to improve performance, as models 17 and 18 are also mis-

matched unstable. The identification scheme eventually chooses model 10,

the only stable choice, although the presence of the three unstable models

disrupted performance considerably. This is an important example of how

sensitive MMAC performance is with regards to the hypotheses used for

identification.

The experiments in this section support the conclusion that the MMAC

identification system performs best under stick commands, rather than to

turbulence excitation or gusts. The performance of the lateral control

system was best at this altitude, since the model used in the model-

following system corresponds closely to the test flight condition. Still,
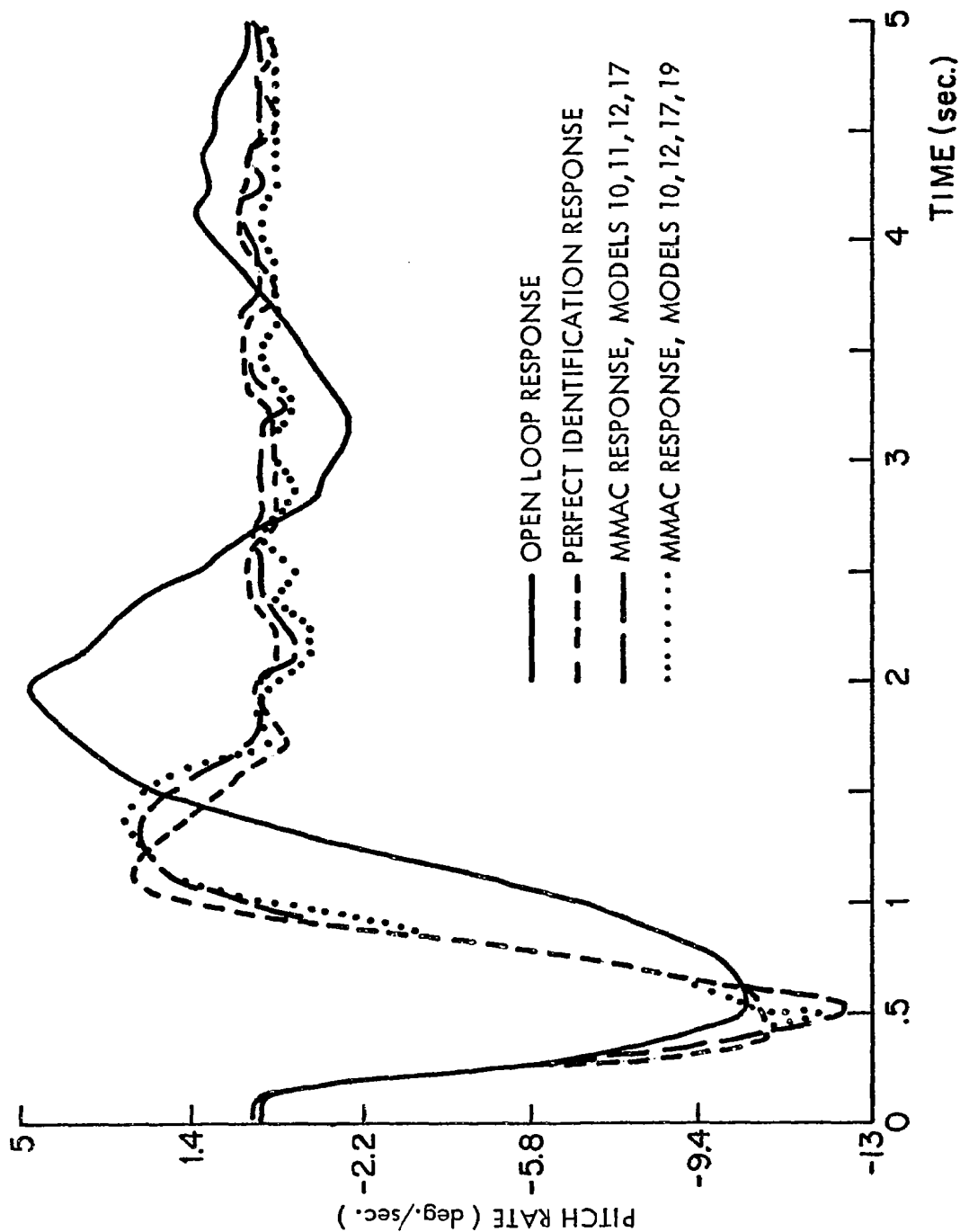
Figure 7.5.1   Pitch Rate Responses at F.C. 11, no turbulence
altitude 6096 meters, speed .6 Mach
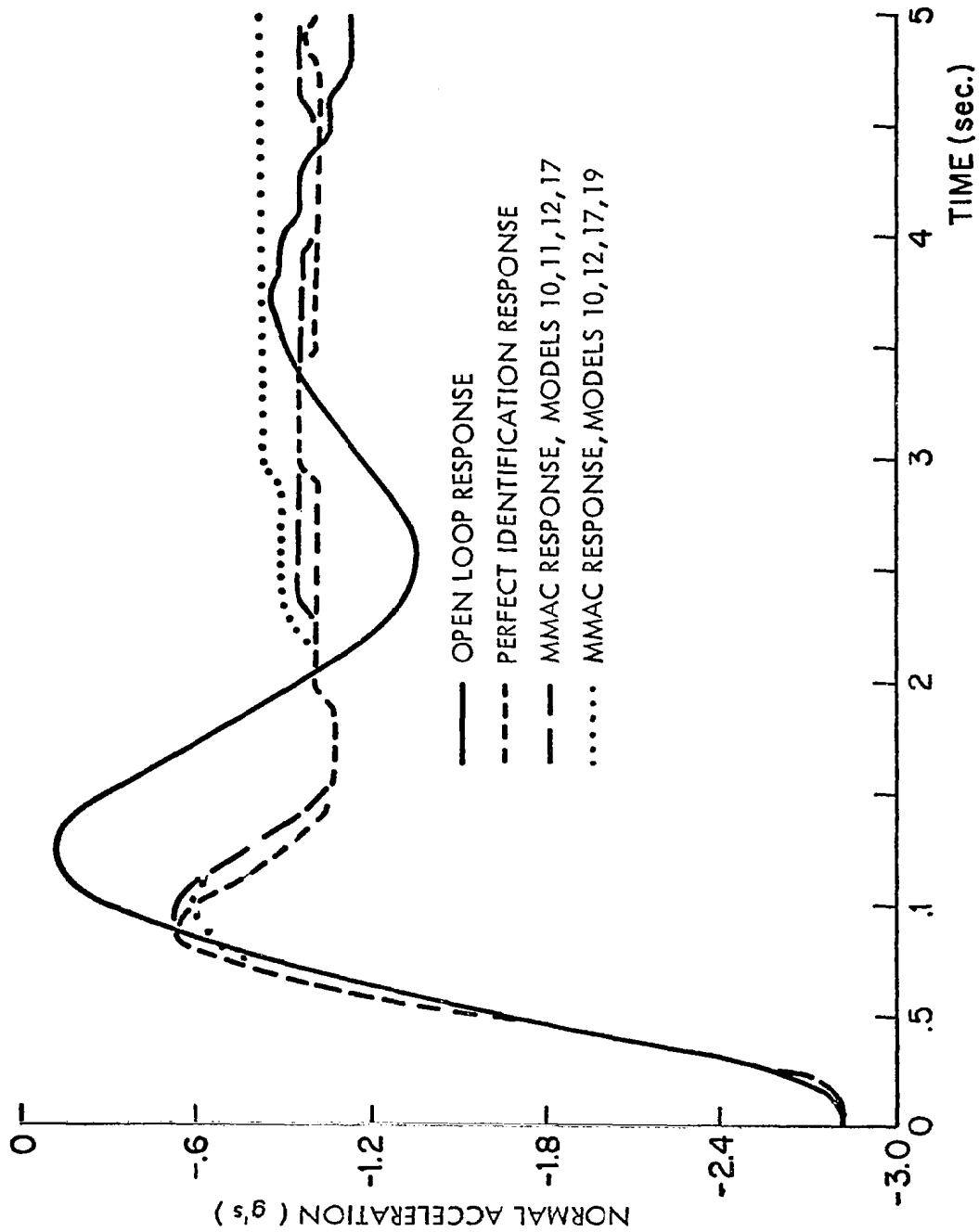
Figure 7.5.2   Normal Acceleration Responses at F.C. 11, no turbulence.
altitude 6096 meters, speed .6 Mach
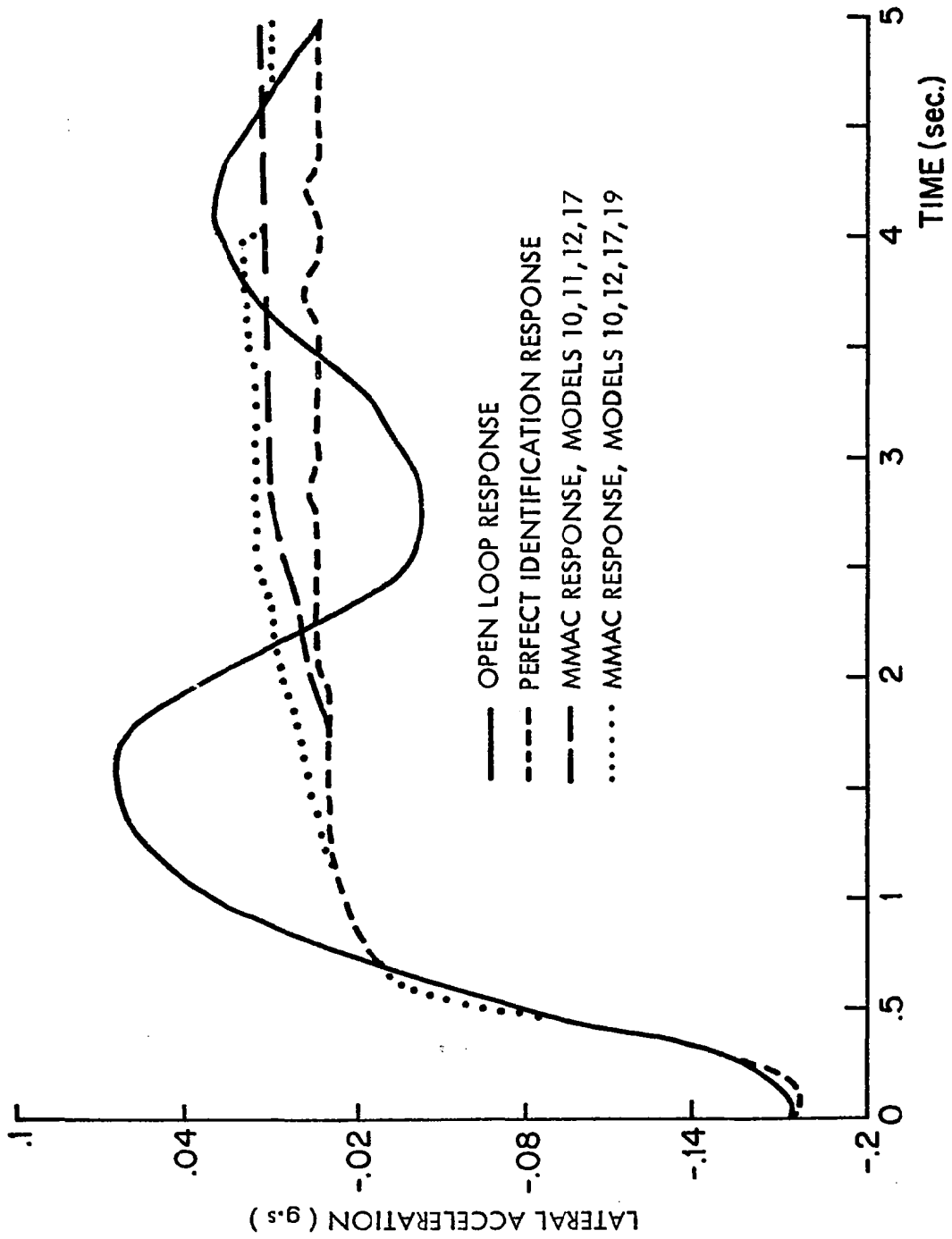
Figure 7.5.3   Lateral Acceleration Responses at F.C. 11, no turbulence
altitude 6096 meters, speed .6 Mach
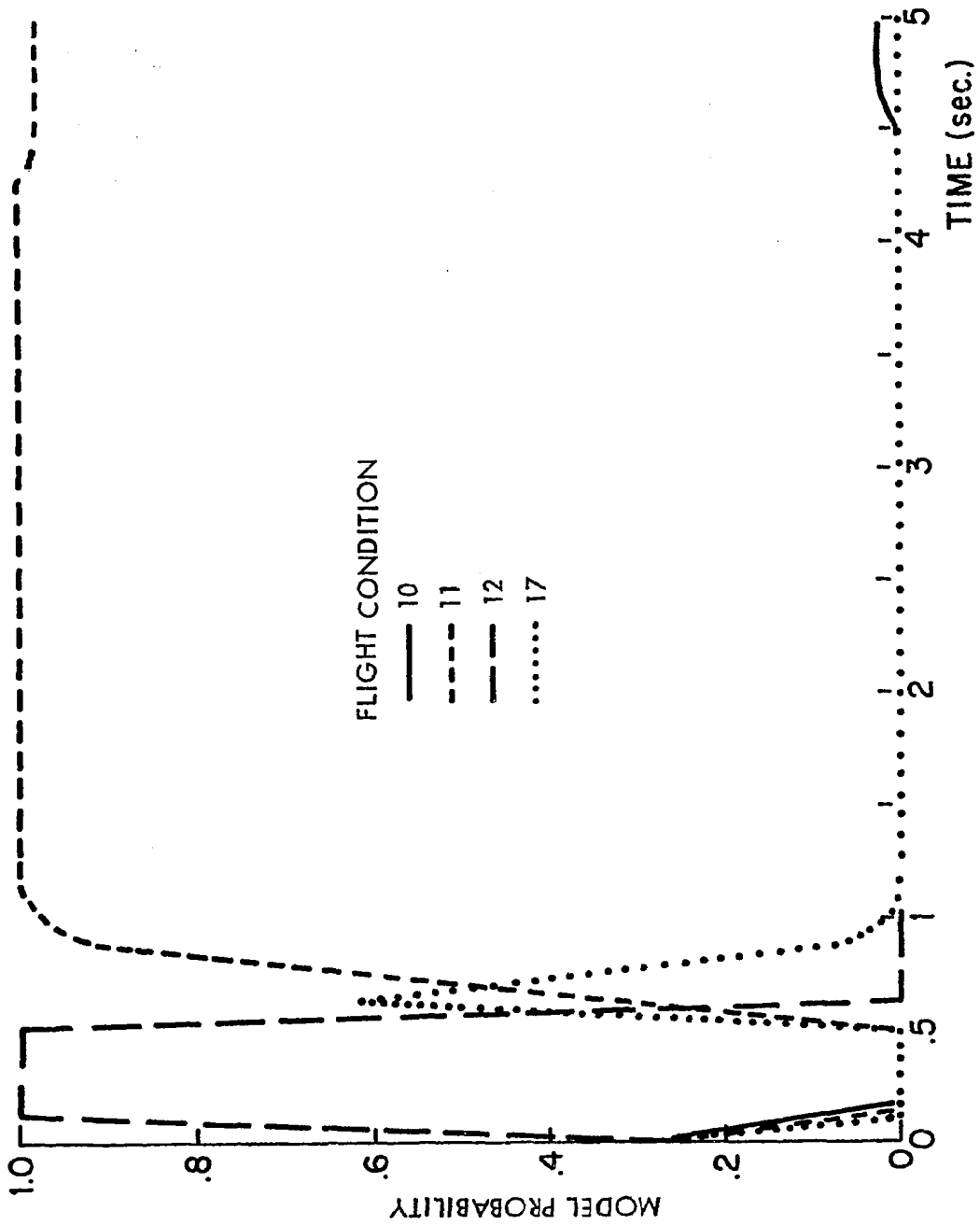
Figure 7.5.4   Longitudinal System Identification Probabilities at F.C. 11,
no turbulence , altitude 6096 meters, speed .6 Mach
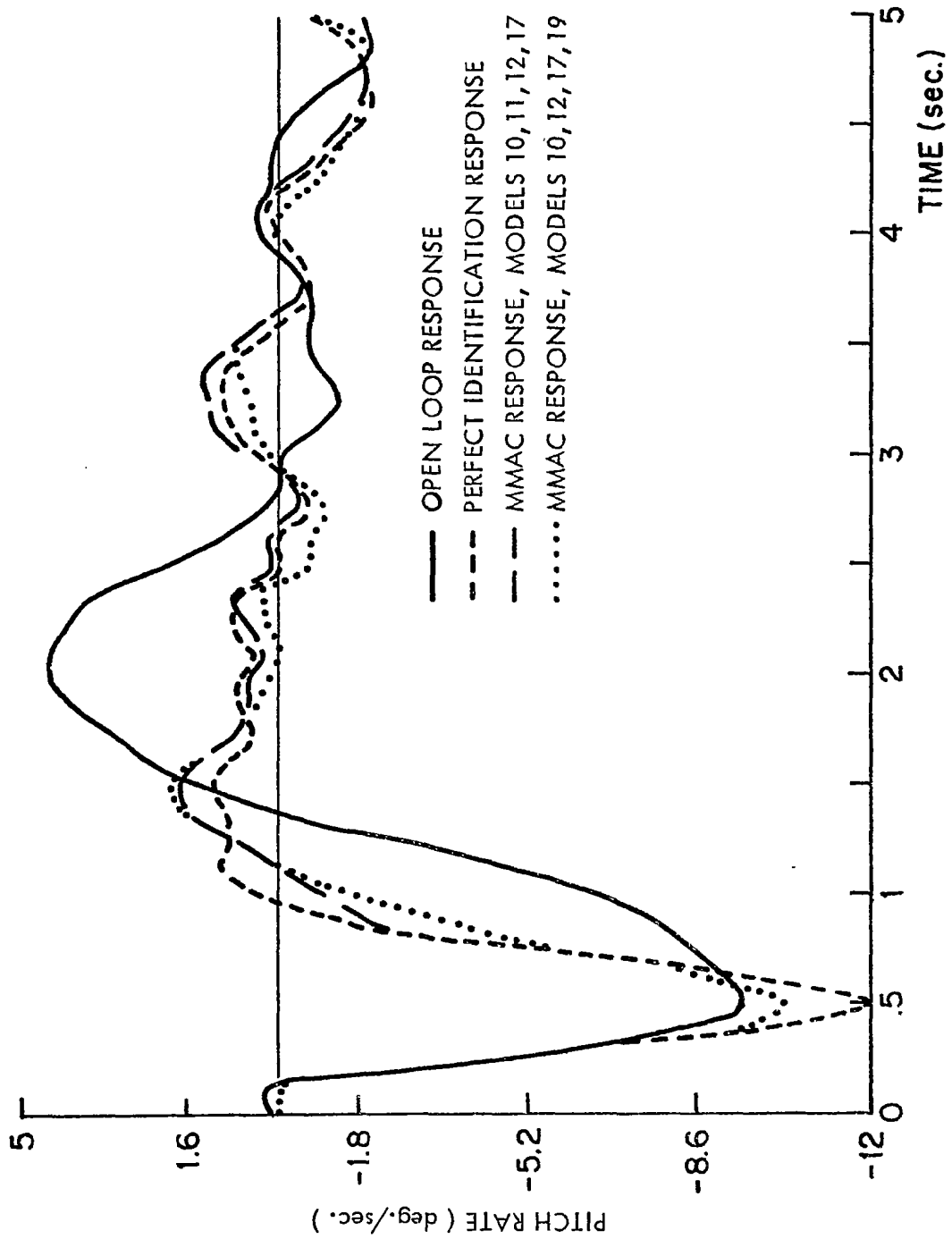
Figure 7.5.5   Pitch Rate Responses at F.C. 11,
4.57 m/sec rms turbulence, altitude
6096 meters, speed .6 Mach
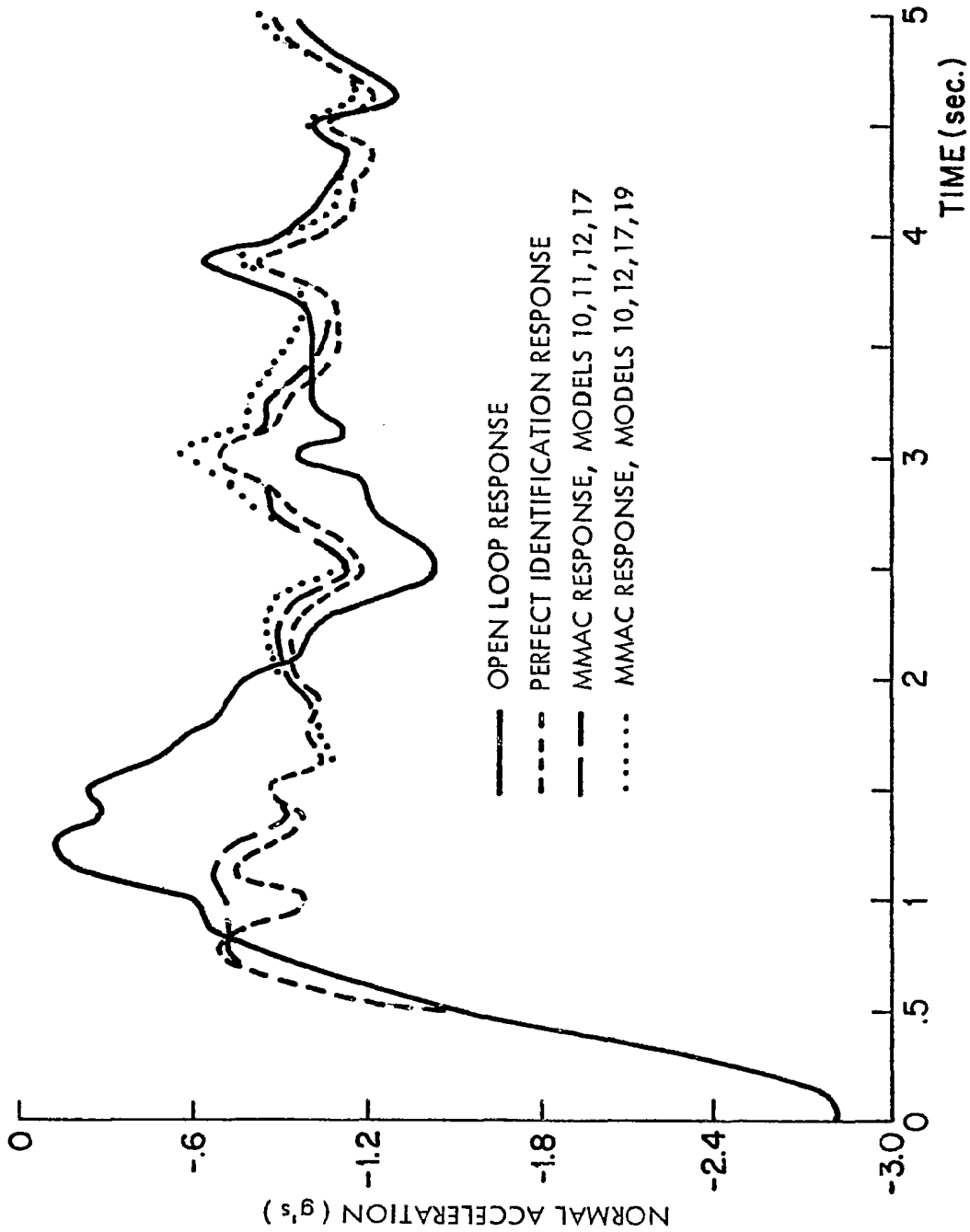
Figure 7.5.6   Normal Acceleration Responses at F.C. 11,
4.57 m/sec rms turbulence,
altitude 6096 meters, speed .6 Mach
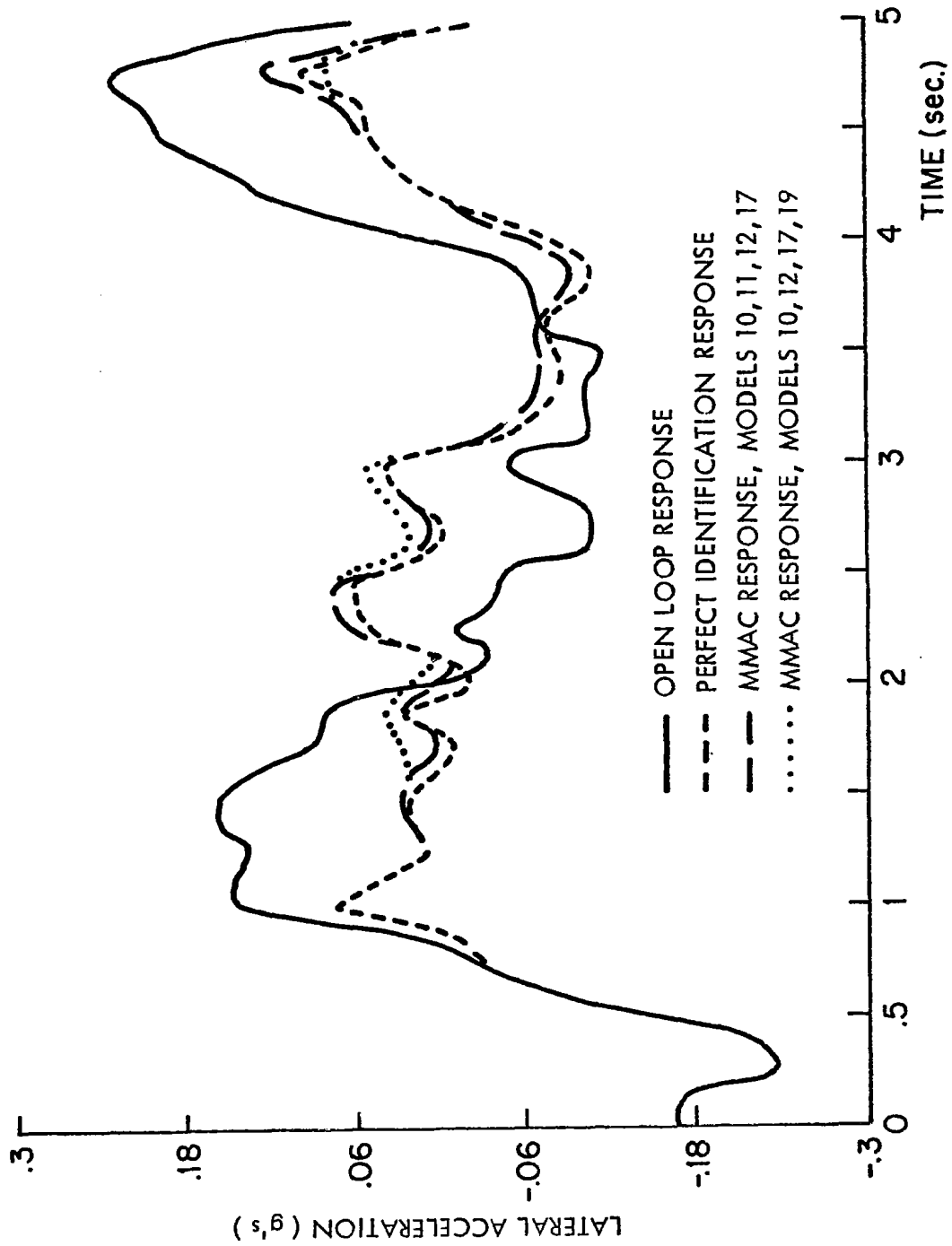
Figure 7.5.7 Lateral Acceleration Responses at F.C. 11,
4.57 m/sec rms turbulence,
altitude 6096 meters, speed .6 Mach
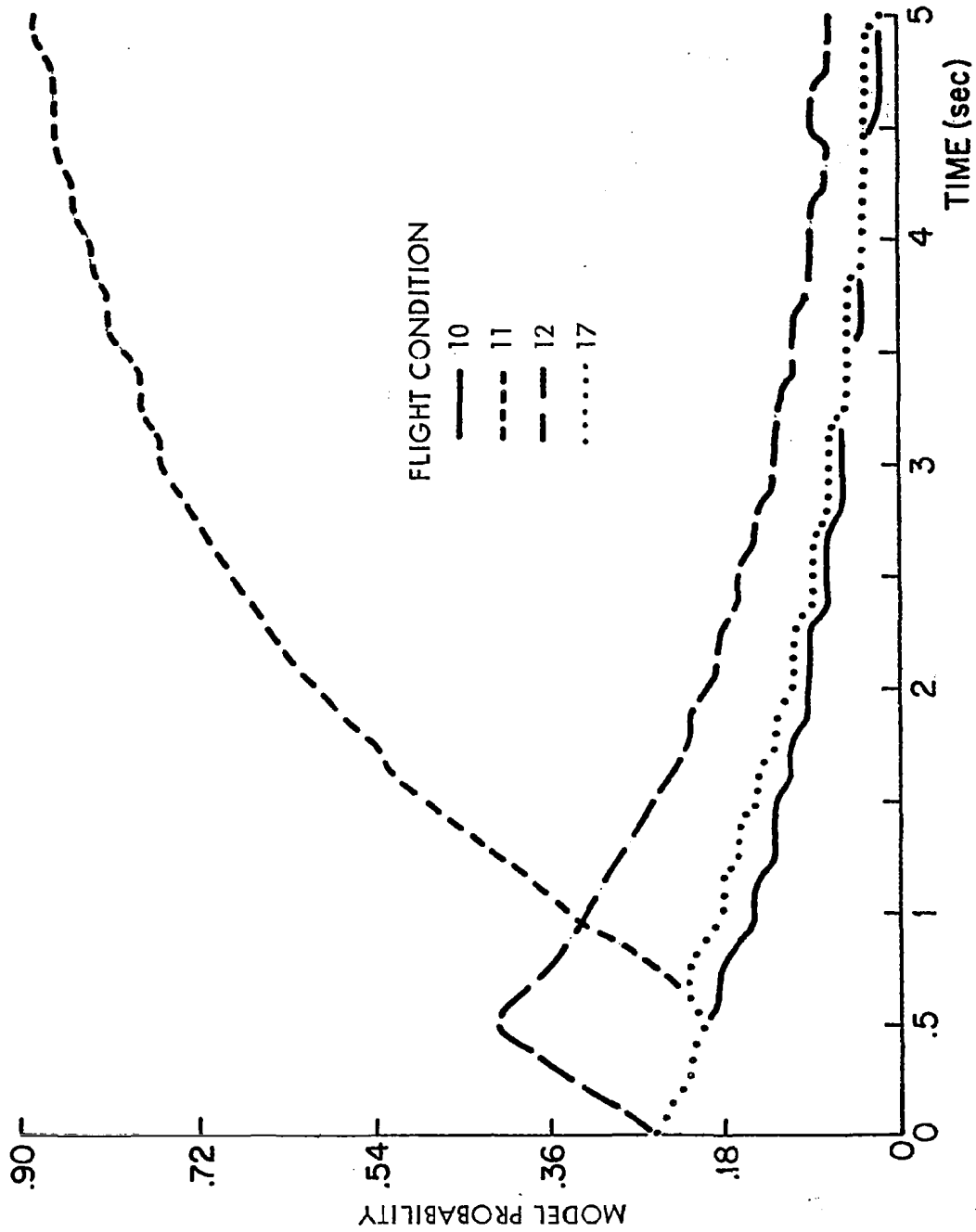
Figure 7.5.8   Low-pass Filtered Longitudinal System Probabilities
                 at F.C. 11, 4.57 m/sec rms turbulence,
                 altitude 6096 meters, speed .6 Mach
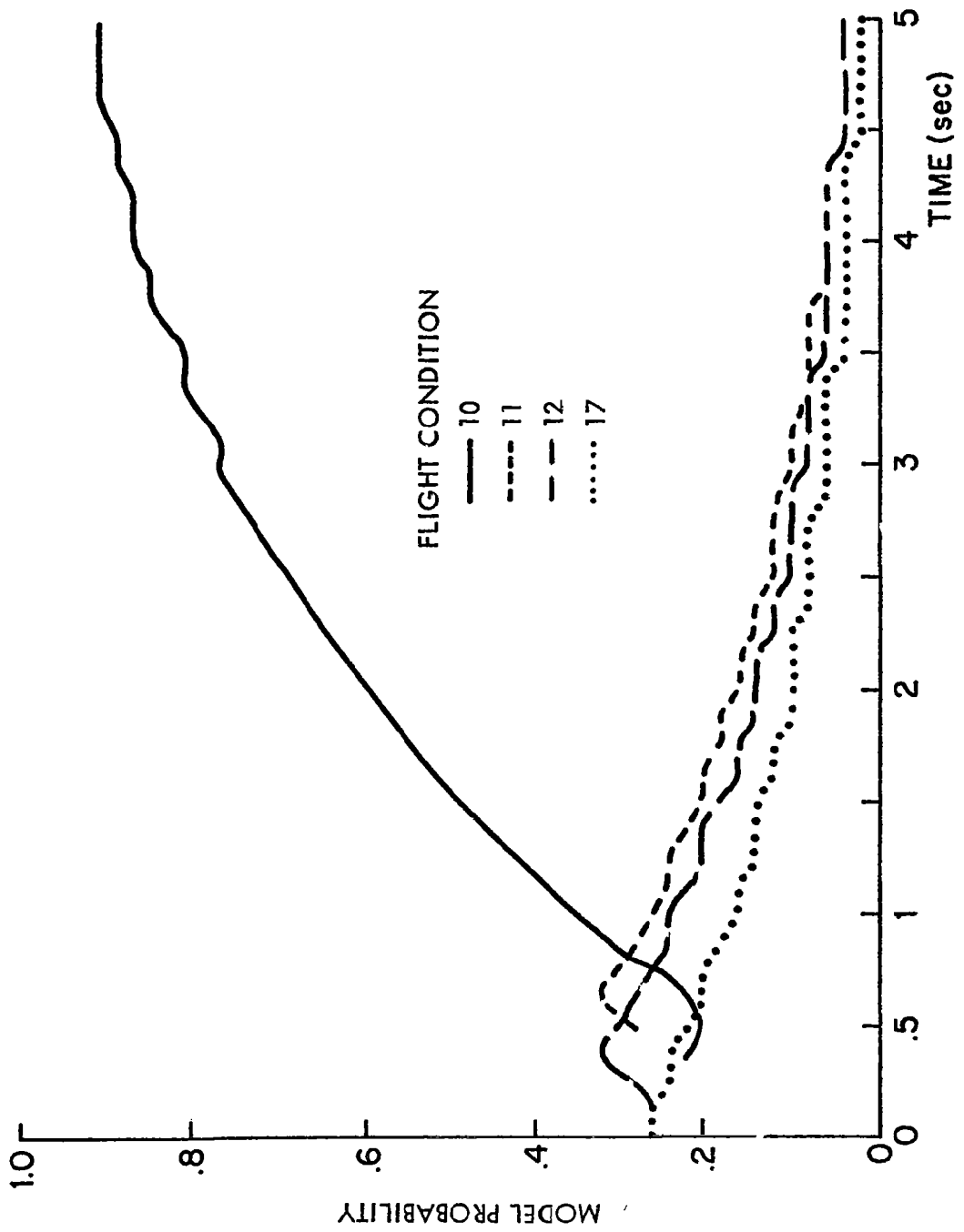
Figure 7.5.9   Low-pass Filtered Lateral System Probabilities
at F.C. 11, 4.57 m/sec rms turbulence,
altitude 6096 meters, speed 6 Mach
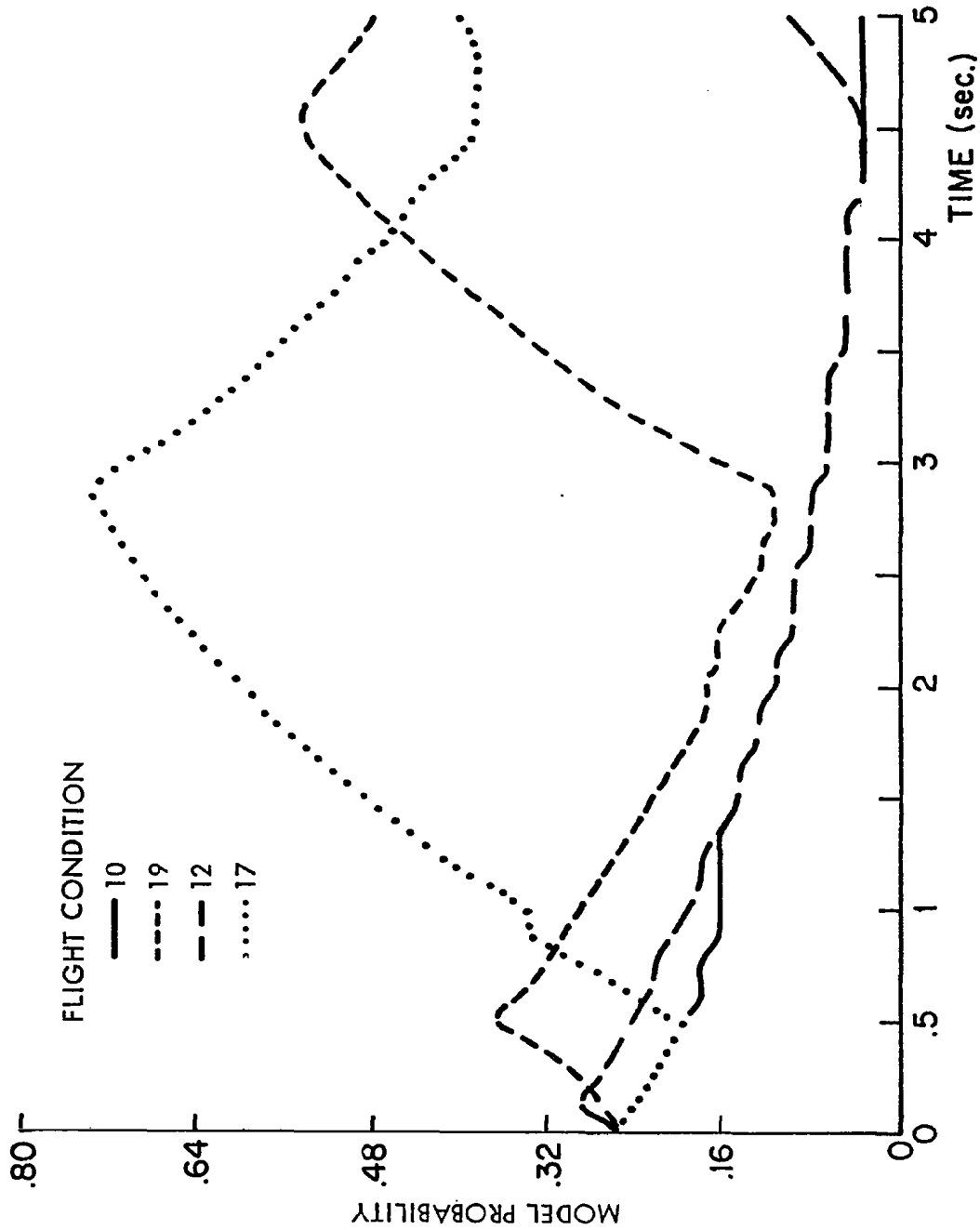
Figure 7.5.10   Low-pass Filtered Longitudinal System Probabilities
at F.C. 11, 4.57 m/sec rms turbulence,
altitude 6096 meters, speed .6 Mach
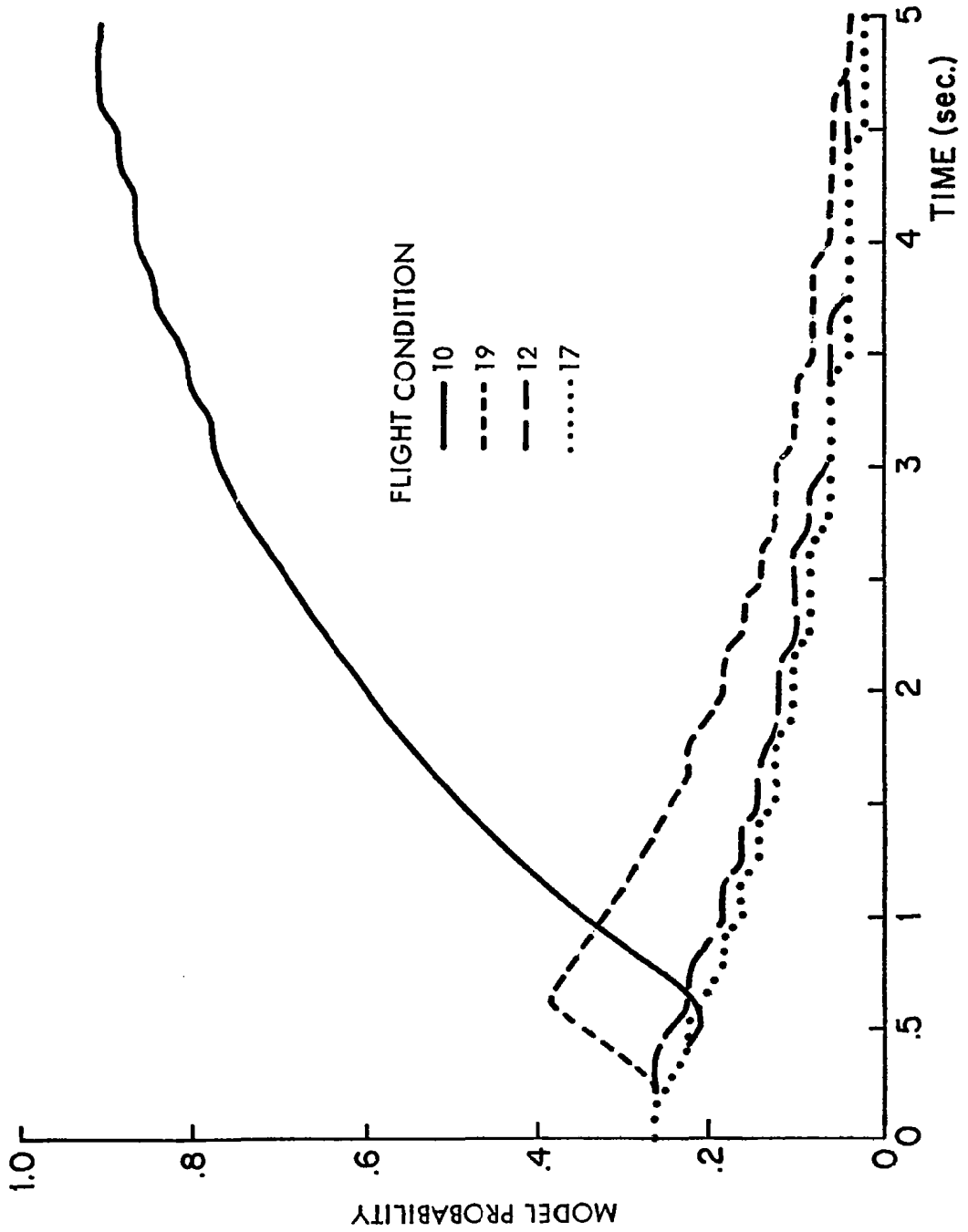
Figure 7.5.11   Low-pass Filtered Lateral System Probabilities at
F.C. 11, 4.57 m/sec rms turbulence,
altitude 6096 meters, speed .6 Mach
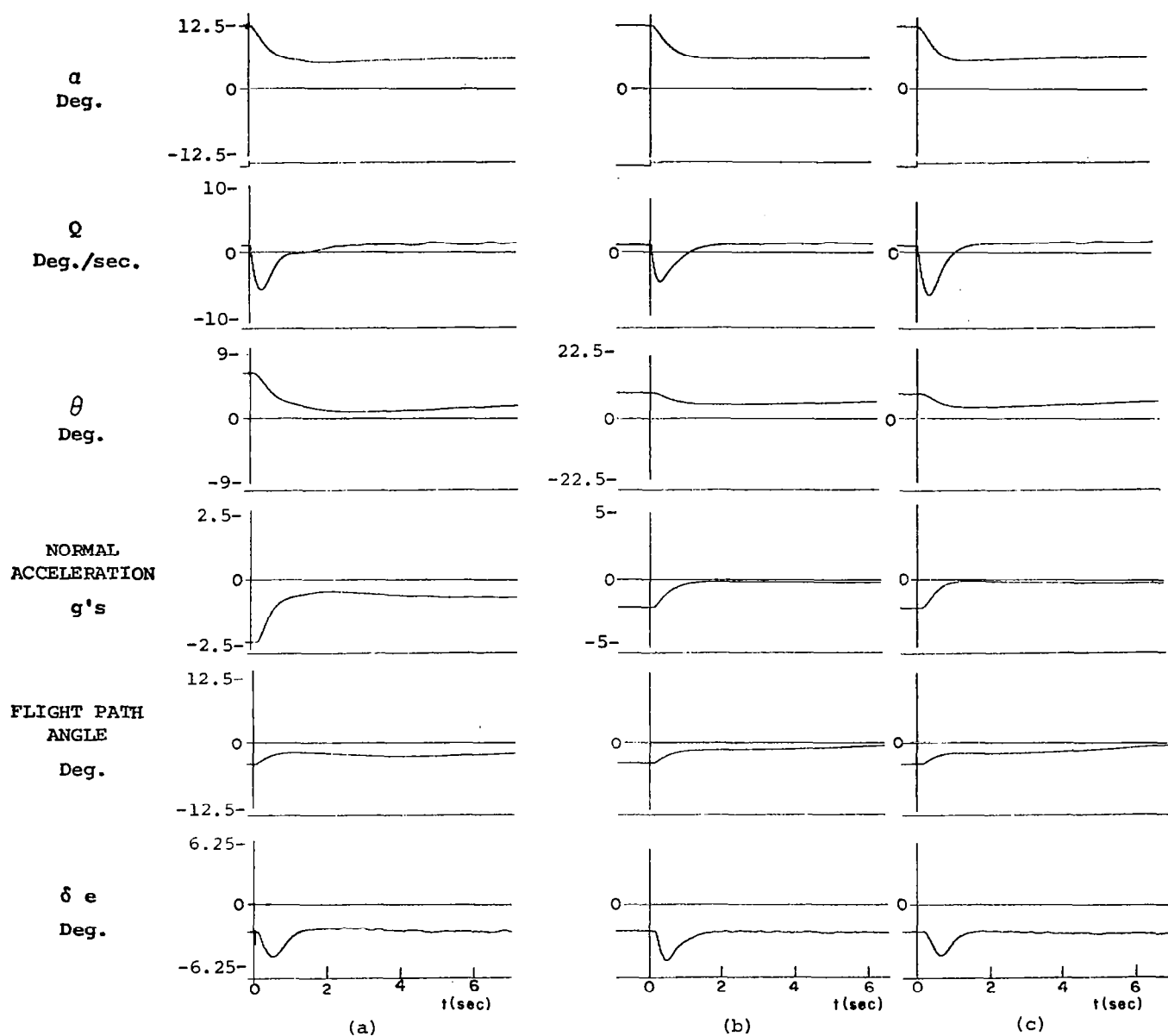
Figure 7.5.12   Longitudinal responses to 6°α, 2°β initial conditions,
no turbulence, altitude 6096 meters, and speed .6 Mach

(a)   MMAC responses, Models 10,11,12,17
(b)   MMAC responses, Models 10,12,17,18
(c)   MMAC responses, Models 6,13,16,17
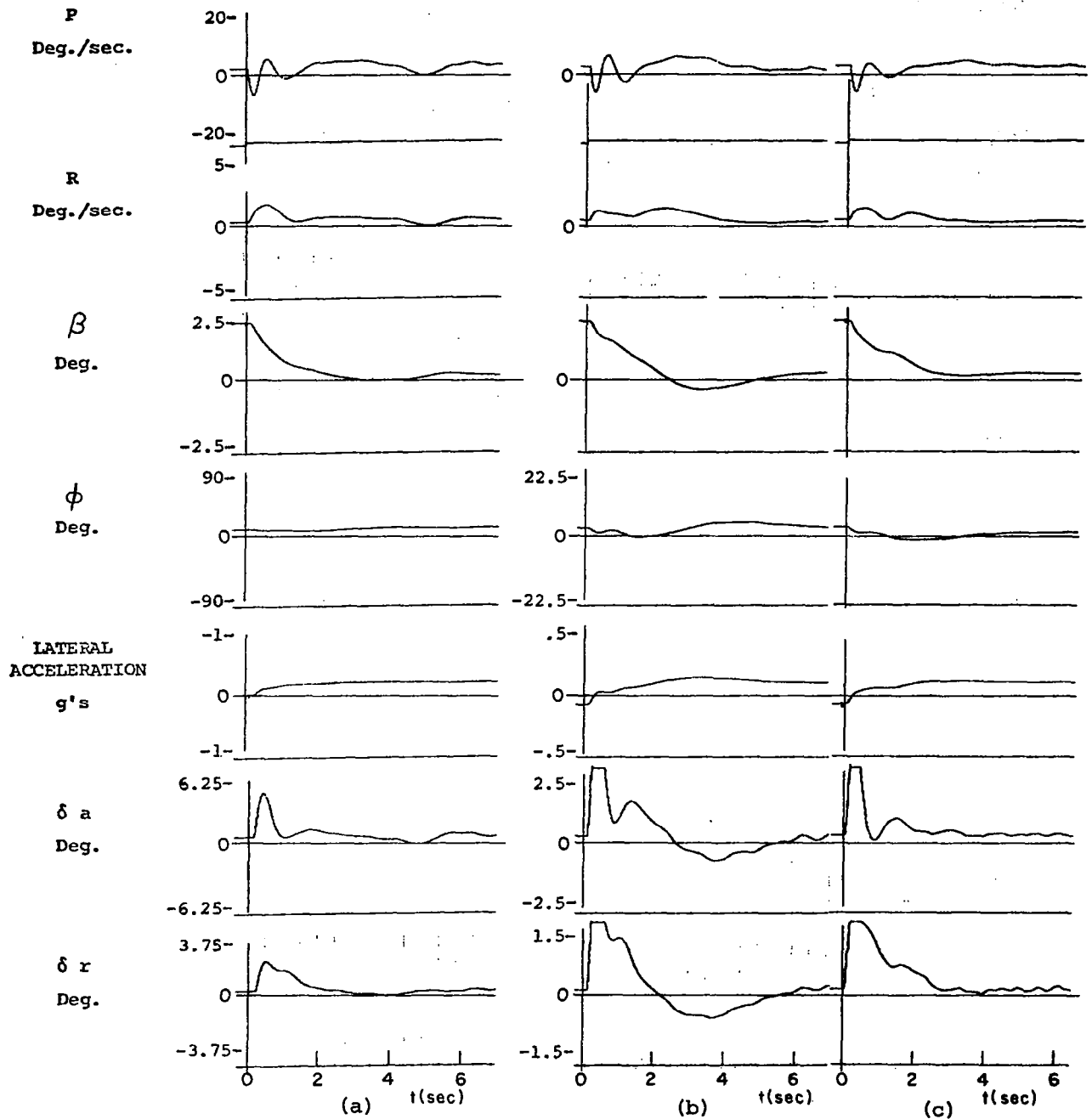
Figure 7.5.13   Lateral responses to 6°α, 2°β initial conditions,
no turbulence, altitude 6096 meters, speed .6 Mach

(a)   MMAC responses, Models 10,11,12,17
(b)   MMAC responses, Models 10,12,17,18
(c)   MMAC responses, Models 6,13,16,17
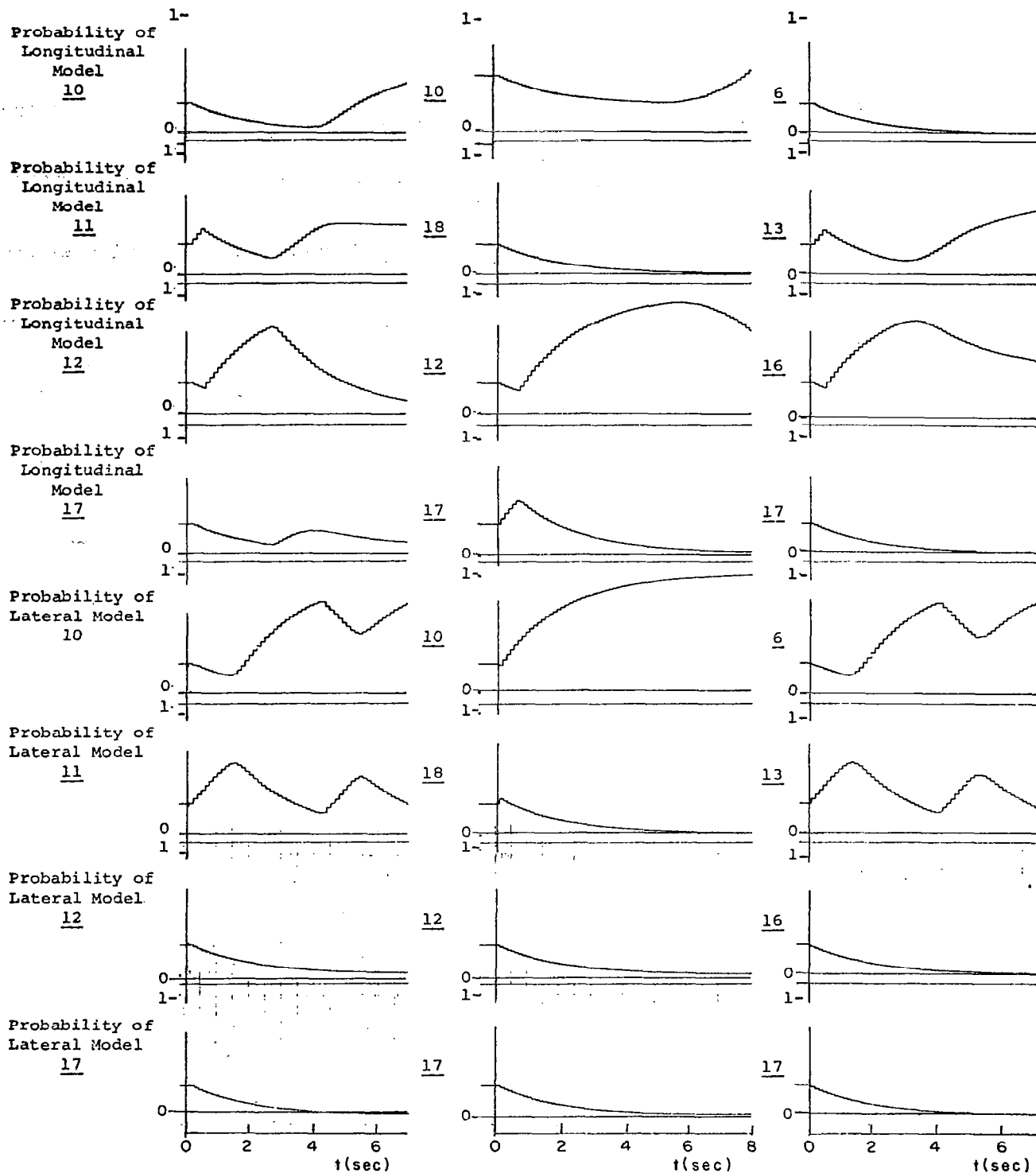
Figure 7.5.14   Control probability response to 6°α, 2°β initial
                 conditions, altitude 6096 meters, speed .6 Mach
                 no turbulence

                 (a)   MMAC responses, Models 10,11,12,17
                 (b)   MMAC responses, Models 10,12,17,18
                 (c)   MMAC responses, Models 6,13,16,17
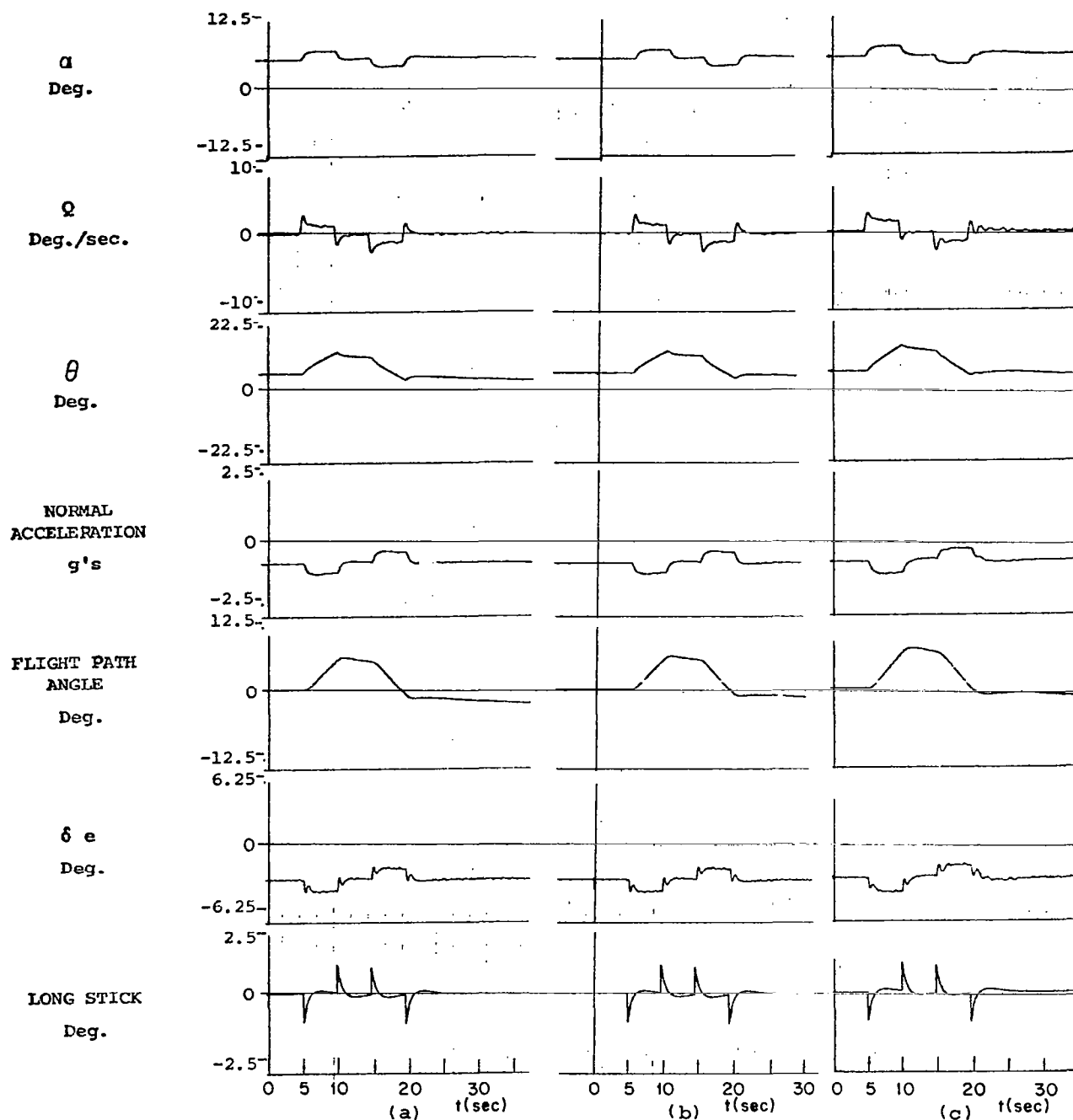
Figure 7.5.15 Longitudinal responses to elevator doublet command, no turbulence, altitude 6096 meters, speed .6 Mach

(a) perfect identification responses
(b) MMAC responses, models 10,11,12,17
(c) MMAC responses, models 10,12,17,18
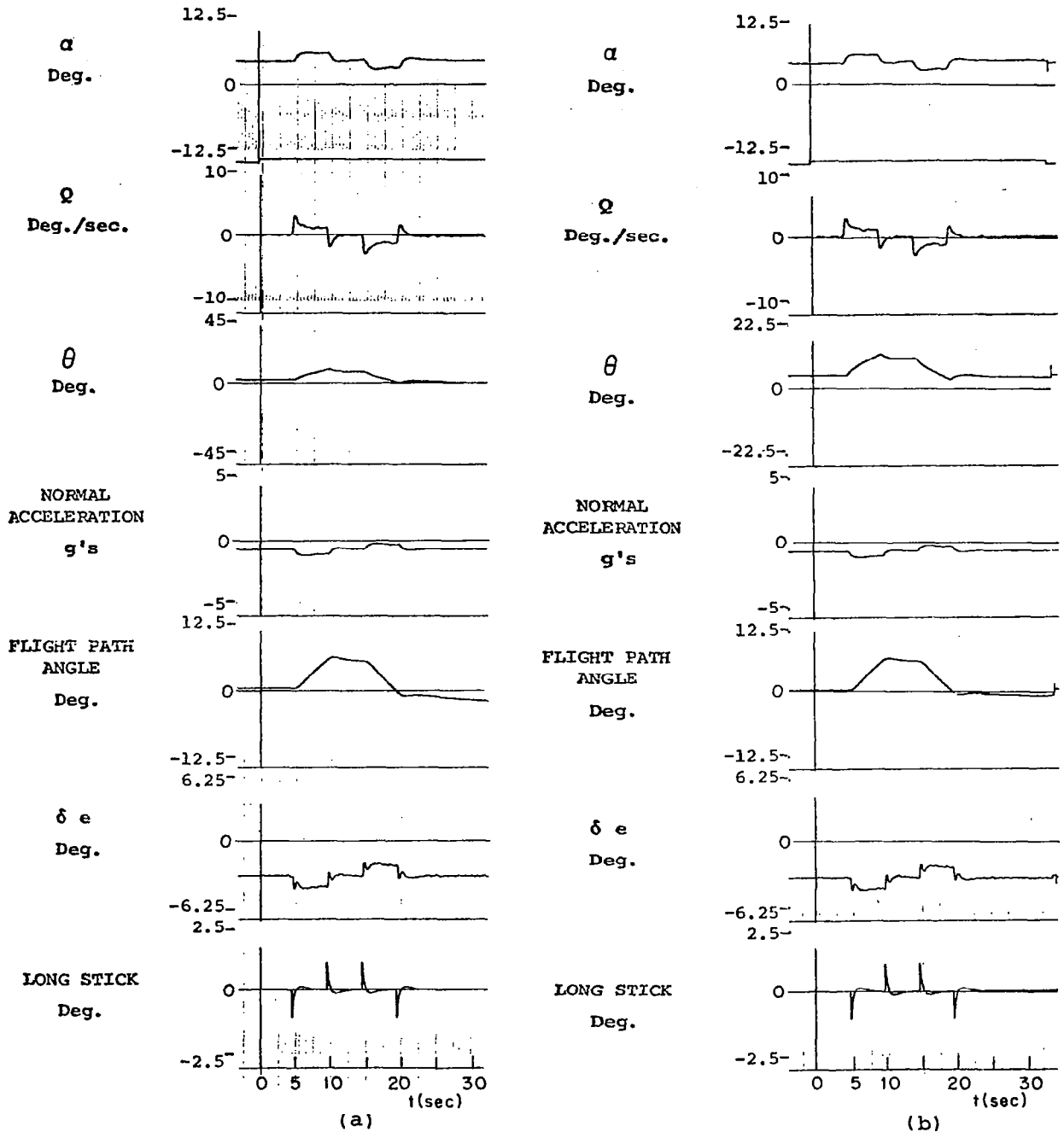
Figure 7.5.16   Longitudinal responses to elevator doublet command,
no turbulence, altitude 6096 meters, speed .6 Mach

(a)   perfect identification responses
(b)   MMAC responses, models 6,13,16,17
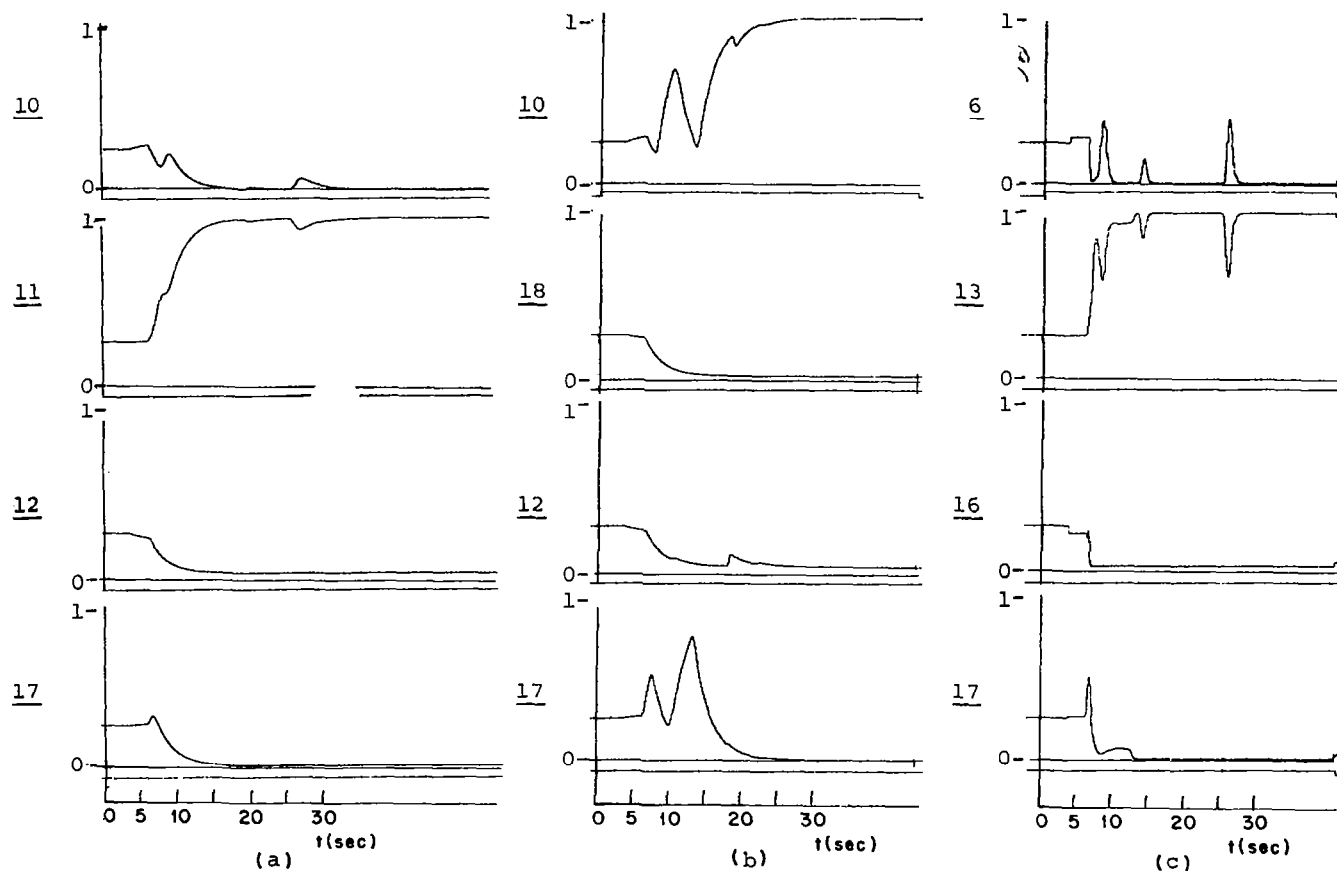
Figure 7.5.17   Control probability responses to elevator doublet command,
no turbulence, altitude 6096 meters, speed .6 Mach

(a)   MMAC responses, models 10,11,12,17
(b)   MMAC responses, models 10,12,17,18
(c)   MMAC responses, models 6,13,16,17
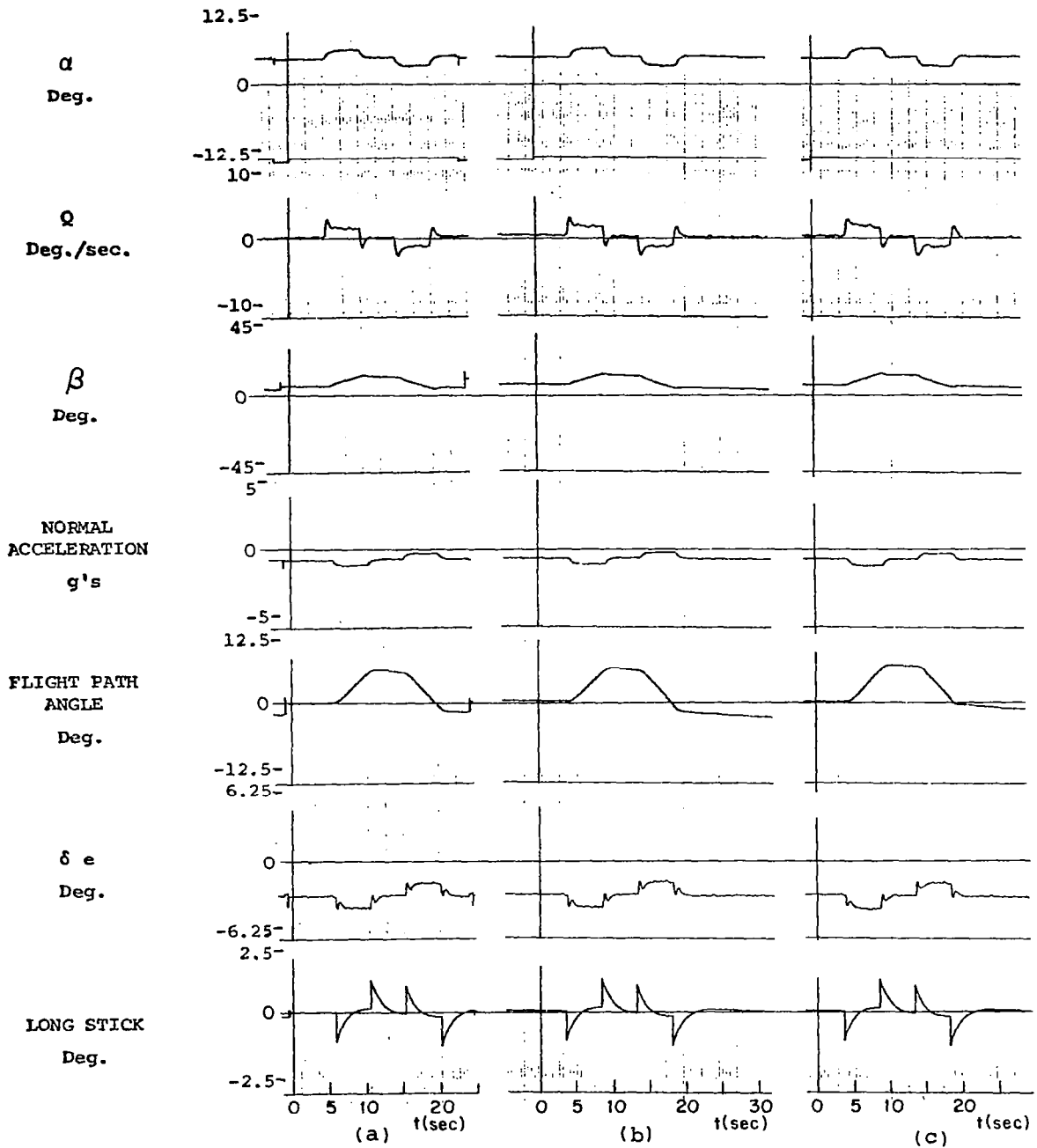
Figure 7.5.18 Longitudinal responses to elevator doublet command,
no turbulence, altitude 6096 meters, speed .6 Mach

(a)   perfect identification responses
(b)   MMAC responses, models 10,11,12,17
(c)   MMAC responses, models 10,12,17,18
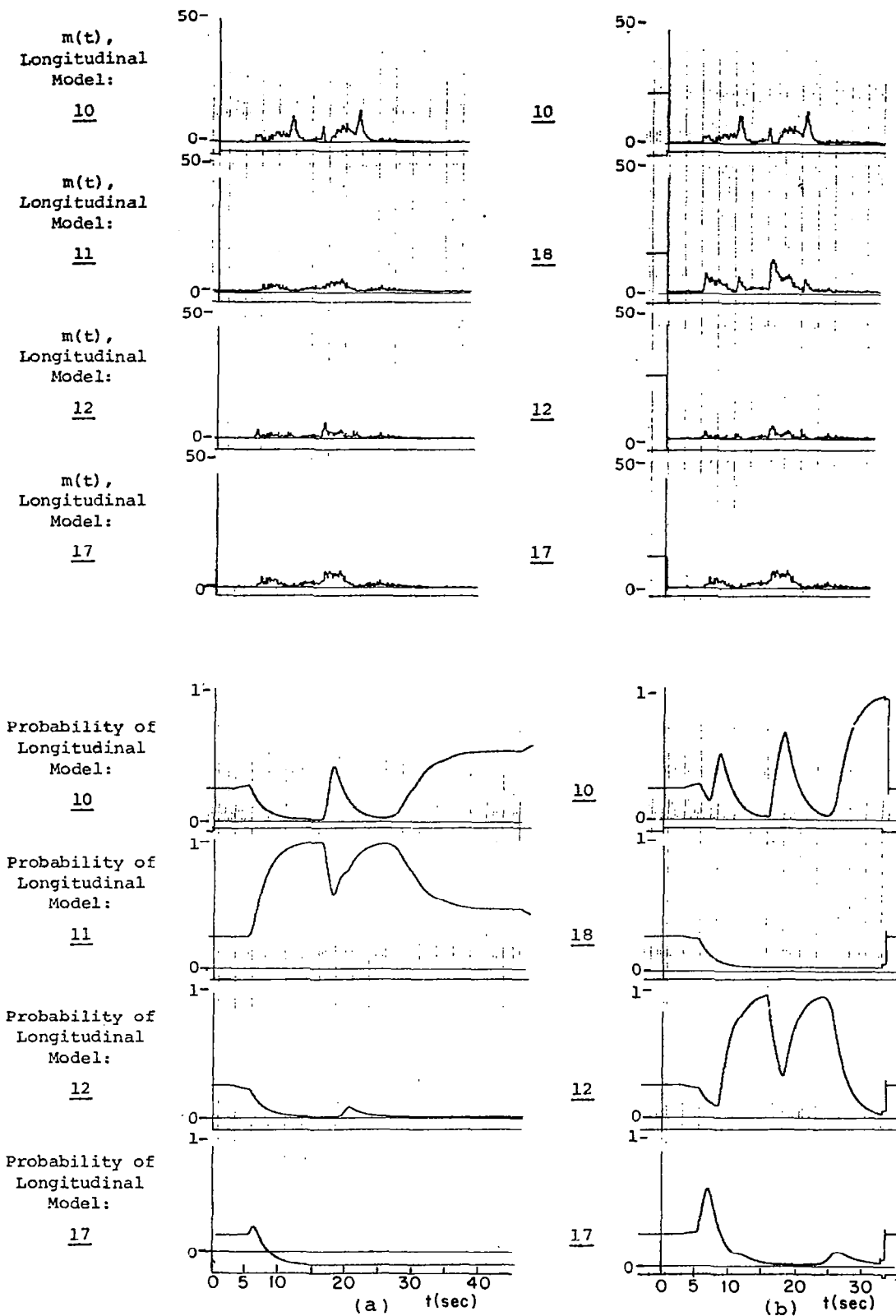
Figure 7.5.19 Longitudinal control probability and m(t) responses to
elevator doublet command, no turbulence, altitude
6096 meters, speed .6 Mach

(a) MMAC responses, models 10,11,12,17
(b) MMAC responses, models 10,12,17,18
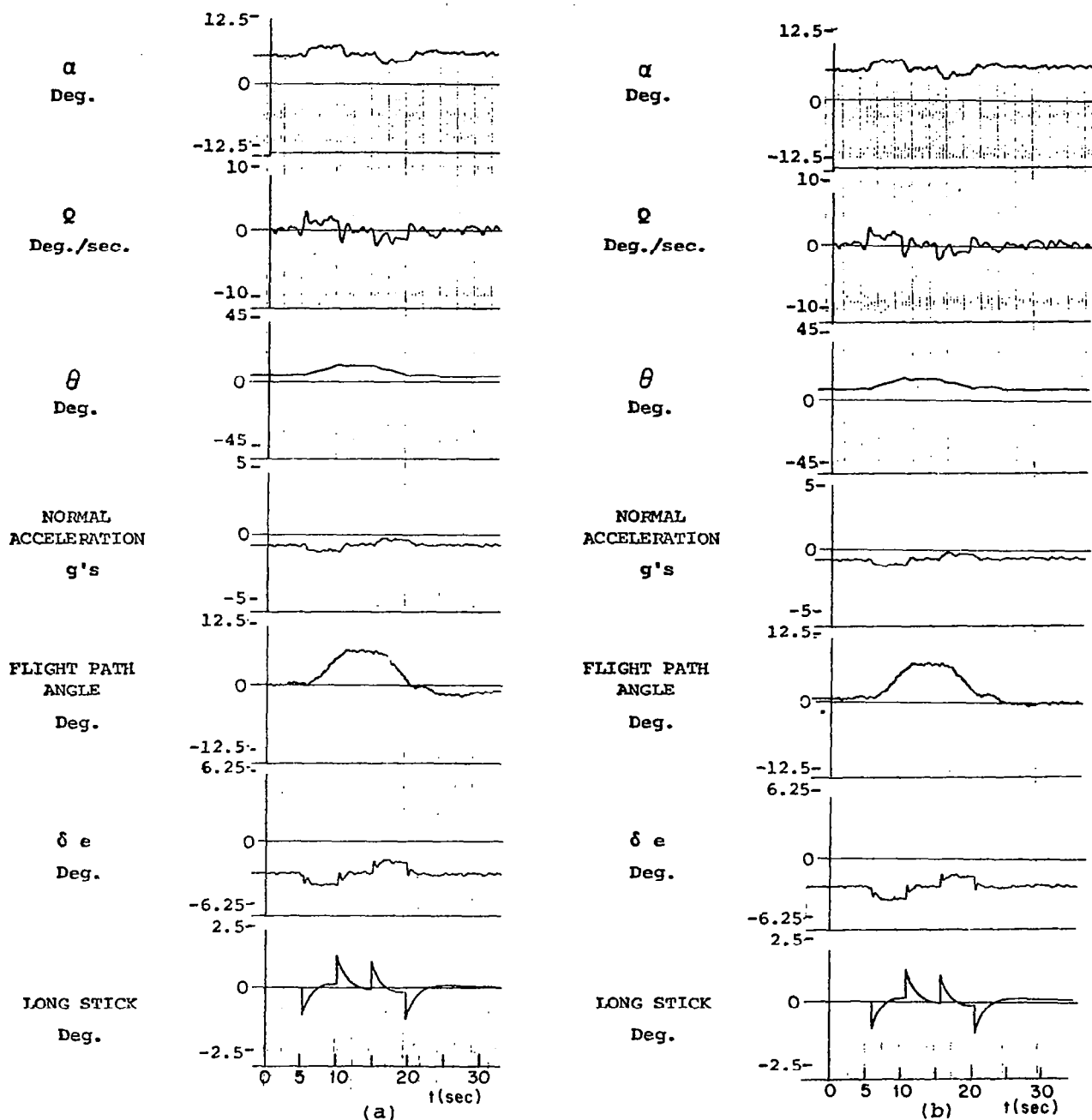
Figure 7.5.20   Longitudinal responses to elevator doublet command,
1.22 m/sec rms turbulence, altitude 6096 meters,
speed .6 Mach

(a)   MMAC responses, models 10,11,12,17
(b)   MMAC responses, models 10,12,17,18
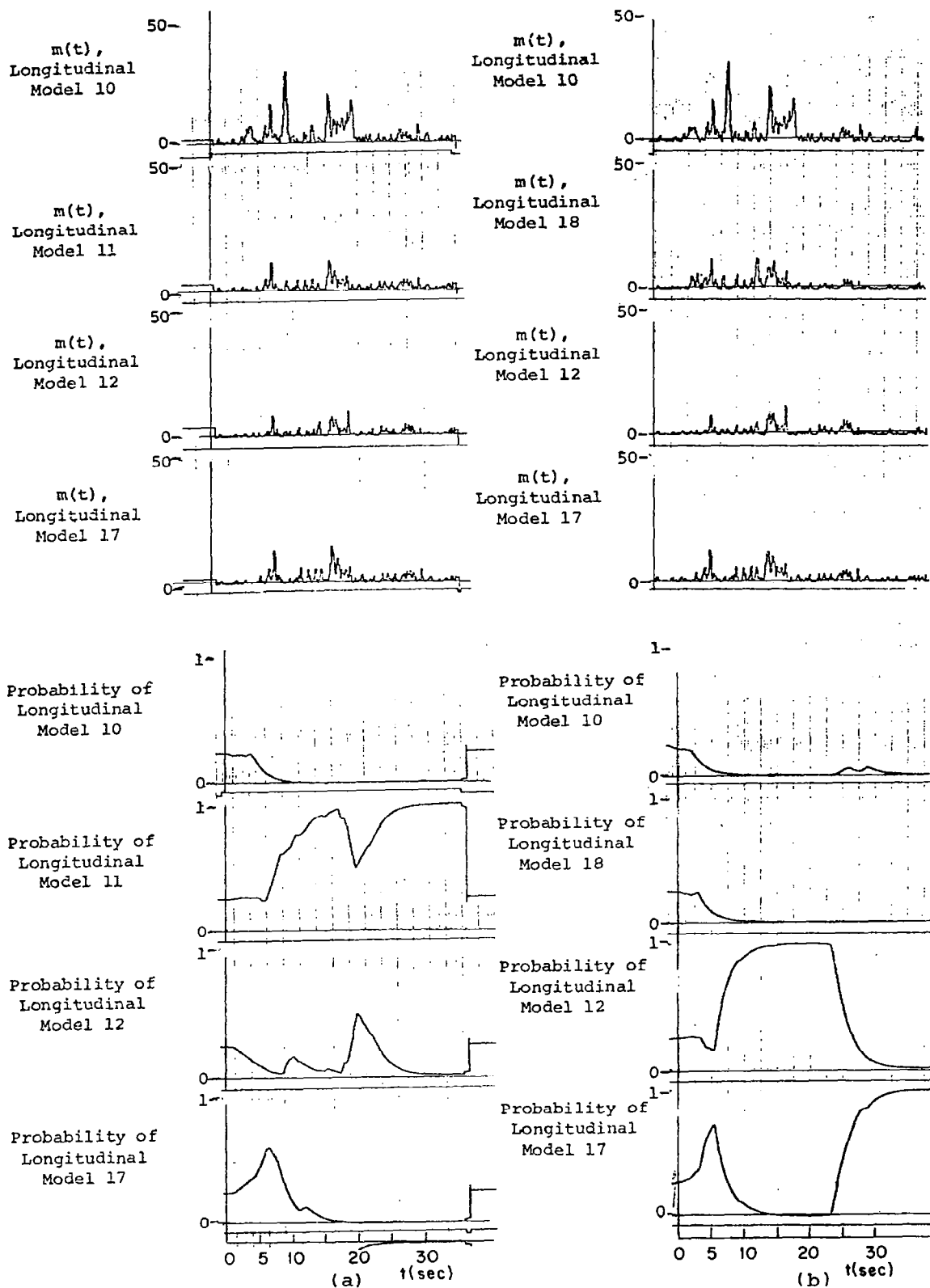
Figure 7.5.21   Control probability and m(t) responses to elevator
doublet command, 1.22 m/sec rms turbulence, altitude
6096 meters, speed .6 Mach

(a)   MMAC responses, models 10,11,12,17
(b)   MMAC responses, models 10,12,17,18
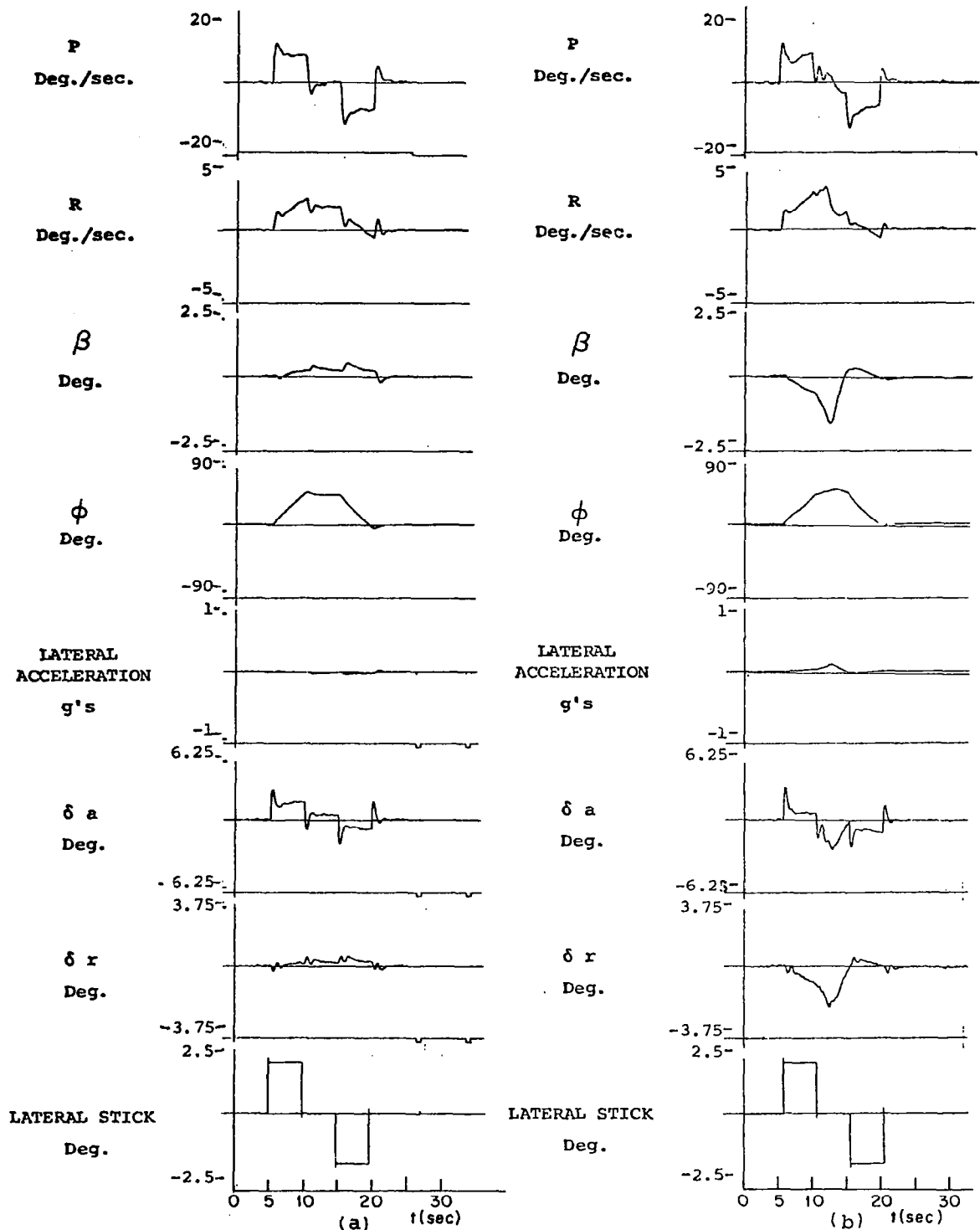
Figure 7.5.22   Lateral responses to aileron doublet command,
                no turbulence, altitude 6096 meters, speed .6 Mach

                (a)   perfect identification responses
                (b)   MMAC responses, models 10,11,12,17
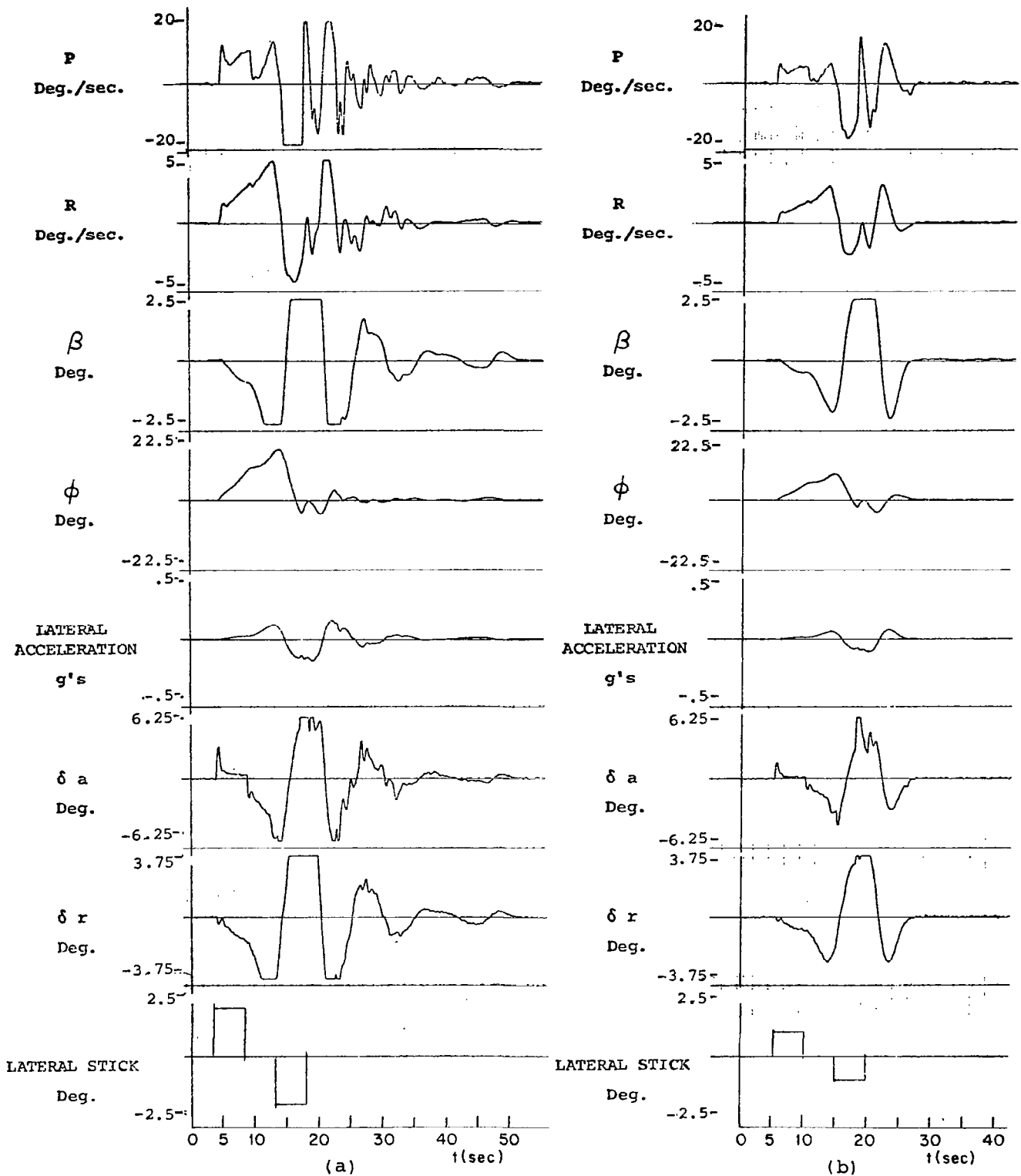
Figure 7.5.23   Lateral responses to aileron doublet command,
no turbulence, altitude 6096 meters, speed .6 Mach

(a)   MMAC responses, models 10,12,17,18, 2° magnitude
(b)   MMAC responses, models 10,12,17,18, 1° magnitude
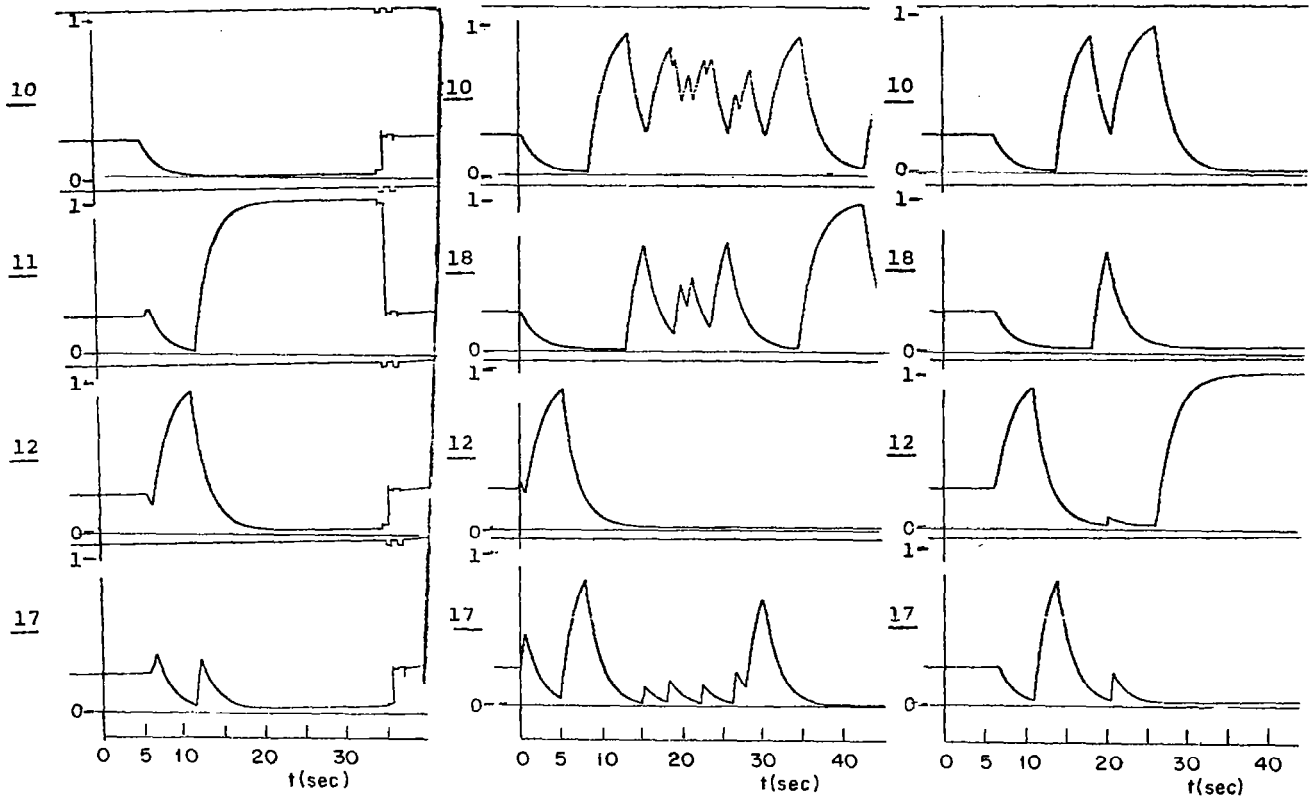
Figure 7.5.24   Control probability responses to aileron doublet
command, zero turbulence, altitude 6096 meters,
speed .6 Mach

(a)   MMAC responses, models 10,11,12,17
(b)   MMAC responses, models 10,12,17,18, 2° magnitude
(c)   MMAC responses, models 10,12,17,18, 1° magnitude

the longitudinal identification system was more accurate than the lateral system.

7.6 Simulations at 40,000 Feet (12192 meters)

The experimental flight condition was flight condition 18, corresponding to a speed of Mach 1.2, a supersonic flight condition. The aircraft was subjected to a 6° angle of attack and a 2° sideslip angle initial perturbation. Figure 7.6.1 show the longitudinal system responses for a perfect identification simulation, and two MMAC simulations. Figure 7.6.2 contains the corresponding lateral system responses. Figure 7.6.3 contains the control probability histories for the two MMAC simulations.

The identification responses indicated in Figure 7.6.3 show good identification. The longitudinal identification erroneously prefers flight condition 19, a close neighbor of the true flight condition. The lateral identification system initially chooses flight condition 17, then it alters between flight condition 19 and 18 when 18 is a hypothesis. This accounts for the slight differences in performance between the two MMAC systems. Figure 7.6.4 contains the longitudinal responses of two MMAC systems, to longitudinal doublet stick commands; there is no turbulence in the experiments. Figure 7.6.4(a) used an MMAC system with hypothesis models 13, 17, 18, 19, while Figure 7.6.4(b) used models 12, 13, 17, 19. Note the similarity in the responses for both experiments, even when the true flight condition is not a hypothesis. Figure 7.6.5

contains the evolution of the control probabilities and weighted sums of residuals m(t) for the longitudinal system. There is a substantial difference in the magnitudes of the weighted residuals m(t) for subsonic and supersonic flight conditions, although there is very little difference between the two supersonic conditions. The MMAC system correctly identifies flight condition 18 when it is a hypothesis. In its absence, it chooses flight condition 19, the other supersonic flight condition.

Figure 7.6.6 is a repeat of the experiments described in Figure 7.6.4 when a moderate level of turbulence (1.22 m/sec rms) is introduced. The responses are again nearly identical. Figure 7.6.7 contains the evolution of the control probabilities and the weighted sum of residuals. The presence of turbulence in these simulations seem to confuse the identification algorithm, making it harder to differentiate between the two supersonic hypotheses. However, the turbulence information is sufficient to differentiate between supersonic and subsonic hypotheses, as illustrated by the initial identification in Figure 7.6.7 b during the quiet period.

Figures 7.6.8 and 7.6.9 describe the lateral system responses to a doublet command in the lateral system under no turbulence. The true hypothesis (model 18) is correctly identified, resulting in good performance. The substantial sideslip angle and lateral acceleration responses in Figure 7.6.8 a are also present in the supersonic experiments with perfect identification, shown in Chapter 6; they are a consequence of the model-following design employed, rather than a shortcoming of the MMAC.

In the absence of the correct hypothesis, Figure 7.6.9 b indicates difficulty in identification. This difficulty is reflected in the bank angle response of Figure 7.6.8 b. The m(t) responses show that the only supersonic hypothesis (model 19) differs widely from the true hypothesis. This indicates a certain degree of inaccuracy present in the lateral identification system.

Figures 7.6.10 and 7.6.11 describe a repeat of the previous lateral system simulations using 1.22 m/sec rms turbulence level. The system responses are qualitatively similar to the previous responses. The true hypothesis is correctly identified, although the presence of turbulence seems to confuse the identification near the end of the doublet command. When the true hypothesis is not present, two subsonic models (12 and 13) are identified.

7.7 Discussion

The performance of the MMAC control system is closely related to the accuracy of its identification algorithm. The experiments in these sections lend support to several conclusions. These experiments were conducted with three different sources of information: turbulence excitation, gust perturbations and stick commands. The identification system performance was best in response to stick commands. The presence of turbulence helped avoid the β^* behavior mentioned in Chapter 4, but did not prove helpful in identifying the correct hypotheses.
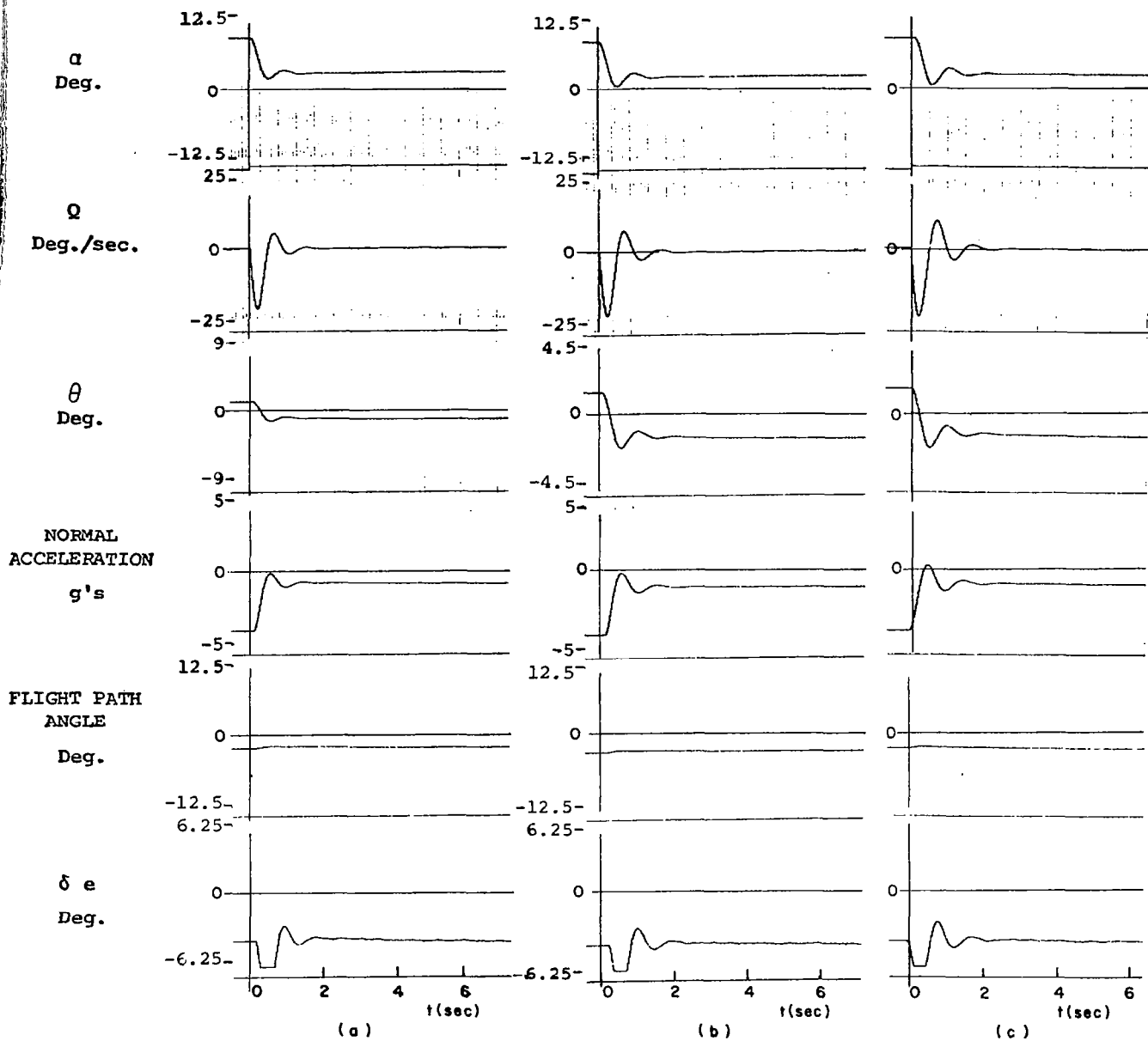
Figure 7.6.1   Longitudinal responses to 6°α, 2°β initial condition,
altitude 12192 meters, speed 1.2 Mach

(a)   perfect identification responses
(b)   MMAC responses, Models 13,17,18,19
(c)   MMAC responses, Models 12,13,17,19
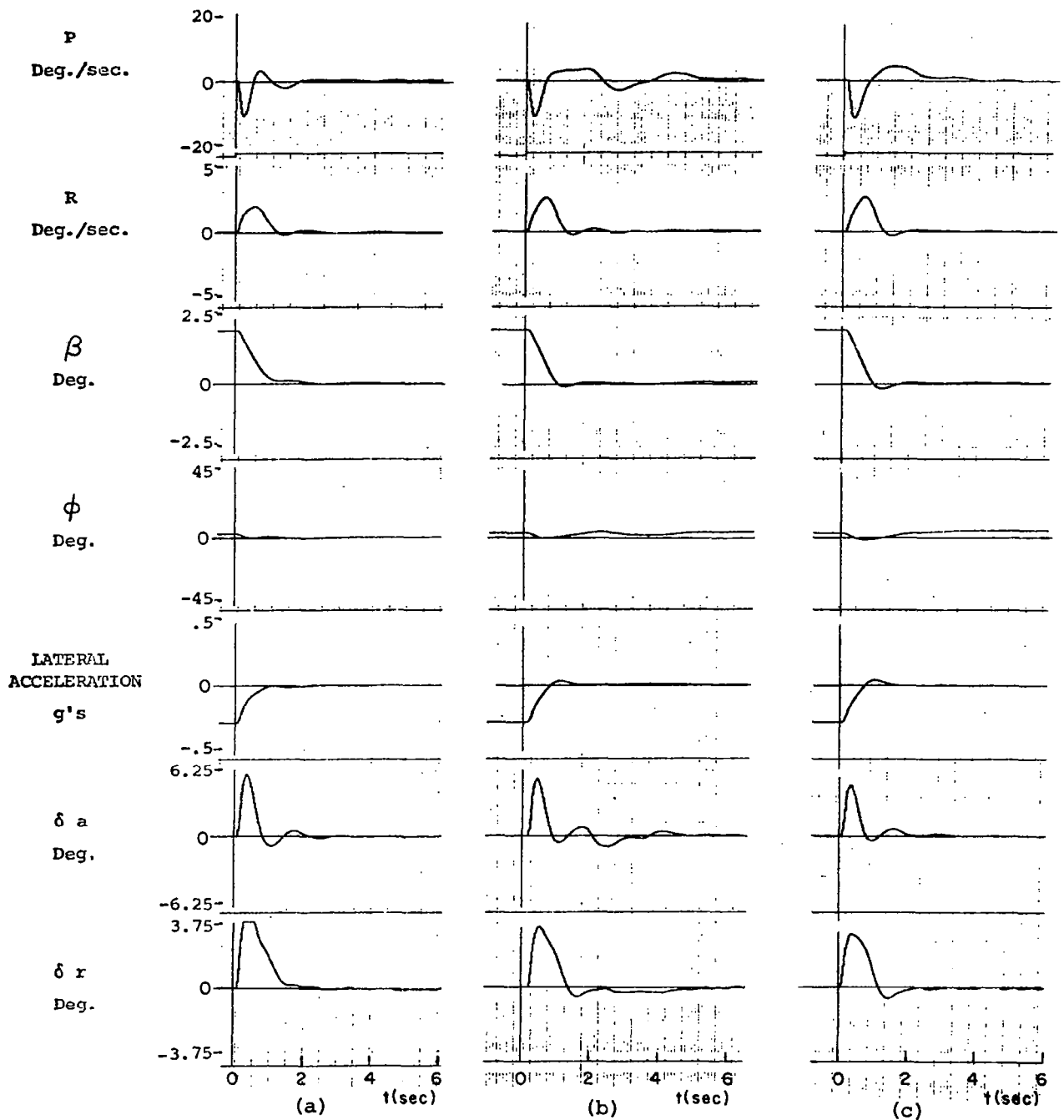
Figure 7.6.2   Lateral responses to 6°α, 2°β initial condition,
altitude 12192 meters, speed 1.2 Mach

(a)   perfect identification responses
(b)   MMAC responses, Models 13,17,18,19
(c)   MMAC responses, Models 12,13,17,19
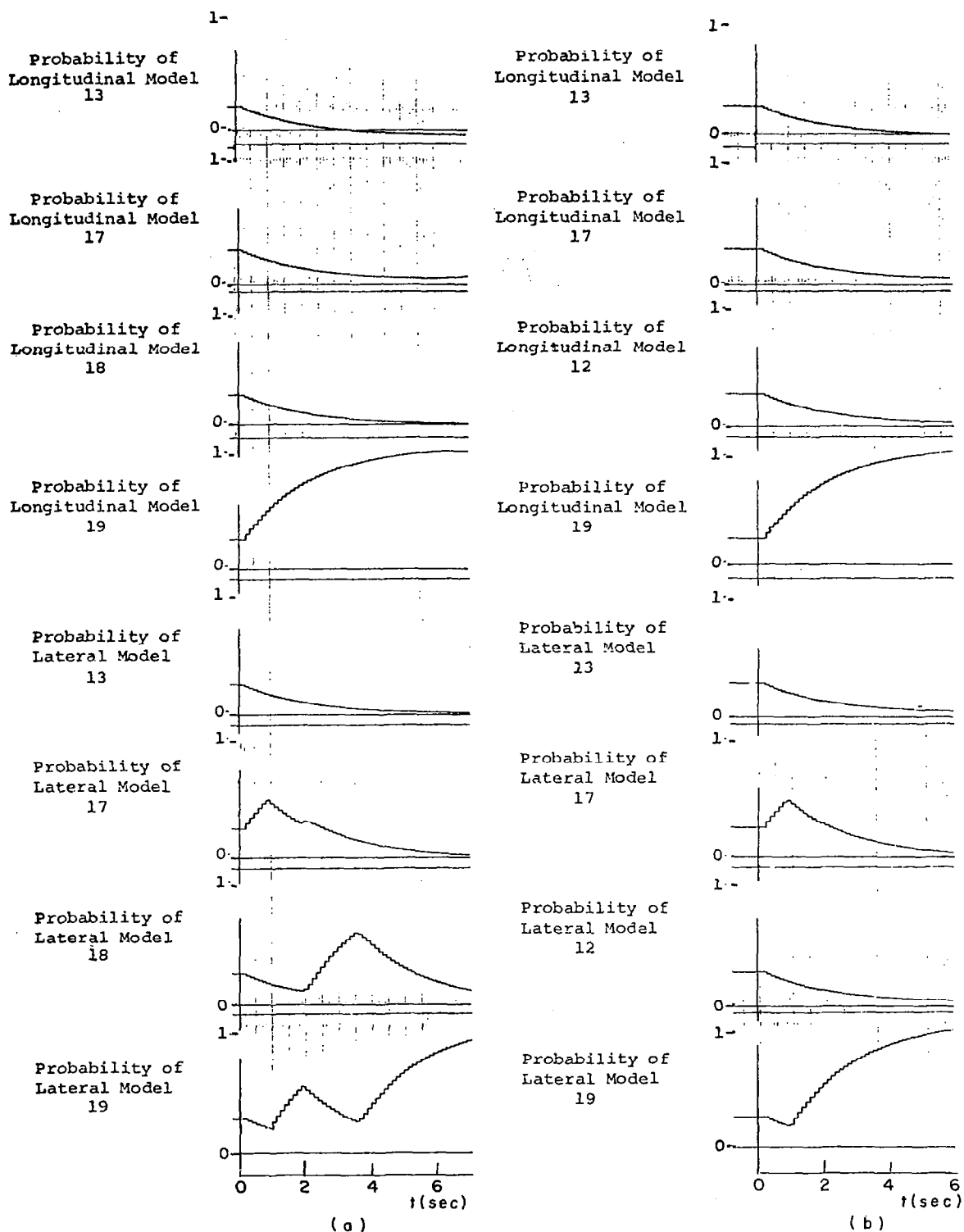
Figure 7.6.3   Control probability responses to 6°α, 2°β initial
condition, altitude 12192 meters, speed 1.2 Mach

(a)   MMAC responses, Models 13,17,18,19
(b)   MMAC responses, Models 12,13,17,19
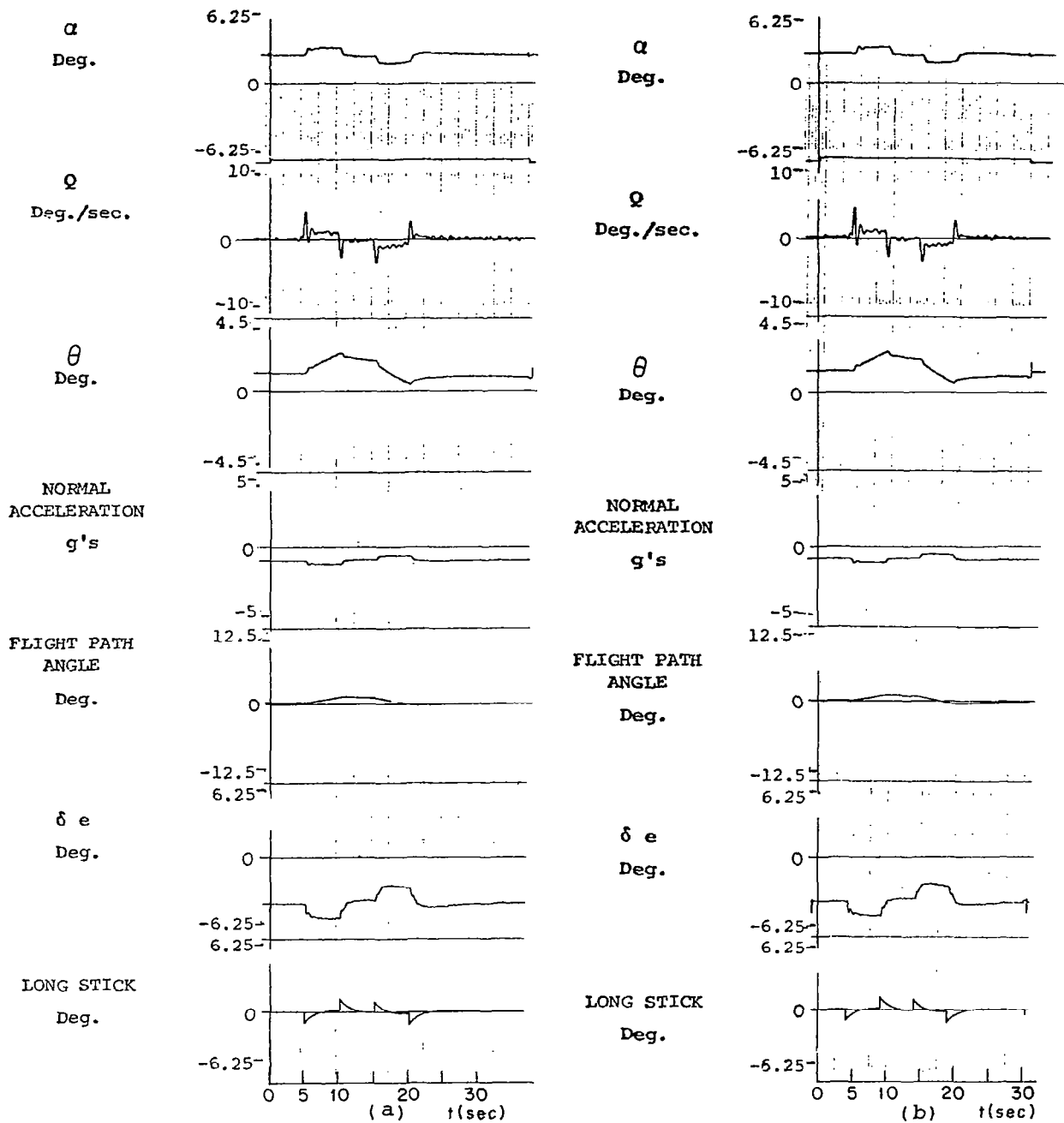
Figure 7.6.4   Longitudinal responses to elevator doublet command,
no turbulence, altitude 12192 meters, speed 1.2 Mach

(a)   MMAC responses, models 13,17,18,19
(b)   MMAC responses, models 12,13,17,19
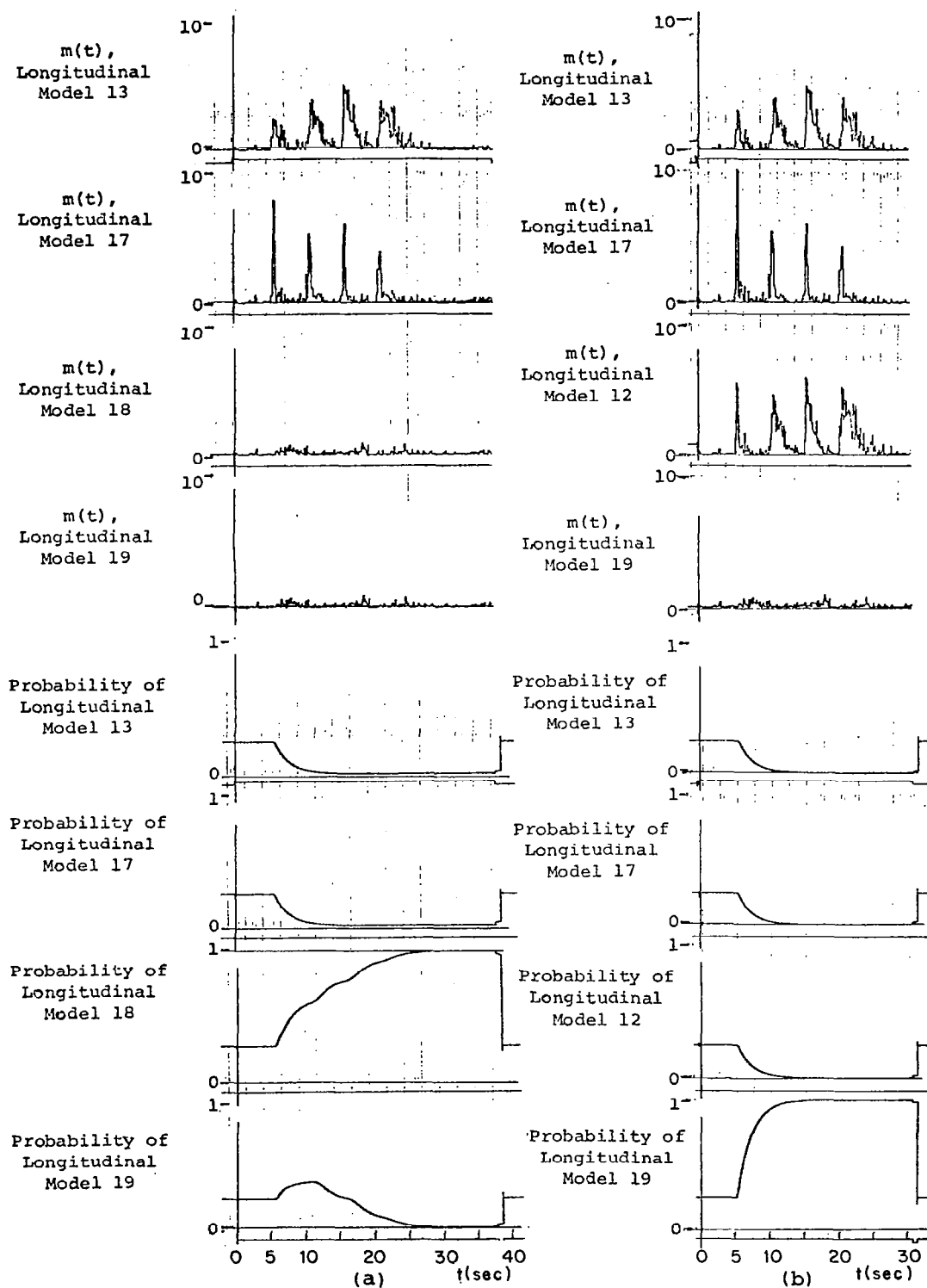
Figure 7.6.5   Control probability and m(t) responses to elevator doublet
command, no turbulence, altitude 12192 meters, speed 1.2 Mach

(a)   MMAC responses, models 13,17,18,19
(b)   MMAC responses, models 12,13,17,19
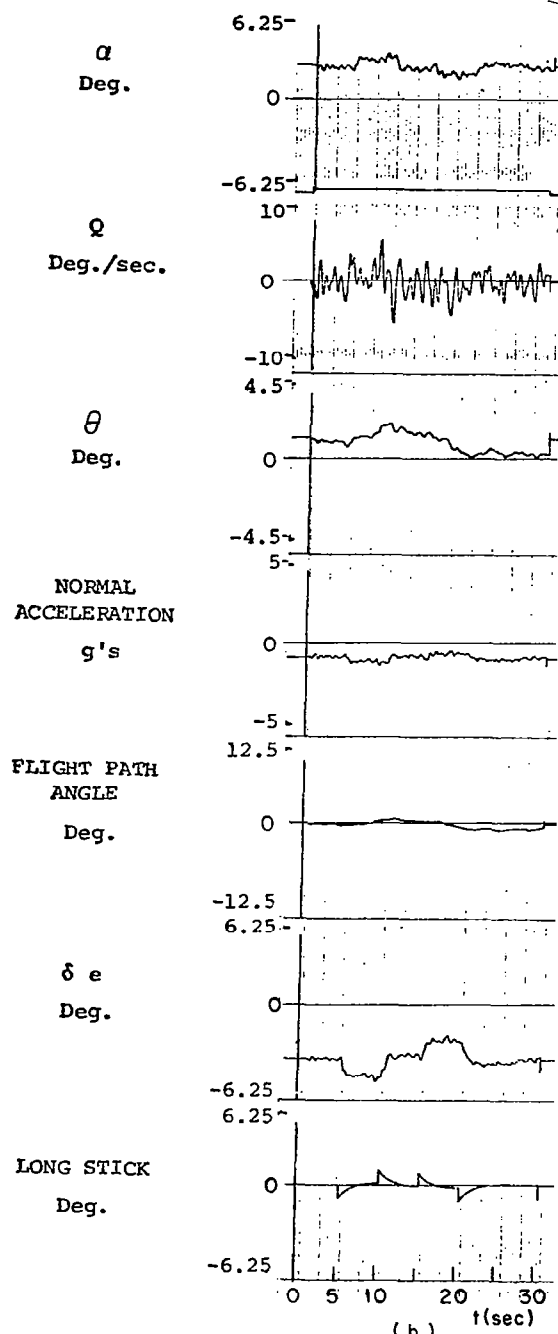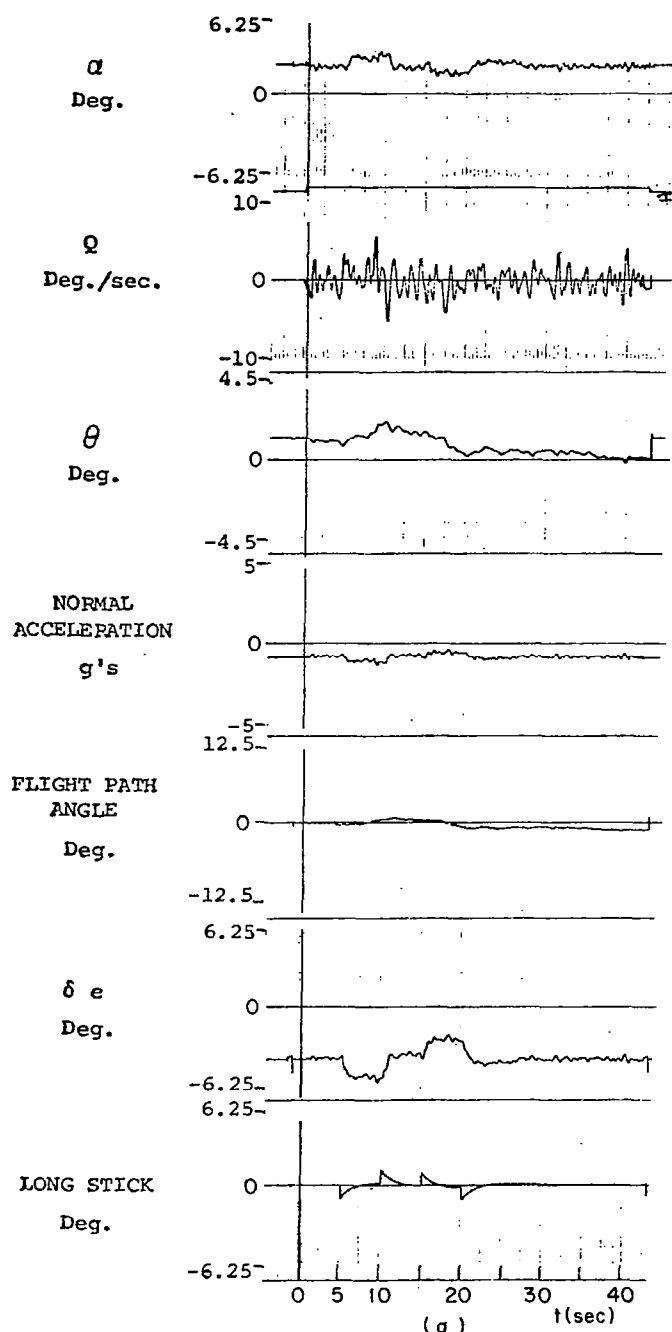
Figure 7.6.6   Longitudinal responses to elevator doublet command,
                1.22 m/sec rms turbulence, altitude 12192 meters,
                speed 1.2 Mach

                (a)   MMAC responses, models 13,17,18,19
                (b)   MMAC responses, models 12,13,17,19
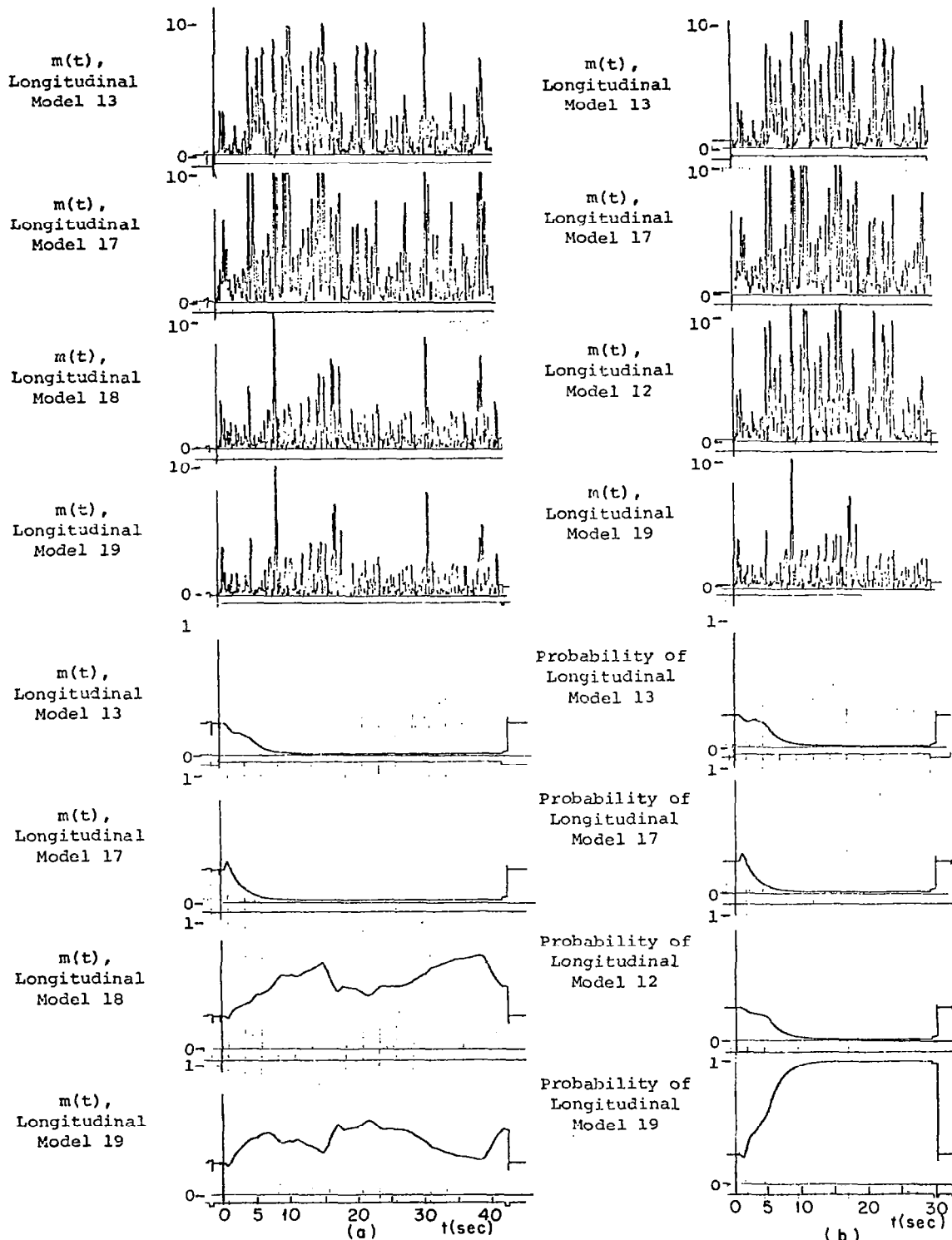
Figure 7.6.7   Longitudinal control probability and m(t) responses to elevator
                doublet command, 1.22 m/sec rms turbulence, altitude 12192 meters,
                speed 1.2 Mach

                (a) MMAC responses, models 13,17,18,19
                (b) MMAC responses, models 12,13,17,19
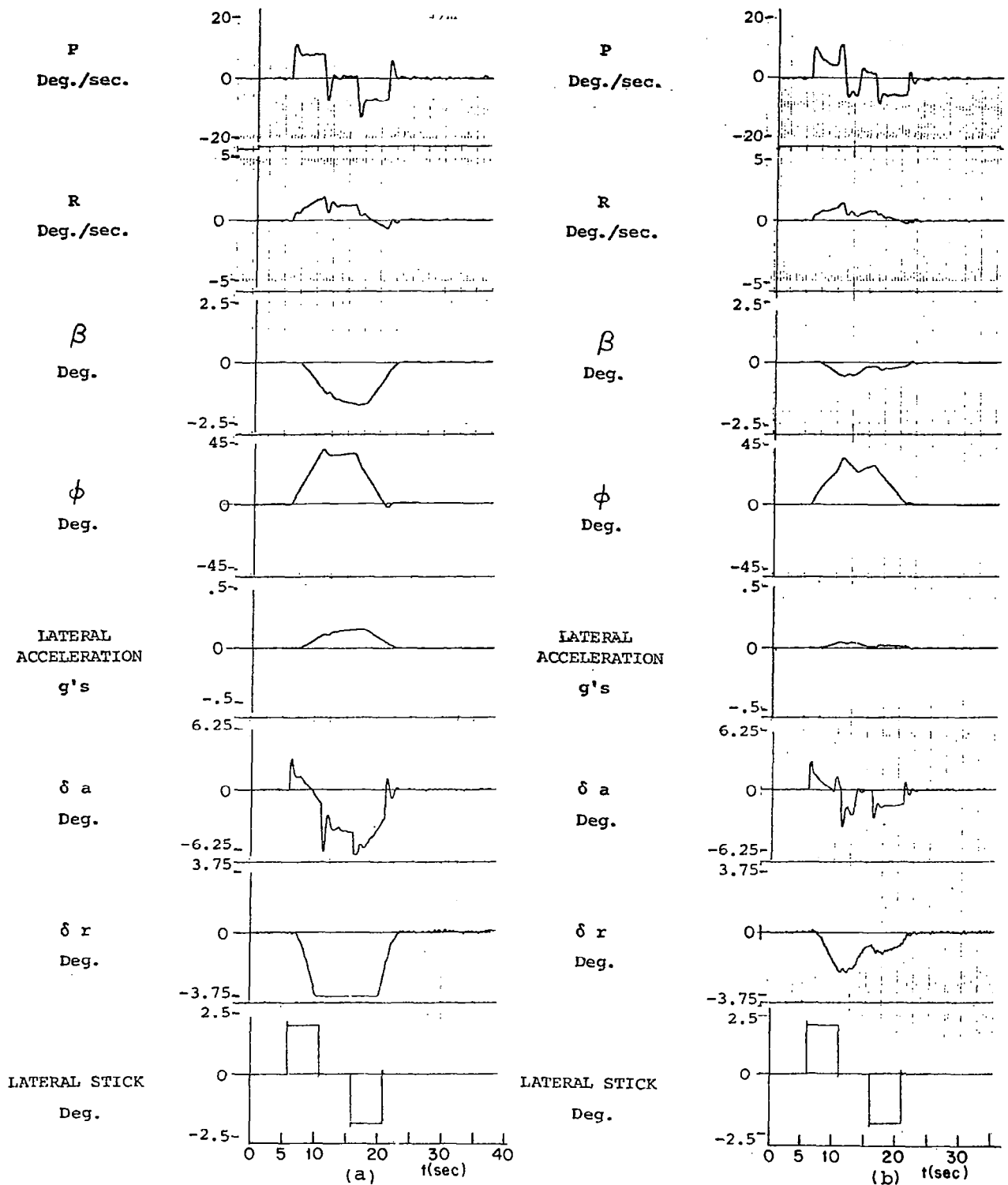
Figure 7.6.8   Lateral system responses to aileron doublet command, no
turbulence, altitude 12192 meters, speed 1.2 Mach

(a)   MMAC responses, models 13,17,18,19
(b)   MMAC responses, models 12,13,17,19
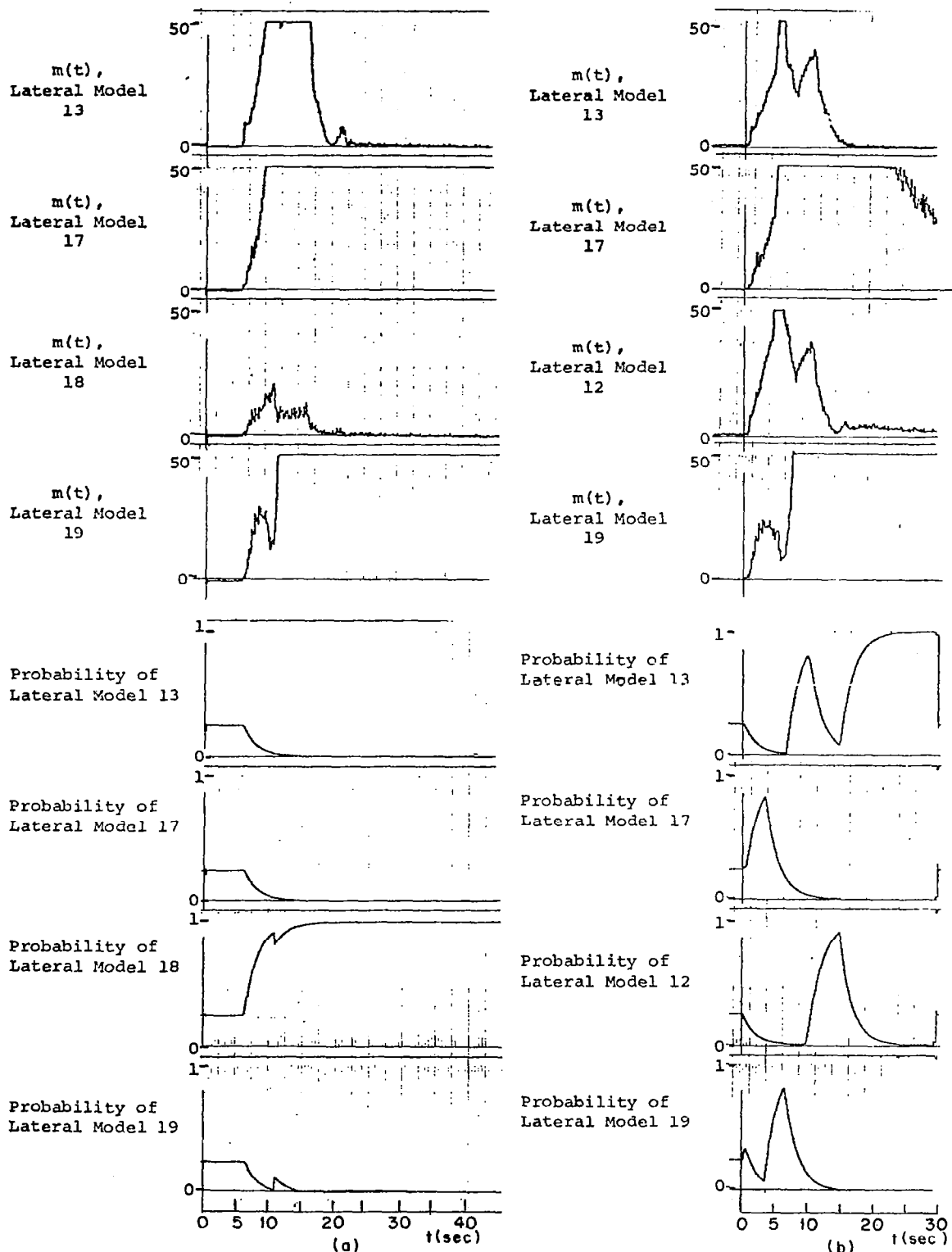
Figure 7.6.9   Lateral control probability and m(t) responses to aileron
                doublet command, no turbulence, altitude 12192 meters,
                speed 1.2 Mach

                (a) MMAC responses, models 13,17,18,19
                (b) MMAC responses, models 12,13,17,19
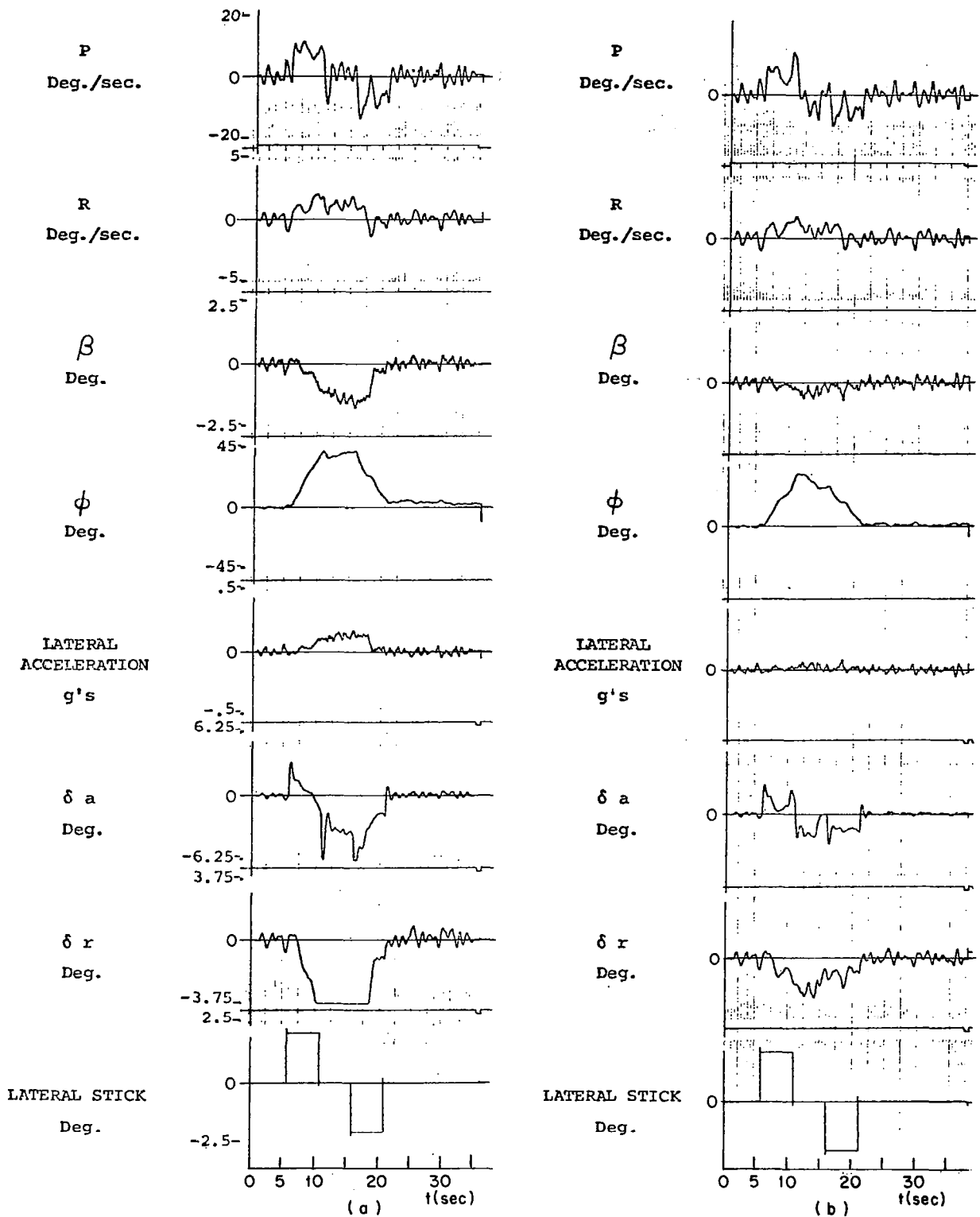
Figure 7.6.10   Lateral system responses to aileron doublet command,
1.22 m/sec rms turbulence, altitude 12192 meters, speed
1.2 Mach

(a)   MMAC responses, models 13,17,18,19
(b)   MMAC responses, models 12,13,17,19
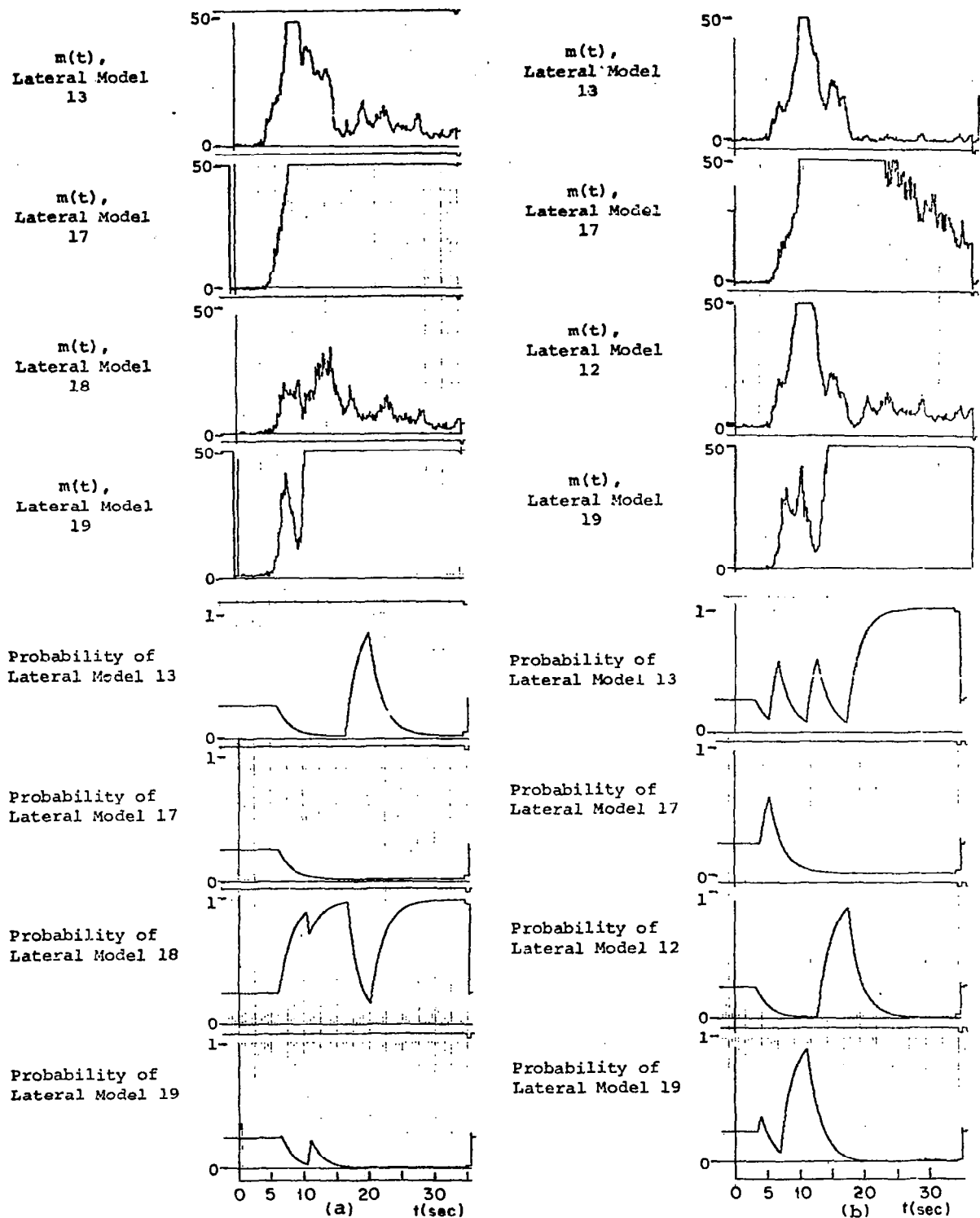
Figure 7.6.11   Lateral control probability and m(t) responses to aileron
doublet command, 1.22 m/sec rms turbulence, altitude 12192
meters, speed I.2 Mach

(a)   MMAC responses, models 13,17,18,19
(b)   MMAC responses, models 12,13,17,19

The lateral system identification responses were poor overall, particularly when contrasted with the longitudinal identification responses. The identification system seemed incapable of differentiating between supersonic and subsonic flight conditions, as well as stable or unstable controller combinations. Furthermore, the fixed-point design philosophy adopted in Chapter 5 proved to be ill-suited for implementation in a multiple-model controller; the shifting identification resulted in uneven control as the feedforward gains switched, and the mismatched controllers were often unstable, indicating high sensitivity to the set of hypothesis models used. On the positive side, the true model was identified correctly when it was included as a hypothesis.

The longitudinal control system was very tolerant of identification errors, unlike the lateral system. This is due partly to the controller designs of Chapter 5; one can see that, when the close neighbors of the actual flight condition are identified, the closed-loop responses of the aircraft is very similar to those obtained with perfect identification. This feature seems essential in the design of any future MMAC-type control systems, since one can seldom assume that the true model is included among the set of hypothesis models.

CHAPTER 8

PILOT SIMULATION EXPERIMENTS

8.1 Introduction

The MMAC simulations described in the previous chapters illustrate the sensitivity of the algorithm's performance to the particular set of hypothesis models used. Due to limitations in available storage and computation time, only a limited number of hypotheses is possible; this number was chosen to be four. It is unreasonable to expect that this number of hypotheses will be adequate for adaptive control of the F-8 aircraft over its entire flight envelope. In order to test the performance of the MMAC system over the entire flight envelope, a scheduling algorithm was designed, based on rough altitude measurements. Using this algorithm, a engineer "pilot" was able to conduct tests of simulated flight using NASA Langley Research Center's nonlinear hybrid simulation of the F-8C aircraft. The experiments shown in this chapter are excerpts from the records of those simulation flights.

8.2 The MMAC Model-Scheduling Algorithm

The basic scheduling algorithm works at five-second intervals, using four hypothesis models; this number of models was chosen to reduce the time required for the MMAC real-time computations. The period was chosen to allow transients in identification to die out. Every five seconds, the algorithm tries to find a model hypothesis older than 10 seconds whose lateral and longitudinal control probabilities are both less than .001. If it

succeeds in finding such a hypothesis, then it tries to replace it by
a "better" one. Using a rough estimate of the current altitude together
with the altitudes of the hypothesis models, the algorithm uses Table
8.2.1 to determine the desired altitude of the new hypothesis. The
dynamic pressures of the models with maximal longitudinal and lateral
control probabilities are averaged to obtain a desirable dynamic pressure.
The algorithm then replaces the undesirable hypothesis model by the model
at the desired altitude whose dynamic pressure is closest to the desired
dynamic pressure. Figure 8.2.1 represents a flow chart of the scheduling
algorithm.

The relevant data used for the MMAC algorithm is stored on-line for
all possible hypotheses. The scheduling algorithm picks out four of
these hypotheses to be the active hypotheses for periods of time. Every
five seconds, it reviews the hypothesis identification to see if there are
candidates which would make "better" hypotheses in the MMAC algorithm.
Once a model is introduced as a hypothesis, it remains one for a least
ten seconds; this provides ample time for the algorithm to identify it
with positive probability if it is a likely hypothesis. Table 8.2.1
represents a schedule of models which attempts to anticipate possible
climbing or driving maneuvers by the pilot.

In sum, this scheduling algorithm represents one feasible solution
to the problem of extending the MMAC algorithm, using only four hypo-
theses, so that it operates over the complete flight envelope. This
algorithm is far from optimal; it represents a way of studying the MMAC's

TABLE 8.2.1

ALTITUDE SCHEDULING TABLE

Actual Altitude (feet) (.3048 m)	Number of Current Hypotheses of Altitude			Desired Altitude (feet) (.3048 m)
	sea level	20,000 ft (6,096 m)	40,000 ft (12,192 m)	
0-5,000	*	*	*	0
	*	2 or more	*	0
5,000-15,000	0	*	*	0
		otherwise		20,000
15,000-25,000	*	*	*	20,000
	*	2 or more	*	40,000
25,000-35,000	*	*	0	40,000
		otherwise		20,000
greater than 35,000	*	*	*	40,000

* indicates number is not relevant.
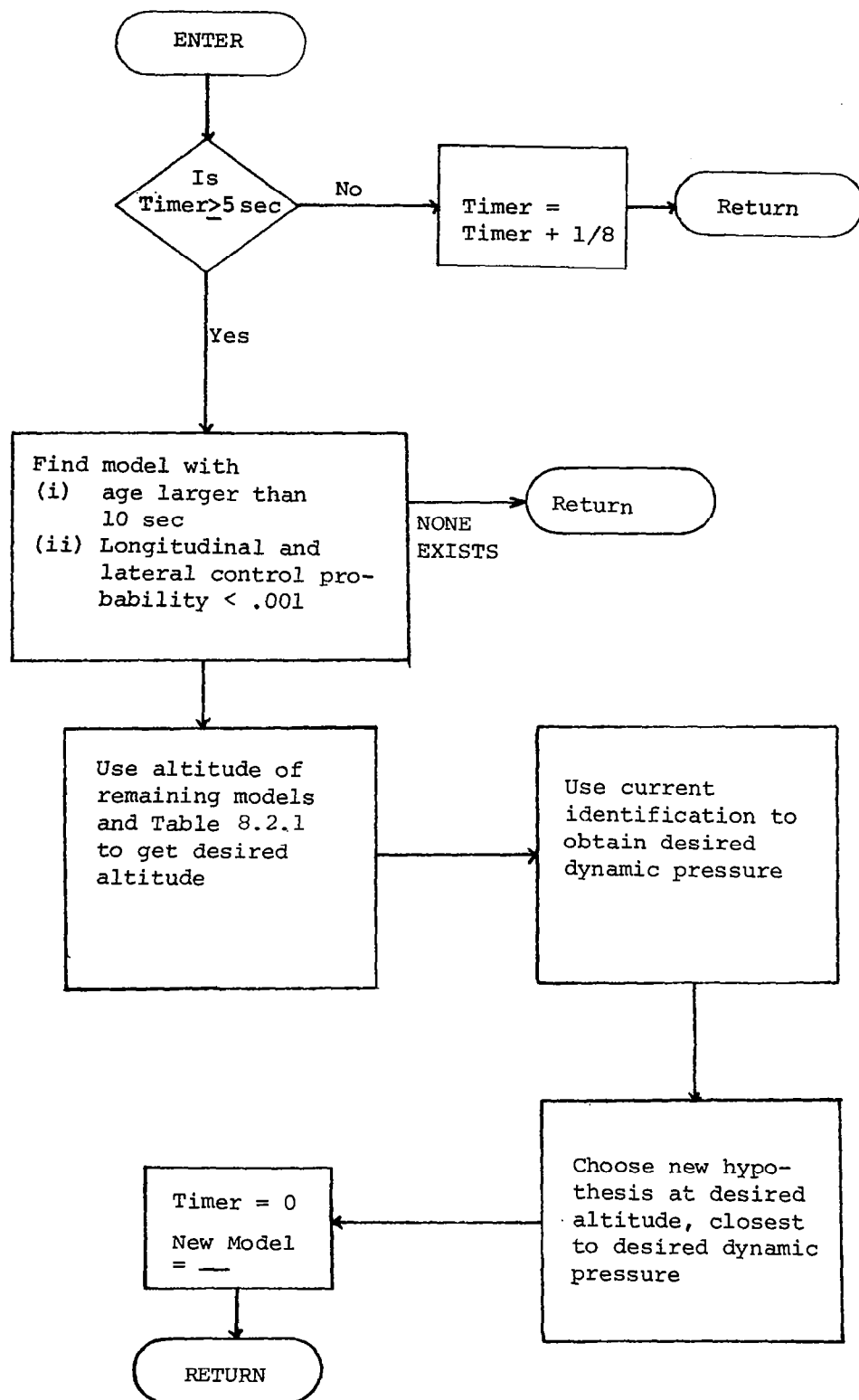
Figure 8.2.1 Flow chart of scheduling algorithm

performance over the entire flight envelope, and it indicates guidelines on which to base better algorithms.

8.3 Identification Experiments

This section discusses the performance of the MMAC identification algorithm during pilot maneuvers. The probability of the various hypotheses are initially equal in each experiment. Figure 8.3.1 shows the aircraft responses and the control probability evolution for the aircraft flying level at 6096 met. at a speed of Mach .83. The small longitudinal maneuvers provide information which identifies model 12, a "close neighbor" of the true flight condition. The absence of any lateral information prevents the probabilities from changing.

Figure 8.3.2 shows the aircraft responses and control probability evolution for the continuation of the experiments shown in Figure 8.3.1. The aircraft is flying level at 6096 met. at a speed of Mach .83. In this figure, small lateral maneuvers provide information to the identification system to correctly identify model 12. The absence of longitudinal information maintains the longitudinal identification constant.

Figure 8.3.3 shows the responses during a repetition of the experiment in Figures 8.3.1 and 8.3.2 using different hypotheses in the MMAC control system. The hypotheses in this experiment are models 11, 12, 13 and 17. The aircraft is flying at level flight at an altitude of 6096 met. and a speed of Mach .82. The pilot first executes a series of small longitudinal maneuvers, then a series of lateral maneuvers.

Note the responses of the control probabilities to the information provided by the aircraft responses. The longitudinal identification system identifies model 12, as the true hypothesis, and the lateral identification system identifies model 13. The true flight conditions are "close" to both of these hypothesis models, lying somewhere in between.

Figure 8.3.4 shows the aircraft responses at an altitude of 13,106 met. and a speed of Mach .87. The MMAC hypotheses are models 11, 12, 13 and 17. The MMAC system identifies flight condition 17, which is very close to the actual flight condition, after the aircraft undergoes some maneuvers in both systems.

Figure 8.3.5 shows the aircraft responses while the aircraft is at level flight, at an altitude of 60.96 met. and a speed of Mach .6. This corresponds exactly to flight condition 11. The MMAC identification converges to the correct hypothesis in both the lateral and longitudinal systems, once information is available.

Figures 8.3.6 and 8.3.7 illustrate the operation of the model scheduling algorithm as the airplane moves through its flight envelope. The center axis marks simultaneous instants of time in the four sets of responses. The aircraft is situated near 9144 met. altitude, at a speed near 1.1 Mach. The initial hypothesis models are 10, 11, 12 and 15, which are subsonic models. Lateral maneuvers provide information to the identification system, leading to lowering model 10's probability near zero. The scheduling algorithm recognizes this, and replaces this

hypothesis by model 18, a supersonic flight condition at an altitude of 12192 met. The longitudinal system quickly identifies this new hypothesis, since it is close in actual speed. This result agrees with the observed behavior in Chapter 7, where the longitudinal identification system distinguished well between subsonic and supersonic hypotheses. The lateral identification system does not respond to this new hypothesis. Figure 8.3.6(a) shows a subsequent change in hypothesis models, replacing model 15 by a higher dynamic pressure model, model 17. This change does not affect current identification.

Figure 8.3.8 shows the longitudinal and lateral control probability and $m(t)$ responses while the aircraft decelerates from a speed of Mach .6 to Mach .44 at an altitude of 6096 met. The initial MMAC hypotheses are models 18, 11, 12 and 17. As the aircraft decelerates, models 18 and 17 are changed to models 13 and 10 respectively. Note the transition of the various control probabilities, from models 12 to model 11 to model 10 as the aircraft decelerates. The longitudinal identification system does not identify model 10, seen by the magnitude of the $m(t)$ response.

Figures 8.3.9 to 8.3.12 show the airplane responses while the airplane is diving from 6096 met to 2438 met. at speeds between .5 Mach and .65 Mach. No turbulence is present in this simulation. The initial MMAC hypotheses are models 13, 11, 12 and 10. The scheduling algorithm replaces model 13 by model 5 and model 10 by model 6. As the airplane descends, the longitudinal system identifies models 10, 12 and 11 in that order, while the lateral system chooses models 11, 12 and 6 in that

order. The actual dynamic pressure of the aircraft is between 300 and
400 pounds per square foot, making models 6 and 11 the closest hypothe-
ses. One should notice that these are the two flight conditions which
the identification system selects.

Figures 8.3.13 to 8.3.16 represent maneuvers at an altitude between
2440 and 3050 met, at a speed of Mach .6, under no turbulence. This
simulation is a continuation of the simulation in Figures 8.3.17 to
8.3.12. This flight condition seems to be near models 6, 11 and 12 in
the longitudinal system, as the identification switches between these
three hypotheses. In the lateral system, models 6 and 11 are identified.
The dynamic pressure of the actual aircraft ranges between 300 and 450
lb/ft^2, in the neighborhood of flight conditions 6, 11 and 12, which
account for the shifting identification.

Figures 8.3.17 to 8.3.20 represent the aircraft responses in a climb
from 1525 met to 9150 met, under no turbulence at subsonic speeds.
Figure 8.3.17 highlights the operation of the model-scheduling algorithm.
Figures 8.3.18 and 8.3.19 show some pitching and banking maneuvers exe-
cuted in the climb. Figure 8.3.20 shows the evolution of the control
probabilities. As the aircraft picks up speed, the longitudinal identi-
fication system follows the transitions from models 5 to 6 and 10 to 11
to 12. The lateral scheme also transitions from 11 to 12. Note the
scheduling of model 12 results in its identification by both systems.
As the aircraft speeds up, model 17 replaces model 10 and model 19 re-
places model 6, to provide for better hypotheses.
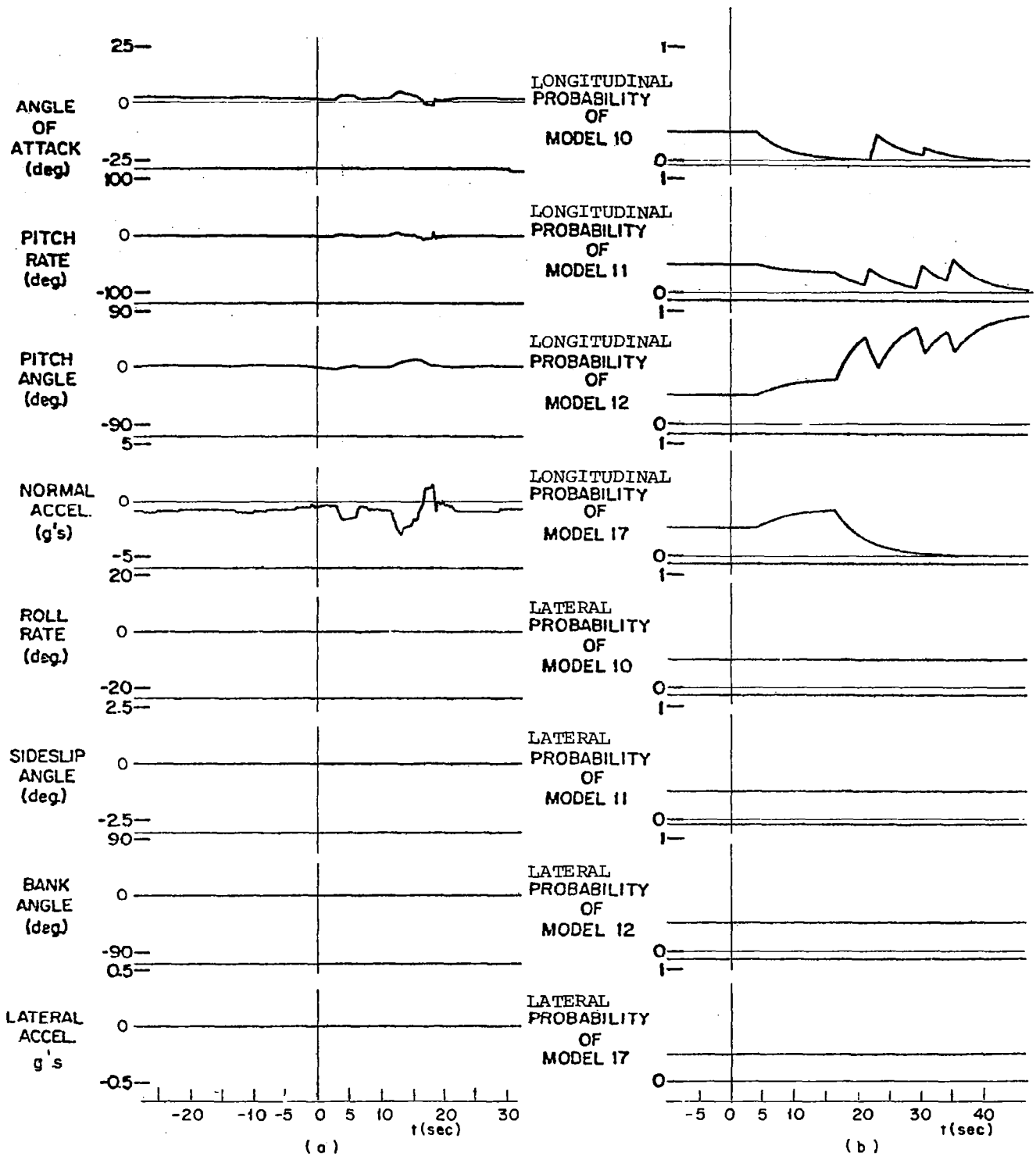
Figure 8.3.1   Responses to Longitudinal system inputs, no turbulence, altitude
6096 meters, speed Mach .83, level flight.
MMAC hypothesis models 10,11,12,17.
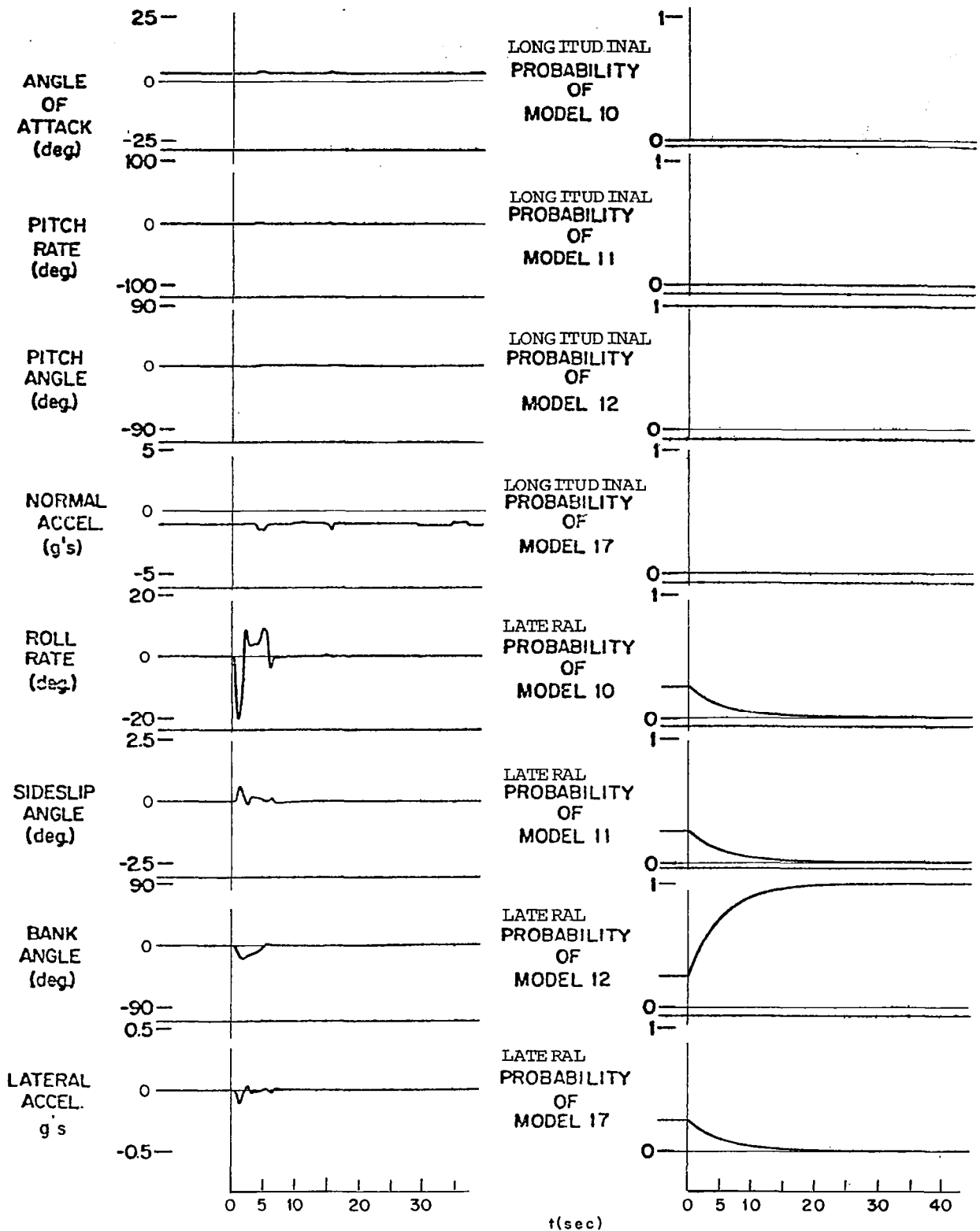
Figure 8.3.2   Responses to Lateral system inputs, no turbulence, altitude
6096 meters, speed Mach .83, level flight.
MMAC hypothesis models 10,11,12,17.
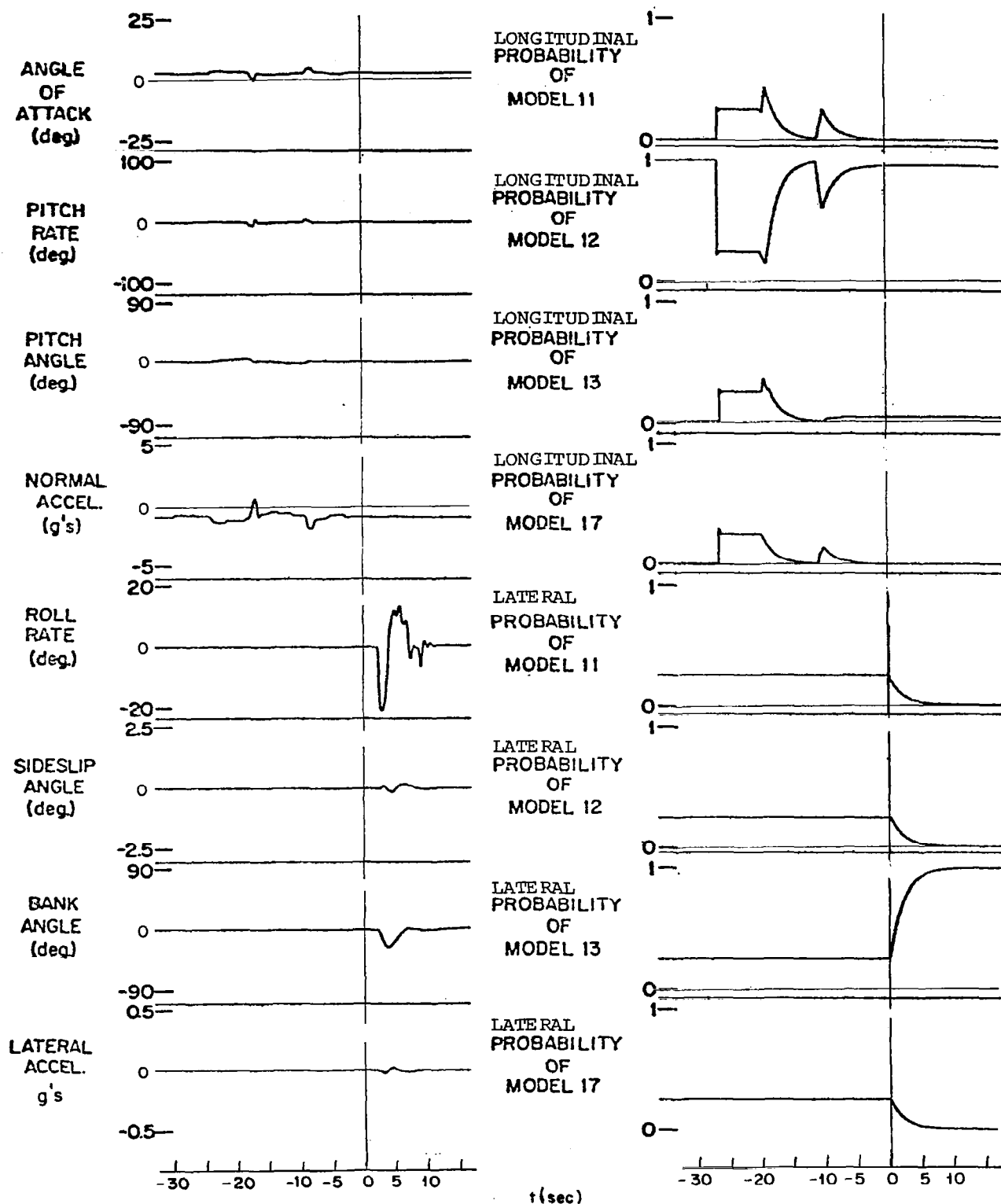
Figure 8.3.3   Responses to longitudinal and lateral system inputs,
no turbulence, altitude 6096 meters, speed .82 Mach,
level flight.
MMAC hypothesis models 11,12,13,17.
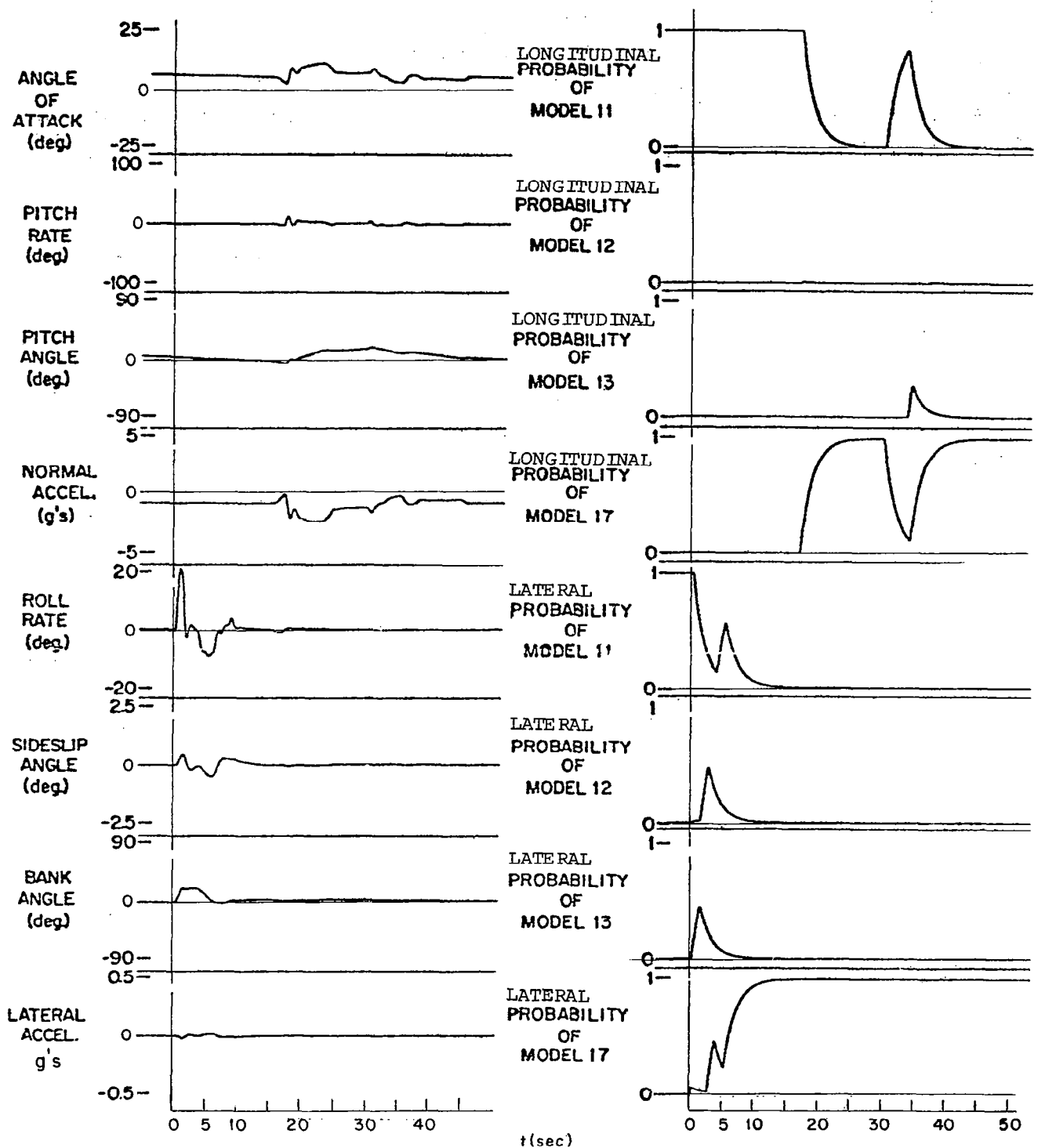
Figure 8.3.4   Responses to longitudinal and lateral system inputs, no turbulence, altitude 13,106 meters, speed .87 Mach, level flight.
MMAC hypothesis models 11,12,13,17.
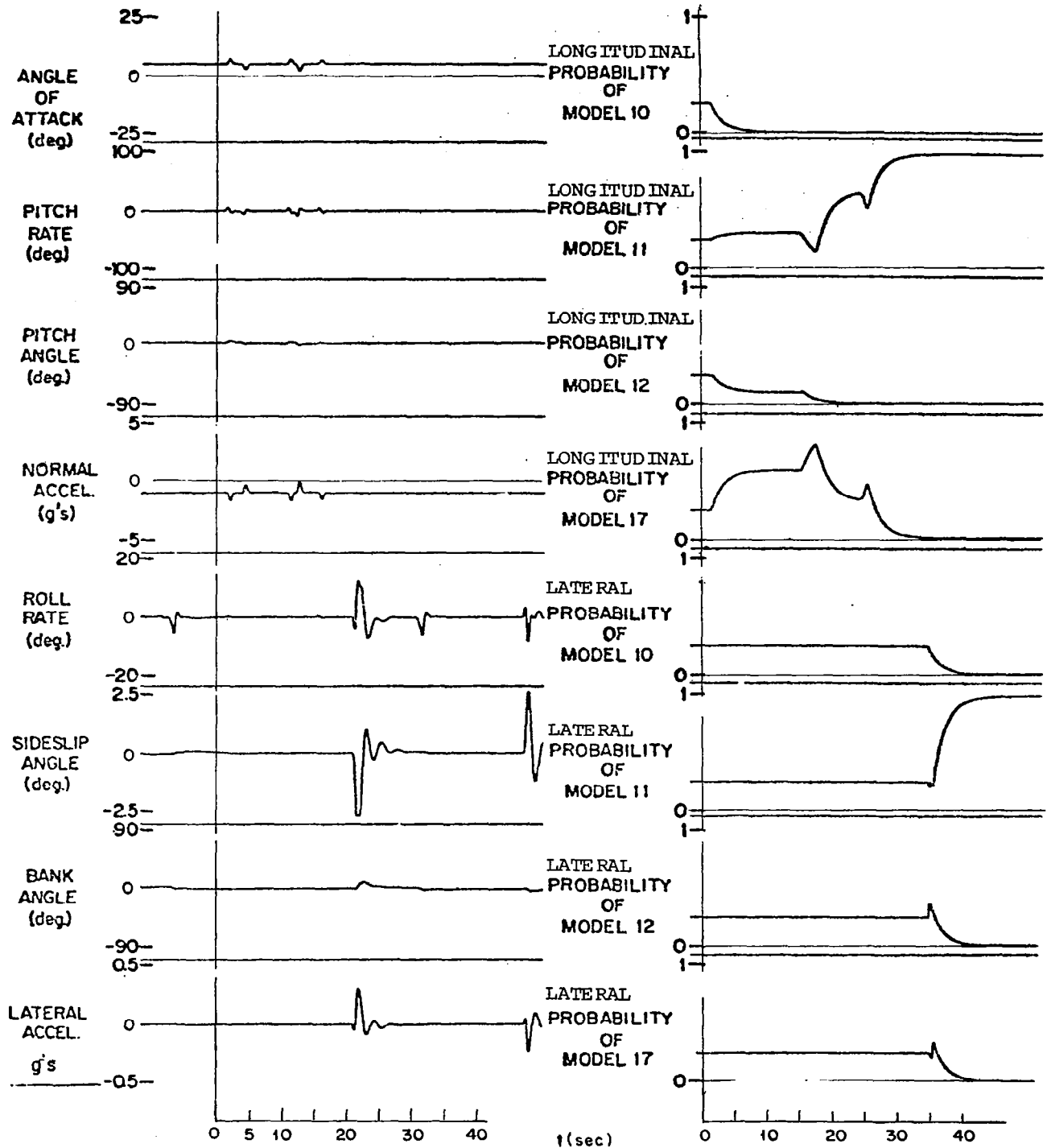
Figure 8.3.5   Responses to longitudinal and lateral system inputs,
no turbulence, altitude 6096 meters, speed .6 Mach.
MMAC hypothesis models 10,11,12,17.
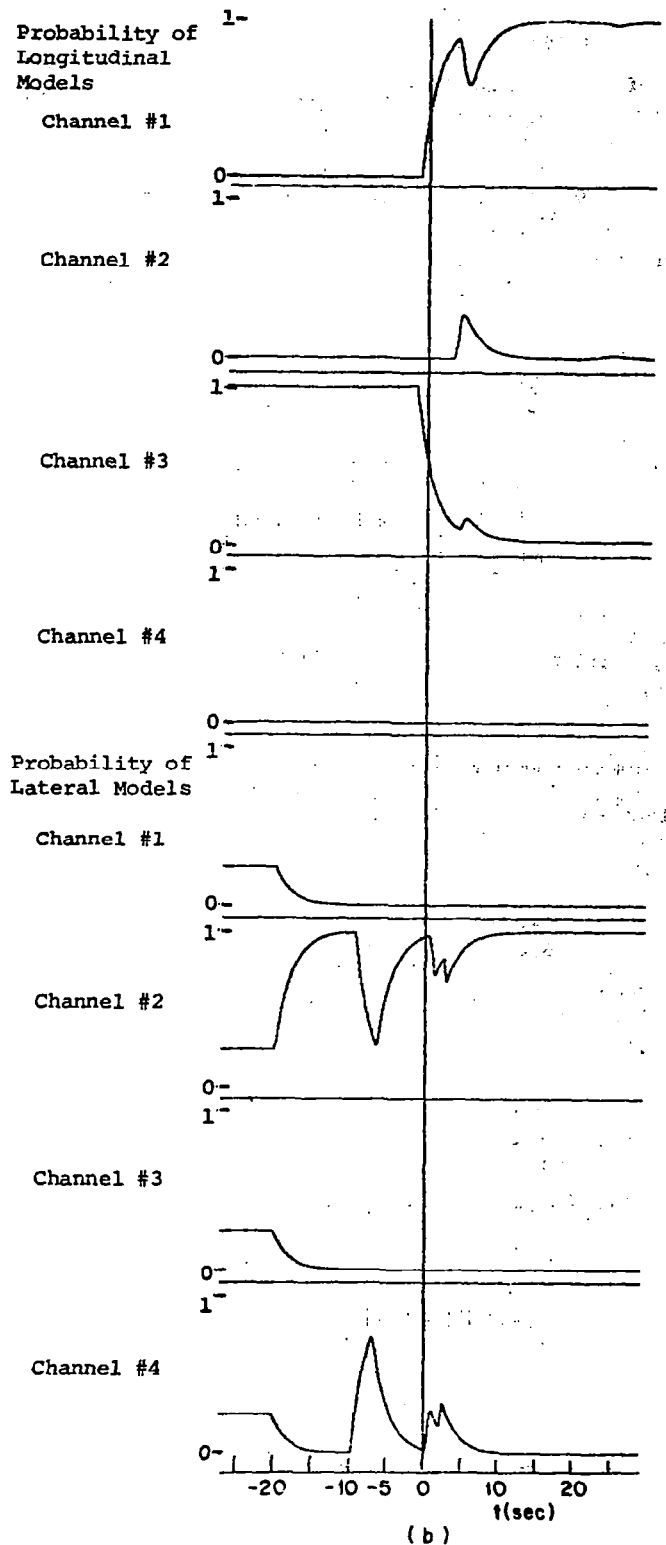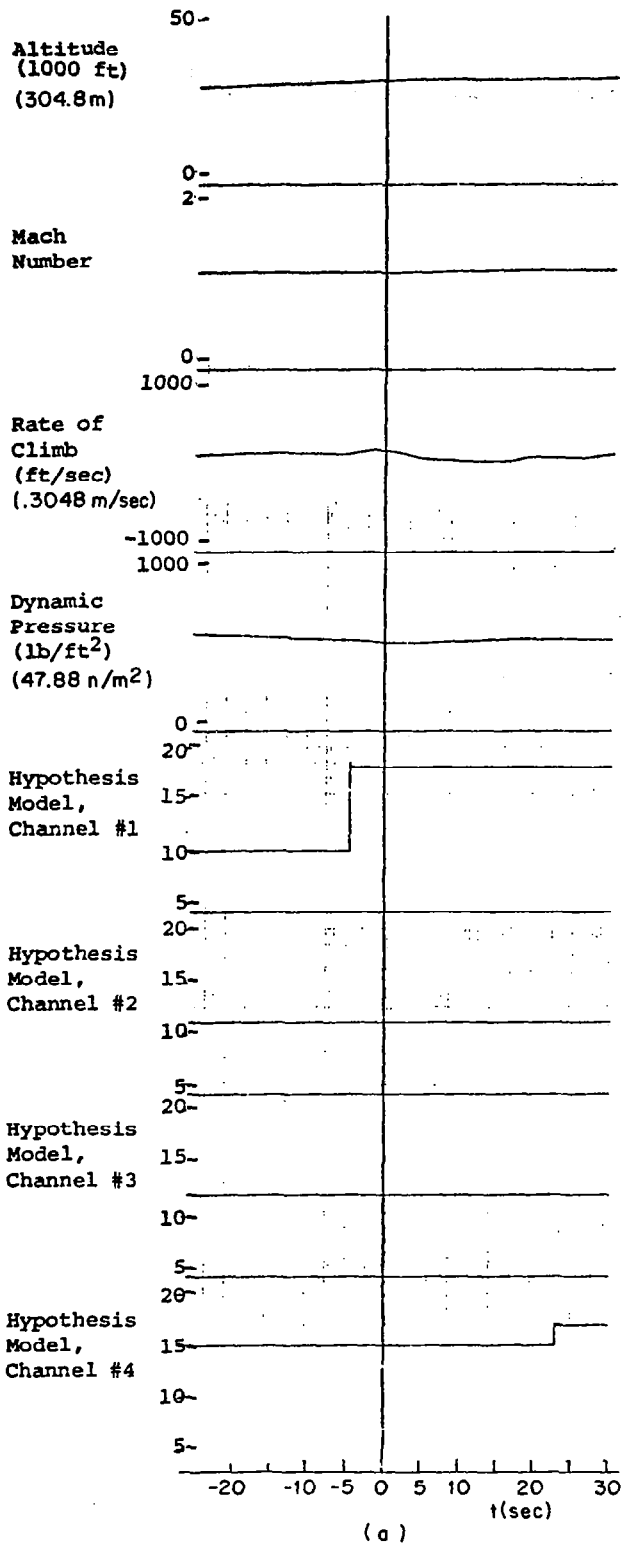
Figure 8.3.6   Global aircraft responses and Identification system
                 responses, during slow climb, no turbulence,
                 altitude ~9144 meters, speed ~1.1 Mach
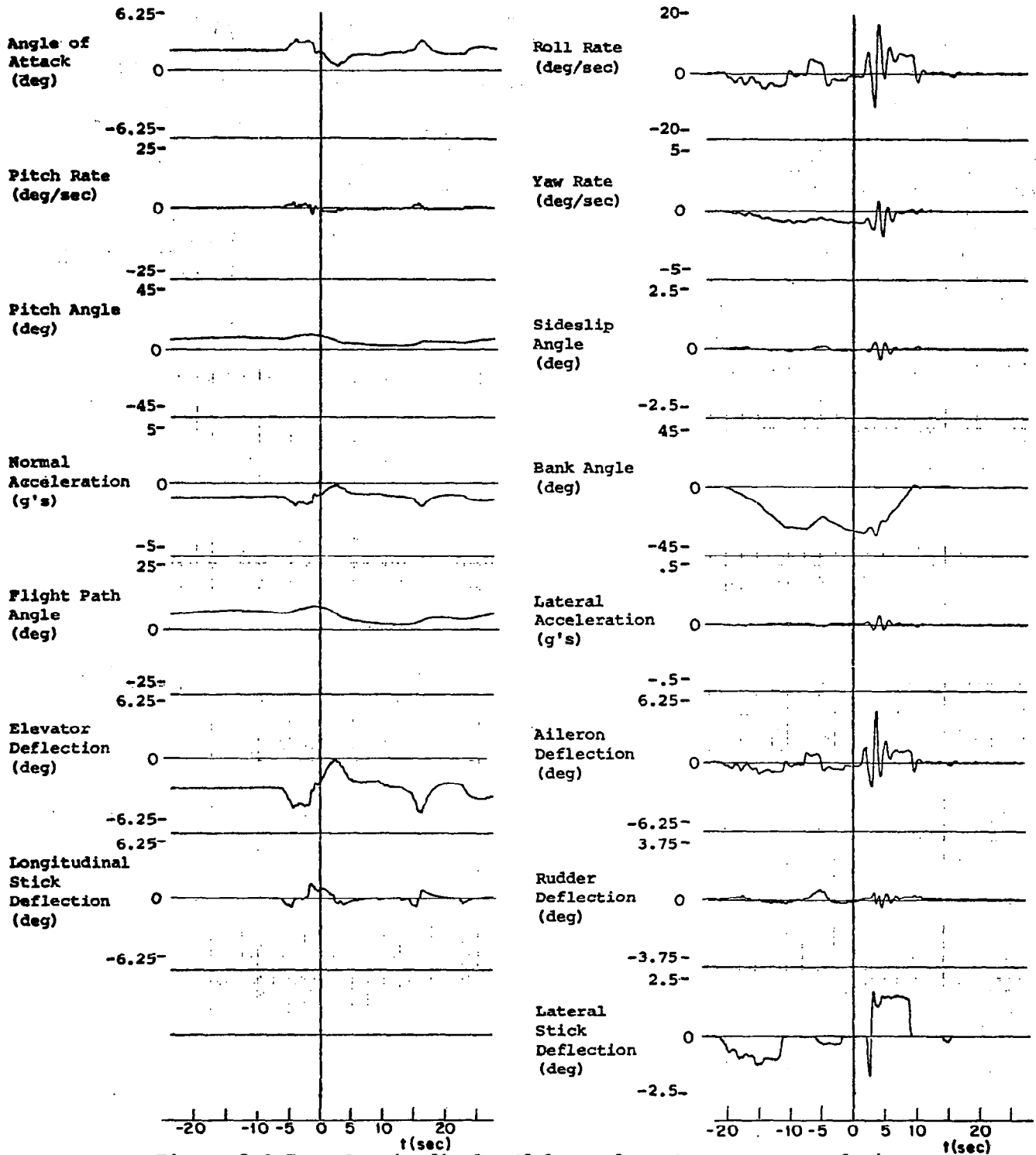
Figure 8.3.7   Longitudinal and lateral system responses during
slow climb, no turbulence, altitude ~9144 meters,
speed ~1.1 Mach.
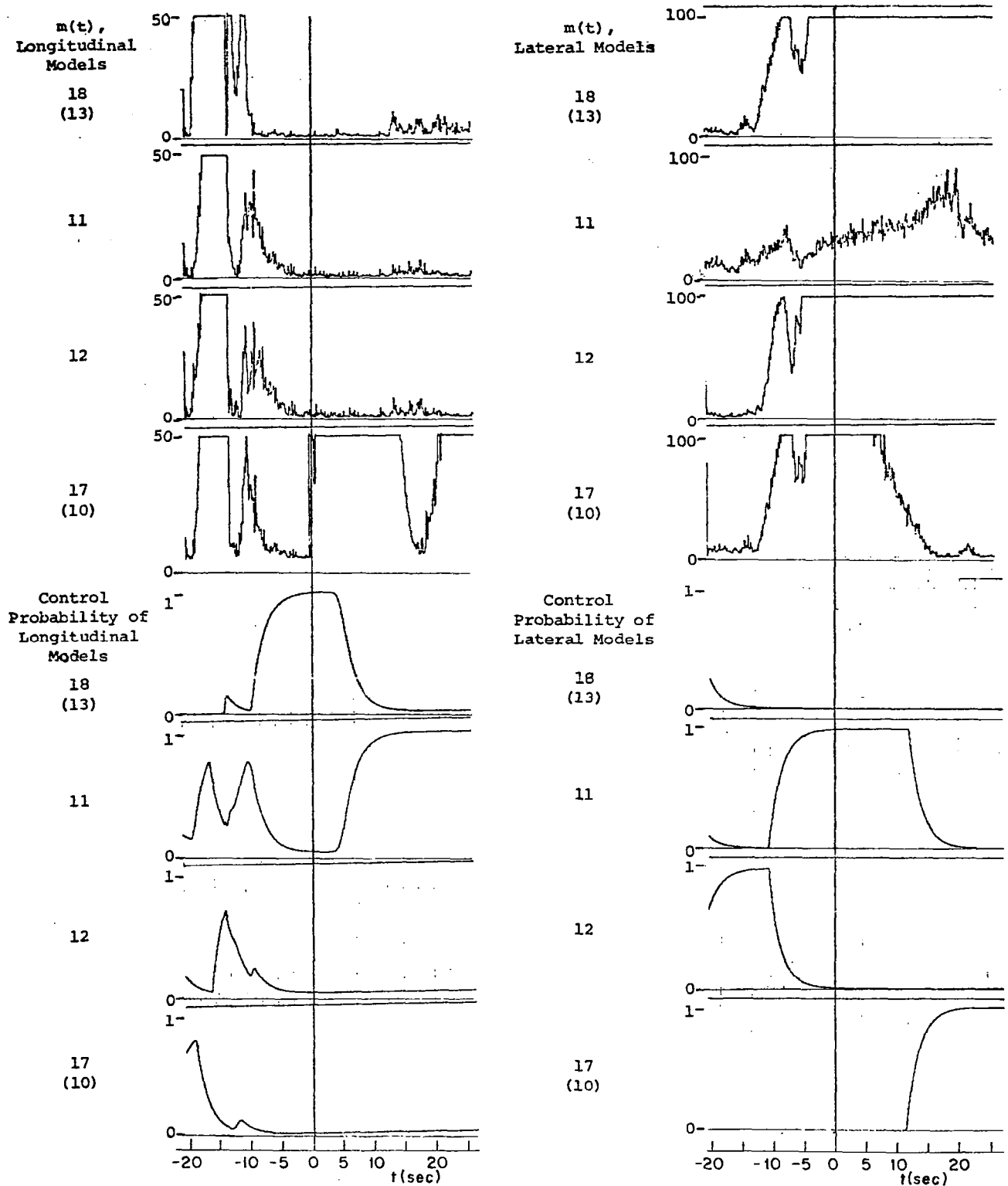
Figure 8.3.8   Control probability and m(t) responses during
               deceleration maneuvers, no turbulence, altitude
               6096 meters, speeds .6 Mach to .44 Mach.

Figure 8.3.9   Global aircraft responses and model scheduling
evolution during diving maneuvers, no turbulence.
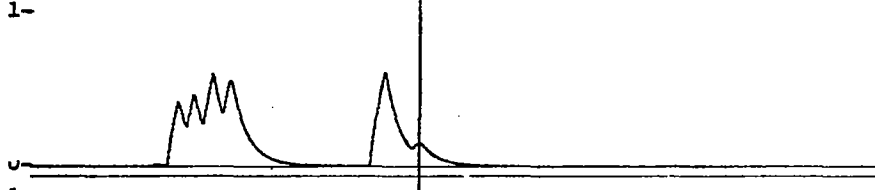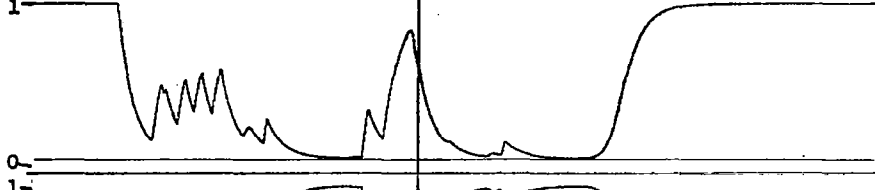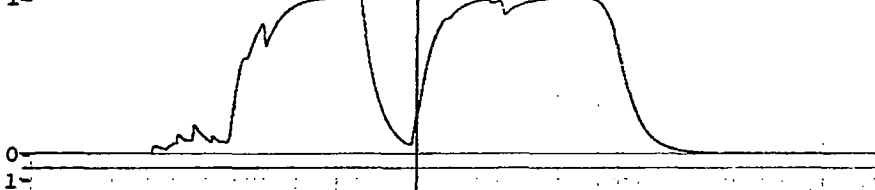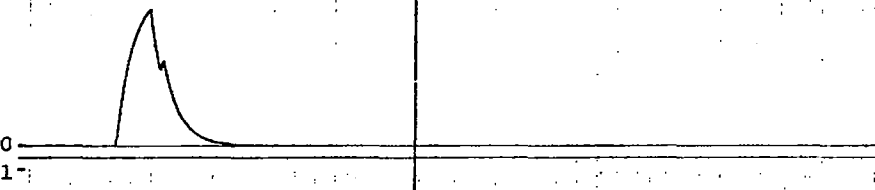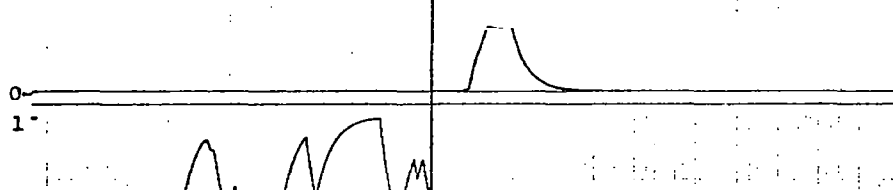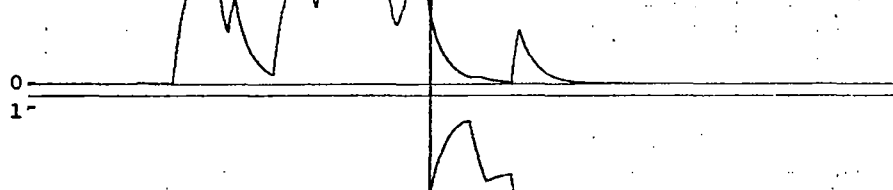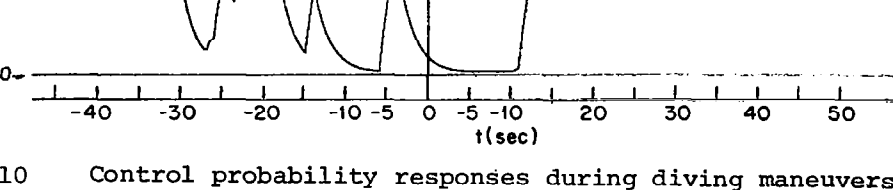
Figure 8.3.10   Control probability responses during diving maneuvers, no turbulence, initial altitude 6096 meters, initial speed .5 Mach.

Figure 8.3.11   Longitudinal system responses during diving maneuvers, no turbulence, initial altitude 6096 meters, initial speed .5 Mach.

Figure 8.3.12   Lateral system responses during diving maneuvers,
no turbulence, initial altitude 6096 meters,
initial speed .5 Mach

Figure 8.3.13   Global aircraft responses and model scheduling evolution
during maneuvers near 2438 meters, no turbulence, speed
.6 Mach
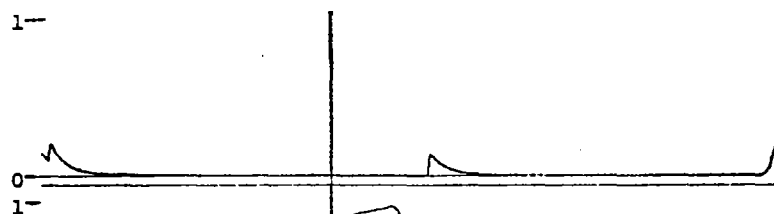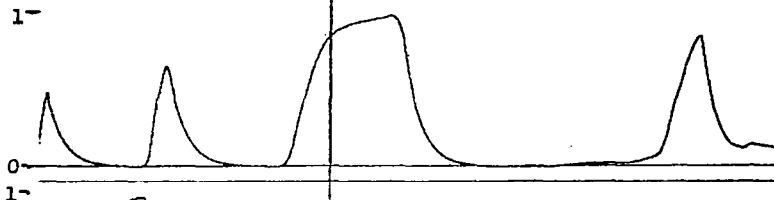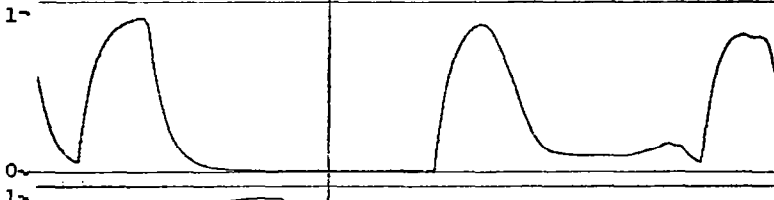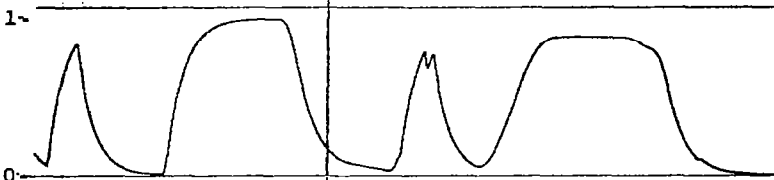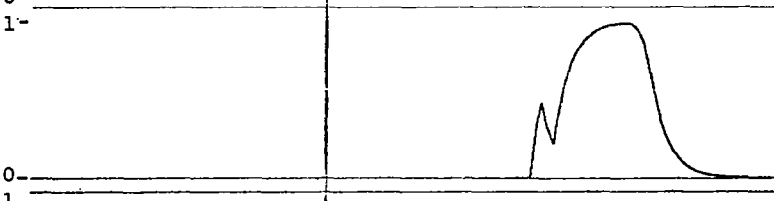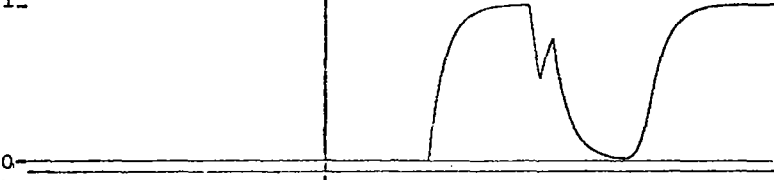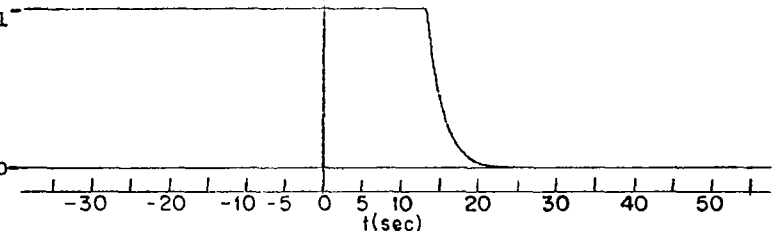
Figure 8.3.14   Control probability responses during maneuvers
near 2438 meters, no turbulence, speed .6 Mach

Figure 8.3.15   Longitudinal system responses during
maneuvers near 2438 meters, no turbulence,
speed .6 Mach

Figure 8.3.16   Lateral system responses during maneuvers near
2438 meters, no turbulence, speed .6 Mach

Figure 8.3.17   Global aircraft responses and model scheduling evolution
during climbing maneuvers, no turbulence, initial altitude
1524 meters, initial speed .51 Mach

Figure 8.3.18   Control probability responses and model scheduling
evolution during climbing maneuvers, no turbulence,
initial altitude 1524 meters, initial speed .51 Mach
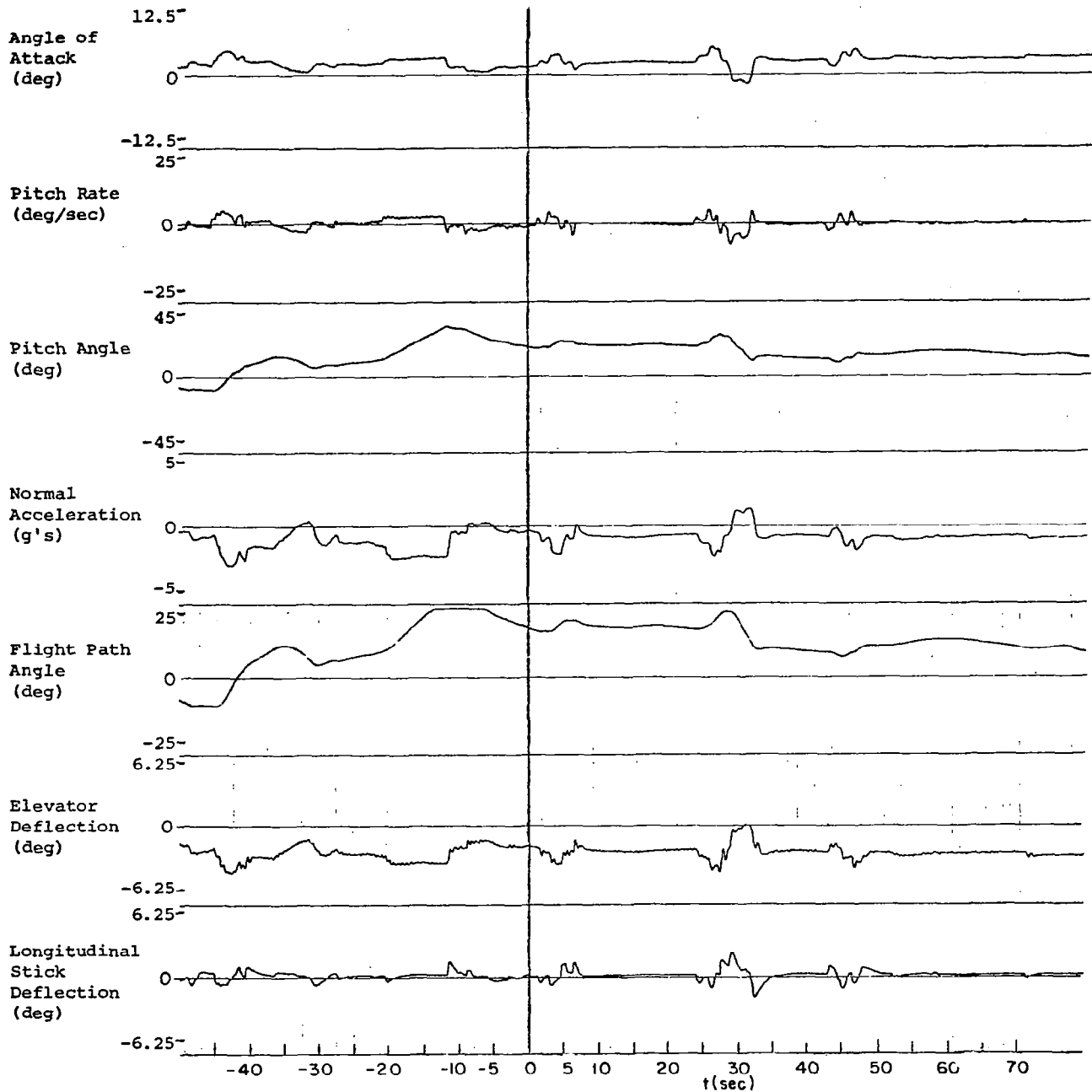
Figure 8.3.19   Longitudinal system responses and model scheduling
                 evolution during climbing maneuvers, no turbulence,
                 initial altitude 1524 meters, initial speed .51 Mach
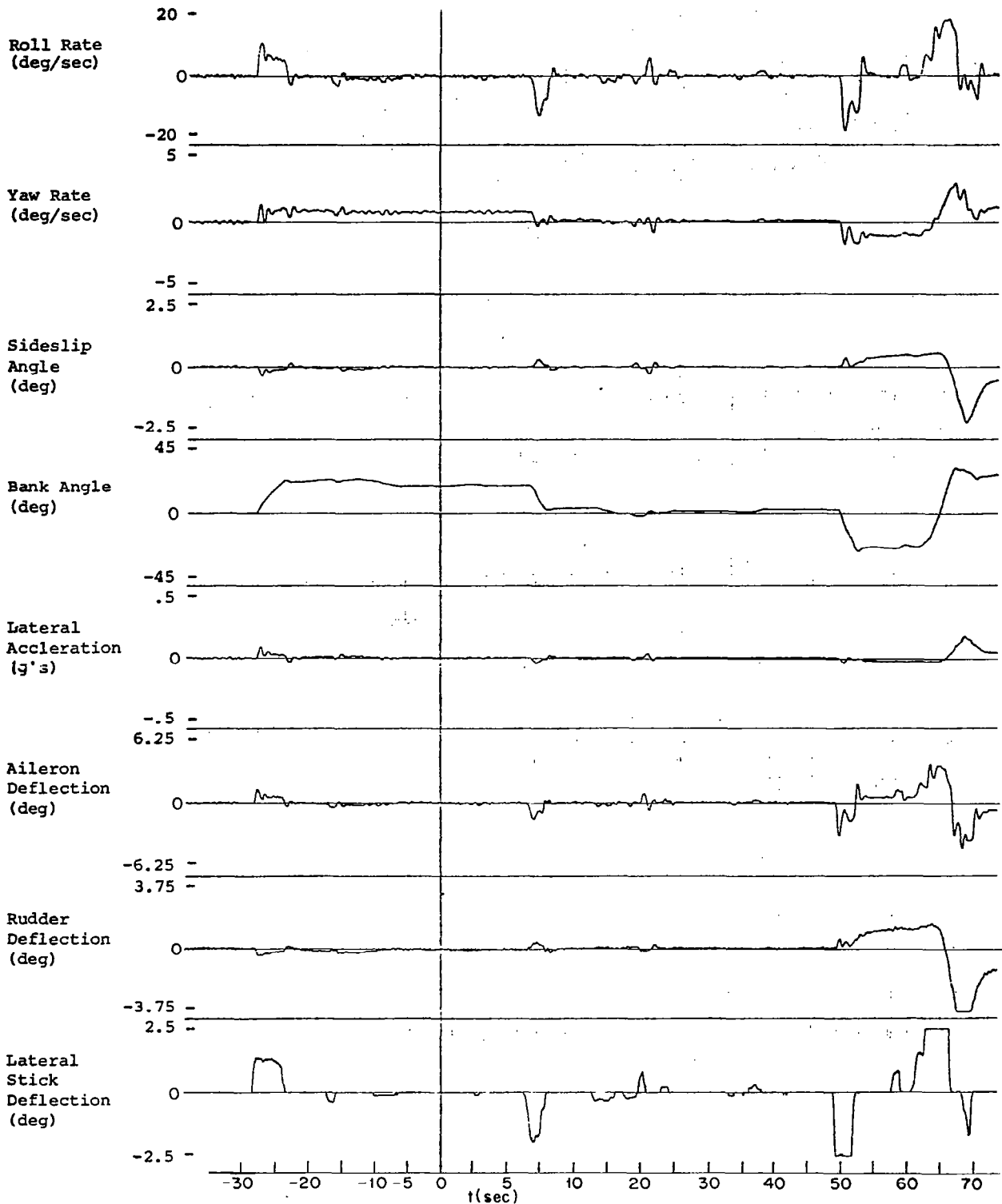
Figure 8.3.20   Lateral system responses and model scheduling
evolution during climbing maneuvers, no turbulence,
initial altitude 1524 meters, initial speed .51 Mach

8.4 Tracking Experiments

The experiments in this section show only the evolution of the con-
trol probabilities and the global aircraft variables as the F-8C aircraft
is flown throughout its flight envelope. The experiments shown are ex-
cerpts from long simulations using an engineer "pilot" to fly the nonlinear
simulation at NASA Langley. No turbulence was present in the simulation.
The purpose of these experiments is to illustrate the way the identifi-
cation algorithm tracks the aircraft across the flight envelope.

Figures 8.4.1 and 8.4.2 describe aircraft responses during an accel-
eration maneuver at 6096 met. altitude. The vertical line indicates
a simultaneous time reference for both figures. The longitudinal iden-
tification system seems to track the velocity changes accurately,
evolving from models 10 to models 11 and 12 as the speed builds up. The
lateral identification system does not track well at all, identifying
only model 10.

Figures 8.4.3 and 8.4.4 show the aircraft responses during a decel-
eration maneuver using the speed brake. The aircraft altitude is 6096
met, and it decelerates from Mach .6 to Mach .38. Figure 8.4.4 shows
the longitudinal identification system tracks the speed changes, shifting
from models 12 to 11 to 10. The lateral identification system does not
respond to these variations in speed.

Figures 8.4.5 and 8.4.6 show aircraft responses during a dive from
1829 met to 305 met altitude, reducing speed from Mach .8 to Mach .6.
The longitudinal identification system wavers between models 7 and 13,

as does the lateral identification system, while the aircraft speed is near .75 Mach. When the aircraft reduces speed, flight condition 7 (very close to the actual condition, with speed .7 Mach at sea level) is identified in both systems.

Figures 8.4.7 and 8.4.8 show the aircraft responses during a climb and acceleration maneuver, from 4572 to 7925 met altitude, and .36 to 1.02 Mach in speed. The hypothesis models in the MMAC system are models 10, 11, 12 and 13. The longitudinal identification system tracks the changing speeds very well, progressing from models 10 to 11 to 12 and 13. The lateral identification system tracks hardly at all, consistently identifying model 10 throughout the simulation.

8.5 Discussion

The performance of the MMAC identification system in experiments using a engineer "pilot" is illustrated in the chapter. The pilot was cautioned against performing severe pitching or rolling maneuvers, recognizing an inherent deficiency in the MMAC identification system which arises from using strictly equilibrium level flight hypotheses. Overall, the longitudinal identification system performed well, tracking properly with minimal error the changes in the operating conditions of the aircraft. The lateral identification system did not track as well, performing best in equilibrium flight experiments. These results are significant when one considers the availability of only two sensors in the longitudinal system (pitch rate and normal acceleration) versus six sensors in the lateral system (yaw rate, roll rate, lateral acceleration, bank angle, aileron and rudder angle).
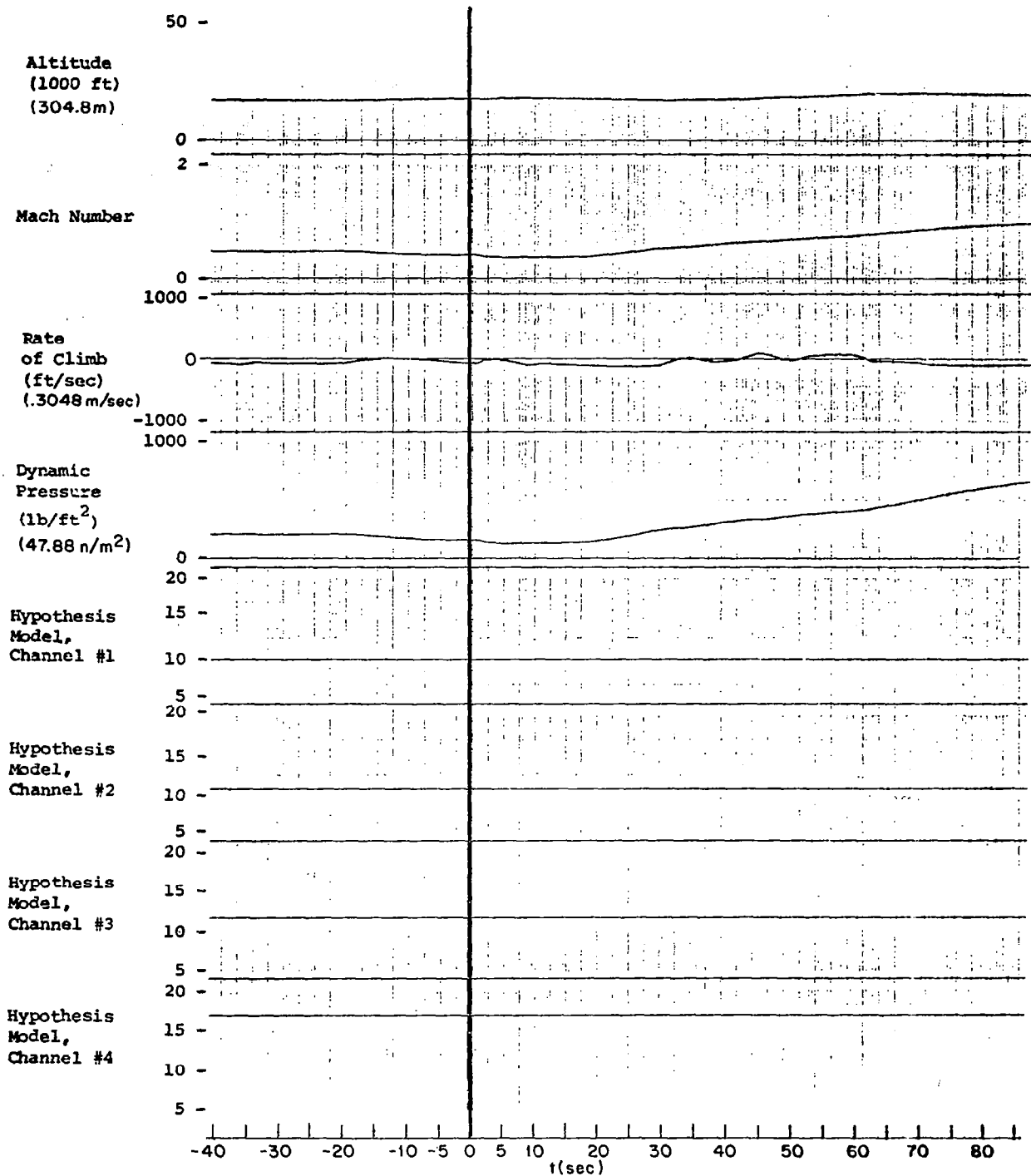
Figure 8.4.1   Global aircraft and model scheduling responses during
                acceleration maneuvers, altitude 6096 meters, speeds
                .4 to 1.02 Mach.

Figure 8.4.2   Control probability responses during acceleration
                maneuvers, altitude 6096 meters, speeds .4 to 1.02
                Mach
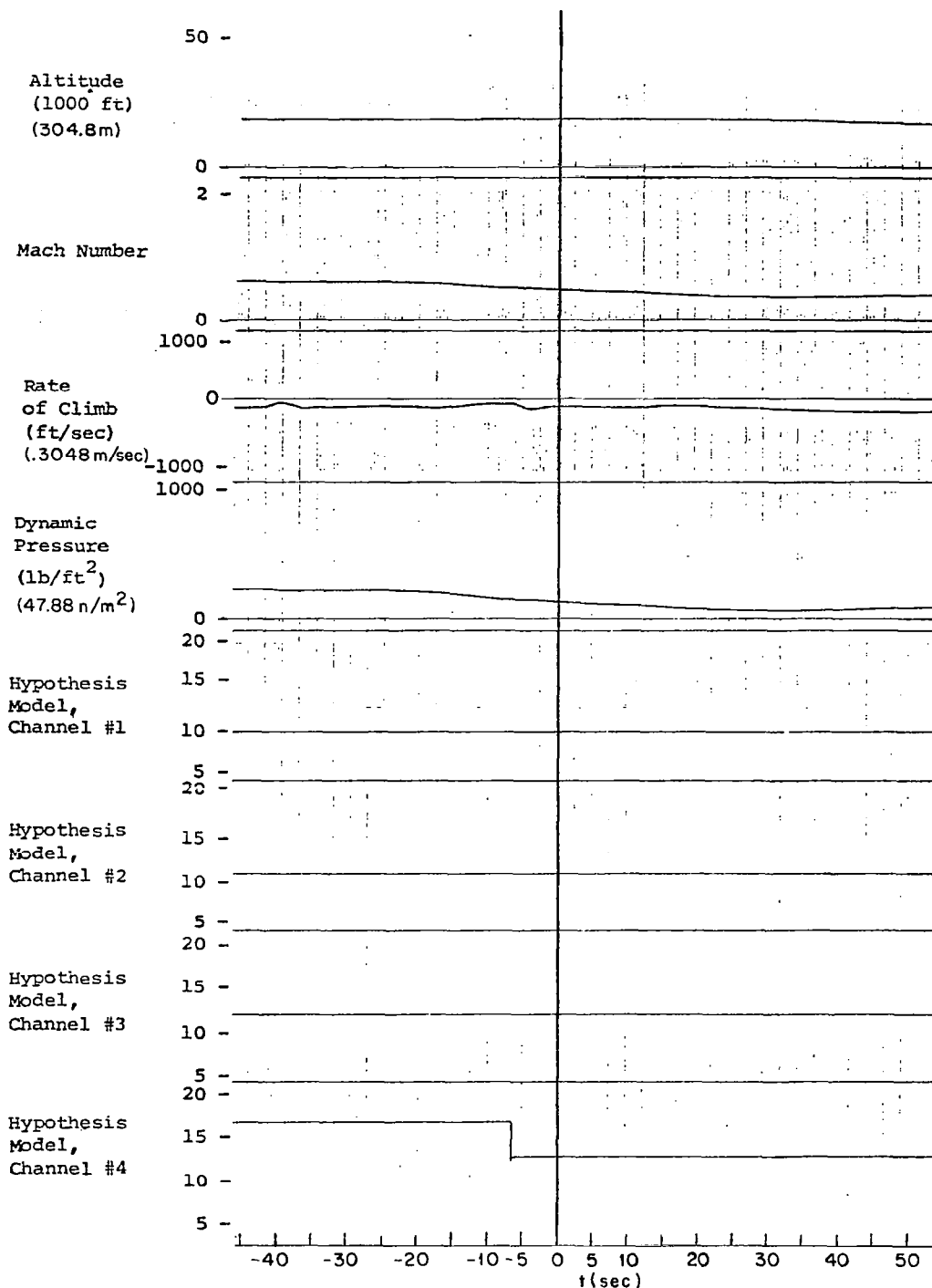
Figure 8.4.3 Global aircraft and model scheduling responses during decelerating maneuvers using speed brake, altitude 6096 meters, speeds .6 to .38 Mach

rrobability of
Longitudinal Models

Channel #1

Channel #2

Channel #3

Channel #4

Probability of
Lateral Models

Channel #1

Channel #2

Channel #3

Channel #4

t(sec)
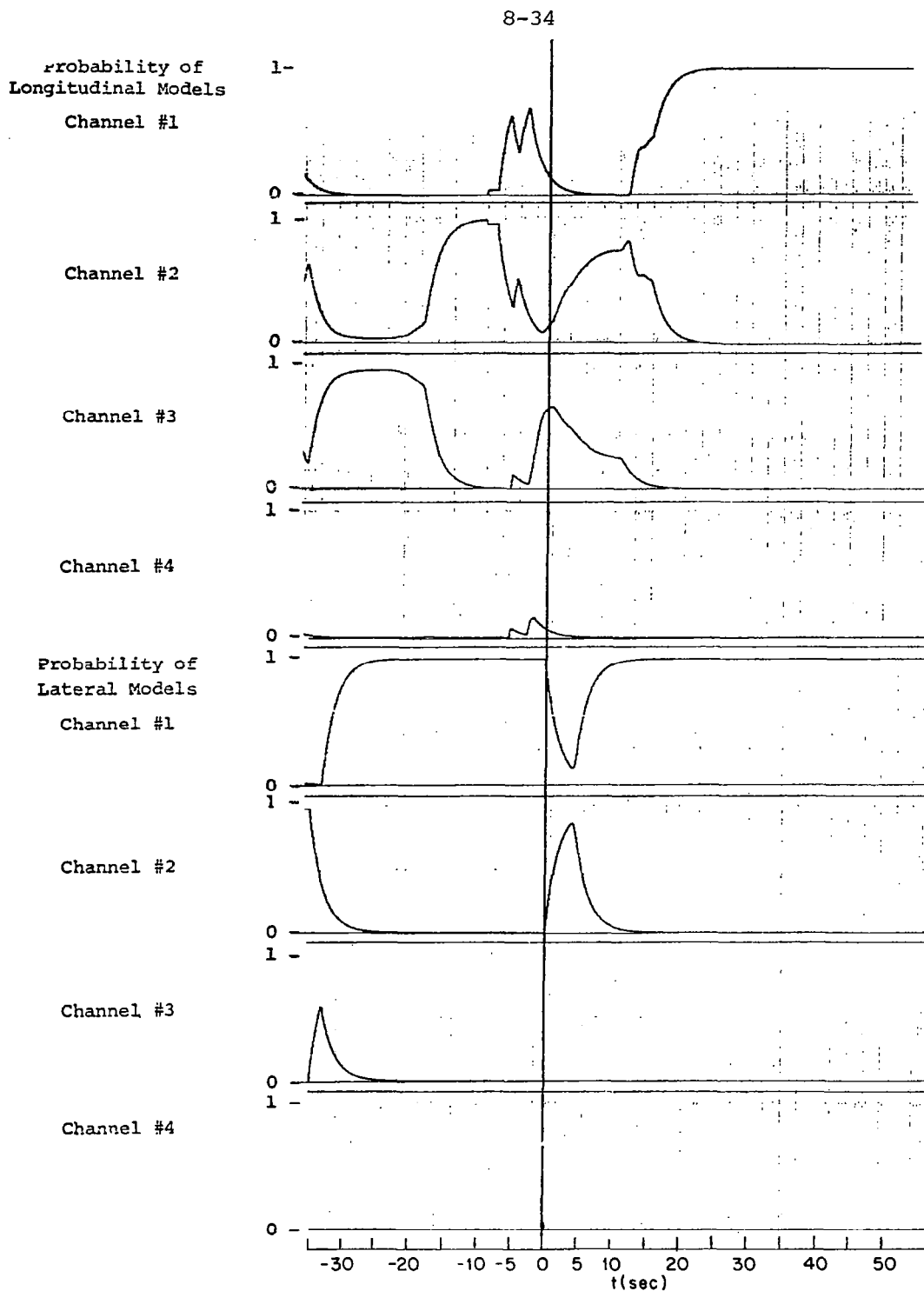
Figure 8.4.4   Control probability responses during decelerating
maneuvers using speed brake, altitude 6096 meters,
speeds .6 to .38 Mach
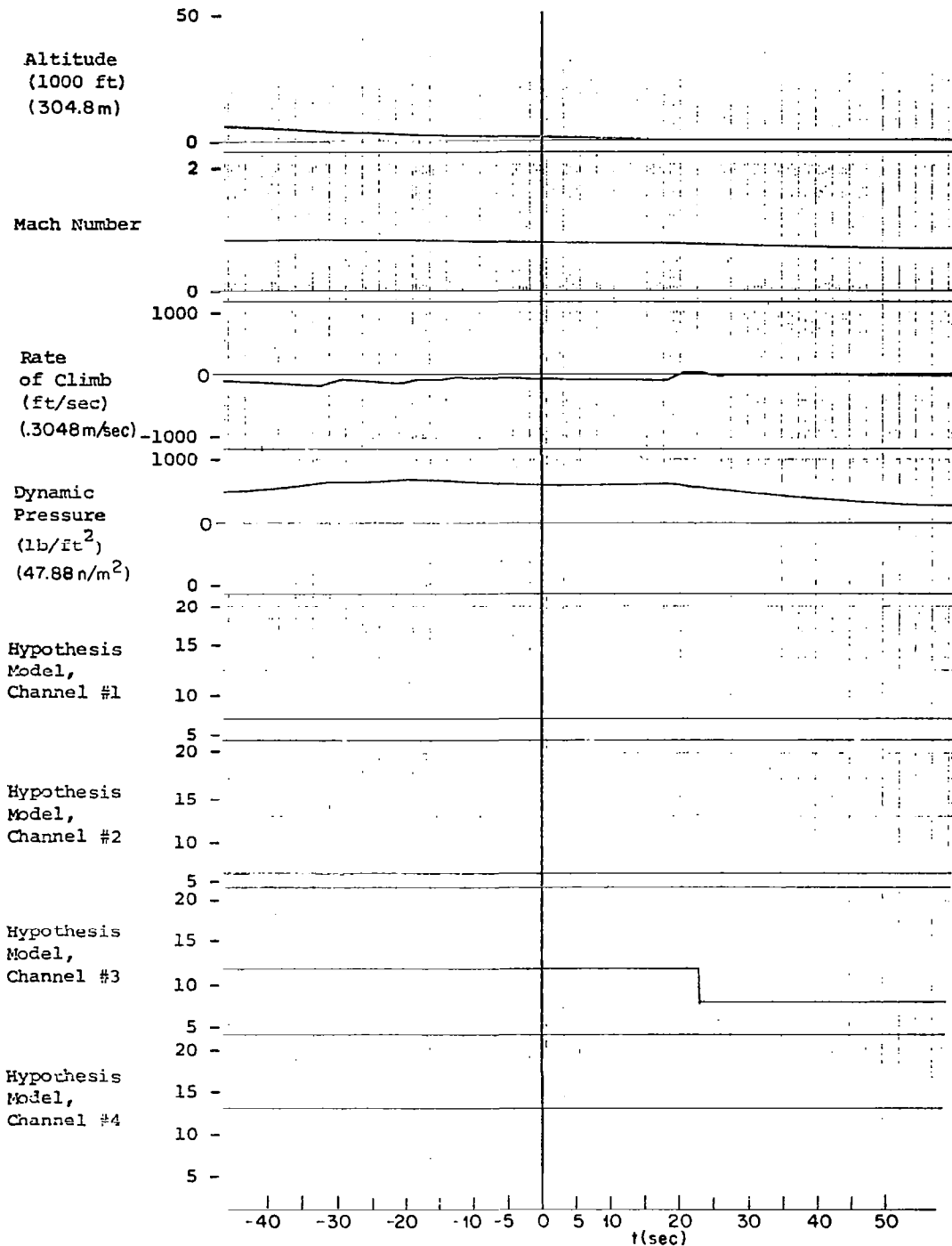
Figure 8.4.5   Global aircraft and model scheduling responses
during descent and deceleration maneuvers, altitude
1829 to 304.8 meters, speed .8 to .6 Mach
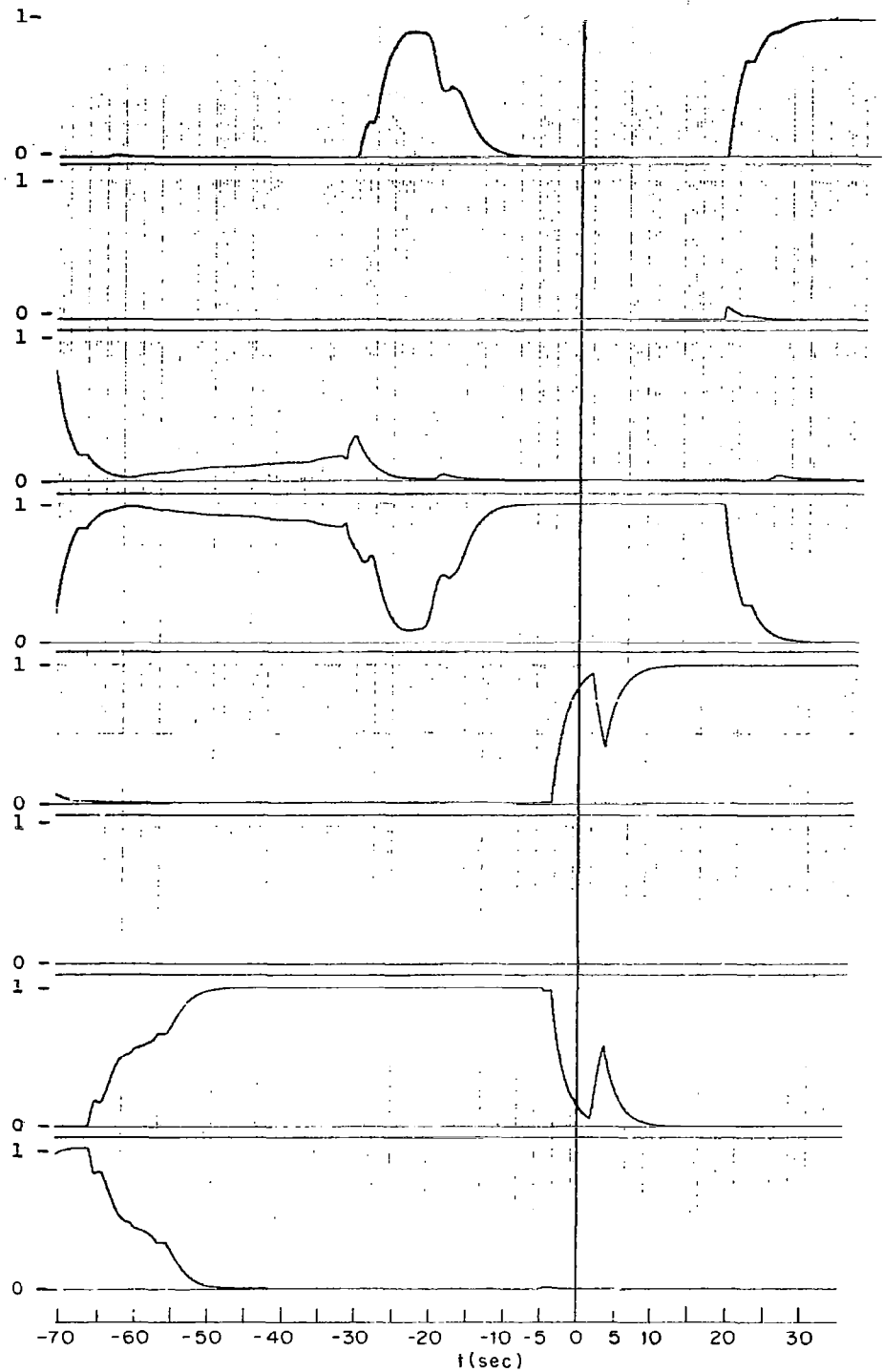
Figure 8.4.6   Control probability responses during descent and
deceleration maneuvers, altitude 1829 to 304.8
meters, speeds .8 to .6 Mach
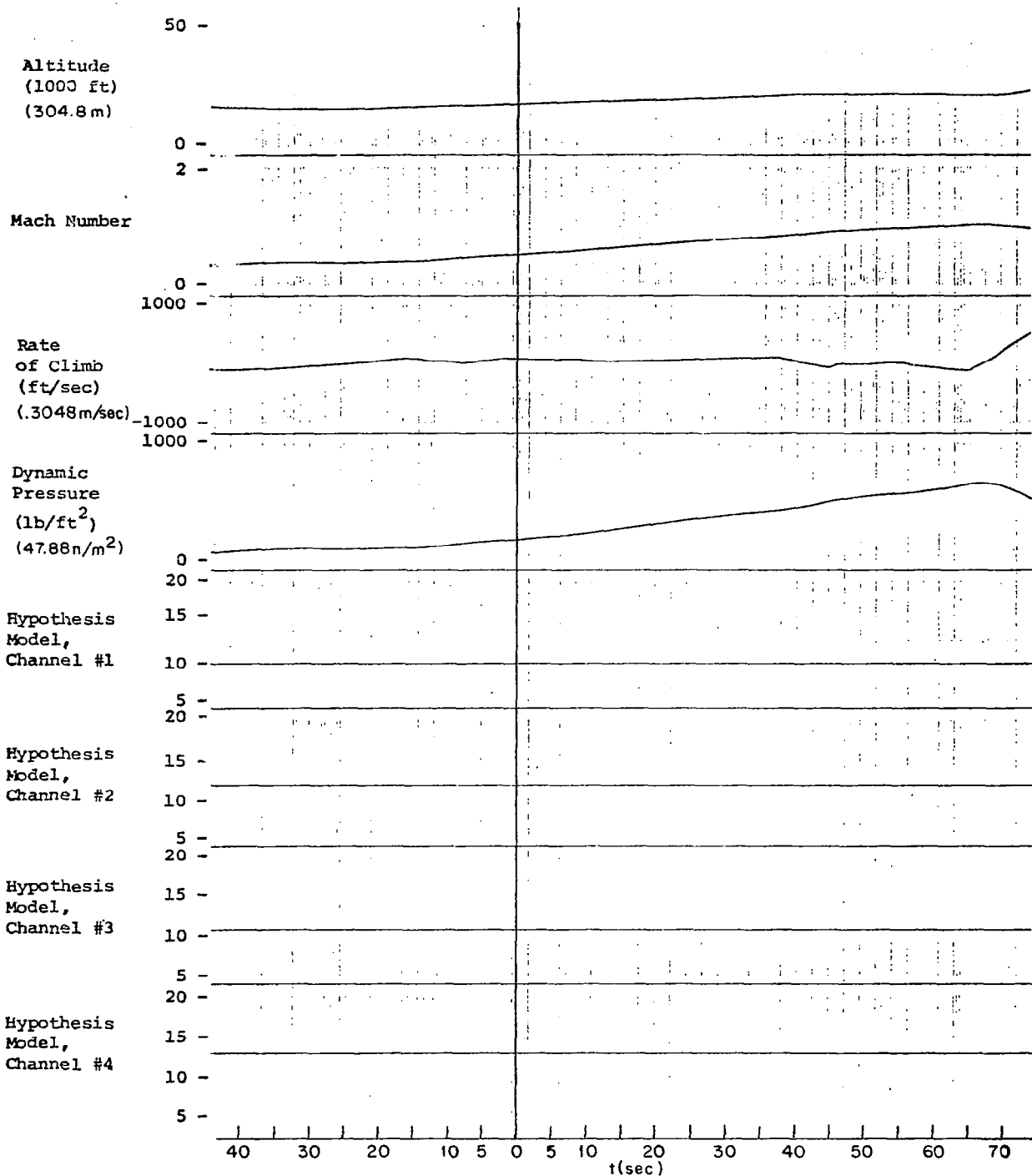
Figure 8.4.7   Global aircraft and model scheduling responses during
combined climbing and accelerating maneuvers, altitude
4572 to 7925 meters, speeds .36 to 1.02 Mach

Figure 8.4.8   Control probability responses during combined
climbing and accelerating maneuvers, altitude
4572 to 7925 meters, speeds .36 to 1.02 Mach

CHAPTER 9

CONCLUSIONS

9.1 Introduction

In this chapter the main conclusions of this study will be sum-
marized from different points of view. Some of the comments will
refer to the MMAC algorithm as a general methodology for stochastic
adaptive control, while other comments will refer to the performance
of the MMAC algorithm in the context of controlling the F-8 aircraft
under the general guidelines adopted with respect to available
sensors and real time computational constraints.

In the reading of this conclusion section the reader should keep
in mind the time frame during which this study was conducted
(April 1974 to September 1976), while this conclusions section is
being written in final form in May 1978. New theoretical results
are currently available; some were obtained as a direct consequence
of this study. If these results had been available at the initiation of
this study, and if incorporated in the MMAC design, the simulation
results and the specific conclusions could have probably been
vastly different.

Finally, the reader should keep in mind the basic objective
of this study: evaluate the concept of the MMAC algorithm as a pos-
sible candidate for adaptive control for aircraft using the F-8 as

the test example. This represents the first exhaustive study of the MMAC methodology for a realistic problem.

9.2 The MMAC Algorithm and the F-8

Given the fact that an F-8 aircraft is currently being used as a test bed for digital-fly-by-wire demonstrations, including tests of failure management systems and advanced control laws, one may pose the question:

> Should the MMAC algorithm, as described in
> this report, be implemented for flight tests?

The answer to this question is a clear NO. The algorithm as currently constituted has severe deficiencies that must be corrected before any flight tests are undertaken.

Specific Deficiencies

The specific deficiencies of the described MMAC algorithm are:

1) Pure handling qualities. These are more serious in the lateral axis than in the longitudinal axis.

2) Unpredictable performance. In the case of typical maneuvers for a fighter aircraft, in both the longitudinal and lateral axes, the equilibrium flight models used in the MMAC algorithm are inadequate, and the response of the control system cannot be predicted.

3) There is no guarantee that the MMAC algorithm,
as described in this report, will not result
in aircraft instabilities for severe aircraft
maneuvers over its flight envelope.

9.3 Reasons for MMAC Deficiencies

The MMAC algorithm yields a very complex and nonlinear closed-loop feedback control system. As such it defies global analysis and it must be tested exhaustively by simulation. Throughout this study and subsequent analysis [34], little insight has been obtained into the the global stability and performance characteristics of the MMAC algorithm. In general, the overall robustness of the algorithm, with respect to the following list of important design variables, is not well understood:

1) Model selection
2) Number of models in MMAC algorithm
3) Nature and accuracy of sensors
4) Changes in levels of wind turbulence
5) Effects of changing sampling times
6) Robustness of Kalman filters for state
   estimation and identification
7) Level of persistent excitation
8) Design, sensitivity, and robustness of the
   control system.

Based upon the theoretical and simulation studies carried out during this research, all of the above issues have to be considered in the design of the MMAC system.

9.4 How should the MMAC algorithm be evaluated?

Even in the absence of global results this study has greatly contributed to the basic understanding of the MMAC algorithm. Its relative performance can only be judged in situations for which the degree of modelling error is not sufficiently severe as to invalidate the methodology employed.

Since only equilibrium flight models were employed in the MMAC design, the robustness and performance of the MMAC algorithm can be evaluated for aircraft motions that are close to equilibrium flight. These are the results presented in Chapters 7 and 8 of this report. For the sake of exposition, the general region for evaluation is defined as maneuvering flight in which motion is as follows:

   (a) Longitudinal motion is restricted to about
        20° change in pitch about equilibrium flight.

   (b) Lateral motion is restricted to about 30°
        change in bank angle about the equilibrium
        flight

There are two ways of evaluating the performance of the entire MMAC system

   1) Identification: If the aircraft is close to a
       particular flight condition, and this flight
       condition is included in the set of model hypo-
       theses, do the model probabilities converge to
       the "correct" flight condition?

2) Closed-Loop Response: If the aircraft is close
    to a particular flight condition, how does the
    MMAC response compare (under both deterministic
    and stochastic conditions) to that obtained if
    the flight condition were known exactly.

Identification performance is easier to check than comparisons of

closed-loop responses. On the other hand, evaluation through

identification performance is not necessarily the most appropriate

way of judging the performance of the closed-loop MMAC algorithm.

The reason is that the actual aircraft dynamics, including the ef-

fects of wind disturbances, are never identical to one of the models

of the MMAC algorithm. Furthermore, the performance of the iden-

tification algorithm is strongly dependent upon the existence of

persistent excitation so as to overcome the β^* -dominance effect.

Closed loop aircraft performance is more difficult to

evaluate, but it is the closed loop performance of any adaptive

control system that matters. In the MMAC context one has to evaluate

the overall response of the aircraft in any particular flight

condition independent of the equilibrium flight models that are

employed by the MMAC algorithm.

With respect to the above two broad ways of evaluating perfor-

mance, and subject to the restrictions on pitch and bank angles noted,

it was concluded that

(a) The MMAC algorithm is in general an adequate adaptive control algorithm and deserves further study.

(b) The longitudinal MMAC system performed much better than the lateral one, both with respect to identification and closed loop performance.

9.5 The Lateral MMAC System

The inferior identification and control performance of the lateral MMAC System can be attributed to several factors

(a) It is difficult to obtain an estimate of key aerodynamic parameters, as influenced by changes in dynamic pressure, from the lateral dynamics. This has been demonstrated by the simulation studies in this report. In several instances the lateral MMAC system could not identify the most probable aircraft flight condition. The fact that one cannot obtain a great deal of information from the lateral dynamics is in agreement with the conclusions reported by Stein et al. [27].

(b) The complexity of the Kalman filters associated with the lateral dynamics, and the fact that fixed levels of wind turbulence were used to design the Kalman filters precluded the careful tuning necessary to have state estimation errors that are consistent with theoretical predictions. It is

conjectured that the Kalman filters used for
the lateral dynamics for several flight con-
ditions are considerably in error. Poorly
designed Kalman filters contribute to both
state estimation errors and poor identifi-
cation through convergence of probabilities
to wrong postulated models.

(c) The poor handling characteristics of the
lateral MMAC system can be directly at-
tributed to the fact that in the model
following approach employed, a single
constant velocity (that of flight condi-
tion 11) was used. This resulted in
uncoordinated turns in other flight con-
ditions, when a particular bank angle
had to be followed. It is suspected that
this shortcoming of the lateral flight
control system introduced bias errors in
the lateral Kalman filters during turning
maneuevers, thus causing additional state
estimation errors and impaired identifi-
cation performance in the later MMAC
system.

The inclusion of the actual inertial velocity V_0 in the model
following control system for the lateral dynamics, and a subsequent
redesign of the Kalman filters for the lateral dynamics should
greatly improve the performance of the lateral identification and
control system. This is due to the fact that the lateral MMAC

system performed well in the vicinity of flight condition 11, as demonstrated in the simulations presented in Chapters 7 and 8.

9.6 The Longitudinal MMAC System

The longitudinal MMAC system performed very well in both its identification accuracy and closed-loop performance throughout the flight envelope, subject to the pitch angle constraints stated. In almost all simulations presented the longitudinal control system correctly identified the correct flight condition when appropriate. Even more important whenever the actual flight condition was not included in the set of hypotheses a close neighbor (in a probabilistic sense) was identified, thus resulting in good closed loop performance.

It is important to stress that in a great variety of simulations with the longitudinal MMAC system, the model hypotheses included several combination that were mismatched unstable. In other words, if the actual flight condition was i and a model j was included in the MMAC algorithm, then if model j was identified the resultant closed-loop system would become unstable.

In all simulations the longitudinal MMAC system never consistently identified a mismatched unstable combination. In the absence of persistent excitations, the β^* dominance effect sometimes could increase the probability of a mismatch unstable combination; however,

this would immediately cause an excitation and in the next measurement the mismatch unstable combination would be rejected. This extremely valuable property of the MMAC system can be evidenced by all piloted simulations, a subset of which has been presented in Chapter 9.

Although the longitudinal MMAC system performed quite well under all simulations performed, its performance could be improved further. These improvements would substantially increase the operating conditions in terms of increased allowable pitch angle longitudinal maneuvers. The main shortcomings of the current longitudinal MMAC design are as follows:

(a) Bias errors are introduced in the longitudinal Kalman filters. These bias errors are introduced through the phugoid mode which was not included in the short period dynamics models. Further bias errors are introduced through inadequate treatment of the elevator trim in the Kalman filter design. The longitudinal Kalman filters should be redesigned so that they estimate the elevator trim through the use of the elevator position measurements. This would enhance the overall accuracy of the longitudinal state estimates, improve the robustness of the individual Kalman filters, further improve the identification accuracy and improve the closed-loop performance.

(b) Persistent (subliminal) excitation through
     elevator motion, through signals known to
     the Kalman filters, should further improve
     the identification accuracy of the longi-
     tudinal MMAC system. Such a persistent
     excitation would overcome the issue of lack
     of information available for identification,
     and will alleviate the β^* -dominance
     phenomenon.

(c) All longitudinal Kalman filters were designed
     using a fixed level of turbulence correspon-
     ding to flight through cumulus clouds. This
     corresponded to increased bandwidth in all
     Kalman filters. When the aircraft was flying
     either in the absence of turbulence or
     moderate turbulence, the accuracy of the
     longitudinal variable estimates, and of the
     identification, degraded because more sensor
     noise passed through the high bandwidth Kalman
     filters than necessary. Future attention
     should be given to enlarging the set of
     hypotheses (and models) in the overall MMAC
     algorithm by having more than one turbulence
     level. This would not necessarily require an
     increase in the number of models operating
     in real time, but could be accomplished through
     modification of the model scheduling algorithm,
     described in Chapter 8, to include a gross
     decision on the level of turbulence actually
     present.

(d) The handling qualities of the longitudinal
MMAC system can be improved through changes
in the control gains, and by providing neutral
aircraft stability.

9.7 General Conclusions

In this section a summary of general conclusions related to the
MMAC algorithm is presented. The subsequent discussions represent
knowledge gained from theoretical and simulation investigations from
the specific F-8 study and additional theoretical and simulation
investigations carried out subsequent to the F-8 study.

a) Structural Advantages: The implementation of the MMAC
algorithm by parallel banks of Kalman filters is appealing because
of the advances made in microprocessor technology. One can vi-
sualize a single chip for implementing each Kalman filter, and
another for the subsequent calculations of the identification pro-
babilities and calculation of the adaptive control. The lack of
any iteration -based calculations makes the concept appealing,
since the total memory and real-time calculations can be precomputed.
It should also be noted that the parallel maximum likelihood
noninterative structure used by Stein et al. [27] has the same
advantages.

b) Identification Properties: As demonstrated in Chapter 4
the identification probabilities can oscillate rapidly between
alternate models in the presence of stochastic disturbances. Such

rapid transitions of the identification probabilities were not suspected before the initiation of this study. These transitions are not necessarily bad, since the actuators will smooth the commanded controls. In the present study, the identification probabilities were low-passed, in an ad-hoc manner, so as to smooth them out.

The rapid probability transitions can be often the result of erroneous initialization of the constant gain Kalman filters, and incorrect design of the digital Kalman filters. Accurate design of the digital Kalman filters is essential for the MMAC algorithm.

The general issue of correct convergence of the MMAC algorithm under closed-loop operation remain an open theoretical question. The on-going doctoral thesis of Greene [34] sheds some understanding on the qualitative properties of the closed-loop MMAC algorithm, but theoretical results that guarantee the asymmptotic convergence of the correct model are not currently available.

Recent results by Baram and Sandell [7], [35], have provided valuable information on the open-loop identification properties of the MMAC algorithm. These results indicate that the MMAC algorithm will converge to the nearest probabilistic neighbor in the presence of persistent excitations. This research provides a well defined metric (distance) that could be used to measure a "stochastic distance" between models, and it may be useful in selecting the model hypotheses that should be implemented in the MMAC algorithm. It

should be stressed, however, that these results do not trivially

extend to convergence properties of the closed-loop MMAC algorithm.

c) Closed-Loop Control Properties: It should be stressed

that the implementation of the MMAC algorithm is not limited to

control designs obtained using the Linear-Quadratic methodology.

Any method for designing the control system can be used in conjuction

with the MMAC identification algorith.

The specific MMAC algorithm presented in this report has a

very special structure. In a regulator context the control $\underline{u}(t)$

is generated by

$$\underline{u}(t) = \sum_{i=1}^{N} P_i(t)\underline{G}_i \hat{\underline{x}}_i(t|t) \tag{9.1}$$

where $P_i(t)$ are the model probabilities generated from the residuals

of the kalman filters, $\underline{G}_i$ are the control gains, and $\hat{\underline{x}}_i(t|t)$

are the state estimates generated by the Kalman filters. It should

be stressed that the control $\underline{u}(t)$ is very sensitive to Kalman filter

errors, because of its double dependence on both the model proba-

bilities $P_i(t)$ and the state estimates $\hat{\underline{x}}_i(t|t)$. Since the system

operates in a stochastic environment the MMAC algorithm may identify

a wrong model for a few measurement; however, the state estimates

of the wrong model may be grossly in error and this will also

influence the generation of erroneous controls.

In aircraft applications the key state variables are measured accurately by gyros and accelerometers. For such problems simple low passing of sensor signals and perhaps the use of low-order Luenberger observers and complementary Kalman filters can be used to generate an overall state estimate $\hat{\underline{x}}(t)$. In this case, it appears that the control should be generated by

$$\underline{u}(t) = \sum_{i=1}^{N} P_i(t)\underline{G}_i(t)\hat{\underline{x}}(t) \qquad (9.2)$$

where the probabilities $P_i(t)$ are still generated from the bank of detailed Kalman filters as described in this report. It is conjectured that the control law (9.2) will be more robust to errors in Kalman filter design than that given by (9.1), for the reason mentioned above. In this method, the Kalman filters would be used primarily for identification rather than for simultaneous identification and control.

In summary, the MMAC algorithm deserves more study from both a theoretical and applied points of view.

CHAPTER 10

REFERENCES

1. IEEE Transactions on Automatic Control, Special Issue on the F-8
    Aircraft, Vol. AC-22, October 1977.

2. J.R. Elliot, "NASA's Advanced Control Law Program for the F-8
    Digital Fly-by-Wire Aircraft," IEEE Trans. on Auto. Control,
    Vol. AC-22, October 1977.

3. G.L. Hartmann et al., "F8-C Digital CCV Flight Control Laws,"
    NASA Contractor Report NASA CR-2629, February 1976.

4. G. Stein, G.L. Hartman, and R.C. Hendrick, "Adaptive Control Law for
    F-8 Flight Test," IEEE Trans. on Auto. Control, Vol.AC-22, Oct. 1977.

5. M. Athans, "The Discrete Time LQG Problem," Annals Economic and
    Social Measurement, Vol. 2, 1972, pp. 449-491.

6. A.E. Bryson, Jr. and Y.-C. Ho, Applied Optimal Control: Optimization,
    Estimation, and Control, Ginn and Company, Waltham, Mass., 1969.

7. Y. Baram, "Information, Consistent Estimation and Dynamic System
    Identification," Ph.D. Thesis, Report ESL-R-718, M.I.T. Electronic
    Systems Laboratory, November 1976.

8. W.H. Lee and M. Athans, "The Discrete Time Compensated Kalman
    Filters," NASA CR-2916, 1977.

9. M. Athans and P.P. Varaiya, "A Survey of Adaptive Stochastic
    Control Methods," Proc. Engineering Foundation Conference on
    Systems Engineering, New England College, Henniker, N.H.,
    August 1975.

10. D.T. Magill, "Optimal Adaptive Estimation of Sampled Processes,"
    IEEE Trans. Automatic Control, Vol. AC-10, 1965, pp. 434-439.

11. D.G. Lainiotis, "Partitioning: A Unifying Framework for Adaptive
    Systems, Parts I and II," Proc. IEEE, Vol. 64, 1976, Part I,
    pp. 1126-1142, Part II, pp. 1182-1197.

12. M. Aoki, "Optimization of Stochastic Systems," N.Y. Academic Press,
    1976, pp. 237-241.

13. A.H. Haddad and J.B. Cruz, Jr., "Nonlinear Filtering for Systems
    with Unknown Parameters," Proc. 2nd Symposium on Nonlinear Esti-
    mation Theory and Its Applications, San Diego, Calif., pp. 147-
    150, 1971.

14. G. Stein, "An Approach to the Parameter Adaptive Control Problems," Ph.D. Thesis, Purdue Univ., Lafayette, Indiana, 1969.

15. G.N. Saridis and T.K. Dao, "A Learning Approach to the Parameter Self Organizing Control Problem," Automatica, Vol. 8, pp. 589-597, 1972.

16. D.G. Lainiotis et al., "Optimal Adaptive Control: A Nonlinear Separation Theorem," Int. J. Control, Vol. 15, 1972, pp. 877-888.

17. D.G. Lainiotis et al., "Optimal Adaptive Estimation: Structure and Parameter Adaptation," IEEE Trans. Auto. Control, Vol. AC-16, 1971 pp. 160-170.

18. D. Willner, "Observation and Control of Partially Unknown Systems," Ph.D. Thesis, Report ESL-R-496, M.I.T. Electronic Systems Laboratory, May 1973.

19. J.D. Desphande, et al., "Adaptive Control of Linear Stochastic Systems," Automatica, Vol. 9, 1973, pp. 107-115.

20. M. Athans and D. Willner, "A Practical Scheme for Adaptive Aircraft Flight Control Systems," Proc. Symposium on Parameter Estimation Techniques and Applications in Aircraft Flight Testing, NASA TN D-7647, NASA Flight Research Center, Edwards, Calif., April 1973, pp. 315-336.

21. E. Tse and Y. Bar-Shalom, "Actively Adaptive Control for Nonlinear Stochastic Systems," Proc. IEEE, Vol. 64, 1976, pp. 1172-1181.

22. K.J. Astrom, "Introduction to Stochastic Control Theory," Academic Press, 1970.

23. A.H. Jazwinski, "Stochastic Processes and Filtering Theory," Academic Press, 1970.

24. J.B. Moore and R.M. Hawkes, "Decision Methods in Dynamic Systems Identification," presented at IEEE Conference on Decision and Control, Houston, Texas, Dec. 1975.

25. S. Kullback, "An Application on Information Theory to Multivariate Analysis, II," Annals of Mathematical Statistics, Vol. 27, pp. 122-145, 1956.

26. M. Athans and C.B. Chang, "Adaptive Estimation and Parameter Identification Using Multiple Model Estimation Algorithm," ESD-TR-76-184, Lincoln Laboratory, M.I.T., 23 June 1976.

27. G.L. Hartmann et al., "F-8C Adaptive Flight Control Laws,"
    NASA CR-2880, 1977.

28. J. Broussard and M. Safonov, "Design of Generalized Discrete Pro-
    portional Integral Controllers by Linear Optimal Control Theory,"
    Technical Information Memorandum, TIM-804-1, TASC, Reading,
    Massachusetts, October 1976.

29. W.H. Lee, M. Athans, D. Castanon, and F. Bacchialoni, "Linear
    Tracking Systems with Application to Aircraft Control System
    Design," ESL Report ESL-P-720, M.I.T. Electronic Systems Labo-
    ratory, January 1977.

30. M. Athans, et al., "The Stochastic Control of the F-8C Aircraft
    Using a Multiple Model Adaptive Control (MMAC) Method, Part I,
    Equilibrium Flight," IEEE Trans. on Automatic Control, Vol. AC-22,
    Oct. 1977.

31. M. Athans et al., "The Stochastic Control of the F8-C Aircraft
    Using the Multiple Model Adaptive Control (MMAC) Method," Proc.
    1975 IEEE Conference on Decision and Control, Houston, Texas,
    December 1975, pp. 217-228.

32. M. Athans and P.L. Falb, Optimal Control, N.Y., McGraw Hill Book
    Co., 1966.

33. M. Athans and A.H. Levis, "On the Optimal Sampled Data Control
    of Strings of Vehicles, "Transportation Science, Vol. 2, No.4,
    November 1968, pp. 362-382.

34. C.S. Greene, Ph.D. Dissertation, MIT (in progress, scheduled for
    completion in Fall 1978).

35. Y. Baram and N. R. Sandell, Jr., "Consistent Estimation of Finite
    Parameter Sets with Application to Linear Systems Identification,"
    IEEE Trans. on Automatic Control, Vol. AC-23, June 1978.

36. B. Etkin, Dynamics of Atmospheric Flight, John Wiley & Sons,
    New York, 1972.

APPENDIX A

Linearized Dynamic Equations for the F-8C Aircraft at Various Flight Conditions

The form of the system equation is

$$\dot{\underline{x}} = \underline{A}\,\underline{x} + \underline{B}\,\underline{u} + \underline{L}\,\xi \qquad\qquad (A.1)$$

For the longitudinal system,

$$\underline{x} = \begin{Bmatrix} q \\ v \\ \alpha \\ \theta \\ \delta_e \\ w \end{Bmatrix} ; \quad \underline{u} = \delta_{ec} \qquad\qquad (A.2)$$

For the lateral system,

$$\underline{x} = \begin{Bmatrix} p \\ r \\ B \\ \phi \\ \delta_a \\ \delta_r \\ w \end{Bmatrix} ; \quad \underline{u} = \begin{bmatrix} \delta_{ac} \\ \delta_{rc} \end{bmatrix}$$

The $\underline{A}$ and $\underline{B}$ matrices are flight-condition dependent, and are listed

in the following pages. The $\underline{L}$ matrices depend on the turbulence level, as discussed in Chapter 3, Section 4; see Section 3.4 for relevant equations defining $\underline{L}$.

FLIGHT CONDITION 5

DYNAMIC PRESSURE 133PSF (6391 N/SQ.M) MACH 0.30 ALTITUDE 0 FT(0 M)

LONGITUDINAL SYSTEM

A-MATRIX
```
-0.4726   -0.0004   -2.0290      0.0      -5.0455    -2.0290
 0.0      -0.0287  -19.4600   -32.2000    -2.5680   -19.4600
 1.0000   -0.0006   -0.8029      0.0      -0.1153    -0.8029
 1.0000    0.0       0.0         0.0       0.0        0.0
 0.0       0.0       0.0         0.0     -12.0000     0.0
 0.0       0.0       0.0         0.0       0.0       -3.3490
```

TRANSPOSE OF B-MATRIX
```
0.0   0.0   0.0   0.0   12.0   0.0
```

LATERAL SYSTEM

A-MATRIX
```
-3.6756    0.3301  -25.7796    0.0      11.5500    4.2460  -25.7796
-0.1575   -0.2985    1.0628    0.0       0.5103   -1.8180    1.0628
 0.1395   -0.9887   -0.2152    0.0951    0.0019    0.0474   -0.2152
 1.0000    0.1404    0.0       0.0       0.0       0.0       0.0
 0.0       0.0       0.0       0.0     -30.0000    0.0       0.0
 0.0       0.0       0.0       0.0       0.0     -25.0000    0.0
 0.0       0.0       0.0       0.0       0.0       0.0      -3.3490
```

TRANSPOSE OF B-MATRIX
```
0.0   0.0   0.0   0.0   30.0    0.0   0.0
0.0   0.0   0.0   0.0    0.0   25.0   0.0
```

FLIGHT CONDITION 6

DYNAMIC PRESSURE 416PSF (19990 N/SO.M)   MACH 0.53   ALTITUDE   0 FT(0 M)

LONGITUDINAL SYSTEM

A-MATRIX

```
-0.7775   -0.0003   -7.0970    0.0      -14.2500   -7.0970
 0.0      -0.0207   -8.7020  -32.2000    -0.9907   -8.7020
 1.0000   -0.0002   -1.4520    0.0       -0.1902   -1.4520
 1.0000    0.0       0.0       0.0        0.0        0.0
 0.0       0.0       0.0       0.0      -12.0000     0.0
 0.0       0.0       0.0       0.0        0.0       -5.9170
```

TRANSPOSE OF B-MATRIX

```
0.0   0.0   0.0   0.0   12.0   0.0
```

LATERAL SYSTEM

A-MATRIX

```
-5.6968    0.0489   -61.8312    0.0       32.4400    11.1000   -61.8312
-0.1920   -0.5495     4.7826    0.0        1.6940    -5.1700     4.7826
 0.0522   -0.9971    -0.3967    0.0543     0.0069     0.0707    -0.3967
 1.0000    0.0522     0.0       0.0        0.0        0.0        0.0
 0.0       0.0        0.0       0.0      -30.0000     0.0        0.0
 0.0       0.0        0.0       0.0        0.0      -25.0000     0.0
 0.0       0.0        0.0       0.0        0.0        0.0       -5.9170
```

TRANSPOSE OF B-MATRIX

```
0.0   0.0   0.0   0.0   30.0    0.0    0.0
0.0   0.0   0.0   0.0    0.0   25.0    0.0
```

FLIGHT CONDITION 7

DYNAMIC PRESSURE 726PSF (34886 N/SQ.M)   MACH 0.70   ALTITUDE   0 FT(· 0 M)

LONGITUDINAL SYSTEM

A-MATRIX

```
-0.9818    -0.0003    -12.8300      0.0      -23.4400    -12.8300
 0.0       -0.0240    -10.0500    -32.2000     1.0050    -10.0500
 1.0000    -0.0001     -2.0080      0.0       -0.2330     -2.0080
 1.0000     0.0         0.0         0.0        0.0         0.0
 0.0        0.0         0.0         0.0      -12.0000      0.0
 0.0        0.0        -7.8150      0.0        0.0        -7.8150
```

TRANSPOSE OF B-MATRIX

```
0.0    0.0    0.0    0.0    12.0    0.0
```

LATERAL SYSTEM

A-MATRIX

```
-7.5552    -0.0837    -95.0785     0.0      48.2300    -95.0785
-0.2260    -0.7394     12.6424     0.0       2.5290     12.6424
 0.0335    -0.9978     -0.5520    0.0411     0.0756     -0.5520
 1.0000     0.0335      0.0        0.0       0.0         0.0
 0.0        0.0         0.0        0.0     -30.0000      0.0
 0.0        0.0         0.0        0.0       0.0        -7.8150
```

TRANSPOSE OF B-MATRIX

```
0.0    0.0    0.0    30.0    0.0     0.0
0.0    0.0    0.0     0.0    25.0    0.0
```

FLIGHT CONDITION 8

DYNAMIC PRESSURE 1098PSF (52762 N/SQ.M)   MACH 0.86   ALTITUDE   0 FT (0 M)

LONGITUDINAL SYSTEM

A-MATRIX
```
-1.1800   -0.0004   -20.9500    0.0       -33.0600   -20.9500
 0.0      -0.0249   -13.7800   -32.2000     1.5900   -13.7800
 1.0000   -0.0001    -2.6730    0.0        -0.2592    -2.6730
 1.0000    0.0        0.0       0.0         0.0        0.0
 0.0       0.0        0.0       0.0       -12.0000     0.0
 0.0       0.0        0.0       0.0         0.0        -9.6010
```

TRANSPOSE OF B-MATRIX
```
0.0   0.0   0.0   0.0   12.0   0.0
0.0
```

LATERAL SYSTEM

A-MATRIX
```
-9.7841   -0.1619   -135.0130    0.0       53.5100    16.9500   -135.0130
-0.2835   -0.9269     25.3940    0.0        2.6870    -8.5560     25.3940
 0.0267   -0.9979     -0.7051    0.0335     0.0158     0.0664     -0.7051
 1.0000    0.0268      0.0       0.0        0.0        0.0         0.0
 0.0       0.0         0.0       0.0      -30.0000     0.0         0.0
 0.0       0.0         0.0       0.0        0.0      -25.0000      0.0
 0.0       0.0         0.0       0.0        0.0        0.0        -9.6010
```

TRANSPOSE OF B-MATRIX
```
0.0   0.0   0.0   0.0   30.0    0.0    0.0
0.0   0.0   0.0   0.0    0.0   25.0    0.0
```

FLIGHT CONDITION 10

DYNAMIC PRESSURE 109PSF (5237 N/SQ.M)   MACH 0.40   ALTITUDE 20000 FT(6095 M)

LONGITUDINAL SYSTEM

A-MATRIX
```
-0.3189   -0.0000    -1.8790     0.0      -4.0600    -1.8790
 0.0      -0.0260   -23.9200   -32.2000   -2.0130   -23.9200
 1.0000   -0.0004    -0.5378     0.0      -0.0771    -0.5378
 1.0000    0.0        0.0        0.0       0.0         0.0
 0.0       0.0        0.0        0.0     -12.0000      0.0
 0.0       0.0        0.0        0.0       0.0        -0.3318
```

TRANSPOSE OF B-MATRIX
```
0.0   0.0   0.0   0.0   12.0   0.0
```

LATERAL SYSTEM

A-MATRIX
```
-2.3503    0.2705   -20.8324    0.0       9.1590     3.6550   -20.8324
-0.1001   -0.1969     0.8597    0.0       0.4085    -1.5410     0.8597
 0.1613   -0.9861    -0.1543    0.0765    0.0011     0.0320    -0.1543
 1.0000    0.1632     0.0       0.0       0.0        0.0        0.0
 0.0       0.0        0.0       0.0     -30.0000     0.0        0.0
 0.0       0.0        0.0       0.0       0.0      -25.0000     0.0
 0.0       0.0        0.0       0.0       0.0        0.0       -0.3318
```

TRANSPOSE OF B-MATRIX
```
0.0   0.0   0.0   0.0   30.0   0.0    0.0
0.0   0.0   0.0   0.0   0.0   25.0    0.0
```

FLIGHT CONDITION 11

DYNAMIC PRESSURE 254PSF (12205 N/SQ.M)   MACH 0.60   ALTITUDE 20000 FT(6095 M)

LONGITUDINAL SYSTEM

A-MATRIX

-0.4877	0.0000	-4.7890	0.0	-8.7430	-4.7890
0.0	-0.0148	-13.8800	-32.2000	-1.0960	-13.8800
1.0000	-0.0002	-0.8361	0.0	-0.1115	-0.8361
1.0000	0.0	0.0	0.0	0.0	0.0
0.0	0.0	0.0	0.0	-12.0000	0.0
0.0	0.0	0.0	0.0	0.0	-0.4977

TRANSPOSE OF B-MATRIX

0.0	0.0	0.0	0.0	12.0	0.0

LATERAL SYSTEM

A-MATRIX

-3.3311	0.0827	-44.6241	0.0	20.6000	8.2570	-44.6241
-0.1261	-0.3135	2.5889	0.0	1.1510	-3.4570	2.5889
0.0773	-0.9962	-0.2306	0.0515	0.0037	0.0456	-0.2306
1.0000	0.0775	0.0	0.0	0.0	0.0	0.0
0.0	0.0	0.0	0.0	-30.0000	0.0	0.0
0.0	0.0	0.0	0.0	0.0	-25.0000	0.0
0.0	0.0	0.0	0.0	0.0	0.0	-0.4977

TRANSPOSE OF B-MATRIX

0.0	0.0	0.0	0.0	30.0	0.0	0.0
0.0	0.0	0.0	0.0	0.0	25.0	0.0

FLIGHT CONDITION 12

DYNAMIC PRESSURE 434PSF (20854 N/SQ.M)   MACH 0.80   ALTITUDE 20000 FT (6095 M)

LONGITUDINAL SYSTEM

A-MATRIX

-0.6696	0.0006	-9.0100	0.0	-15.7700	-9.0100
0.0	-0.0136	-14.1100	-32.2000	-0.4330	-14.1100
1.0000	-0.0001	-1.2140	0.0	-0.1394	-1.2140
1.0000	0.0	0.0	0.0	0.0	0.0
0.0	0.0	0.0	0.0	-12.0000	0.0
0.0	0.0	0.0	0.0	0.0	-0.6636

TRANSPOSE OF B-MATRIX

0.0	0.0	0.0	0.0	12.0	0.0

LATERAL SYSTEM

A-MATRIX

-4.6880	-0.0237	-66.2474	0.0	32.8200	12.5800	-66.2474
-0.1526	-0.4400	9.3089	0.0	1.8620	-5.5400	9.3089
0.0458	-0.9980	-0.3217	0.0387	0.0067	0.0514	-0.3217
1.0000	0.0459	0.0	0.0	0.0	0.0	0.0
0.0	0.0	0.0	0.0	-30.0000	0.0	0.0
0.0	0.0	0.0	0.0	0.0	-25.0000	0.0
0.0	0.0	0.0	0.0	0.0	0.0	-0.6636

TRANSPOSE OF B-MATRIX

0.0	0.0	0.0	0.0	30.0	0.0	0.0
0.0	0.0	0.0	0.0	0.0	25.0	0.0

FLIGHT CONDITION 13

DYNAMIC PRESSURE 550PSF (26429 N/SQ.M)   MACH 0.90   ALTITUDE 20000 FT (6095 M)

LONGITUDINAL SYSTEM

A-MATRIX

-0.7900	-12.7300	0.0	-19.2700	-12.7300
0.0	-16.6400	-32.2000	-0.6549	-16.6400
1.0000	-1.4560	0.0	-0.1519	-1.4560
1.0000	0.0	0.0	0.0	0.0
0.0	0.0	0.0	-12.0000	0.0
0.0	0.0	0.0	0.0	-0.7466

TRANSPOSE OF B-MATRIX

0.0	0.0	0.0	12.0	0.0

LATERAL SYSTEM

A-MATRIX

-5.7284	-81.0659	0.0	36.5000	-81.0659
-0.1812	11.4848	0.0	2.0910	11.4848
0.0393	-0.3662	0.0344	0.0081	-0.3662
1.0000	0.0	0.0	0.0	0.0
0.0	0.0	0.0	-30.0000	0.0
0.0	0.0	0.0	0.0	0.0
0.0	0.0	0.0	0.0	-0.7466

TRANSPOSE OF B-MATRIX

0.0	0.0	0.0	30.0	0.0	0.0
0.0	0.0	0.0	0.0	25.0	0.0

FLIGHT CONDITION 14

DYNAMIC PRESSURE 978PSF (46995 N/SQ.M)   MACH 1.20   ALTITUDE 20000 FT(6095 M)

LONGITUDINAL SYSTEM

A-MATRIX

-0.4149	0.0006	-43.0400	0.0	-25.2500	-43.0400
0.0	-0.0020	-16.6800	-32.2000	-0.8813	-16.6800
1.0000	0.0000	-1.5880	0.0	-0.1647	-1.5880
1.0000	0.0	0.0	0.0	0.0	0.0
0.0	0.0	0.0	0.0	-12.0000	0.0
0.0	0.0	0.0	0.0	0.0	-0.9955

TRANSPOSE OF B-MATRIX

0.0	0.9	0.0	0.0	12.0	0.0

LATERAL SYSTEM

A-MATRIX

-5.0204	-0.0982	-128.0840	0.0	22.0500	11.3400	-128.0840
-0.0851	-0.7923	17.1258	0.0	0.7944	-3.2930	17.1258
0.0259	-0.9985	-0.4844	0.0258	0.0059	0.0177	-0.4844
1.0000	0.0260	0.0	0.0	0.0	0.0	0.0
0.0	0.0	0.0	0.0	-30.0000	-25.0000	0.0
0.0	0.0	0.0	0.0	0.0	0.0	0.0
0.0	0.0	0.0	0.0	0.0	0.0	-0.9955

TRANSPOSE OF B-MATRIX

0.0	0.0	0.0	30.0	0.0	0.0
0.0	0.0	0.0	0.0	25.0	0.0

FLIGHT CONDITION 15

DYNAMIC PRESSURE 135PSF (6487 N/SQ.M)   MACH 0.70   ALTITUDE 40000 FT(12191 M)

LONGITUDINAL SYSTEM

A-MATRIX

```
-0.2719    0.0006    -2.8930      0.0      -5.4080    -2.8930
 0.0      -0.0090   -23.2000    -32.2000   -1.2470   -23.2000
 1.0000   -0.0002    -0.4433      0.0      -0.0584    -0.4433
 1.0000    0.0        0.0         0.0       0.0        0.0
 0.0       0.0        0.0         0.0     -12.0000     0.0
 0.0       0.0        0.0         0.0       0.0       -0.5421
```

TRANSPOSE OF B-MATRIX

```
 0.0       0.0        0.0         0.0      12.0        0.0
```

LATERAL SYSTEM

A-MATRIX

```
-1.6739    0.1486   -27.1511      0.0      12.0700     4.9210   -27.1511
-0.0679   -0.1585     1.8334      0.0       0.6412    -2.0670     1.8334
 0.1226   -0.9921    -0.1235      0.0471    0.0017     0.0251    -0.1235
 1.0000    0.1234     0.0         0.0       0.0        0.0        0.0
 0.0       0.0        0.0         0.0     -30.0000     0.0        0.0
 0.0       0.0        0.0         0.0       0.0      -25.0000     0.0
 0.0       0.0        0.0         0.0       0.0        0.0       -0.5421
```

TRANSPOSE OF B-MATRIX

```
 0.0       0.0        0.0         0.0      30.0        0.0        0.0
 0.0       0.0        0.0         0.0       0.0       25.0        0.0
```

FLIGHT CONDITION 16

DYNAMIC PRESSURE 176PSF (8457 N/SQ.M)   MACH 0.80   ALTITUDE 40000 FT (12191 M)

LONGITUDINAL SYSTEM

A-MATRIX

```
-0.3297     0.0007    -4.0010      0.0       -7.3630     -4.0010
 0.0       -0.0102   -18.9200    -32.2000    -1.1270    -18.9200
 1.0000    -0.0001    -0.5358      0.0       -0.0657     -0.5358
 1.0000     0.0        0.0         0.0        0.0         0.0
 0.0        0.0        0.0         0.0      -12.0000      0.0
 0.0        0.0        0.0         0.0        0.0        -0.6196
```

TRANSPOSE OF B-MATRIX

```
0.0    0.0    0.0    0.0    12.0    0.0
```

LATERAL SYSTEM

A-MATRIX

```
-1.9434     0.0957    -34.7524     0.0        15.6700      6.2860    -34.7524
-0.0742    -0.1885      3.3114     0.0         0.8758     -2.6880      3.3114
 0.0937    -0.9952     -0.1420     0.0413      0.0025      0.0278     -0.1420
 1.0000     0.0940      0.0        0.0         0.0         0.0         0.0
 0.0        0.0         0.0        0.0       -30.0000      0.0         0.0
 0.0        0.0         0.0        0.0         0.0       -25.0000      0.0
 0.0        0.0         0.0        0.0         0.0         0.0        -0.6196
```

TRANSPOSE OF B-MATRIX

```
0.0    0.0    0.0    0.0    30.0    0.0    0.0
0.0    0.0    0.0    0.0    25.0    0.0    0.0
```

FLIGHT CONDITION 17

DYNAMIC PRESSURE 223PSF (10715 N/SQ.M)   MACH 0.90   ALTITUDE 40000 FT(12191 M)

LONGITUDINAL SYSTEM

A-MATRIX

-0.4018	-0.0008	-5.8580	0.0	-9.2880	-5.8580
0.0	-0.0113	-23.4000	-32.2000	-1.0480	-23.4000
1.0000	-0.0001	-0.6532	0.0	-0.0729	-0.6532
1.0000	0.0	0.0	0.0	0.0	0.0
0.0	0.0	0.0	0.0	-12.0000	0.0
0.0	0.0	0.0	0.0	0.0	-0.6970

TRANSPOSE OF B-MATRIX

0.0	0.0	0.0	0.0	12.0	0.0

LATERAL SYSTEM

A-MATRIX

-2.6459	0.0167	-43.3851	0.0	19.4000	7.2990	-43.3851
-0.0987	-0.2240	4.9200	0.0	1.1150	-3.1440	4.9200
0.0743	-0.9968	-0.1596	0.0368	0.0033	0.0279	-0.1596
1.0000	0.0744	0.0	0.0	0.0	0.0	0.0
0.0	0.0	0.0	0.0	-30.0000	0.0	0.0
0.0	0.0	0.0	0.0	0.0	-25.0000	0.0
0.0	0.0	0.0	0.0	0.0	0.0	-0.6970

TRANSPOSE OF B-MATRIX

0.0	0.0	0.0	0.0	30.0	0.0	0.0
0.0	0.0	0.0	0.0	0.0	25.0	0.0

FLIGHT CONDITION 18

DYNAMIC PRESSURE 397PSF (19077 N/SQ.M)   MACH 1.20   ALTITUDE 40000 FT(12191 M)

LONGITUDINAL SYSTEM

A-MATRIX

```
-0.2798    0.0001   -21.6900     0.0     -13.4900   -21.6900
 0.0      -0.0013   -23.0000   -32.2000    0.8560    -23.0000
 1.0000    0.0       -0.7761     0.0      -0.0867     -0.7761
 1.0000    0.0        0.0        0.0       0.0         0.0
 0.0       0.0        0.0        0.0     -12.0000      0.0
 0.0       0.0        0.0        0.0       0.0        -0.9294
```

TRANSPOSE OF B-MATRIX

```
 0.0   0.0   0.0   0.0   12.0   0.0
```

LATERAL SYSTEM

A-MATRIX

```
-2.6763    0.0141   -65.8833    0.0      14.1600     6.3540   -65.8833
-0.0868   -0.3714     8.6148    0.0       0.6752    -2.3340     8.6148
 0.0492   -0.9983    -0.2100    0.0276    0.0024     0.0153    -0.2100
 1.0000    0.0493     0.0       0.0       0.0        0.0         0.0
 0.0       0.0        0.0       0.0     -30.0000     0.0         0.0
 0.0       0.0        0.0       0.0       0.0      -25.0000      0.0
 0.0       0.0        0.0       0.0       0.0        0.0        -0.9294
```

TRANSPOSE OF B-MATRIX

```
 0.0   0.0   0.0   0.0   30.0   0.0   0.0
 0.0   0.0   0.0   0.0   25.0   0.0   0.0
```

FLIGHT CONDITION 19.

DYNAMIC PRESSURE   537PSF (25804 N/SQ.M)   MACH 1.40   ALTITUDE   40000 FT (12191 M)

LONGITUDINAL SYSTEM

A-MATRIX

-0.2970	0.0001	-25.2100	0.0	-14.3100	-25.2100
0.0	-0.0030	-29.7200	-32.2000	1.1230	-29.7200
1.0000	-0.0000	-0.7770	0.0	-0.0861	-0.7770
1.0000	0.0	0.0	0.0	0.0	0.0
0.0	0.0	0.0	0.0	-12.0000	0.0
0.0	0.0	0.0	0.0	0.0	-1.0840

TRANSPOSE OF B-MATRIX

0.0	0.0	0.0	12.0	0.0
0.0				

LATERAL SYSTEM

A-MATRIX

-2.8733	0.0139	-85.9576	0.0	13.2700	6.1350	-85.9576
-0.1138	-0.3995	7.4019	0.0	0.3848	-2.3750	7.4019
0.0477	-0.9984	-0.2224	0.0237	0.0024	0.0128	-0.2224
1.0000	0.0478	0.0	0.0	0.0	0.0	0.0
0.0	0.0	0.0	0.0	-30.0000	0.0	0.0
0.0	0.0	0.0	0.0	0.0	-25.0000	0.0
0.0	0.0	0.0	0.0	0.0	0.0	-1.0840

TRANSPOSE OF B-MATRIX

0.0	0.0	0.0	30.0	0.0	0.0
0.0	0.0	0.0	0.0	25.0	0.0

FLIGHT CONDITION 20

DYNAMIC PRESSURE 703PSF (33781 N/SQ.M)   MACH 1.60   ALTITUDE 40000 FT(12191 M)

LONGITUDINAL SYSTEM

A-MATRIX

-0.3028	0.0000	-27.8500	0.0	-15.7100	-27.8500
0.0	-0.0080	-38.6900	-32.2000	1.3800	-38.6900
1.0000	-0.0000	-0.7656	0.0	-0.0847	-0.7656
1.0000	0.0	0.0	0.0	0.0	0.0
0.0	0.0	0.0	0.0	-12.0000	0.0
0.0	0.0	0.0	0.0	0.0	-1.2390

TRANSPOSE OF B-MATRIX

0.0	0.0	0.0	0.0	12.0	0.0

LATERAL SYSTEM

A-MATRIX

-3.0301	-0.0152	-99.7334	0.0	12.4600	5.9800	-99.7334
-0.0977	-0.4147	6.5254	0.0	0.0987	-2.4240	6.5254
0.0360	-0.9990	-0.2407	0.0207	0.0022	0.0109	-0.2407
1.0000	0.0360	0.0	0.0	0.0	0.0	0.0
0.0	0.0	0.0	0.0	-30.0000	0.0	0.0
0.0	0.0	0.0	0.0	0.0	-25.0000	0.0
0.0	0.0	0.0	0.0	0.0	0.0	-1.2390

TRANSPOSE OF B-MATRIX

0.0	0.0	0.0	0.0	30.0	0.0	0.0
0.0	0.0	0.0	0.0	0.0	25.0	0.0

APPENDIX B

Reduced Short-Period Models for Longitudinal Dynamics

of the F-8C Aircraft

The reduced equations are of the form

$$\dot{\underline{x}} = A \, \underline{x} + B \, \underline{u} + \underline{L} \, \xi \tag{B.1}$$

where

$$\underline{x} = \begin{Bmatrix} q \\ \alpha \\ \delta_e \\ w \end{Bmatrix} \; ; \; \underline{u} = \delta_{ec} \tag{B.2}$$

Matrices $\underline{A}$ and $\underline{B}$ are flight-condition dependent, and are listed on the following pages. The $\underline{L}$-matrix depends also on the turbulence level; see Section 3.4 for relevant equations.

FLIGHT CONDITION 5

DYNAMIC PRESSURE 133PSF (6391 N/SQ.M)   MACH 0.30   ALTITUDE   0 FT(0 M)

LONGITUDINAL SYSTEM - REDUCED STATE

A-MATRIX
```
-0.4726   -2.0290   -5.0455    0.0
 1.0000   -0.8029   -0.1153    0.0
 0.0        0.0    -12.0000    0.0
 0.0        0.0      0.0      -3.3490
```

TRANSPOSE OF B-MATRIX
```
0.0   0.0   12.0   0.0
```

FLIGHT CONDITION 6

DYNAMIC PRESSURE 416PSF (19990 N/SQ.M)   MACH 0.53   ALTITUDE   0 FT(0 M)

LONGITUDINAL SYSTEM - REDUCED STATE

A-MATRIX
```
-0.7775   -7.0970   -14.2500    0.0
 1.0000   -1.4520    -0.1902    0.0
 0.0        0.0     -12.0000    0.0
 0.0        0.0       0.0      -5.9170
```

TRANSPOSE OF B-MATRIX
```
0.0   0.0   12.0   0.0
```

FLIGHT CONDITION 7

DYNAMIC PRESSURE 726PSF (34886 N/SQ.M)   MACH 0.70   ALTITUDE   0 FT(0 M)

LONGITUDINAL SYSTEM - REDUCED STATE

A-MATRIX
```
-0.9818   -12.8300   -23.4400    0.0
 1.0000    -2.0080     -0.2330    0.0
 0.0         0.0       -12.0000    0.0
 0.0         0.0         0.0      -7.8150
```

TRANSPOSE OF B-MATRIX
```
0.0   0.0   12.0   0.0
```

FLIGHT CONDITION 8

DYNAMIC PRESSURE 1098PSF (52762 N/SQ.M)   MACH 0.86   ALTITUDE   0 FT(0 M)

LONGITUDINAL SYSTEM - REDUCED STATE

A-MATRIX
```
-1.1800   -20.9500   -33.0600    0.0
 1.0000    -2.6730     -0.2592    0.0
 0.0         0.0       -12.0000    0.0
 0.0         0.0         0.0      -9.6010
```

TRANSPOSE OF B-MATRIX
```
0.0   0.0   12.0   0.0
```

PLIGHT CONDITION 10

DYNAMIC PRESSURE 109PSF (5237 N/SQ.M)   MACH 0.40   ALTITUDE 20000 FT(6095 M)

LONGITUDINAL SYSTEM - REDUCED STATE

A-MATRIX
```
-0.3189   -1.8790    -4.0600     0.0
 1.0000   -0.5378    -0.0771     0.0
 0.0       0.0       -12.0000    0.0
 0.0       0.0        0.0       -0.3318
```

TRANSPOSE OF B-MATRIX
```
0.0   0.0   12.0   0.0
```


PLIGHT CONDITION 11

DYNAMIC PRESSURE 254PSF (12205 N/SQ.M)   MACH 0.60   ALTITUDE 20000 FT(6095 M)

LONGITUDINAL SYSTEM - REDUCED STATE

A-MATRIX
```
-0.4877   -4.7890    -8.7430     0.0
 1.0000   -0.8361    -0.1115     0.0
 0.0       0.0       -12.0000    0.0
 0.0       0.0        0.0       -0.4977
```

TRANSPOSE OF B-MATRIX
```
0.0   0.0   12.0   0.0
```

FLIGHT CONDITION 12

DYNAMIC PRESSURE 434PSF (20854 N/SQ.M)   MACH 0.80   ALTITUDE 20000 FT(6095 M)

LONGITUDINAL SYSTEM - REDUCED STATE

```
A-MATRIX
-0.6696   -9.0100   -15.7700    0.0
 1.0000   -1.2140    -0.1394    0.0
 0.0        0.0     -12.0000    0.0
 0.0        0.0       0.0      -0.6636
```

```
TRANSPOSE OF B-MATRIX
0.0   0.0   12.0   0.0
```

FLIGHT CONDITION 13

DYNAMIC PRESSURE 550PSF (26429 N/SQ.M)   MACH 0.90   ALTITUDE 20000 FT(6095 M)

LONGITUDINAL SYSTEM - REDUCED STATE

```
A-MATRIX
-0.7900   -12.7300   -19.2700    0.0
 1.0000    -1.4560    -0.1519    0.0
 0.0         0.0     -12.0000    0.0
 0.0         0.0       0.0      -0.7466
```

```
TRANSPOSE OF B-MATRIX
0.0   0.0   12.0   0.0
```

FLIGHT CONDITION 14

DYNAMIC PRESSURE   978PSF (46995 N/SQ.M)   MACH 1.20   ALTITUDE 20000 FT (6095 M)

LONGITUDINAL SYSTEM - REDUCED STATE

A-MATRIX
-0.4149   -43.0400   -25.2500   0.0
 1.0000   -1.5880   -0.1647   0.0
 0.0   0.0   -12.0000   0.0
 0.0   0.0   0.0   -0.9955

TRANSPOSE OF B-MATRIX
0.0   0.0   12.0   0.0

FLIGHT CONDITION 15

DYNAMIC PRESSURE   135PSF (6487 N/SQ.M)   MACH 0.70   ALTITUDE 40000 FT(12191 M)

LONGITUDINAL SYSTEM - REDUCED STATE

A-MATRIX
-0.2719   -2.8930   -5.4080   0.0
 1.0000   -0.4433   -0.0584   0.0
 0.0   0.0   -12.0000   0.0
 0.0   0.0   0.0   -0.5421

TRANSPOSE OF B-MATRIX
0.0   0.0   12.0   0.0

FLIGHT CONDITION 16

DYNAMIC PRESSURE   176PSF (8457 N/SQ.M)   MACH 0.80   ALTITUDE   40000 FT (12191 M)

LONGITUDINAL SYSTEM - REDUCED STATE

A-MATRIX
-0.3297   -4.0010   -7.3630   0.0
 1.0000   -0.5358   -0.0657   0.0
 0.0   0.0   -12.0000   0.0
 0.0   0.0   0.0   -0.6196

TRANSPOSE OF B-MATRIX
0.0   0.0   12.0   0.0

FLIGHT CONDITION 17

DYNAMIC PRESSURE   223PSF (10715 N/SQ.M)   MACH 0.90   ALTITUDE   40000 FT (12191 M)

LONGITUDINAL SYSTEM - REDUCED STATE

A-MATRIX
-0.4018   -5.8580   -9.2880   0.0
 1.0000   -0.6532   -0.0729   0.0
 0.0   0.0   -12.0000   0.0
 0.0   0.0   0.0   -0.6970

TRANSPOSE OF B-MATRIX
0.0   0.0   12.0   0.0

FLIGHT CONDITION 18

DYNAMIC PRESSURE 397PSF (19077 N/SQ.M)   MACH 1.20   ALTITUDE 40000 FT(12191 M)

LONGITUDINAL SYSTEM - REDUCED STATE

A-MATRIX
```
-0.2798   -21.6900   -13.4900    0.0
 1.0000    -0.7761    -0.0867    0.0
 0.0         0.0      -12.0000    0.0
 0.0         0.0        0.0      -0.9294
```

TRANSPOSE OF B-MATRIX
```
0.0   0.0   12.0   0.0
```

FLIGHT CONDITION 19

DYNAMIC PRESSURE 537PSF (25804 N/SQ.M)   MACH 1.40   ALTITUDE 40000 FT(12191 M)

LONGITUDINAL SYSTEM - REDUCED STATE

A-MATRIX
```
-0.2970   -25.2100   -14.3100    0.0
 1.0000    -0.7770    -0.0861    0.0
 0.0         0.0      -12.0000    0.0
 0.0         0.0        0.0      -1.0840
```

TRANSPOSE OF B-MATRIX
```
0.0   0.0   12.0   0.0
```

FLIGHT CONDITION 20

DYNAMIC PRESSURE 703PSF (33781 N/SQ.M)   MACH 1.60   ALTITUDE 40000 FT (12191 M)

LONGITUDINAL SYSTEM - REDUCED STATE

A-MATRIX

-0.3028	-27.8500	-15.7100	0.0
1.0000	-0.7656	-0.0847	0.0
0.0	0.0	-12.0000	0.0
0.0	0.0	0.0	-1.2390

TRANSPOSE OF B-MATRIX

0.0	0.0	12.0	0.0

APPENDIX C

The MMAC Identification Algorithm

C.1 Problem Statement

Consider a linear, time invariant system with a parameter vector $\underline{\gamma}$ belonging to a finite set $\{\underline{\gamma}_1, \underline{\gamma}_2, \ldots, \underline{\gamma}_N\}$. Characterize the possible systems by the parameter subscript, by the vector difference equations

$$\underline{x}(t+1) = \underline{A}_i\underline{x}(t) + \underline{B}_i\underline{u}(t) + \underline{L}_i\underline{\xi}(t) \qquad (C.1)$$

The measurement equations, as discussed in Chapter 4, are given by

$$\underline{z}(t) = \underline{C}_i\underline{x}(t) + \underline{\theta}(t) \qquad (C.2)$$

The state, control, and observation variables $\underline{x}(t)$, $\underline{u}(t)$ and $\underline{z}(t)$ are all elements of finite-dimensional Euclidean spaces. The vectors $\underline{\xi}(t)$, $\underline{\theta}(t)$, are mutually independent, white-noise gaussian random processes taking values in a finite dimensional space, with zero mean, and known covariances, expressed as

$$\underline{\theta}(t) = N(\underline{0}; \underline{\Theta}(t)) \qquad (C.3)$$

$$\underline{\xi}(t) = N(\underline{0}; \underline{\Xi}(t)) \qquad (C.4)$$

The elements $\underline{A}_i$, $\underline{B}_i$, $\underline{L}_i$ and $\underline{C}_i$ are appropriately dimensioned linear matrices. Let $Z(t)$ represent the sequence:

$$Z(t) \triangleq \{\underline{u}(0), \underline{u}(1), \ldots, \underline{u}(t-1); \underline{z}(1), \underline{z}(2), \ldots, \underline{z}(t)\} \qquad (C.5)$$

The first question posed is, given a sequence $Z(t)$, what is the conditional probability density of $\underline{x}(t)$, $(p(\underline{x}(t)|Z(t))$?

Denote by H_i the event that the unknown parameters $\underline{\gamma}$ are equal

to $\underline{Y}_i$. Let H denote a random hypothesis variable, taking discrete values as H_i, i = 1, ..., N. Assume there is a probability distribution at time t, such that

$$P(H = H_i \text{ at } t | Z(t)) = P_i(t). \tag{C.6}$$

The probability density of H can be written as

$$p(H | Z(t)) = \sum_{i=1}^{N} \delta(H - H_i) P_i(t)$$

Consider now $p(\underline{x}(t+1) | Z(t+1))$. From the definition of marginal densities, one obtains

$$p(\underline{x}(t+1) | Z(t+1)) = \int_H p(\underline{x}(t+1), H | Z(t+1)) dH \tag{C.8}$$

From Bayes' Rule, it follows that

$$p(\underline{x}(t+1), H | Z(t+1)) = p(\underline{x}(t+1) | H, Z(t+1)) p(H | Z(t)) \tag{C.9}$$

Substituting equations (C.7) and (C.9) into (C.8) and integrating yields

$$p(\underline{x}(t+1) | Z(t+1)) = \sum_{i=1}^{N} P_i(t+1) p(\underline{x}(t+1) | H_i, Z(t+1)). \tag{C.10}$$

Consider $p(\underline{x}(t) | H_i, Z(t))$. Under the hypothesis that $H = H_i$, the system and observations described by equations (C.1) and (C.2) represent a linear, time-invariant system driven by Gaussian white noise with Gaussian-corrupted linear observations. Hence, the conditional distributions are also Gaussian, and can be obtained using a Kalman filter [5]. Hence, for each i, $p(\underline{x}(t) | H_i, Z(t))$ can be constructed with a Kalman filter. Additionally, using Bayes' rule, the following relationships follow:

$$p(\underline{x}(t)|H_i, Z(t)) = \frac{p(\underline{z}(t)|H_i, \underline{x}(t))p(\underline{x}(t)|H_i, Z(t-1))}{p(\underline{z}(t)|H_i, Z(t-1))} \qquad (C.11)$$

$$p(\underline{x}(t)|H_i, Z(t-1)) = \int p(\underline{x}(t)|H_i, x(t-1))p(\underline{x}(t-1)|H_i, Z(t-1))d\underline{x}(t-1)$$

$$(C.12)$$

Since the conditional densities $p(\underline{x}(t) \; H_i, \; Z(t))$ are Gaussian, they can be characterized by their means and covariances. Denote these as

$$\hat{\underline{x}}_i(t) \overset{\Delta}{=} E\{\underline{x}(t)|H_i, Z(t)\} \qquad (C.13)$$

$$\underline{\Sigma}_i(t|t) = E\{(\underline{x}(t)-\hat{\underline{x}}_i(t))(\underline{x}(t)-\hat{\underline{x}}_i(t))'|H_i, Z(t)\} \qquad (C.14)$$

It is well known from the theory of Kalman filtering [32] that the $\underline{\Sigma}_i(t)$ are precomputable, according to the relations

$$\underline{\Sigma}_i(t+1|t) = \underline{A}_i\underline{\Sigma}_i(t|t)\underline{A}_i' + \underline{\Xi}(t) \qquad (C.15)$$

$$\underline{\Sigma}_i(t+1|t+1) = \underline{\Sigma}_i(t+1|t) - \underline{\Sigma}_i(t+1|t)\underline{C}_i'[\underline{C}_i\underline{\Sigma}_i(t+1|t)\underline{C}_i' + \underline{\Theta}(t)]^{-1}.$$

$$\cdot \; \underline{C}_i\underline{\Sigma}_i(t+1|t) \qquad (C.16)$$

With this notation, using equation (C.10), the conditional mean of $\underline{x}(t)$ given $Z(t)$ is

$$\hat{\underline{x}}(t) = E\{\underline{x}(t)|Z(t)\} = \int \underline{x}(t)p(\underline{x}(t)|Z(t))d\underline{x}(t) = \sum_{i=1}^{N} P_i(t)\hat{\underline{x}}_i(t)$$

$$(C.17)$$

Hence, using the output of N Kalman filters, each working with a different set of dynamics, H_i, the conditional mean can be determined. The Kalman filter equations are:

$$\hat{\underline{x}}_i(t+1|t) = \underline{A}_i\hat{\underline{x}}_i(t) + \underline{B}_i\underline{u}(t) \qquad (C.18)$$

$$\hat{\underline{x}}_i(t+1) = \hat{\underline{x}}_i(t+1|t) + \underline{\Sigma}_i(t|t)\underline{C}'_i\underline{\Theta}^{-1}(t+1)(\underline{z}(t+1)-\underline{C}_i\hat{\underline{x}}_i(t+1|t))$$

$$(C.19)$$

The remaining question consists of determining the probabilities $P_i(t)$. Consider the conditional density $p(H|Z(t))$ defined by equation (C.7). Use of Bayes' rule yields

$$p(H|Z(t+1) = p(H|\underline{z}(t+1), u(t), Z(t)) = \frac{p(H,\underline{z}(t+1)|\underline{u}(t), Z(t))}{p(\underline{z}(t+1))|\underline{u}(t), Z(t))}$$

$$= \frac{p(\underline{z}(t+1)|H, Z(t), \underline{u}(t))p(H|Z(t), \underline{u}(t))}{p(\underline{z}(t+1)|Z(t), u(t))} \qquad (C.20)$$

Since $\underline{u}(t)$ is a constant in this derivation, then

$$p(H|Z(t), \underline{u}(t)) = p(H|Z(t)). \qquad (C.21)$$

Using equations (C.7) and (C.20), one obtains

$$P_i(t+1) = \frac{p(\underline{z}(t+1)|H_i, \underline{u}(t), Z(t))}{p(\underline{z}(t+1)|\underline{u}(t), z(t))} P_i(t) \qquad (C.22)$$

The density $p(\underline{z}(t+1)|H_i, \underline{u}(t), Z(t))$ is Gaussian and can be calculated from the ith Kalman filter, as

$$p(\underline{z}(t+1)|H_i, \underline{u}(t), Z(t)) \sim N(\underline{C}_i\hat{\underline{x}}_i(t+1|t), \underline{S}_i(t+1)) \qquad (C.23)$$

where

$$\underline{S}_i(t+1) = \underline{C}_i\underline{\Sigma}_i(t+1|t)\underline{C}'_i + \underline{\Theta}(t+1) \qquad (C.24)$$

The quantity $\underline{C}_i\hat{\underline{x}}_i(t+1|t)$ is the predicted measurement at t+1 and $\underline{S}_i$ is the residual covariance associated with the ith Kalman filter.

The density $p(\underline{z}(t+1)|Z(t), u(t))$ can be computed using marginal

densities as:

$$p(\underline{z}(t+1) | Z(t), \underline{u}(t)) = \int p(\underline{z}(t+1), H | Z(t), \underline{u}(t)) dH$$

$$= \int p(\underline{z}(t+1) | H, Z(t)) p(H | Z(t)) dH \quad \text{from Bayes' rule}$$

$$= \sum_{j=1}^{N} P_j(t) p(\underline{z}(t+1) | H_j, \underline{u}(t), Z(t)) \qquad (C.25)$$

using equation (C.7) and integrating.

Thus, combining equations (C.23), (C.24), and (C.25) with (C.22), one obtains

$$P_i(t+1) = \frac{p(\underline{z}(t+1) | H_i, \underline{u}(t), Z(t))}{\sum_{j=1}^{N} P_j(t) p(\underline{z}(t+1) | H_j, \underline{u}(t), Z(t))} P_i(t) \qquad (C.26)$$

Let m be the dimension of the space of $\underline{z}(t)$ (i.e., the number of measurements).

Let the residual vectors $\underline{r}_i(t)$ be defined as

$$\underline{r}_i(t) \triangleq \underline{z}(t+1) - \underline{C}_i \hat{\underline{x}}_i(t+1 | t); \qquad i = 1, 2, \ldots, N \qquad (C.27)$$

Then

$$p(\underline{z}(t+1) | H_i, \underline{u}(t), Z(t)) = (2\pi)^{-\frac{m}{2}} (\det \underline{S}_i(t+1))^{-\frac{1}{2}} \cdot$$

$$\cdot e^{-\frac{1}{2} \underline{r}_i'(t+1) \underline{S}_i^{-1}(t+1) \underline{r}_i(t+1)} \qquad (C.28)$$

Define β_i as

$$\beta_i(t+1) = (2\pi)^{-\frac{m}{2}} \det(\underline{S}_i(t+1))^{-\frac{1}{2}} \qquad (C.29)$$

It was mentioned previously that $\beta_i^*(t)$ is precomputable for all

$i = 1,...N$, and all t. With this notation, equation (C.26) becomes

$$P_i(t+1) = \frac{\beta_i(t+1) e^{-\frac{1}{2} \underline{r}_i'(t+1)\underline{S}_i^{-1}(t+1)\underline{r}_i(t+1)}}{\sum_{j=1}^{N} \beta_j(t+1)P_j(t)e^{-\frac{1}{2} \underline{r}_j'(t+1)\underline{S}_j^{-1}(t+1)\underline{r}_j(t+1)}} P_i(t) \qquad (C.30)$$

In the special case of statistically stationary noises, that is, $\underline{\Xi}(t) = \underline{\Xi}$, $\underline{\Theta}(t) = \underline{\Theta}$ constant for all t, time invariant Kalman filters can be designed which are the steady state limits of the Kalman filters discussed previously. These limits exist under appropriate observability assumptions. Define

$$\underline{\Sigma}_i = \lim_{t\to\infty} \underline{\Sigma}_i(t|t) = (\underline{M}_i^{-1} + \underline{C}_i' \underline{\Theta}^{-1}\underline{C}_i)^{-1} \qquad (C.31)$$

$$\underline{M}_i = \lim_{t\to\infty} \underline{\Sigma}_i(t+1|t) = \underline{A}_i\underline{\Sigma}_i\underline{A}_i' + \underline{\Xi} \qquad (C.32)$$

Then, $\underline{S}_i$ can be defined accordingly as in equation (C.24), by

$$\underline{S}_i = \underline{C}_i\underline{M}_i\underline{C}_i' + \underline{\Theta} \qquad (C.33)$$

$$\beta_i = (2\pi)^{-\frac{m}{2}} (\det \underline{S}_i)^{-\frac{1}{2}}. \qquad (C.34)$$

For this special case, the evolution of the probabilities is given by

$$P_i(t+1) = \frac{\beta_i \, e^{-\frac{1}{2}(\underline{r}_i'(t+1)\underline{S}_i^{-1}\underline{r}_i(t+1))}}{\sum_{j=1}^{N} \beta_j \, e^{-\frac{1}{2}(\underline{r}_j'(t+1)\underline{S}_j^{-1}\underline{r}_j(t+1))} P_j(t)} P_i(t) \qquad (C.35)$$

APPENDIX D

Linearized Acceleration Equations

The equations for normal and lateral acceleration in terms of the
state variables used in the models of Chapter 3, are given in Etkin [36];
the acceleration at the center of gravity of the airplane are given by

$$N_z = - \frac{V}{g} (q - \dot{\alpha} - p\beta) - \cos\theta\cos\phi \tag{D.1}$$

$$N_y = \frac{V}{g} (\dot{\beta} + r - p\alpha) - \cos\theta\sin\phi \tag{D.2}$$

For the purposes of designing the Kalman filters the pseudomeasurements
$\tilde{a}_{nz}$ and $\tilde{a}_y$ were defined, where

$$\tilde{a}_{nz} = N_z + \cos\theta\cos\phi \tag{D.3}$$

$$\tilde{a}_y = N_y + \cos\theta\sin\phi - \phi \tag{D.4}$$

For the purposes of developing a linear equation for a_{nz} and a_y,
the longitudinal and lateral systems are assumed to be independent;
thus lateral variables in (D.3) and longitudinal variables in (D.4) are
set to their trim values. Hence,

$$a_{nz} = - \frac{V_0}{g} (q - \dot{\alpha}) \tag{D.5}$$

$$a_y = \frac{V_0}{g} (\dot{\beta} + r - p\alpha_0) - \phi \tag{D.6}$$

where $\dot{\alpha}$ and $\dot{\beta}$ are the linearized expressions given in Appendix A, and α_0
is the value of the trim angle of attack. The coefficients of equations
(D.5) and (D.6) are tabulated in this appendix for each flight condition.

Linearized Normal Acceleration Equations

Flight Condition	q	v	α	θ	δ_e	δ_{ec}	w
5	0.0	0.006	8.352	0.0	1.199	0.0	0.0
6	0.0	0.004	26.680	0.0	3.496	0.0	0.0
7	0.0	0.003	48.730	0.0	5.656	0.0	0.0
8	0.0	0.002	79.710	0.0	7.730	0.0	0.0
10	0.0	0.005	5.928	0.0	0.993	0.0	0.0
11	0.0	0.004	16.150	0.0	2.154	0.0	0.0
12	0.0	0.003	31.280	0.0	3.592	0.0	0.0
13	0.0	0.002	42.200	0.0	4.401	0.0	0.0
14	0.0	-0.001	61.370	0.0	6.363	0.0	0.0
15	0.0	0.004	9.329	0.0	1.229	0.0	0.0
16	0.0	0.003	12.890	0.0	1.580	0.0	0.0
17	0.0	0.002	17.680	0.0	1.973	0.0	0.0
18	0.0	0.0	28.000	0.0	3.129	0.0	0.0
19	0.0	0.000	32.710	0.0	3.625	0.0	0.0
20	0.0	0.000	36.830	0.0	4.076	0.0	0.0

Linearized Lateral Acceleration Equations

Flight Condition	p	r	β	φ	w	δ_a	δ_r
5	0.000	0.118	-2.240	-0.010	0.0	0.020	0.493
6	0.001	0.054	-7.300	-0.002	0.0	0.126	1.300
7	-0.001	0.053	-13.400	-0.001	0.0	0.277	1.840
8	-0.003	0.062	-21.000	-0.001	0.0	0.472	1.980
10	-0.006	0.180	-1.990	-0.013	0.0	0.015	0.413
11	0.001	0.074	-4.460	-0.003	0.0	0.071	0.882
12	-0.000	0.050	-8.290	-0.001	0.0	0.174	1.320
13	-0.000	0.049	-10.600	-0.001	0.0	0.234	1.380
14	-0.002	0.057	-18.700	-0.001	0.0	0.230	0.686
15	-0.004	0.167	-2.600	-0.008	0.0	0.036	0.528
16	-0.002	0.116	-3.420	-0.005	0.0	0.089	0.755
17	-0.001	0.086	-4.320	-0.003	0.0	0.086	0.552
18	-0.000	0.063	-7.580	-0.002	0.0	0.061	0.669
19	-0.000	0.066	-9.370	-0.002	0.0	0.101	0.537
20	-0.001	0.050	-11.600	-0.001	0.0	0.105	0.527

APPENDIX E

Linearized Discrete-Time Models for the F-8C Aircraft

The basic equations for converting the continuous-time models of Appendix A to discrete-time sampled-data models are described in Appendix F. For the longitudinal system, the complete deterministic continuous-time model is of the form

$$
\underline{\dot{x}} = \frac{d}{dt}
\begin{pmatrix}
q \\
v \\
\alpha \\
\theta \\
\delta_e \\
\delta_{ec} \\
w
\end{pmatrix}
= \underline{A}_i
\begin{pmatrix}
q \\
v \\
\alpha \\
\theta \\
\delta_e \\
\delta_{ec} \\
w
\end{pmatrix}
+ \underline{B}_i \, \dot{\delta}_{ec}
\tag{E.1}
$$

where the matrices $\underline{A}_i$, $\underline{B}_i$ were described in Chapter 3 and Appendix A. To convert to a sampled-data system, $\dot{\delta}_{ec}$ was assumed to be piecewise constant at 1/8 of a second. The resulting sampled-data system is described as

$$
\underline{x}(t+1) =
\begin{pmatrix}
q \\
v \\
\alpha \\
\theta \\
\delta_e \\
\delta_{ec} \\
w
\end{pmatrix}
(t+1) = \underline{A}_d^i
\begin{pmatrix}
q \\
v \\
\alpha \\
\theta \\
\delta_e \\
\delta_{ec} \\
w
\end{pmatrix}
(t) + \underline{B}_d^i \, \dot{\delta}_{ec}(t)
\tag{E.2}
$$

The deterministic continuous-time linearized equations for the lateral system are of the form:

$$\dot{\underline{x}} = \frac{d}{dt}\begin{pmatrix} p \\ r \\ B \\ \phi \\ \delta_a \\ \delta_r \\ \delta_{ac} \\ \delta_{rc} \\ w \end{pmatrix} = \underline{A}_i\underline{x} + \underline{B}_i\begin{pmatrix} \dot{\delta}_{ac} \\ \dot{\delta}_{rc} \end{pmatrix} \tag{E.3}$$

where $\underline{A}_i$, $\underline{B}_i$ are described in Chapter 3 and Appendix A. The continuous time lateral system can be divided into two subsystems as explained in Chapter 7, of the form:

$$\dot{\underline{x}}^1 = \frac{d}{dt}\begin{pmatrix} p \\ r \\ B \\ \phi \\ w \end{pmatrix} = \underline{A}_i^1\underline{x}_1 + \underline{B}_i^1\begin{pmatrix} \delta_a \\ \delta_r \end{pmatrix} \tag{E.4}$$

$$\dot{\underline{x}}^2 = \frac{d}{dt}\begin{pmatrix} \delta_a \\ \delta_r \\ \delta_{ac} \\ \delta_{rc} \end{pmatrix} = \underline{A}_i^2\underline{x}_2 + \begin{pmatrix} 0 & 0 \\ 0 & 0 \\ 1 & 0 \\ 0 & 1 \end{pmatrix}\begin{pmatrix} \dot{\delta}_{ac} \\ \dot{\delta}_{rc} \end{pmatrix} \tag{E.5}$$

Discretizing each of these systems at 1/8 of a second with the procedure described in Chapter 5 yields an overall system of the form:

$$
\underline{x}^3(t+1) =
\begin{bmatrix} p \\ r \\ B \\ \phi_w \\ \delta_a \\ \delta_r \\ \delta_{ac} \\ \delta_{rc} \end{bmatrix}
(t+1) =
\left[
\begin{array}{c:c:c}
\underline{A}_d^{i1} & \underline{B}_d^{i1} & \\
(5{\times}5) & 2{\times}5 & 0 \\
\hdashline
& & \underline{A}_d^{i2} \\
0 & & 4{\times}4
\end{array}
\right]
\underline{x}^3(t) +
\left[
\begin{array}{c}
\underline{0} \\
5{\times}2 \\
\hline
\underline{B}_d^{i2}
\end{array}
\right]
\begin{bmatrix} \dot{\delta}_{ac} \\ \dot{\delta}_{rc} \end{bmatrix}
(t)
$$

$$(E.6)$$

A simple permutation of the states results in the system

$$
x(t+1) =
\begin{bmatrix} p \\ r \\ B \\ \phi \\ \delta_a \\ \delta_r \\ \delta_{ac} \\ \delta_{rc} \\ w \end{bmatrix}
= \underline{A}_d^i \; \underline{x}(t) + \underline{B}_d^i
\begin{bmatrix} \dot{\delta}_{ac} \\ \dot{\delta}_{rc} \end{bmatrix}
(t)
\qquad (E.7)
$$

The matrices in equations (E.2) and (E.7) are displayed in this appendix.

FLIGHT CONDITION 6

DYNAMIC PRESSURE 416PSF (19990 N/SQ.M)   MACH 0.53   ALTITUDE   0 FT(0 M)

LONGITUDINAL SYSTEM

AD-MATRIX
```
 0.8589  -0.0000  -0.7578   0.0001  -0.8416  -0.8164  -0.5241
-0.3026   0.9974  -0.9066  -4.0200   0.0733  -0.0029  -0.6215
 0.1068  -0.0000   0.7869   0.0001  -0.0746  -0.0473  -0.1530
 0.1170  -0.0000  -0.0501   1.0000  -0.0680  -0.0384  -0.0395
 0.0      0.0      0.0      0.0      0.2231   0.7769   0.0
 0.0      0.0      0.0      0.0      0.0      1.0000   0.0
 0.0      0.0      0.0      0.0      0.0      0.0      0.4773
```

TRANSPOSE OF BD-MATRIX
```
-0.0384  -0.0012  -0.0017  -0.0013   0.0603   0.1250   0.0
```

LATERAL SYSTEM

AD-MATRIX
```
 0.4720   0.3690  -5.2500  -0.0204   2.9000   0.8710   0.0      0.0     -3.5100
-0.0146   0.8960   0.6220   0.0021   0.1670  -0.6260   0.0      0.0      0.4400
 0.0059  -0.1150   0.8940   0.0065   0.0007   0.0510   0.0      0.0     -0.0799
 0.0885   0.0229  -0.3730   0.9999   0.2030   0.0630   0.0      0.0     -0.2910
 0.0      0.0      0.0      0.0      0.0235   0.0      0.9760   0.9560   0.0
 0.0      0.0      0.0      0.0      0.0      0.0439   0.0      0.0      0.0
 0.0      0.0      0.0      0.0      0.0      0.0      1.0000   1.0000   0.0
 0.0      0.0      0.0      0.0      0.0      0.0      0.0      0.0      0.0
 0.0      0.0      0.0      0.0      0.0      0.0      0.0      0.0      0.4773
```

TRANSPOSE OF BD-MATRIX
```
 0.0  0.0  0.0  0.0  0.0925  0.0  0.1250  0.0     0.0
 0.0  0.0  0.0  0.0  0.0868  0.0  0.0     0.1250  0.0
```

FLIGHT CONDITION 5

DYNAMIC PRESSURE 133PSF (6391 N/SQ.M)   MACH 0.30   ALTITUDE   0 FT(0 M)

LONGITUDINAL SYSTEM

AD-MATRIX
```
 0.9279  -0.0000  -0.2329   0.0001  -0.3115  -0.2959  -0.1891
-0.3894   0.9965  -2.2780  -4.0180  -0.0962  -0.1248  -1.8520
 0.1148  -0.0001   0.8901   0.0001  -0.0308  -0.0201  -0.0903
 0.1208  -0.0000  -0.0150   1.0000  -0.0247  -0.0138  -0.0131
 0.0      0.0      0.0      0.0       0.2231   0.7769   0.0
 0.0      0.0      0.0      0.0       0.0      1.0000   0.0
 0.0      0.0      0.0      0.0       0.0      0.0      0.6580
```

TRANSPOSE OF BD-MATRIX
```
-0.0138  -0.0063  -0.0008  -0.0005   0.0603   0.1250   0.0
```

LATERAL SYSTEM

AD-MATRIX
```
 0.6090   0.1990  -2.5100  -0.0163   1.1500   0.3960   0.0      0.0     -2.0100
-0.0143   0.9540   0.1540   0.0009   0.0509  -0.2260   0.0      0.0      0.1270
 0.0153  -0.1180   0.9400   0.0116   0.0079   0.0236   0.0      0.0     -0.0508
 0.0991   0.0266  -0.1700   0.9990   0.0781   0.0256   0.9760   0.0     -0.1470
 0.0      0.0      0.0      0.0      0.0235   0.0      0.0      0.9560   0.0
 0.0      0.0      0.0      0.0      0.0      0.0439   1.0000   0.0      0.0
 0.0      0.0      0.0      0.0      0.0      0.0      0.0      1.0000   0.0
 0.0      0.0      0.0      0.0      0.0      0.0      0.0      0.0      0.0
 0.0      0.0      0.0      0.0      0.0      0.0      0.0      0.0      0.6580
```

TRANSPOSE OF BD-MATRIX
```
 0.0   0.0   0.0   0.0   0.0   0.0925   0.0868   0.1250   0.0
 0.0   0.0   0.0   0.0   0.0   0.0      0.0      0.0      0.1250
```

FLIGHT CONDITION 7

DYNAMIC PRESSURE   726PSF (34886 N/SQ.M)   MACH 0.70   ALTITUDE   0 FT(0 M)

LONGITUDINAL SYSTEM

AC-MATRIX

0.8009	-1.2870	0.0000	-1.3340	-1.3180	-0.7886
-0.3058	-0.9524	-4.0190	0.2919	0.1543	-0.5694
0.1003	0.6980	0.0000	-0.1130	-0.0712	-0.1970
0.1140	-0.0872	1.0000	-0.1098	-0.0624	-0.0638
0.0	0.0	0.0	0.2231	0.7769	0.0
0.0	0.0	0.0	0.0	1.0000	0.0
0.0	0.0	0.0	0.0	0.0	0.3765

TRANSPOSE OF BD-MATRIX

-0.0624	0.0053	-0.0026	-0.0021	0.0603	0.1250
0.0					

LATERAL SYSTEM

AD-MATRIX

0.3710	-7.0300	-0.0218	3.9100	1.0000	0.0	0.0	-4.0500
-0.0141	1.5100	0.0040	0.2380	-0.8920	0.0	0.0	-0.9540
0.0039	0.8200	0.0048	-0.0048	0.0679	0.0	0.0	-0.1250
0.0800	-0.5270	0.9990	0.2830	0.0788	0.9760	0.0	-0.3790
0.0	0.0	0.0	0.0235	0.0	0.0	0.9560	0.0
0.0	0.0	0.0	0.0	0.0439	1.0000	0.0	0.0
0.0	0.0	0.0	0.0	0.0	0.0	1.0000	0.0
0.0	0.0	0.0	0.0	0.0	0.0	0.0	0.3765

TRANSPOSE OF BD-MATRIX

0.0	0.0	0.0	0.0925	0.0	0.0	0.1250	0.0
0.0	0.0	0.0	0.0	0.0868	0.0	0.0	0.1250

FLIGHT CONDITION 8

DYNAMIC PRESSURE 1098PSF (52762 N/SQ.M)   MACH 0.86   ALTITUDE   0 FT(0 M)

LONGITUDINAL SYSTEM

AD-MATRIX

```
 0.7336   -0.0000   -1.9510    0.0001   -1.7990   -1.8180   -1.0590
-0.3228    0.9969   -1.1950   -4.0190    0.4425    0.2371   -0.6222
 0.0931   -0.0000    0.5946    0.0000   -0.1475   -0.0933   -0.2420
 0.1105   -0.0000   -0.1361    1.0000   -0.1515   -0.0868   -0.0929
 0.0       0.0       0.0       0.0       0.2231    0.7769    0.0
 0.0       0.0       0.0       0.0       0.0       1.0000    0.0
 0.0       0.0       0.0       0.0       0.0       0.0       0.3012
```

TRANSPOSE OF BD-MATRIX

```
-0.0868    0.0082   -0.0034   -0.0029    0.0603    0.1250    0.0
```

LATERAL SYSTEM

AD-MATRIX

```
 0.6370    0.2750   -8.3800    3.8800   -0.0227    0.9070    0.0       0.0      -4.0500
 0.7110   -0.0138    2.8400    0.2330    0.0063   -0.9520    0.0       0.0       1.6000
-0.1040    0.0032    0.7160   -0.0061   -0.0037    0.0709    0.0       0.0      -0.1860
 0.0328    0.0712   -0.6730   -0.2900    0.9990    0.0788    0.0       0.0      -0.4480
 0.0       0.0       0.0       0.0       0.0       0.0       0.9760    0.9560    0.0
 0.0       0.0       0.0       0.0       0.0       0.0439    0.0       0.0       0.0
 0.0       0.0       0.0       0.0       0.0       0.0       1.0000    0.0       0.0
 0.0       0.0       0.0       0.0       0.0       0.0       0.0       1.0000    0.0
 0.0       0.0       0.0       0.0       0.0       0.0       0.0       0.0       0.3012
```

TRANSPOSE OF BD-MATRIX

```
 0.0   0.0   0.0   0.0   0.0   0.0925   0.1250   0.0      0.0
 0.0   0.0   0.0   0.0   0.0   0.0868   0.0      0.1250   0.0
```

FLIGHT CONDITION 10

DYNAMIC PRESSURE 109PSF (5237 N/SQ.M)   MACH 0.40   ALTITUDE 20000 FT (6095 M)

LONGITUDINAL SYSTEM

AD-MATRIX

```
 0.9470   -0.2216   -0.0000   -0.2540   -0.2400   -0.2169
-0.4271   -2.8540   -4.0190   -0.0692   -0.0953   -2.7950
 0.1179    0.9212    0.0001   -0.0243   -0.0155   -0.0772
-0.1220   -0.0141    1.0000   -0.0200   -0.0112   -0.0139
 0.0       0.0       0.0       0.2231    0.7769    0.0
 0.0       0.0       0.0       0.0       1.0000    0.0
 0.0       0.0       0.0       0.0       0.0       0.9594
```

TRANSPOSE OF BD-MATRIX

```
-0.0112   -0.0049   -0.0004   -0.0006    0.0603    0.1250    0.0
```

LATERAL SYSTEM

AD-MATRIX

```
 0.7230    0.1710   -2.2100   -0.0112    0.9860    0.3750    0.0    0.0    -2.1600
-0.0096    0.9680    0.1190    0.0006    0.0443   -0.1920    0.0    0.0     0.1160
 0.0183   -0.1190    0.9500    0.0094    0.0079    0.0199    0.0    0.0    -0.0492
 0.1070   -0.0281   -0.1450    1.0000    0.0653    0.0232    0.9760 0.9560 -0.1430
 0.0       0.0       0.0       0.0       0.0235    0.0439    0.0    0.0     0.0
 0.0       0.0       0.0       0.0       0.0       0.0       0.0    0.0     0.0
 0.0       0.0       0.0       0.0       0.0       0.0       1.0000 1.0000  0.0
 0.0       0.0       0.0       0.0       0.0       0.0       0.0    0.0     0.9594
```

TRANSPOSE OF BD-MATRIX

```
 0.0       0.0       0.0       0.0       0.0925    0.0       0.0    0.0
 0.0       0.0       0.0       0.0       0.0       0.0868    0.1250 0.0
```

FLIGHT CONDITION 11

DYNAMIC PRESSURE 254PSF (12205 N/SQ.M)   MACH 0.60   ALTITUDE 20000 FT (6095 M)

LONGITUDINAL SYSTEM

AD-MATRIX
```
 0.9064   -0.5443   -0.0000   -0.5334   -0.5100   -0.5271
-0.3468   -1.5780   -4.0210    0.0274   -0.0252   -1.5280
 0.1137    0.8668    0.0000   -0.0476   -0.0297   -0.1294
 0.1198   -0.0352    1.0000   -0.0425   -0.0239   -0.0345
 0.0       0.0       0.0       0.2231    0.7769    0.0
 0.0       0.0       0.0       0.0       1.0000    0.0
 0.0       0.0       0.0       0.0       0.0       0.9397
```

TRANSPOSE OF BD-MATRIX
```
-0.0239   -0.0020   -0.0011   -0.0008    0.0603    0.1250    0.0
```

LATERAL SYSTEM

AD-MATRIX
```
 0.6370    0.3020   -4.4200   -0.0154    2.1000    0.7760    0.0      -4.2700
-0.0110    0.9410    0.3450    0.0011    0.1240   -0.4260    0.0       0.3350
 0.0088   -0.1180    0.9270    0.0063    0.0035    0.0363    0.0      -0.0712
 0.1010    0.0228   -0.2980    0.9990    0.1410    0.0520    0.9760   -0.2910
 0.0       0.0       0.0       0.0       0.0       0.0       0.0       0.0
 0.0       0.0       0.0       0.0       0.0       0.0439    0.0       0.0
 0.0       0.0       0.0       0.0       0.0       0.0       1.0000    0.0
 0.0       0.0       0.0       0.0       0.0       0.0       0.0       0.9397
```

TRANSPOSE OF BD-MATRIX
```
 0.0    0.0925    0.0      0.1250   0.0
 0.0    0.0       0.0868   0.0      0.1250
```

FLIGHT CONDITION 12

DYNAMIC PRESSURE 434PSF (20854 N/SQ.M)   MACH 0.80   ALTITUDE 20000 FT (6095 M)

LONGITUDINAL SYSTEM

AD-MATRIX
```
 0.8571   -0.9781   -0.0001   -0.9337   -0.9059   -0.9366
-0.3425   -1.5090   -4.0220    0.1437    0.0448   -1.4440
 0.1086    0.7981    0.0000   -0.0796   -0.0489   -0.1944
 0.1172   -0.0644    1.0000   -0.0755   -0.0426   -0.0626
 0.0       0.0       0.0       0.2231    0.7769    0.0
 0.0       0.0       0.0       0.0       1.0000    0.0
 0.0       0.0       0.0       0.0       0.0       0.9204
```

TRANSPOSE OF BD-MATRIX
```
-0.0426    0.0007   -0.0018   -0.0014    0.0603    0.1250    0.0
```

LATERAL SYSTEM

AD-MATRIX
```
 0.5380   -5.9100   -0.0161    3.1100    1.0600    0.0       0.0      -5.6400
-0.0108    1.1400    0.0028    0.1940   -0.6640    0.0       0.0       1.0900
 0.0053    0.8700    0.0046   -0.0019    0.0516    0.0       0.0      -0.1260
 0.0937   -0.4130    0.9990    0.2140    0.0752    0.9760    0.9560   -0.4010
 0.0       0.0       0.0       0.0235    0.0       0.0       0.0       0.0
 0.0       0.0       0.0       0.0       0.0439    1.0000    0.0       0.0
 0.0       0.0       0.0       0.0       0.0       0.0       1.0000    0.0
 0.0       0.0       0.0       0.0       0.0       0.0       0.0       0.9204
```

TRANSPOSE OF BD-MATRIX
```
 0.0       0.0       0.0925    0.0       0.0       0.1250    0.0       0.0
 0.0       0.0       0.0       0.0868    0.0       0.0       0.1250    0.0
```

FLIGHT CONDITION 13

DYNAMIC PRESSURE 550PSF (26429 N/SQ.M)   MACH 0.90   ALTITUDE 20000 FT (6095 M)

LONGITUDINAL SYSTEM

```
AD-MATRIX
  0.8198   -0.0001   -1.3380    0.0001   -1.1140   -1.0940   -1.2730
 -0.3560    0.9983   -1.7160   -4.0210    0.1763    0.0511   -1.6320
  0.1051   -0.0000    0.7498    0.0000   -0.0940   -0.0578   -0.2398
  0.1153   -0.0000   -0.0892    1.0000   -0.0912   -0.0517   -0.0864
  0.0       0.0       0.0       0.0       0.2231    0.7769    0.0
  0.0       0.0       0.0       0.0       0.0       1.0000    0.0
  0.0       0.0       0.0       0.0       0.0       0.0       0.9109
```

```
TRANSPOSE OF BD-MATRIX
 -0.0517    0.0006   -0.0021   -0.0017    0.0603    0.1250    0.0
                                                    0.1250    0.0
```

LATERAL SYSTEM

```
AD-MATRIX
  0.4690   -6.7500   -0.0168    3.2700    1.0400    0.0       0.0      -6.4000
 -0.0122    1.3900    0.0031    0.2110   -0.7350    0.0       0.0       1.3300
  0.0045    0.8480    0.0041   -0.0038    0.0552    0.0       0.0      -0.1460
  0.0884   -0.4840    0.9990    0.2290    0.0765    0.9760    0.0      -0.4690
  0.0       0.0       0.0       0.0235    0.0439    0.0       0.9560    0.0
  0.0       0.0       0.0       0.0       0.0       1.0000    0.0       0.0
  0.0       0.0       0.0       0.0       0.0       0.0       1.0000    0.0
  0.0       0.0       0.0       0.0       0.0       0.0       0.0       0.9109
```

```
TRANSPOSE OF BD-MATRIX
  0.0       0.0925    0.0       0.0       0.1250    0.0       0.0       0.0
  0.0       0.0       0.0868    0.0       0.0       0.1250    0.0       0.0
```

FLIGHT CONDITION 14

DYNAMIC PRESSURE 978PSF (46995 N/SQ.M)   MACH 1.20   ALTITUDE 20000 FT(6095 M)

LONGITUDINAL SYSTEM

AD-MATRIX

```
 0.6618   -4.2360    0.0001   -1.3280   -0.0001   -1.3820   -3.9560
-0.3478   -1.2790    0.9997    0.2216   -4.0240    0.0627   -1.1810
 0.0984    0.5463    0.0000   -0.1163   -0.0000   -0.0722   -0.4309
 0.1092   -0.2929    0.0000   -0.1152    1.0000   -0.0664   -0.2806
 0.0       0.0       0.0       0.2231    0.0       0.7769    0.0
 0.0       0.0       0.0       0.0       0.0       1.0000    0.0
 0.0       0.0       0.0       0.0       0.0       0.0       0.8830
```

TRANSPOSE OF BD-MATRIX

```
-0.0664    0.0007   -0.0026   -0.0023    0.0603    0.1250    0.0
```

LATERAL SYSTEM

AD-MATRIX

```
 0.5140  -10.8000   -0.0202    2.0500    0.9200    0.7450    0.0     -10.1000
-0.0043    1.9400    0.0033    0.0825   -0.3770    0.7840    0.0       1.8200
 0.0029    0.7970    0.0030   -0.0009    0.0279   -0.1090    0.0      -0.1940
 0.0920   -0.7780    0.9990    0.1410    0.0675    0.0362    0.9560   -0.7450
 0.0       0.0       0.0       0.0235    0.0439    0.0       0.0       0.0
 0.0       0.0       0.0       0.0       0.0       0.9760    0.0       0.0
 0.0       0.0       0.0       0.0       0.0       0.0       1.0000    0.0
 0.0       0.0       0.0       0.0       0.0       0.0       0.0       0.8830
```

TRANSPOSE OF BD-MATRIX

```
 0.0       0.0       0.0       0.0       0.0868    0.0       0.1250    0.0
 0.0       0.0       0.0       0.0       0.0925    0.0       0.0       0.0
```

FLIGHT CONDITION 15

DYNAMIC PRESSURE 135PSF (6487 N/SQ.M)   MACH 0.70   ALTITUDE 40000 FT (12191 M)

LONGITUDINAL SYSTEM

```
AD-MATRIX
  0.9450  -0.3433  -0.0002  -0.3385  -0.3200   0.0     -0.3317
 -0.4229  -2.7690  -4.0230  -0.0056  -0.0439   0.0     -2.6760
  0.1186   0.9247   0.0000  -0.0298  -0.0181   0.0     -0.0731
  0.1220  -0.0219   1.0000  -0.0267  -0.0149   0.0     -0.0214
  0.0      0.0      0.0      0.2231   0.7769   0.9760   0.0
  0.0      0.0      0.0      0.0      1.0000   0.0      0.0
  0.0      0.0      0.0      0.0      0.0      1.0000   0.9345
```

```
TRANSPOSE OF BD-MATRIX
 -0.0149  -0.0026  -0.0007  -0.0005   0.0603   0.1250   0.0
```

LATERAL SYSTEM

```
AD-MATRIX
  0.7880   0.2090  -2.9900  -0.0092   1.3500   0.5260   0.0      0.0     -2.8900
 -0.0058   0.9660   0.2350   0.0007   0.0739  -0.2560   0.0      0.0      0.2280
 -0.0143  -0.1200   0.9460   0.0058   0.0064   0.0233   0.0      0.0     -0.0526
  0.1120   0.0245  -0.1940   1.0000   0.0884   0.0329   0.0      0.0     -0.1890
  0.0      0.0      0.0      0.0      0.0235   0.0      0.9560   0.0      0.0
  0.0      0.0      0.0      0.0      0.0      0.0439   0.0      0.0      0.0
  0.0      0.0      0.0      0.0      0.0      0.0      1.0000   0.0      0.0
  0.0      0.0      0.0      0.0      0.0      0.0      0.0      0.0      0.9345
```

```
TRANSPOSE OF BD-MATRIX
  0.0      0.0      0.0925   0.0      0.1250   0.0
  0.0      0.0      0.0      0.0868   0.0      0.1250
```

FLIGHT CONDITION 16

DYNAMIC PRESSURE 176ESF (8457 N/SQ.M)   MACH 0.80   ALTITUDE 40000 FT(12191 M)

LONGITUDINAL SYSTEM

AD-MATRIX

```
 0.9300   0.0001  -0.4690  -0.0002  -0.4568  -0.4336  -0.4509
-0.3886   0.9987  -2.2220  -4.0220  -0.0188  -0.0301  -2.1360
 0.1172  -0.0000   0.9059   0.0000  -0.0393  -0.0237  -0.0909
 0.1212  -0.0000  -0.0300   1.0000  -0.0361  -0.0202  -0.0292
 0.0      0.0      0.0      0.0      0.2231   0.7769   0.0
 0.0      0.0      0.0      0.0      0.0      1.0000   0.0
 0.0      0.0      0.0      0.0      0.0      0.0      0.9255
```

TRANSPOSE OF BD-MATRIX

```
-0.0202  -0.0008  -0.0007  -0.0021   0.0603   0.1250   0.0
```

LATERAL SYSTEM

AD-MATRIX

```
 0.7620   0.2540  -3.7500  -0.0102   1.7300   0.6550   0.0     -3.6000
-0.0058   0.9510   0.4170   0.0011   0.1010  -0.3310   0.0      0.4010
 0.0109  -0.1200   0.9330   0.0050   0.0046   0.0282   0.0     -0.0649
 0.1100   0.0226  -0.2450   1.0000   0.1130   0.0419   0.0     -0.2380
 0.0      0.0      0.0      0.0      0.0235   0.0439   0.9763   0.0
 0.0      0.0      0.0      0.0      0.0      0.0      0.9560   0.0
 0.0      0.0      0.0      0.0      0.0      0.0      1.0000   0.0
 0.0      0.0      0.0      0.0      0.0      0.0      0.0      0.9255
```

TRANSPOSE OF BD-MATRIX

```
 0.0      0.0      0.0925   0.0      0.0      0.1250
 0.0      0.0      0.0      0.0868   0.0      0.0
```

FLIGHT CONDITION 17

DYNAMIC PRESSURE 223PSF (10715 N/SQ.M)   MACH 0.90   ALTITUDE 40000 FT(12191 M)

LONGITUDINAL SYSTEM

AD-MATRIX

```
 0.9083   -0.0001   -0.6750    0.0002   -0.5689   -0.5434   -0.6456
-0.4190    0.9986   -2.7060   -4.0220    0.0571   -0.0115   -2.5870
 0.1153   -0.0000    0.8793    0.0000   -0.0484   -0.0291   -0.1161
 0.1201   -0.0000   -0.0435    1.0000   -0.0453   -0.0254   -0.0422
 0.0       0.0       0.0       0.0       0.2231    0.7769    0.0
 0.0       0.0       0.0       0.0       0.0       1.0000    0.0
 0.0       0.0       0.0       0.0       0.0       0.0       0.9166
```

TRANSPOSE OF BD-MATRIX

```
-0.0254   -0.0015   -0.0010   -0.0009    0.0603    0.1250    0.0
```

LATERAL SYSTEM

AD-MATRIX

```
 0.6970   -4.4700    0.2970   -0.0110    2.0600    0.7210    0.0      -4.2600
-0.0076    0.6170    0.9340    0.0014    0.1250   -0.3860    0.0       0.5910
-0.0086    0.9190   -0.1190    0.0045    0.0026    0.0312    0.0      -0.0780
 0.1050   -0.2960    0.0219    1.0000    0.1370    0.0475    0.0      -0.2880
 0.0       0.0       0.0       0.0       0.0235    0.0       0.9760    0.0
 0.0       0.0       0.0       0.0       0.0       0.0439    0.0       0.9560
 0.0       0.0       0.0       0.0       0.0       0.0       1.0000    0.0
 0.0       0.0       0.0       0.0       0.0       0.0       0.0       0.9166
```

TRANSPOSE OF BD-MATRIX

```
 0.0    0.0    0.0925    0.0      0.1250    0.0    0.0    0.0
 0.0    0.0    0.0       0.0868   0.0       0.0    0.0    0.1250
```

FLIGHT CONDITION 18

DYNAMIC PRESSURE   397PSF   (19077 N/SQ.M)   MACH 1.20   ALTITUDE   40000 FT(12191 M)

LONGITUDINAL SYSTEM

AD-MATRIX

0.8098	-2.3980	-0.0000	-0.7820	-0.7716	-2.2570
-0.4091	-2.3730	-4.0250	0.2309	0.1241	-2.2280
0.1105	0.7549	-0.0000	-0.0673	-0.0406	-0.2339
0.1162	-0.1577	1.0000	-0.0643	-0.0364	-0.1516
0.0	0.0	0.0	0.2231	0.7769	0.0
0.0	0.0	0.0	0.0	1.0000	0.0
0.0	0.0	0.0	0.0	0.0	0.8903

TRANSPOSE OF BD-MATRIX

-0.0364	0.0043	-0.0014	-0.0012	0.0603	0.1250	0.0

LATERAL SYSTEM

AD-MATRIX

0.6940	0.4440	-6.6800	-0.0125	1.5000	0.6170	0.0	-6.2700
-0.0058	0.8890	1.0500	0.0018	0.0742	-0.2810	0.0	0.9860
0.0058	-0.1170	0.8860	0.0033	-0.0005	0.0217	0.0	-0.1090
0.1050	0.0252	-0.0447	0.9990	0.0994	0.0417	0.0	-0.4300
0.0	0.0	0.0	0.0	0.0235	0.0	0.0	0.0
0.0	0.0	0.0	0.0	0.0	0.0439	0.9560	0.0
0.0	0.0	0.0	0.0	0.0	0.0	1.0000	0.0
0.0	0.0	0.0	0.0	0.0	0.0	0.0	0.8903

TRANSPOSE OF BD-MATRIX

0.0	0.0	0.0	0.0	0.0925	0.0	0.0	0.0
0.0	0.0	0.0	0.0	0.0	0.0868	0.1250	0.0

FLIGHT CONDITION 19

DYNAMIC PRESSURE 537PSF (25804 N/SQ.M)   MACH 1.40   ALTITUDE 40000 FT (12191 M)

LONGITUDINAL SYSTEM

AD-MATRIX

0.7835	0.0000	-0.0000	-2.7570	-0.8169	-0.8130	-2.5690
-0.4555	0.9996	-4.0240	-3.0630	0.2813	0.1541	-2.8460
-0.1094	-0.0000	0.0000	0.7310	-0.0706	-0.0425	-0.2549
0.1150	0.0000	1.0000	-0.1823	-0.0677	-0.0385	-0.1742
0.0	0.0	0.0	0.0	0.2231	0.7769	0.0
0.0	0.0	0.0	0.0	0.0	1.0000	0.0
0.0	0.0	0.0	0.0	0.0	0.0	0.8733

TRANSPOSE OF BD-MATRIX

0.0055	-0.0015	0.0603	0.1250	0.0		
-0.0385	-0.0013					

LATERAL SYSTEM

AD-MATRIX

0.6700	0.5740	-8.6100	-0.0138	1.3900	0.5700	0.0	-8.0100
-0.0089	0.8940	0.9290	0.0014	0.0373	-0.2870	0.0	-0.8680
0.0057	-0.1160	0.8870	0.0028	0.0022	0.0215	0.0	-0.1080
0.1040	-0.0307	-0.5800	0.9990	0.0922	0.0393	0.0	-0.5540
0.0	0.0	0.0	0.0	0.0235	0.0	0.9560	0.0
0.0	0.0	0.0	0.0	0.0	0.0439	0.0	0.0
0.0	0.0	0.0	0.0	0.0	0.0	1.0000	0.0
0.0	0.0	0.0	0.0	0.0	0.0	0.0	0.8733

TRANSPOSE OF BD-MATRIX

0.0	0.0	0.0925	0.0	0.1250	0.0
0.0	0.0	0.0	0.0868	0.0	0.1250

FLIGHT CONDITION 20

DYNAMIC PRESSURE   703PSF (33781 N/SQ.M)   MACH 1.60   ALTITUDE   40000 FT (12191 M)

LONGITUDINAL SYSTEM

AD-MATRIX
```
 0.7647   -3.0260   -0.0000   -0.8878   -0.8887   -2.7900
-0.5185   -4.0090   -4.0230    0.3508    0.1917   -3.6880
 0.1086    0.7144    0.0000   -0.0766   -0.0460   -0.2688
 0.1142   -0.2008    1.0000   -0.0741   -0.0422   -0.1905
 0.0       0.0       0.0       0.2231    0.7769    0.0
 0.0       0.0       0.0       0.0       1.0000    0.0
 0.0       0.0       0.0       0.0       0.0       0.8565
```

TRANSPOSE OF BD-MATRIX
```
-0.0422    0.0068   -0.0016   -0.0014    0.0603    0.1250    0.0
```

LATERAL SYSTEM

AD-MATRIX
```
 0.6590   -9.9200   -0.0140    1.2800    0.5390    0.0       0.0      -9.1300
 0.8990    0.8270    0.0011    0.0046   -0.2930    0.0       0.0       0.7660
-0.1170    0.8950    0.0025    0.0030    0.0211    0.0       0.0      -0.0994
-0.0329   -0.6710    0.9990    0.0858    0.0379    0.0       0.0      -0.6370
 0.0       0.0       0.0       0.0235    0.0       0.9760    0.9560    0.0
 0.0       0.0       0.0       0.0       0.0439    0.0       0.0       0.0
 0.0       0.0       0.0       0.0       0.0       1.0000    1.0000    0.0
 0.0       0.0       0.0       0.0       0.0       0.0       0.0       0.8565
```

TRANSPOSE OF BD-MATRIX
```
 0.0   0.0   0.0   0.0925   0.0       0.0       0.1250   0.0
 0.0   0.0   0.0   0.0      0.0868    0.1250    0.0      0.0
```

APPENDIX F

OUTLINE OF COMPENSATOR DESIGN PROCEDURE

F.1 Problem Statement

Consider a linear, time invariant stochastic system whose state equation is modeled as

$$\dot{\underline{x}}(t) = \underline{A}\,\underline{x}(t) + \underline{B}\,\underline{u}(t) + \underline{L}\,\underline{\xi}(t) \tag{F.1}$$

where $\underline{x}$, $\underline{u}$, and $\underline{\xi}$ are elements of finite dimentional spaces, and $\underline{\xi}(t)$ is a white noise, zero-mean, Gaussian random process with covariance defined by

$$E\{\underline{\xi}(t)\ \underline{\xi}'(s)\} = \underline{\Xi}\ \delta(t-s) \tag{F.2}$$

where $\underline{\Xi}$ is the intensity matrix and $\delta(t-s)$ is the Dirac delta function. Additionally, $\underline{A}$, $\underline{B}$ and L are appropriately dimensioned time-invariant matrices.

Observations on the state vector $\underline{x}(t)$ are defined by linear equations, corrupted by white noise Gaussian processes according to the model

$$\underline{z}(t) = \underline{C}\,\underline{x}(t) + \underline{\theta}(t) \tag{F.3}$$

where

$$E\{\underline{\theta}(t)\} = \underline{0} \tag{F.4}$$

$$E\{\underline{\theta}(t)\underline{\theta}'(s)\} = \underline{\Theta}\ \delta(t-s) \tag{F.5}$$

$$E\{\underline{\theta}(t)\underline{\xi}'(s)\} = \underline{0} \quad \text{for all t, s} \tag{F.6}$$

where $\underline{\Theta}$ is the noise intensity matrix.

The initial state $\underline{x}(0)$ is assumed to be a Gaussian random variable, with mean $\underline{x}_0$ and covariance $\underline{\Sigma}_0$. Associated with this problem is a quadratic cost functional of the form

$$J_T = \lim_{T \to \infty} \frac{1}{T}\,E\{\underline{x}(T)'\underline{S}\,\underline{x}(T) + \int_0^T (\underline{x}'(t)\underline{Q}\underline{x}(t) + \underline{u}'(t)\underline{R}\underline{u}(t))dt\} \tag{F.7}$$

where $\underline{S}$, $\underline{Q} \geq 0$, $\underline{R} > \underline{0}$ for all t.

The cost functional J_T represents the objectives of the design, and must be chosen in the design process. Thus, the matrices $\underline{S}$, $\underline{Q}$ and $\underline{R}$ must be chosen to specify the design. Additional parameter choices are values of the covariance matrices $\underline{\Xi}$ and $\underline{\Theta}$, reflecting the confidence one has in the system observations (F.3) and the mathematical model (F.1).

F.2 The Separation Theorem and Control Gain Design

The optimal solution of the stochastic control problem described in F.1 can be obtained as the combined solution of two problems: one of estimation and one of control. This is known as the separation theorem [5]. The control problem solution is given by

$$\underline{u}(t) = -\underline{G}\ \hat{\underline{x}}(t) \tag{F.8}$$

where $\hat{\underline{x}}(t)$ is the minimum variance estimate of the state, given measurements $\{\underline{z}(t)\}$, and $\underline{G}$ is obtained from

$$\underline{G} = -\underline{R}^{-1}\underline{B}\ \underline{K} \tag{F.9}$$

where $\underline{K}$ is the unique positive definite symmetric solution matrix of the algebraic Riccati equation

$$\underline{0} = -\ \underline{K}\ \underline{A} - \underline{A}\ \underline{K} - \underline{Q} + \underline{K}\ \underline{B}\ \underline{R}^{-1}\underline{B}\ \underline{K} \tag{F.10}$$

F.3 Discrete-time Formulation and Estimation

Control algorithms for the F-8C aircraft will be implemented using a digital computer. Hence, the control action $\underline{u}(t)$ will change only at discrete intervals. Assume these intervals are equispaced τ seconds apart. Then, an equivalent system description can be obtained, as in [33], of the form

$$\underline{x}((n+1)\tau) = \underline{A}_d\underline{x}(n\tau) + \underline{B}_d \underline{u}(n\tau) + \underline{\eta}(n\tau) \qquad (F.11)$$

where

$$\underline{A}_d = e^{\underline{A}\tau} \qquad (F.12)$$

$$\underline{B}_d = \int_0^\tau e^{\underline{A}t}\underline{B} \; dt \qquad (F.13)$$

and $\underline{\eta}(n\tau)$ is a stationary discrete-time, zero-mean white noise sequence with covariance $\underline{N}$, where

$$\underline{N} = \int_0^\tau e^{\underline{A}t} \underline{L} \; \Xi \; \underline{L}' \; e^{\underline{A}'t} dt \qquad (F.14)$$

Assuming that the observations $\underline{z}(t)$ are available only at the sampling intervals τ, the minimum variance estimate of the state $\underline{x}$ is obtained by a discrete Kalman filter [23], described by:

$$\hat{\underline{x}}(t+1|t) = \underline{A}_d \; \hat{\underline{x}}(t|t) + \underline{B}_d \; u(t) \qquad (F.15)$$

$$\hat{\underline{x}}(t+1|t+1) = \hat{\underline{x}}(t+1|t) + \underline{H}(\underline{z}(t+1) - \underline{C} \; \underline{x}(t+1|t)) \qquad (F.16)$$

where the Kalman filter gain matrix $\underline{H}$ is obtained by

$$\underline{\Sigma}_1 = \underline{A}_d' \; \underline{\Sigma} \; \underline{A}_d + \underline{N} \qquad (F.17)$$

$$\underline{\Sigma} = \underline{\Sigma}_1 - \underline{\Sigma}_1\underline{C}' (\Theta + \underline{C} \; \underline{\Sigma}_1 \; \underline{C}')\underline{C} \; \underline{\Sigma}_1 \qquad (F.18)$$

$$\underline{H} = \underline{\Sigma} \; \underline{C}' \; \Theta^{-1} \qquad (F.19)$$

F.4 Discrete-Time Control Gain Design

The gains obtained in Section C.2 used instantaneous feedback of the state vector $\underline{x}(t)$ to obtain a decision vector $\underline{u}(t)$. Since the estimate of the state is available only at discrete intervals $n\tau$, and the control action is constant during each interval, these gains should be discretized so that

$$\underline{u}(n\tau) = \underline{G}_d \; \hat{\underline{x}}(n\tau|n\tau) \tag{F.20}$$

The gains $\underline{G}_d$ are chosen to approximate closest the deterministic closed-loop response of the continuous-time system. The closed-loop continuous-time system is

$$\underline{x}((n+1)\tau) = e^{(\underline{A} - \underline{B}\,\underline{G})\tau}\underline{x}(n\tau) \tag{F.21}$$

The closed-loop response of the discrete-time system is

$$\underline{x}((n+1)\tau) = (\underline{A}_d - \underline{B}_d\underline{G}_d)\underline{x}(n\tau) \tag{F.22}$$

The $\underline{G}_d$ which minimizes $\left|\left|\underline{A}_d - \underline{B}_d\underline{G}_d - e^{(\underline{A} - \underline{B}\,\underline{G})\tau}\right|\right|$ is obtained using generalized inverses,

$$\hat{\underline{G}} = (\underline{B}_d{}'\,\underline{B}_d)^{-1}\underline{B}_d{}'(\underline{A}_d - e^{(\underline{A} - \underline{B}\,\underline{G})\tau}) \tag{F.23}$$

APPENDIX G

Continuous Time Control Gains

Although the MMAC algorithm is a sampled-data algorithm, the control gains were initially designed as continuous time gains using the LQG methodology described in Appendix F. Using the matrices of Appendix A, the deterministic longitudinal system is represented by

$$\dot{\underline{x}} = \begin{pmatrix} A & B \\ \hline 0 & 0 \end{pmatrix} \underline{x} + \begin{pmatrix} 0 \\ 1 \end{pmatrix} \underline{u} \tag{G.1}$$

where $\underline{u} = \dot{\delta}_{ec}$, $\underline{x} = \begin{pmatrix} q \\ v \\ \alpha \\ \theta \\ \delta_e \\ w \\ \delta_{ec} \end{pmatrix}$ (G.2)

Transposing the states δ_{ec} and w yields the state vector

$$\hat{\underline{x}} = \begin{pmatrix} q \\ v \\ \alpha \\ \theta \\ \delta_e \\ \delta_{ec} \\ w \end{pmatrix} \tag{G.3}$$

The longitudinal control variable $\dot{\delta}_{ec}$ is given by

$$\dot{\delta}_{ec} = \underline{u} = - \underline{G}_{lon} \, \underline{\hat{x}}. \tag{G.4}$$

The matrices $\underline{G}_{lon}$ are tabulated in this appendix.

The deterministic equations for the lateral system are given by

$$\dot{\underline{x}} = \begin{pmatrix} \underline{A} & \underline{B} \\ 0 & 0 \end{pmatrix} \underline{x} + \begin{bmatrix} \underline{0} \\ 1 & 0 \\ 0 & 1 \end{bmatrix} \underline{u} \tag{G.5}$$

where A,B are the lateral system matrices of Appendix A, and

$$\underline{u} = \begin{pmatrix} \dot{\delta}_{ac} \\ \dot{\delta}_{rc} \end{pmatrix}, \qquad \underline{x} = \begin{bmatrix} p \\ r \\ \beta \\ \phi \\ \delta_a \\ \delta_r \\ w \\ \delta_{ac} \\ \delta_{rc} \end{bmatrix} \tag{G.6}$$

Switching the order of the states yields the state vector

$$\underline{x} = \begin{bmatrix} p \\ r \\ \beta \\ \phi \\ \delta_a \\ \delta_r \\ \delta_{ac} \\ \delta_{rc} \\ w \end{bmatrix} \tag{G.7}$$

$$\hat{\underline{x}} = \begin{Bmatrix} p \\ r \\ \beta \\ \phi \\ \delta_a \\ \delta_r \\ \delta_{ac} \\ \delta_{rc} \\ w \end{Bmatrix} \tag{G.7}$$

The control value $\underline{u}$ is derived in Chapter 9 to be of the form

$$\dot{\delta}_{ac}(t) = \underline{G}^a_m \, \underline{x}_m(t) - \underline{G}^a_F \, \hat{\underline{x}}(t) \tag{G.8}$$

where $\underline{x}_m(t) = \begin{Bmatrix} p_m \\ r_m \\ \beta_m \\ \phi_m \\ \delta_{am} \\ \delta_{rm} \end{Bmatrix}$ \hfill (G.9)

$\underline{x}_m$ represents the model states. Similarly

$$\dot{\delta}_{rc}(t) = \underline{G}^r_m \underline{x}_n(t) - \underline{G}^r_F \, \hat{\underline{x}}(t) \tag{G.10}$$

The matrices $\underline{G}^a_m$, $\underline{G}^a_F$, $\underline{G}^r_m$ and $\underline{G}^r_F$ are tabulated for each flight condition.

Continuous Feedback Gain, Elevator Rate

Flight Condition	q	v	α	θ	δ_e	δ_{ec}	w
5	-4.118	-.0017	.274	.0024	1.712	6.411	2.014
6	-4.827	-.0011	-.600	.0099	5.36	11.34	5.25
7	-5.543	-.00086	-2.037	.0068	9.587	15.168	8.763
8	-6.33	-.00026	-3.3	.0032	14.67	18.76	13.84
10	-4.485	-.00182	.767	-.0433	1.403	5.80	3.43
11	-4.541	-.0015	.7089	.0103	3.19	8.75	7.14
12	-5.146	-.0019	-.383	.0121	6.21	12.21	12.19
13	-5.39	.000024	-.229	.0026	7.83	13.71	16.66
14	-4.272	-.00032	18.96	-.000027	9.05	14.74	41.06
15	-4.42	-.0025	1.28	-.234	1.95	6.84	4.55
16	-4.57	-.0024	.997	-.0304	2.706	8.06	5.90
17	-4.67	.00021	1.308	-.0033	3.47	9.12	8.10
18	-3.65	.000096	13.59	-.714	4.35	10.22	21.84
19	-3.575	-.00028	14.89	.00187	4.611	10.52	25.19
20	-3.69	-.00024	15.88	.0017	5.192	11.16	27.22

Feedforward Control Gains, Aileron Rate

Continuous Time

Flight Condition	p_m	r_m	β_m	ϕ_m	δ_{am}	δ_{rm}
5	-1.9070	-.94700	2.88900	-9.2850	-12.650	-.62190
6	-1.6830	-1.6820	4.26600	-9.1810	-7.5740	-.19190
7	-1.5570	-3.7940	16.3100	-8.8650	-6.3890	-.98210
8	-1.4940	-6.5150	39.3300	-8.4400	-6.6620	-1.7190
10	-1.9410	-1.1120	3.05400	-9.2760	-13.710	-.50490
11	-1.7710	-1.4300	2.18800	-9.2080	-9.1440	.20380
12	-1.6500	-2.5930	6.51100	-9.0340	-7.2720	.06132
13	-1.6150	-3.3530	11.4100	-8.9130	-7.0410	-.17550
14	-1.7270	-5.0800	17.3000	-8.8380	-9.0530	2.5650
15	-1.8740	-1.2740	2.19600	-9.2200	-11.660	.14930
16	-1.8160	-1.4710	1.96100	-9.1820	-10.220	.39940
17	-1.7700	-1.6670	2.36300	-9.1520	-9.2310	.46860
18	-1.8280	-2.5790	2.90100	-9.0670	-10.740	2.0440
19	-1.8700	-.78300	.719800	-9.2760	-11.380	1.1460
20	-1.8830	1.3280	-2.37600	-9.3710	-11.800	.04392

Feedback Control Gains, Aileron Rate

Continuous Time

Flight Condition	p	r	β	φ	δ_a	δ_r	δ_{ac}	δ_{rc}	ω
5	1.68200	3.48200	-12.8100	9.03200	.688100	.044570	6.41600	.448700	-7.17900
6	1.18000	3.50600	-18.3700	9.06500	1.40800	-.044630	9.19100	.253400	-8.16900
7	.868500	4.85800	-27.5200	8.84800	1.73700	-.451200	1.02100	-.198700	-9.39800
8	.605700	6.80700	-41.1000	8.53300	1.69100	-.947200	10.0600	-.557200	-10.8900
10	2.21200	4.09200	-13.8100	9.05600	.708000	.080690	6.50300	.588900	-12.7900
11	1.70000	4.02900	-18.5300	9.07200	1.25800	.071160	8.67800	.510700	-16.5400
12	1.32400	4.16100	-20.4400	9.00300	1.62100	-.039070	9.85900	.318300	-16.9400
13	1.10900	4.87400	-24.9600	8.91300	1.61700	-.267400	9.85000	-01.0880	-20.0070
14	1.28300	8.36200	-40.5800	8.87300	1.13200	-.293500	8.24100	-.128400	-30.7100
15	2.47500	4.36600	-17.0600	9.09200	1.03700	.148200	7.86800	.771000	-15.1400
16	2.27100	4.21500	-18.0600	9.09000	1.24000	.158900	8.60600	.758800	-15.7600
17	1.94200	4.10400	-18.6500	8.98900	1.33400	.121000	8.93400	.648200	-15.9700
18	1.97500	6.83700	-29.1900	9.10200	1.03600	-.052790	7.88200	.311300	-23.1700
19	1.90600	7.55600	-39.0100	9.12800	.908100	-.124700	7.38000	.212300	-31.9400
20	1.94300	7.54800	-45.2300	9.12600	.811700	-.121200	6.97500	.319700	-37.6600

Feedforward Control Gains, Rudder Rate

Continuous Time

Flight Condition	p_m	r_m	β_m	ϕ_m	δ_{am}	δ_{rm}
5	.062090	2.56500	4.21500	-.074120	3.12000	-5.11400
6	-.156800	10.7800	-6.74100	-1.39400	-.344000	-5.25500
7	-.352400	17.8000	-26.8000	-2.64200	-1.08200	-4.99300
8	-.510600	24.8400	-51.6100	-3.73800	-1.25800	-6.67800
10	.014270	2.01100	4.26000	-.268300	2.91200	-5.14900
11	-.115600	6.51200	1.04700	-1.05800	.262900	-5.55600
12	-.257500	11.9400	-9.25500	-1.94500	-.856300	-5.75000
13	-.327600	14.6000	-17.4600	-2.38600	-1.14000	-6.00700
14	-.324100	24.3000	-40.3000	-2.83600	-1.06900	-14.3300
15	-.107900	3.10300	4.38700	-.867900	1.01600	-5.61500
16	-.147200	4.59200	3.58200	-1.11800	.316900	-5.92100
17	-.176700	6.10600	2.15200	-1.31200	-.188600	-6.40900
18	-.220500	1.07500	-2.36100	-1.72700	-.535000	-11.3500
19	-.028890	13.4900	-7.67700	-.982700	1.03700	-12.6800
20	.117200	16.4300	-14.2600	-.441400	2.09200	-14.0400

Feedback Control Gains, Rudder Rate

Continuous Time

Flight Condition	p	r	β	ϕ	δ_a	δ_r	δ_{ac}	δ_{rc}	ω
5	.466000	-6.01500	.398600	.551800	.079640	.611600	.252800	5.52000	-4.86500
6	.616800	-10.2300	3.63500	1.40200	.121500	2.85200	.142700	11.9400	-14.4400
7	.675300	-12.5600	-1.04500	2.22900	.114600	5.01600	-.112000	15.8400	-28.5300
8	.696800	-13.6700	-17.9000	2.88600	.156800	6.05800	-.314500	17.4000	-47.7700
10	.577900	-6.28600	.536500	.639100	.091140	.537500	.331700	5.16500	-2.05000
11	.648900	-8.32100	1.06300	1.13100	.135800	1.60900	.287700	8.96200	-4.72000
12	.640300	-9.49900	-5.54800	1.65500	.149600	2.92900	.179300	12.1000	-15.4400
13	.676000	-10.8700	-4.84400	1.96300	.120800	3.54900	-.006127	13.3200	-17.4200
14	.633700	-15.0300	-12.8300	1.91200	.091330	2.43300	-07.2320	11.0300	-34.5800
15	.670700	-6.39500	-1.60800	.978000	.133400	.763400	.434400	6.15100	-5.25000
16	.640000	-6.46900	-3.80100	1.10900	.149400	1.02000	.427400	7.11700	-8.35200
17	.598200	-6.71100	-5.94100	1.19500	.147100	1.22700	.365100	7.81700	-11.5000
18	.642500	-8.54200	-13.7400	1.33800	.114200	1.09900	.175400	7.40800	-22.9000
19	.617200	-12.4700	-5.60300	.505800	.121800	1.43800	.119600	8.47700	-19.4900
20	.499600	-17.4600	8.80500	-.131200	.156600	1.85600	.180100	9.62900	-11.8800

APPENDIX H

Discrete Time Control Gains

This appendix contains the discrete time control gains used in the pilot command designs of Chapters 5 and 6. For the longitudinal system, the commanded elevator rate is obtained from

$$\dot{\delta}_{ec}(t) = \underline{G} \ (\underline{G}_p s(t) - \hat{\underline{x}}(t)) \tag{H.1}$$

where $\hat{\underline{x}}(t)$ is the minimum variance estimate of the state, $\underline{x}(t)$

$$x(t) = \begin{bmatrix} q \\ v \\ \alpha \\ \theta \\ \delta_e \\ \delta_{ec} \\ w \end{bmatrix}(t) \tag{H.2}$$

and s is the pilot stick deflection, as discussed in Chapter 5. The gains $\underline{G}_p$ are tabulated in Chapter 5. The elements of the matrix $\underline{G}$ are listed in this appendix for each flight condition.

In the lateral system, there are two control variables. As discussed in Chapter 6, the commanded aileron rate can be computed as

$$\dot{\delta}_{ac}(t) = \underline{G}_m^a \ \underline{x}_m(t) - \underline{G}_F^a \ \hat{\underline{x}}(t) \tag{H.3}$$

Feedback Control Gains, Elevator Rate

Flight Condition	q	v	α	θ	δ_e	δ_{ec}	w
5	-2.641	-0.001	0.000	0.000	1.133	5.218	1.384
6	-2.193	-0.000	0.845	0.006	2.641	7.874	2.571
7	-1.996	-0.000	1.138	0.003	3.911	9.480	3.370
8	-1.884	-0.000	1.810	0.001	5.178	10.820	4.344
10	-2.804	-0.001	0.867	-0.027	0.966	4.820	2.660
11	-2.456	-0.001	1.209	0.008	1.824	6.590	4.743
12	-2.208	-0.001	1.290	0.008	2.927	8.259	6.785
13	-2.073	0.000	1.858	0.001	3.386	8.877	8.566
14	-1.017	-0.000	10.880	0.000	3.094	9.128	18.770
15	-2.753	-0.002	1.358	-0.148	1.260	5.490	3.361
16	-2.608	-0.002	1.309	-0.015	1.623	6.212	4.084
17	-2.450	0.000	1.724	0.001	1.937	6.785	5.282
18	-1.300	-0.000	8.859	0.000	1.934	7.211	12.900
19	-1.175	-0.000	9.876	0.001	1.971	7.352	14.170
20	-1.135	-0.000	10.310	0.001	2.130	7.643	14.720

Feedback Control Gains, Aileron Rate

Flight Condition	p	r	β	ϕ	δ_a	δ_r	δ_{ac}	δ_{rc}	w
5	1.145	3.095	-10.300	6.088	0.485	-0.021	5.293	0.221	-1.365
6	0.746	2.616	-12.720	5.538	0.922	-0.133	7.200	0.094	-1.246
7	0.552	3.128	-16.410	5.381	1.110	-0.410	7.905	-0.165	0.076
8	0.396	4.239	-21.590	5.323	1.058	-0.814	7.782	-0.541	3.104
10	1.514	3.612	-11.080	6.045	0.500	0.008	5.343	0.326	-1.725
11	1.073	3.232	-13.520	5.488	0.828	-0.051	6.797	0.213	-2.176
12	0.827	2.946	-13.350	5.342	1.043	-0.137	7.611	0.133	-1.094
13	0.700	3.301	-15.520	5.368	1.040	-0.290	7.624	-0.083	-0.427
14	0.841	5.364	-24.980	5.574	0.750	-0.299	6.514	-0.237	0.772
15	1.610	3.686	-12.910	5.608	0.699	0.030	6.232	0.407	-2.257
16	1.441	3.450	-13.170	5.425	0.817	0.018	6.712	0.375	-2.297
17	1.220	3.283	-13.270	5.401	0.872	-0.017	6.942	0.295	-2.099
18	1.290	5.423	-20.550	5.609	0.703	-0.128	6.261	0.028	-2.169
19	1.253	6.398	-28.780	5.845	0.619	-0.218	5.930	-0.098	-3.438
20	1.302	6.657	-34.870	5.976	0.554	-0.251	5.659	-0.077	-4.827

Feedforward Control Gains, Aileron Rate

Flight Condition	p_m	r_m	β_m	ϕ_m	δ_{am}	δ_{rm}
5	-1.301	-1.012	2.895	-6.314	-8.698	-0.947
6	-1.035	-0.453	1.906	-5.675	-4.621	-0.655
7	-0.955	-0.342	1.598	-5.513	-3.728	-0.550
8	-0.944	-0.344	1.583	-5.473	-3.704	-0.545
10	-1.311	-1.165	2.975	-6.246	-9.366	-0.954
11	-1.083	-0.584	2.178	-5.637	-5.576	-0.744
12	-0.986	-0.409	1.782	-5.451	-4.257	-0.613
13	-0.981	-0.392	1.739	-5.479	-4.121	-0.599
14	-1.098	-0.569	2.220	-5.734	-5.596	-0.764
15	-1.169	-0.831	2.569	-5.741	-7.329	-0.853
16	-1.096	-0.672	2.310	-5.541	-6.176	-0.782
17	-1.062	-0.580	2.154	-5.503	-5.512	-0.737
18	-1.151	-0.754	2.506	-5.742	-6.731	-0.853
19	-1.209	-0.835	2.660	-5.976	-7.366	-0.899
20	-1.243	-0.907	2.760	-6.095	-7.847	-0.92~

Feedforward Control Gains, Rudder Rate

Flight Condition	p_m	r_m	β_m	ϕ_m	δ_{am}	δ_{rm}
5	0.080	0.332	-0.142	0.172	2.478	-0.054
6	-0.076	-0.044	0.109	-0.442	-0.444	-0.026
7	-0.150	-0.101	0.291	-0.788	-0.920	-0.090
8	-0.191	-0.127	0.386	-0.983	-1.158	-0.123
10	0.053	0.333	-0.003	0.048	2.578	-0.133
11	-0.049	0.032	0.014	-0.362	0.062	-0.001
12	-0.127	-0.083	0.220	-0.695	-0.785	-0.062
13	-0.157	-0.111	0.299	-0.830	-1.006	-0.089
14	-0.159	-0.119	0.296	-0.841	-1.067	-0.085
15	-0.033	0.154	0.052	-0.314	0.950	-0.064
16	-0.062	0.069	0.057	-0.433	0.273	-0.030
17	-0.085	0.005	0.092	-0.524	-0.197	-0.024
18	-0.110	-0.014	0.134	-0.646	-0.410	-0.031
19	0.013	0.094	-0.165	-0.079	0.495	0.068
20	0.102	0.162	-0.370	0.346	1.081	0.136

Feedback Control Gains, Rudder Rate

Flight Condition	p	r	β	ϕ	δ_a	δ_r	δ_{ac}	δ_{rc}	ω
5	0.307	-4.243	-0.399	0.311	0.047	0.384	0.209	4.593	-0.701
6	0.300	-4.675	-1.387	0.758	0.060	1.172	0.195	7.970	-2.301
7	0.256	-4.018	-7.093	1.004	0.064	1.521	0.161	9.212	-4.352
8	0.217	-3.187	-17.180	1.137	0.080	1.489	0.146	9.492	-6.577
10	0.387	-4.592	-0.197	0.345	0.056	0.356	0.261	4.359	-0.766
11	0.369	-4.692	-1.268	0.644	0.073	0.816	0.253	6.641	-1.859
12	0.305	-3.988	-7.037	0.885	0.081	1.143	0.248	8.014	-4.024
13	0.300	-4.128	-8.023	1.007	0.071	1.298	0.186	8.479	-5.273
14	0.311	-6.163	-17.880	1.059	0.058	1.054	0.115	7.620	-10.390
15	0.420	-4.313	-2.107	0.537	0.077	0.465	0.323	5.013	-1.217
16	0.381	-3.979	-3.999	0.619	0.082	0.565	0.322	5.600	-1.670
17	0.345	-3.817	-5.829	0.686	0.080	0.636	0.294	5.997	-2.161
18	0.377	-4.585	-13.030	0.805	0.071	0.583	0.201	5.766	-4.193
19	0.343	-6.769	-8.749	0.269	0.065	0.771	0.169	6.406	-5.265
20	0.264	-9.416	-1.182	-0.123	0.079	0.992	0.211	7.048	-5.933

APPENDIX I

Continuous Time Closed-Loop Eigenvalues of Control System

The control gains were designed initially in continuous time using the matrices of Appendix A, yielding a closed-loop system of the form

$$\dot{\underline{x}} = (\underline{A} - \underline{B}\ \underline{G})\ \underline{x} \qquad\qquad (I.1)$$

The eigenvalues of $(\underline{A} - \underline{B}\ \underline{G})$ are tabulated below. Conjugate pairs are listed together.

| | Longitudinal System | |
| Flight Condition | Eigenvalues | |
	Real Part	Imaginary Part
5	-3.349	0
	-12.125	0
	-3.041	±3.6702
	-1.506	0
	-.000499	0
	-.00137	0
6	-5.917	0
	-12.76	0
	-4.668	±6.557
	-3.48	0
	-.0161	0
	-.000045	0

7	-7.815	0
	-13.484	0
	-5.59	±8.69
	-5.49	0
	-.0000233	0
	-.02157	0
8	-9.601	0
	-14.01	0
	-6.303	±10.703
	-8.0	0
	-.02386	0
	-.0000145	0
10	-.332	0
	-.00327	0
	-.00025	0
	-12.08	0
	-2.732	±3.28
	-1.137	0
11	-.4977	0
	-.000173	0
	-.00647	0
	-3.806	±5.019
	-2.133	0
	-12.34	0

12	-.6636	0
	-12.88	0
	-4.787	±6.97
	-3.646	0
	-.0000867	0
	-.00941	0
13	-.747	0
	-13.139	0
	-5.12	±7.897
	-4.586	0
	-.0121	0
	-.0000106	0
14	-.00251	0
	-.996	0
	-.00000377	0
	-5.177	±9.918
	-13.36	0
	-5.027	0
15	-.5421	0
	-12.14	0
	-3.083	±3.840
	-1.2484	0
	-.00982	0
	-.0000616	0

16	−.6196	0
	−12.25	0
	−3.524	±4.538
	−1.635	0
	−.000872	0
	−.6196	0
17	−.697	0
	−.0000534	0
	−12.38	0
	−3.85	±5.212
	−2.113	0
	−.0055	0
18	−.929	0
	−12.61	0
	−4.04	±6.96
	−2.536	0
	−.0189	0
	−.0185	0
19	−1.084	0
	−12.65	0
	−4.097	±7.31
	−2.747	0
	−.0000288	0
	−.00203	0
20	−1.239	0
	−12.743	0
	−4.252	±7.697
	−2.986	0
	−.0000062	0
	−.00684	0

Closed-loop Eigenvalues, Lateral System

Continuous Time

FC #										
5	-29.999	-24.887	-2.536	-2.536	-5.164	-1.846	-2.078	-2.078	-3.349
	0.0	0.0	4.007	-4.007	0.0	0.0	2.184	-2.184	0.0
	29.999	24.887	4.742	4.742	5.164	1.846	3.015	3.015	3.349
6	-29.989	-24.217	-3.667	-3.667	-4.812	-4.812	-3.853	-7.759	-5.917
	0.0	0.0	5.020	-5.020	4.566	-4.566	0.0	0.0	0.0
	29.989	24.217	6.216	6.216	6.633	6.633	3.853	7.759	5.917
7	-29.945	-23.459	-4.078	-4.078	-6.775	-6.775	-9.556	-5.231	-7.815
	0.0	0.0	5.540	-5.540	6.238	-6.238	0.0	0.0	0.0
	29.945	23.459	6.879	6.879	9.209	9.209	9.556	5.231	7.815
8	-29.844	-23.359	-7.313	-7.313	-4.293	-4.293	-11.251	-6.209	-9.600
	0.0	0.0	7.950	-7.950	5.226	-5.226	0.0	0.0	0.0
	29.844	23.359	10.802	10.802	6.764	6.764	11.251	6.209	9.600
10	-30.000	-24.921	-2.265	-2.265	-4.497	-1.721	-1.850	-1.850	-0.332
	0.0	0.0	3.931	-3.931	0.0	0.0	2.037	-2.037	0.0
	30.000	24.921	4.537	4.537	4.497	1.721	2.752	2.752	0.332
11	-29.996	-24.641	-3.140	-3.140	-6.125	-2.861	-3.306	-3.306	-0.498
	0.0	0.0	4.863	-4.863	0.0	0.0	3.373	-3.373	0.0
	29.996	24.641	5.789	5.789	6.125	2.861	4.723	4.723	0.498
12	-29.979	-24.201	-3.554	-3.554	-4.865	-4.865	-3.863	-7.528	-0.664
	0.0	0.0	5.229	-5.229	5.063	-5.063	0.0	0.0	0.0
	29.979	24.201	6.323	6.323	7.021	7.021	3.863	7.528	0.664
13	-29.961	-24.166	-5.337	-5.337	-3.565	-3.665	-8.141	-4.506	-0.747
	0.0	0.0	5.801	-5.801	5.283	-5.283	0.0	0.0	0.0
	29.961	24.166	7.882	7.882	6.430	6.430	8.141	4.506	0.747

Closed-loop Eigenvalues, Lateral System

Continuous Time

FC #									
FC# 14	-29.962	-24.833	-3.904	-3.904	-3.098	-3.098	-6.893	-4.876	-0.996
	0.0	0.0	6.547	-6.547	4.435	-4.435	0.0	0.0	0.0
	29.962	24.833	7.623	7.623	5.410	5.410	6.893	4.876	0.996
FC# 15	-29.999	-24.871	-2.467	-2.467	-4.860	-1.950	-2.180	-2.180	-0.542
	0.0	0.0	4.349	-4.349	0.0	0.0	2.475	-2.475	0.0
	29.999	24.871	5.000	5.000	4.860	1.950	3.298	3.298	0.542
FC# 16	-29.996	-24.794	-2.739	-2.739	-5.374	-2.225	-2.565	-2.565	-0.620
	0.0	0.0	4.659	-4.659	0.0	0.0	2.950	-2.950	0.0
	29.996	24.794	5.405	5.405	5.374	2.225	3.909	3.909	0.620
FC# 17	-29.994	-24.739	-5.900	-2.998	-2.998	-2.476	-2.838	-2.838	-0.697
	0.0	0.0	0.0	4.869	-4.869	0.0	3.424	-3.424	0.0
	29.994	24.739	5.900	5.718	5.718	2.476	4.447	4.447	0.697
FC# 18	-29.995	-24.869	-2.725	-2.725	-2.545	-2.545	-5.385	-2.759	-0.929
	0.0	0.0	4.727	-4.727	3.822	-3.822	0.0	0.0	0.0
	29.995	24.869	5.456	5.456	4.592	4.592	5.385	2.759	0.929
FC# 19	-29.993	-24.880	-2.867	-2.867	-2.600	-2.600	-5.256	-3.289	-1.084
	0.0	0.0	4.986	-4.986	3.660	-3.660	0.0	0.0	0.0
	29.993	24.880	5.751	5.751	4.490	4.490	5.256	3.289	1.084
FC# 20	-29.993	-24.890	-3.088	-3.088	-2.605	-2.605	-5.151	-3.870	-1.239
	0.0	0.0	5.177	-5.177	3.567	-3.567	0.0	0.0	0.0
	29.993	24.890	6.028	6.028	4.417	4.417	5.151	3.870	1.239

APPENDIX J

C* Criterion for Handling Qualities [3]

There are numerous desirable specifications on handling qualities.
The handling quality of an aircraft is often expressed by means of a
"pilot rating" from one to ten (Cooper-Harper scale) with a rating
of one for the best handling aircraft. However, in practical aircraft
design no single handling quality criterion is the ultimate. The
C*-criterion is a particular criterion expressed in terms of the short-
period response of the aircraft. It is a general concept which includes
the traditional short period damping requirements, and incorporates the
notion of response to pilot inputs.

The usual definition of the C* quantity is

$$C^* = a_z + V_{co}q \tag{J.1}$$

where V_{co} is the "crossover" velocity, the velocity at which the con-
tribution of pitch rate q equals the contribution of normal accelera-
tion a_z to the C* response.

The C* response of the aircraft can be determined in terms of
the system response to a step input. Figure J.1 contains the regions
of the C* envelope. Responses typical of the various regions can be
identified as:

Region 1:   optimum response

Region 2:   non-critical operation of vehicle
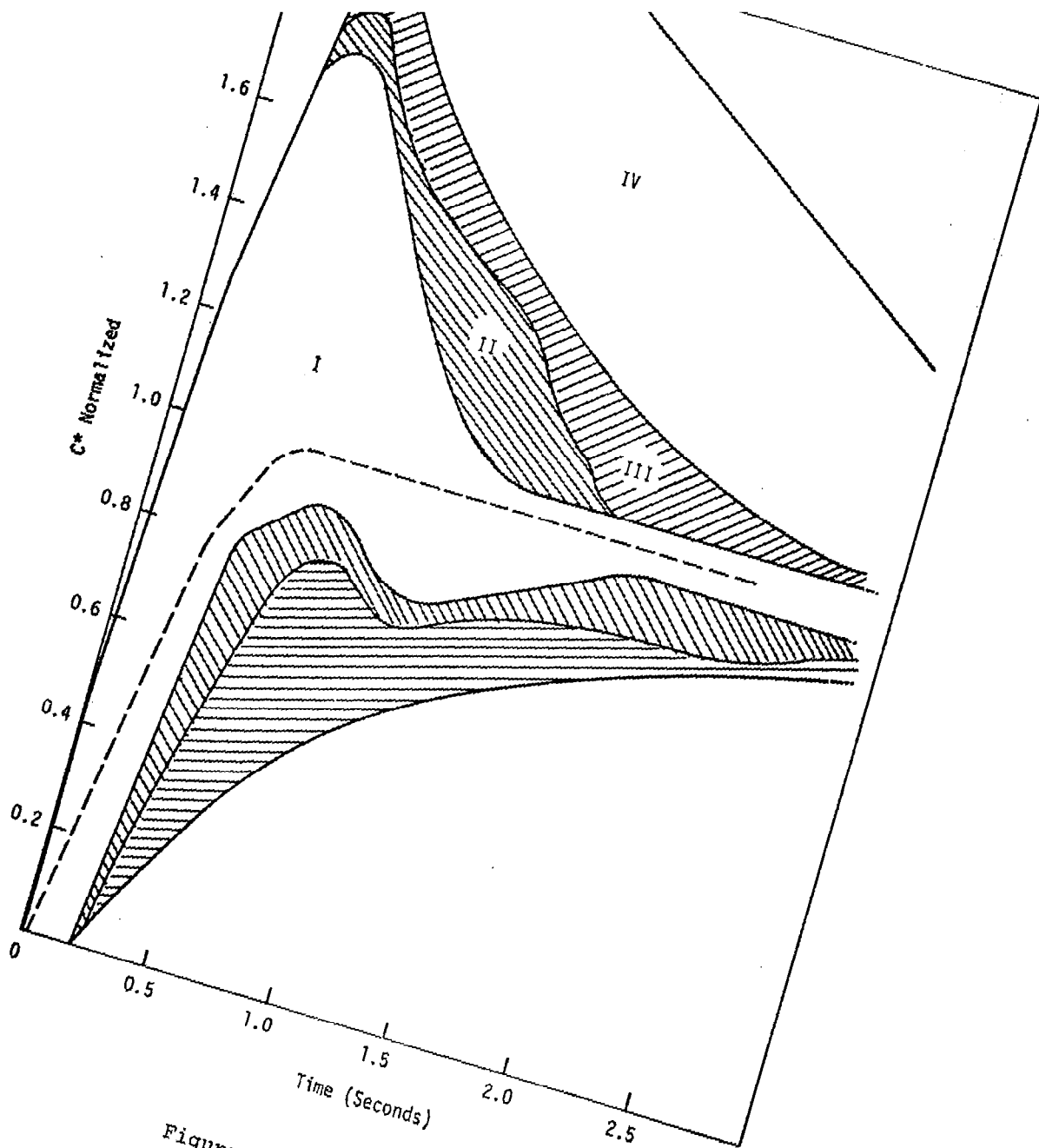
Figure J.1   C* Envelope

Region 3:   conditions not covered by 1, 2, and 4

Region 4:   power approach response

For the purposes of obtaining desirable C* handling qualities during normal operation, the step response of the system must lie in Region I.

Various studies have been made to determine the crossover velocity at various flight conditions. With respect to the F-8C aircraft dynamics, V_{co} can be approximate for all flight conditions as

$$V_{co} \approx 10 \text{ g's-seconds} \tag{J.2}$$

where the units of q are radians per second and the units of a_z are g's.

Thus, the C* quantity defined as

$$C^* \approx a_z + 10q \tag{J.3}$$

represents a desirable handling qualities balance between q and a_z for the F-8C aircraft. This quantity represents a useful criterion for the evaluation of the short-period performance of the aircraft.

APPENDIX K

Kalman Filter Gains

The update equation of the Kalman filter is given in Appendix F
and Appendix C as

$$\hat{\underline{x}}(t) = \hat{\underline{x}}(t|t-1) + \underline{H}\left(\underline{z}(t) - \underline{C}\,\hat{\underline{x}}(t|t-1)\right) \tag{K.1}$$

The matrix $\underline{C}$ is obtained from Appendix D and Chapter 3. The predicted
value of the state is obtained using the discrete matrices of Appendix E.
For the longitudinal system, $\underline{z}$ consists of the vector

$$\underline{z} = \begin{pmatrix} q \\ a_z \end{pmatrix} \tag{K.2}$$

The transpose of the matrix $\underline{H}$ is tabulated in this appendix for each
flight condition.

For the lateral system,

$$\underline{z} = \begin{pmatrix} a_y \\ p \\ r \\ \phi \\ \delta_a \\ \delta_r \end{pmatrix} \tag{K.3}$$

The transpose of the matrix $\underline{H}$ is tabulated in this appendix.

Longitudinal Kalman Filter Gains

Flight Condition	q	v	α	θ	δ_e	δ_{ec}	w
5	0.401	17.500	0.163	0.023	-0.025	0.0	-0.767
	0.030	-1.580	0.030	0.011	0.003	0.0	-0.064
6	0.452	24.110	0.077	0.008	-0.060	0.0	-0.314
	0.041	-2.094	0.020	0.008	0.006	0.0	-0.042
7	0.459	30.250	0.045	0.002	-0.085	0.0	-0.149
	0.038	-1.979	0.014	0.006	0.006	0.0	-0.029
8	0.469	40.940	0.027	-0.000	-0.102	0.0	-0.075
	0.031	-2.063	0.010	0.004	0.006	0.0	-0.017
10	0.274	6.296	0.125	0.044	-0.000	0.0	-0.417
	0.019	-0.415	0.021	0.014	0.000	0.0	-0.031
11	0.367	14.400	0.083	0.025	-0.043	0.0	-0.252
	0.028	-1.792	0.018	0.011	0.004	0.0	-0.029
12	0.408	19.380	0.056	0.011	-0.068	0.0	-0.143
	0.033	-1.794	0.015	0.008	0.005	0.0	-0.026
13	0.420	-308.200	0.063	0.190	-0.077	0.0	-0.111
	0.036	27.770	0.012	-0.009	0.006	0.0	-0.022
14	0.591	27.850	0.035	0.012	-0.061	0.0	-0.110
	0.037	-3.417	0.010	0.008	0.006	0.0	-0.009
15	0.330	11.300	0.089	0.040	-0.028	0.0	-0.285
	0.018	-1.238	0.018	0.013	0.002	0.0	-0.022
16	0.358	11.060	0.080	0.034	-0.036	0.0	-0.245
	0.021	-1.215	0.017	0.013	0.003	0.0	-0.021
17	0.336	-312.600	0.110	0.197	-0.000	0.0	-0.237
	0.027	43.950	0.010	-0.011	0.000	0.0	-0.019
18	0.565	2.293	0.052	0.031	-0.000	0.0	-0.174
	0.031	-0.279	0.013	0.012	0.000	0.0	-0.011
19	0.563	1.032	0.046	0.028	-0.000	0.0	-0.154
	0.032	-0.064	0.013	0.011	0.000	0.0	-0.010
20	0.552	0.957	0.042	0.027	-0.000	0.0	-0.138
	0.033	-0.025	0.012	0.011	-0.000	0.0	-0.009

Lateral Kalman Filter Gains

Flight Condition	p	r	β	φ	δ_a	δ_r	δ_ac	δ_rc	w
5	-0.020	0.006	-0.018	-0.025	0.0	0.0	0.0	0.0	-0.024
	0.669	-0.040	0.010	0.040	0.0	0.0	0.0	0.0	-0.024
	-0.642	0.082	-0.058	-0.193	0.0	0.0	0.0	0.0	-0.024
	0.152	-0.046	0.055	0.149	0.0	0.0	0.0	0.0	-0.024
	0.0	0.0	0.0	0.0	0.200	0.0	0.0	0.0	0.0
	0.0	0.0	0.0	0.0	0.0	0.200	0.0	0.0	0.0
6	-0.025	0.019	-0.020	-0.038	0.0	0.0	0.0	0.0	-0.002
	0.657	-0.067	0.004	0.024	0.0	0.0	0.0	0.0	-0.002
	-1.070	0.204	-0.055	-0.214	0.0	0.0	0.0	0.0	-0.002
	0.093	-0.051	0.027	0.085	0.0	0.0	0.0	0.0	-0.002
	0.0	0.0	0.0	0.0	0.200	0.0	0.0	0.0	0.0
	0.0	0.0	0.0	0.0	0.0	0.200	0.0	0.0	0.0
7	-0.020	0.034	-0.020	-0.035	0.0	0.0	0.0	0.0	0.005
	-0.538	-0.087	0.002	0.012	0.0	0.0	0.0	0.0	0.005
	-1.390	0.386	-0.053	-0.180	0.0	0.0	0.0	0.0	0.005
	0.044	-0.043	0.013	0.037	0.0	0.0	0.0	0.0	0.005
	0.0	0.0	0.0	0.0	0.200	0.0	0.0	0.0	0.0
	0.0	0.0	0.0	0.0	0.0	0.200	0.0	0.0	0.0
8	-0.001	0.045	-0.019	-0.028	0.0	0.0	0.0	0.0	0.007
	0.421	-0.089	-0.000	0.004	0.0	0.0	0.0	0.0	0.007
	-1.430	0.533	-0.045	-0.136	0.0	0.0	0.0	0.0	0.007
	0.014	-0.032	0.007	0.018	0.0	0.0	0.0	0.0	0.007
	0.0	0.0	0.0	0.0	0.200	0.0	0.0	0.0	0.0
	0.0	0.0	0.0	0.0	0.0	0.200	0.0	0.0	0.0
10	-0.021	0.005	-0.015	-0.022	0.0	0.0	0.0	0.0	-0.057
	0.402	-0.026	0.011	0.048	0.0	0.0	0.0	0.0	-0.057
	-0.415	0.045	-0.043	-0.150	0.0	0.0	0.0	0.0	-0.057
	0.183	-0.036	0.054	0.160	0.0	0.0	0.0	0.0	-0.057
	0.0	0.0	0.0	0.0	0.200	0.0	0.0	0.0	0.0
	0.0	0.0	0.0	0.0	0.0	0.200	0.0	0.0	0.0

Lateral Kalman Filter Gains

Flight Condition	p	r	β	ϕ	δ_a	δ_r	δ_{ac}	δ_{rc}	w
11	-0.021	0.009	-0.016	-0.032	0.0	0.0	0.0	0.0	-0.034
	0.474	-0.040	0.006	0.040	0.0	0.0	0.0	0.0	-0.034
	-0.645	-0.092	-0.041	-0.187	0.0	0.0	0.0	0.0	-0.034
	0.154	-0.045	0.037	0.133	0.0	0.0	0.0	0.0	-0.034
	0.0	0.0	0.0	0.0	0.200	0.0	0.0	0.0	0.0
	0.0	0.0	0.0	0.0	0.0	0.200	0.0	0.0	0.0
12	-0.015	0.021	-0.020	-0.032	0.0	0.0	0.0	0.0	-0.016
	0.369	-0.067	0.002	0.019	0.0	0.0	0.0	0.0	-0.016
	-1.090	0.292	-0.054	-0.191	0.0	0.0	0.0	0.0	-0.016
	0.072	-0.046	0.020	0.053	0.0	0.0	0.0	0.0	-0.016
	0.0	0.0	0.0	0.0	0.200	0.0	0.0	0.0	0.0
	0.0	0.0	0.0	0.0	0.0	0.200	0.0	0.0	0.0
13	-0.015	0.026	-0.020	-0.032	0.0	0.0	0.0	0.0	-0.012
	0.360	-0.068	0.002	0.017	0.0	0.0	0.0	0.0	-0.012
	-1.090	0.319	-0.051	-0.182	0.0	0.0	0.0	0.0	-0.012
	0.065	-0.044	0.016	0.042	0.0	0.0	0.0	0.0	-0.012
	0.0	0.0	0.0	0.0	0.200	0.0	0.0	0.0	0.0
	0.0	0.0	0.0	0.0	0.0	0.200	0.0	0.0	0.0
14	-0.047	0.028	-0.016	-0.043	0.0	0.0	0.0	0.0	-0.008
	0.445	-0.074	0.003	0.020	0.0	0.0	0.0	0.0	-0.008
	-1.180	0.251	-0.032	-0.146	0.0	0.0	0.0	0.0	-0.008
	0.075	-0.035	0.012	0.045	0.0	0.0	0.0	0.0	-0.008
	0.0	0.0	0.0	0.0	0.200	0.0	0.0	0.0	0.0
	0.0	0.0	0.0	0.0	0.0	0.200	0.0	0.0	0.0
15	-0.020	0.005	-0.014	-0.023	0.0	0.0	0.0	0.0	-0.037
	0.412	-0.035	0.007	0.043	0.0	0.0	0.0	0.0	-0.037
	-0.566	0.064	-0.037	-0.150	0.0	0.0	0.0	0.0	-0.037
	0.165	-0.036	0.044	0.155	0.0	0.0	0.0	0.0	-0.037
	0.0	0.0	0.0	0.0	0.200	0.0	0.0	0.0	0.0
	0.0	0.0	0.0	0.0	0.0	0.200	0.0	0.0	0.0

Lateral Kalman Filter Gains

Flight Condition	p	r	β	φ	δ_a	δ_r	δ_{ac}	δ_{rc}	w
16	-0.018	0.007	-0.015	-0.027	0.0	0.0	0.0	0.0	-0.031
	0.408	-0.048	0.005	0.035	0.0	0.0	0.0	0.0	-0.031
	-0.765	0.116	-0.043	-0.177	0.0	0.0	0.0	0.0	-0.031
	0.134	-0.042	0.039	0.131	0.200	0.0	0.0	0.0	-0.031
	0.0	0.0	0.0	0.0	0.0	0.200	0.0	0.0	0.0
	0.0	0.0	0.0	0.0	0.0	0.0	0.0	0.0	0.0
17	-0.013	0.010	-0.018	-0.028	0.0	0.0	0.0	0.0	-0.025
	0.389	-0.055	0.003	0.028	0.0	0.0	0.0	0.0	-0.025
	-0.882	0.173	-0.049	-0.196	0.0	0.0	0.0	0.0	-0.025
	0.106	-0.047	0.033	0.102	0.200	0.0	0.0	0.0	-0.025
	0.0	0.0	0.0	0.0	0.0	0.200	0.0	0.0	0.0
	0.0	0.0	0.0	0.0	0.0	0.0	0.0	0.0	0.0
18	-0.019	0.014	-0.017	-0.037	0.0	0.0	0.0	0.0	-0.017
	0.412	-0.064	0.003	0.024	0.0	0.0	0.0	0.0	-0.017
	-1.030	0.202	-0.040	-0.174	0.0	0.0	0.0	0.0	-0.017
	0.092	-0.042	0.025	0.086	0.200	0.0	0.0	0.0	-0.017
	0.0	0.0	0.0	0.0	0.0	0.200	0.0	0.0	0.0
	0.0	0.0	0.0	0.0	0.0	0.0	0.0	0.0	0.0
19	-0.024	0.013	-0.015	-0.042	0.0	0.0	0.0	0.0	-0.016
	0.498	-0.054	0.003	0.031	0.0	0.0	0.0	0.0	-0.016
	-0.861	0.128	-0.030	-0.167	0.0	0.0	0.0	0.0	-0.016
	0.118	-0.040	0.023	0.103	0.200	0.0	0.0	0.0	-0.016
	0.0	0.0	0.0	0.0	0.0	0.200	0.0	0.0	0.0
	0.0	0.0	0.0	0.0	0.0	0.0	0.0	0.0	0.0
20	-0.028	0.012	-0.013	-0.045	0.0	0.0	0.0	0.0	-0.014
	0.535	-0.045	0.003	0.035	0.0	0.0	0.0	0.0	-0.014
	-0.724	0.087	-0.022	-0.150	0.0	0.0	0.0	0.0	-0.014
	0.136	-0.036	0.020	0.115	0.200	0.0	0.0	0.0	-0.014
	0.0	0.0	0.0	0.0	0.0	0.200	0.0	0.0	0.0
	0.0	0.0	0.0	0.0	0.0	0.0	0.0	0.0	0.0

APPENDIX L

Discrete Time Eigenvalues

In the absence of pilot commands, the complete filtering and control system can be described by the equations:

$$\underline{x}(t+1) = \underline{A}_d \, \underline{x}(t) + \underline{B}_d \, \underline{u}(t) + \underline{L} \, \xi(t) \tag{L.1}$$

$$\underline{\tilde{x}}(t+1) = \underline{A}_d \, \underline{\hat{x}}(t) + \underline{B}_d \, \underline{u}(t) \tag{L.2}$$

$$\underline{\hat{x}}(t) = \underline{\tilde{x}}(t) + \underline{H}(\underline{z}(t) - \underline{C} \, \underline{\tilde{x}}(t)) \tag{L.3}$$

$$\underline{u}(t) = -\underline{G} \, \underline{\hat{x}}(t) \tag{L.4}$$

$$\underline{z}(t) = \underline{C} \, \underline{x}(t) + \underline{\theta}(t) \tag{L.5}$$

The eigenvalues of the system are the eigenvalues of the closed-loop control system matrix $(\underline{A}_d - \underline{B}_d\underline{G})$ and the eigenvalues of the Kalman filter $(\underline{I} - \underline{H} \, \underline{C})\underline{A}_d$.

The eigenvalues of the closed loop control system matrix $(\underline{A}_d - \underline{B}_d\underline{G})$ and the Kalman filter matrix $(\underline{I} - \underline{H} \, \underline{C})\underline{A}_d$ are tabulated below for each flight condition in the longitudinal and lateral system. Three numbers are given for each eigenvalue, its real part, its imaginary part, and its magnitude.

Longitudinal System

Closed-loop Control Eigenvalues, Flight Condition 5

0.2215	0.6332	0.9996	0.9996	0.7934	0.6580
0.0	-0.2993	0.0056	-0.0056	0.0	0.0
0.2215	0.7004	0.9996	0.9996	0.7934	0.6580

Closed-loop KBF Eigenvalues, Flight Condition 5

0.9965	0.4389	1.0000	0.2263	0.8248	0.9965
-0.0120	0.2904	0.0	0.0	0.0	0.0120
0.9966	0.5262	1.0000	0.2263	0.8248	0.9966

Closed-loop Control Eigenvalues, Flight Condition 6

0.3964	0.3964	0.2006	1.0000	0.9980	0.6488	0.4773
0.4257	-0.4257	0.0	0.0	0.0	0.0	0.0
0.5817	0.5817	0.2006	1.0000	0.9980	0.6488	0.4773

Closed-loop KBF Eigenvalues, Flight Condition 6

1.0000	0.9972	0.1631	0.1631	0.5485	0.2432	0.9972
0.0	-0.0066	0.2819	-0.2819	0.0	0.0	0.0066
1.000	0.9972	0.3257	0.3257	0.5485	0.2432	0.9972

Longitudinal System

Closed-loop Control Eigenvalues, Flight Condition 7

```
0.2458    0.2458   0.1808   1.0000   0.9973   0.5071   0.3765
0.4783   -0.4783   0.0      0.0      0.0      0.0      0.0
0.5377    0.5377   0.1808   1.0000   0.9973   0.5071   0.3765
```

Closed-loop KBF Eigenvalues, Flight Condition 7

```
 0.9974   1.0000   0.0265   0.0265   0.2964   0.2964   0.9974
-0.0047   0.0      0.2223  -0.2223   0.0683  -0.0683   0.0047
 0.9974   1.0000   0.2239   0.2239   0.3041   0.3041   0.9974
```

Closed-loop Control Eigenvalues, Flight Condition 8

```
0.0983    0.0983   0.1641   1.0000   0.9970   0.3686   0.3012
0.5017   -0.5017   0.0      0.0      0.0      0.0      0.0
0.5112    0.5112   0.1641   1.0000   0.9970   0.3686   0.3012
```

Closed-loop KBF Eigenvalues, Flight Condition 8

```
 0.9982   1.0000  -0.0587  -0.0587   0.2169   0.2169   0.9982
-0.0014   0.0      0.1350  -0.1350   0.1252  -0.1252   0.0014
 0.9982   1.0000   0.1472   0.1472   0.2504   0.2504   0.9982
```

Longitudinal System

Closed-loop Control Eigenvalues, Flight Condition 10

0.2204	0.6546	0.6546	0.8675	1.0000	0.9996	0.9594
0.0	0.2868	-0.2868	0.0	0.0	0.0	0.0
0.2204	0.7146	0.7146	0.8675	1.0000	0.9996	0.9594

Closed-loop KBF Eigenvalues, Flight Condition 10

0.9992	1.0000	0.7303	0.7303	0.2231	0.8789	0.9992
-0.0127	0.0	0.2418	-0.2418	0.0	0.0	0.0127
0.9993	1.0000	0.7693	0.7693	0.2231	0.8789	0.9993

Closed-loop Control Eigenvalues, Flight Condition 11

0.2124	0.5128	0.5128	0.9999	0.9993	0.7665	0.9397
0.0	0.3740	-0.3740	0.0	0.0	0.0	0.0
0.2124	0.6347	0.6347	0.9999	0.9993	0.7665	0.9397

Closed-loop KBF Eigenvalues, Flight Condition 11

0.9979	0.2346	1.0000	0.5797	0.5797	0.7399	0.9979
-0.0088	0.0	0.0	0.2870	-0.2870	0.0	0.0088
0.9979	0.2346	1.0000	0.6469	0.6469	0.7399	0.9979

Longitudinal System

Closed-loop Control Eigenvalues, Flight Condition 12

0.3717	0.3717	0.1978	1.0000	0.9988	0.6360	0.9204
0.4421	-0.4421	0.0	0.0	0.0	0.0	0.0
0.5776	0.5776	0.1978	1.0000	0.9988	0.6360	0.9204

Closed-loop KBF Eigenvalues, Flight Condition 12

0.9973	1.0000	0.4172	0.4712	0.5755	0.2713	0.9973
-0.0082	0.0	0.3039	-0.3039	0.0	0.0	0.0082
0.9974	1.0000	0.5162	0.5162	0.5755	0.2713	0.9974

Closed-loop Control Eigenvalues, Flight Condition 13

0.3088	0.3088	0.1910	0.9985	1.0000	0.5669	0.9109
0.4700	-0.4700	0.0	0.0	0.0	0.0	0.0
0.5624	0.5624	0.1910	0.9985	1.0000	0.5669	0.9109

Closed-loop KBF Eigenvalues, Flight Condition 13

0.9994	1.0000	0.3166	0.3166	0.2983	0.4905	0.9980
0.0	0.0	0.3167	-0.3167	0.0	0.0	0.0
0.9994	1.0000	0.4478	0.4478	0.2983	0.4905	0.9980

Longitudinal System

Closed-loop Control Eigenvalues, Flight Condition 14

0.1730	0.1730	0.5366	1.0000	0.9997	0.1819	0.8830
0.5412	-0.5412	0.0	0.0	0.0	0.0	0.0
0.5682	0.5682	0.5366	1.0000	0.9997	0.1819	0.8830

Closed-loop KBF Eigenvalues, Flight Condition 14

0.9998	0.9998	1.0000	0.0725	0.3926	0.2717	0.9998
-0.0011	0.0	0.0	0.3331	0.0	0.0	0.0011
0.9998	0.9998	1.0000	0.3409	0.3926	0.2717	0.9998

Closed-loop Control Eigenvalues, Flight Condition 15

0.2184	0.6082	0.6082	0.8557	1.0000	0.9988	0.9345
0.0	0.3190	-0.3190	0.0	0.0	0.0	0.0
0.2184	0.6868	0.6868	0.8557	1.0000	0.9988	0.9345

Closed-loop KBF Eigenvalues, Flight Condition 15

0.9983	0.2273	1.0000	0.6938	0.6938	0.8435	0.9983
-0.0109	0.0	0.0	0.2462	-0.2462	0.0	0.0109
0.9984	0.2273	1.000	0.7362	0.7362	0.8435	0.9984

Longitudinal System

Closed-loop Control Eigenvalues, Flight Condition 16

0.5507	0.5507	0.2150	0.8155	1.0000	0.9998	0.9255
0.3532	-0.3532	0.0	0.0	0.0	0.0	0.0
0.6543	0.6543	0.2150	0.8155	1.0000	0.9998	0.9255

Closed-loop KBF Eigenvalues, Flight Condition 16

0.9982	0.2313	0.6433	0.6433	0.7941	0.9982
-0.0100	0.0	0.2653	-0.2653	0.0	0.0100
0.9983	0.2313	0.6959	0.6959	0.7941	0.9983

Closed-loop Control Eigenvalues, Flight Condition 17

0.5025	0.5025	0.2113	0.7684	1.0000	0.9993	0.9166
0.3852	-0.3852	0.0	0.0	0.0	0.0	0.0
0.6332	0.6332	0.2113	0.7684	1.0000	0.9993	0.9166

Closed-loop KBF Eigenvalues, Flight Condition 17

0.9989	1.0000	0.6056	0.6056	0.7469	0.2231
0.0	0.0	0.3383	-0.3383	0.0	0.0
0.9989	1.0000	0.6937	0.6937	0.7469	0.2231

Longitudinal System

Closed-loop Control Eigenvalues, Flight Condition 18

0.4006	0.4006	0.2041	0.7299	1.0000	0.9998	0.8903
0.4802	-0.4802	0.0	0.0	0.0	0.0	0.0
0.6254	0.6254	0.2041	0.7299	1.0000	0.9998	0.8903

Closed-loop KBF Eigenvalues, Flight Condition 18

0.9999	1.0000	0.3283	0.3283	0.6294	0.2231	0.9999
-0.0012	0.0	0.4210	-0.4210	0.0	0.0	0.0012
0.9999	1.0000	0.5339	0.5339	0.6294	0.2231	0.9999

Closed-loop Control Eigenvalues, Flight Condition 19

0.3776	0.3776	0.2030	0.7112	1.0000	0.9997	0.8733
-0.4960	-0.4960	0.0	0.0	0.0	0.0	0.0
0.6234	0.6234	0.2030	0.7112	1.0000	0.9997	0.8733

Closed-loop KBF Eigenvalues, Flight Condition 19

0.9998	1.0000	0.2987	0.2987	0.5880	0.2231	0.9998
-0.0025	0.0	0.4269	-0.4269	0.0	0.0	0.0025
0.9998	1.0000	0.5211	0.5211	0.5880	0.2231	0.9998

Longitudinal System

Closed-loop Control Eigenvalues, Flight Condition 20

0.3480	0.2004	0.6908	1.0000	0.9991	0.8565
-0.5072	0.0	0.0	0.0	0.0	0.0
0.6151	0.2004	0.6908	1.0000	0.9991	0.8565

0.3480
0.5072
0.6151

Closed-loop KBF Eigenvalues, Flight Condition 20

1.0000	0.2810	0.2810	0.5570	0.2231	0.9995
0.0	0.4338	-0.4338	0.0	0.0	0.0022
1.0000	0.5169	0.5169	0.5570	0.2231	0.9995

0.9995
-0.0022
0.9995

Lateral System

Closed-loop Control Eigenvalues, Flight Condition 5

-0.0542	0.6977	0.6977	0.7767	0.7767	0.8260	0.5453	0.6580
0.0	0.4082	-0.4082	0.2648	-0.2648	0.0	0.0	0.0
0.0542	0.8083	0.8083	0.8206	0.8206	0.8260	0.5453	0.6580

Closed-loop KBF Eigenvalues, Flight Condition 5

0.2064	0.9919	0.9440	0.7450	0.5801	0.0351	1.0000	0.0188	1.0000
0.0	0.0	0.0	0.0	0.0	0.0	0.0	0.0	0.0
0.2064	0.9919	0.9440	0.7450	0.5801	0.0351	1.0000	0.0188	1.0000

Closed-loop Control Eigenvalues, Flight Condition 6

0.5622	0.6447	0.6447	0.4049	-0.1341	-0.1625	0.7233	0.4773
-0.5122	0.4687	-0.4687	0.0	0.0	0.0	0.0	0.0
0.7605	0.7971	0.7971	0.4049	0.1341	0.1625	0.7233	0.4773

Closed-loop KBF Eigenvalues, Flight Condition 6

0.1148	0.9942	0.7799	0.4648	0.0351	1.0000	0.0188	1.0000
0.0	0.0	0.0	0.0	0.0	0.0	0.0	0.0
0.1148	0.9942	0.7799	0.4648	0.0351	1.0000	0.0188	1.0000

Lateral System

Closed-loop Control Eigenvalues, Flight Condition 7

0.4602	0.5940	-0.2395	-0.1709	0.6805	0.3228	0.3765
-0.5993	-0.5101	0.0	0.0	0.0	0.0	0.0
0.7556	0.7829	0.2395	0.1709	0.6805	0.3228	0.3765

Closed-loop KBF Eigenvalues, Flight Condition 7

0.0768	0.9962	0.6036	0.4076	0.0351	1.0000	0.0188	1.0000
0.0	0.0	-0.0950	0.0	0.0	0.0	0.0	0.0
0.0768	0.9962	0.6110	0.4076	0.0351	1.0000	0.0188	1.0000

Closed-loop Control Eigenvalues, Condition 8

0.3570	0.5904	0.6550	-0.2542	-0.1652	0.2518	0.3012
-0.6666	-0.4701	0.0	0.0	0.0	0.0	0.0
0.7562	0.7547	0.6550	0.2542	0.1652	0.2518	0.3012

Closed-loop KBF Eigenvalues, Condition 8

0.9970	0.0553	0.4251	0.3609	0.0351	1.0000	0.0188	1.0000
0.0	0.0	-0.1251	0.0	0.0	0.0	0.0	0.0
0.9970	0.0553	0.4432	0.3609	0.0351	1.0000	0.0188	1.0000

Lateral System

Closed-loop Control Eigenvalues, Flight Condition 10

Real	-0.0048	0.7208	0.7208	0.7982	0.7982	0.6068	0.8357	0.9594	-0.0570
Imag	0.0	0.4148	-0.4148	0.2508	-0.2508	0.0	0.0	0.0	0.0
Mag	0.0048	0.8316	0.8316	0.8367	0.8367	0.6068	0.8357	0.9594	0.0570

Closed-loop KBF Eigenvalues, Flight Condition 10

Real	0.5992	0.5992	0.8135	0.9895	1.0000	0.0188	1.0000
Imag	-0.1594	0.1594	0.0	0.0	0.0	0.0	0.0
Mag	0.6200	0.6200	0.8135	0.9895	1.0000	0.0188	1.0000

Closed-loop Control Eigenvalues, Flight Condition 11

Real	0.6381	0.6381	0.6952	0.6952	0.7707	0.5134	-0.1165	-0.0899	0.9397
Imag	-0.4905	0.4905	0.3972	-0.3972	0.0	0.0	0.0	0.0	0.0
Mag	0.8048	0.8048	0.8007	0.8007	0.7707	0.5134	0.1165	0.0899	0.9397

Closed-loop KBF Eigenvalues, Flight Condition 11

Real	0.5184	0.5184	0.7949	0.9945	0.9332	0.0351	1.0000
Imag	-0.0619	0.0619	0.0	0.0	0.0	0.0	0.0
Mag	0.5221	0.5221	0.7949	0.9945	0.9332	0.0351	1.0000

Lateral System

Closed-loop Control Eigenvalues, Flight Condition 12

0.5368	0.5368	0.6398	0.4336	-0.1592	0.7330	0.9204
0.5415	-0.5415	-0.5044	0.0	-0.0018	0.0	0.0
0.7625	0.7625	0.8148	0.4336	0.1592	0.7330	0.9204

Closed-loop KBF Eigenvalues, Flight Condition 12

0.3216	0.9957	0.6817	0.9178	0.0351	0.0188	1.0000
0.0	0.0	0.0	0.0	0.0	0.0	0.0
0.3216	0.9957	0.6817	0.9178	0.0351	0.0188	1.0000

Closed-loop Control Eigenvalues, Flight Condition 13

0.5073	0.5073	0.6251	0.3925	-0.1587	-0.1901	0.7053	0.9109
0.5786	-0.5786	-0.5045	0.0	0.0	0.0	0.0	0.0
0.7695	0.7695	0.8033	0.3925	0.1587	0.1901	0.7053	0.9109

Closed-loop KBF Eigenvalues, Flight Condition 13

0.2783	0.9963	0.6256	0.9137	0.0351	0.0188	1.0000
0.0	0.0	0.0804	0.0	0.0	0.0	0.0
0.2783	0.9963	0.6308	0.9137	0.0351	0.0188	1.0000

Lateral System

Closed-loop Control Eigenvalues, Flight Condition 14

0.5093	0.5093	0.6737	0.6737	0.4461	-0.1046	0.6705	-0.1441	0.8830
0.6168	-0.6168	0.4356	-0.4356	0.0	0.0	0.0	0.0	0.0
0.7999	0.7999	0.8023	0.8023	0.4461	0.1046	0.6705	0.1441	0.8830

Closed-loop KBF Eigenvalues, Flight Condition 14

0.2369	0.9951	0.5971	0.5971	0.8838	0.0351	1.0000	0.0188	1.0000
0.0	0.0	0.1198	-0.1198	0.0	0.0	0.0	0.0	0.0
0.2369	0.9951	0.6090	0.6090	0.8838	0.0351	1.0000	0.0188	1.0000

Closed-loop Control Eigenvalues, Flight Condition 15

0.7050	0.7050	0.7680	0.7680	0.6027	-0.0924	-0.0232	0.8236	0.9345
0.4633	-0.4633	0.3027	-0.3027	0.0	0.0	0.0	0.0	0.0
0.8436	0.8436	0.8255	0.8255	0.6027	0.0924	0.0232	0.8236	0.9345

Closed-loop KBF Eigenvalues, Flight Condition 15

0.6008	0.6008	0.8192	0.9681	0.9949	0.0351	1.0000	0.0188	1.0000
0.1632	-0.1632	0.0	0.0	0.0	0.0	0.0	0.0	0.0
0.6226	0.6226	0.8192	0.9681	0.9949	0.0351	1.0000	0.0188	1.0000

Lateral System

Closed-loop Control Eigenvalues, Flight Condition 16

0.6792	0.7323	0.5748	-0.1134	-0.0430	0.8086	0.9255
0.4874	-0.3554	0.0	0.0	0.0	0.0	0.0
0.8360	0.8139	0.5748	0.1134	0.0430	0.8086	0.9255

Closed-loop KBF Eigenvalues, Flight Condition 16

0.5699	0.9935	0.9570	0.8207	0.0351	1.0000	0.0188	1.0000
0.1437	0.0	0.0	0.0	0.0	0.0	0.0	0.0
0.5877	0.9935	0.9570	0.8207	0.0351	1.0000	0.0188	1.0000

Closed-loop Control Eigenvalues, Flight Condition 17

0.6513	0.7039	0.5400	-0.1233	0.7966	-0.0595	0.9166
0.4960	-0.4009	0.0	0.0	0.0	0.0	0.0
0.8186	0.8101	0.5400	0.1233	0.7966	0.0595	0.9166

Closed-loop KBF Eigenvalues, Flight Condition 17

0.5377	0.9961	0.9383	0.8083	0.0351	1.0000	0.0188	1.0000
-0.1181	0.0	0.0	0.0	0.0	0.0	0.0	0.0
0.5505	0.9961	0.9383	0.8083	0.0351	1.0000	0.0188	1.0000

Lateral System

Closed-loop Control Eigenvalues, Flight Condition 18

0.6446	0.7220	0.7220	0.5554	-0.0885	0.7732	-0.0569	0.8903
-0.4984	0.4102	-0.4102	0.0	0.0	0.0	0.0	0.0
0.8148	0.8304	0.8304	0.5554	0.0885	0.7732	0.0569	0.8903

Closed-loop KBF Eigenvalues, Flight Condition 18

0.4968	0.7916	0.9924	0.9048	0.0351	1.0000	0.0188	1.0000
-0.0924	0.0	0.0	0.0	0.0	0.0	0.0	0.0
0.5053	0.7916	0.9924	0.9048	0.0351	1.0000	0.0188	1.0000

Closed-loop Control Eigenvalues, Flight Condition 19

0.6299	0.7280	0.7280	0.5531	-0.0816	-0.0816	0.7457	0.8733
-0.5254	0.3900	-0.3900	0.0	0.0118	-0.0118	0.0	0.0
0.8203	0.8259	0.8259	0.5531	0.0825	0.0825	0.7457	0.8733

Closed-loop KBF Eigenvalues, Flight Condition 19

0.4732	0.9936	0.8844	0.7830	0.0351	1.0000	0.0188	1.0000
-0.1051	0.0	0.0	0.0	0.0	0.0	0.0	0.0
0.4848	0.9936	0.8844	0.7830	0.0351	1.0000	0.0188	1.0000

Lateral System

Closed-loop Control Eigenvalues, Flight Condition 20

-0.1173	-0.0702	0.6256	0.7317	0.7317	0.5535	0.7142	0.8565
0.0	0.0	-0.5466	0.3749	-0.3749	0.0	0.0	0.0
0.1173	0.0702	0.8307	0.8222	0.8222	0.5535	0.7142	0.8565

Closed-loop KBF Eigenvalues, Flight Condition 20

0.4688	0.9927	0.8646	0.7828	0.0351	1.0000	0.0188	1.0000
-0.0764	0.0	0.0	0.0	0.0	0.0	0.0	0.0
0.4750	0.9927	0.8646	0.7828	0.0351	1.0000	0.0188	1.0000

APPENDIX M

Sampled-Data Second Order High-Pass Filters

The desired transfer function of a second-order high-pass filter is given by

$$H(s) = \frac{s^2}{(s+a)^2} \tag{M.1}$$

where a is the desired break-frequency. A simple two-state-variable model is given by

$$\begin{pmatrix} \dot{x}_1 \\ x_2 \end{pmatrix} = \begin{pmatrix} -a & 0 \\ -a & -a \end{pmatrix} \begin{pmatrix} x_1 \\ x_2 \end{pmatrix} + \begin{pmatrix} -a \\ -a \end{pmatrix} u \tag{M.2}$$

$$y = x_1 + x_2 + u \tag{M.3}$$

The transfer function $H(s)$ is given by

$$H(s) = \frac{Y(s)}{U(s)} = \frac{s^2}{s^2+a^2} \tag{M.4}$$

Using the discretizing methods described in Appendix F, one obtains the following discrete-time realization for a sampling period of $\frac{1}{8}$ of a second:

$$\begin{pmatrix} x_1 \\ x_2 \end{pmatrix} (t+1) = \begin{pmatrix} a_d & 0 \\ -b_d & a_d \end{pmatrix} \begin{pmatrix} x_1(t) \\ x_2(t) \end{pmatrix} + \begin{pmatrix} a_d-1 \\ -b_d \end{pmatrix} u(t) \tag{M.5}$$

$$Y(t+1) = x_1(t+1) + u(t+1) + x_2(t+1) \tag{M.6}$$

where $\quad a_d = e^{-\frac{a}{8}}$ (M.7)

$\qquad b = \frac{a}{8} \, e^{-\frac{a}{8}}$ (M.8)

and a is the break frequency in radians.

1. Report No. NASA CR-3089	2. Government Accession No.	3. Recipient's Catalog No.
4. Title and Subtitle INVESTIGATION OF THE MULTIPLE MODEL ADAPTIVE CONTROL (MMAC) METHOD FOR FLIGHT CONTROL SYSTEMS		5. Report Date May 1979
		6. Performing Organization Code
7. Author(s) M. Athans, Y. Baram, D. Castanon, K. P. Dunn, C. S. Green, W. H. Lee, N. R. Sandell, Jr., and A. S. Willsky		8. Performing Organization Report No.
		10. Work Unit No.
9. Performing Organization Name and Address Electronic Systems Laboratory Massachusetts Institute of Technology Cambridge, Massachusetts 92139		
		11. Contract or Grant No. NSG-1018
		13. Type of Report and Period Covered Contractor Report
12. Sponsoring Agency Name and Address National Aeronautics and Space Administration Washington, DC 20546		
		14. Sponsoring Agency Code

15. Supplementary Notes

Langley Technical Monitors: Jarrell R. Elliott and Joseph Gera

Final Report

16. Abstract

The stochastic adaptive control of the NASA F-8C digital-fly-by-wire aircraft using the Multiple Model Adaptive Control (MMAC) method is presented. The report discusses the selection of the performance criteria for the lateral and the longitudinal dynamics, the design of the Kalman filters for different operating conditions, the identification algorithm associated with the MMAC method, the control system design, and simulation results obtained using the real time simulator of the F-8 aircraft at the NASA Langley Research Center.

17. Key Words (Suggested by Author(s)) Flight control, Adaptive, Identification, Digital, F-8C	18. Distribution Statement Unclassified – Unlimited Subject Category 08

19. Security Classif. (of this report) Unclassified	20. Security Classif. (of this page) Unclassified	21. No. of Pages 420	22. Price* $13.25